University of Stavanger

FACULTY OF SCIENCE AND TECHNOLOGY

MASTER'S THESIS

Study programme/specialisation: MSc. in Petroleum Engineering Drilling and Well Technology	Spring/ Autumn semester, 2018 Confidential
Author: Beder Mohammad Al Furati	(signature of author)
Programme coordinator: Supervisor(s): Carl Lasse Hermansson (External), Bernt Sigve Aadnøy (Internal)	
Title of master's thesis: **An evaluation of inflow control technologies on the Neptune Energy Gjøa field**	
Credits: 60	
Keywords: Inflow Control ICD, AICD, AICV, NETool, Eclipse, Completion Engineering, Sandscreens, Gjøa Field, Neptune Energy	Number of pages: 145 + supplemental material/other: 68 Stavanger, 13.07.2018

Master's Thesis
PETMAS

An evaluation of inflow control technologies on the Neptune Energy Gjøa field

Beder Mohammad Al Furati

Faculty of Science and Technology
Department of Petroleum Technology
University of Stavanger
Stavanger
2018

Abstract

Operators are constantly looking for new ways to increase production and recovery in oil and gas wells by application of Intelligent Well Completions and Inflow Control Technology (ICT). For the latter, one of the main challenges is to quantify the potential upside with the application of this technology. In this context, dynamic simulators such as Eclipse™ and static simulators such as Landmark NETool™ are commonly used to try and demonstrate a change in production behavior compared to a conventional completion. The traditional way of doing this is to simulate and predict performance using a preliminary reservoir model prior to drilling the wells. This can present a series of uncertainties, and it all comes down to the accuracy of the geological understanding and reservoir approximations. It can lead to false conclusions based on poor and erroneous models. Additionally, lack of understanding of how inflow control technology works, combined with conservatism, often makes a non-ICT completion the default go-to strategy when it comes completing new wells.

In this study, a different approach to the challenge was pursued. Together with Neptune Energy Norway, two existing oil wells on the Gjøa field were analyzed. At the time of construction, these wells were not completed with IC Technology. The objective of the study was to investigate whether or not an ICT completion would have been beneficial in terms of improved oil recovery, and/or lower gas/water production, and potentially to what degree. The main methodology was based on establishing Landmark NETool models with input from the existing reservoir model, and subsequently calibrating the models to match the production history of the wells. The well designs were then modified to include different types of inflow control technologies.

The two candidate oil wells chosen for the study indicated different behaviors with the inclusion of inflow control. Well B3, which suffered from excessive gas production, showed promising results with both standard nozzle-ICDs and with AICVs. This can be attributed to the mitigation of the heel-toe effect and restrictive choking of gas producing intervals which promoted production from the toe of the well. On the other hand, well B1 did not show significant improvements when simulated with ICT. Previously suffering from excessive water production and immobilized the oil reserves, the results showed an increase in water production both with standard and autonomous inflow control. This result is however linked to some uncertainties. There are also other significant benefits to ICT that can justify the inclusion of inflow control in the well design.

Acknowledgement

This thesis was written for the Department of Energy and Petroleum Engineering at the University of Stavanger during the spring of 2018. It marks the end of my Master's degree within Drilling and Well Technology. I hope that the results and learnings from this thesis will help enhance the knowledge regarding inflow control technologies in the industry.

The process of conducting this study has provided me with extensive knowledge about different disciplines within the oil industry. Not only does the thesis consider well engineering, but it also discusses topics within the reservoir and production disciplines. This has helped me expand my competence and improve my analytic and critical thinking skills.

I would like to show my greatest gratitude towards my family for the great love and support that they have provided me with throughout my life. Without their encouragements and support, I would not have been able to come this far. This thesis is dedicated to them.

I would also like to thank Neptune Energy for letting me write this thesis, and giving me the access to valuable data for the study. Many thanks to my supervisors Lasse Hermansson and Bernt Aadnøy. Sitting at the Neptune offices, I was always provided with great support, guidance and input for the thesis. Additionally, thanks to Gerhard Våland Sund, Mehryar Nasseri, Allan Ritchie, Leif Erik Øen and Dwayne Werner Martins for the entertaining conversations and lunch breaks. Your company made the time at Neptune both enjoyable and appreciated. Furthermore, I would like to thank engineers Torunn Haugvaldstad, Neal Hewitt, Andrea Reinholdtsen and Claire Le Maitre for providing the input to the simulation work. The input and assistance from Tendeka and InflowControl is also greatly valued. Many thanks to Terje Moen at Ridge for the discussions regarding inflow control and reservoir dynamics.

Lastly, I am thankful towards all the friends and people I have gotten to know during my five years of study in Stavanger. Your companionship has made the time away from home worthwhile.

Table of Contents

List of Figures

List of Tables

List of Abbreviations

AFD	Autonomous Flowcontroller Device
AFI	Annular Flow Isolation
AICD	Autonomous Inflow Control Device
AICT	Autonomous Inflow Control Technology
AICV	Autonomous Interval Control Valve
BC	Base Case
BHP	Bottom-Hole Pressure
ECP	External Casing Packer
EOR	Enhanced Oil Recovery
ERD	Extended Reach Drilling
ERV	Enhanced Recovery Valve
FCV	Flow Control Valve
GOC	Gas-Oil Contact
GOR	Gas/Oil Ratio
IC	Inflow Control
ICD	Inflow Control Device
ICT	Inflow Control Technology
ICV	Interval Control Valve
ID	Inner Diameter
LFE	Laminar Flow Element
MLT	Multilateral Technology
NCS	Norwegian Continental Shelf
OBM	Oil-Based Mud
OD	Outer Diameter
OHGP	Open-Hole Gravel Pack
OWC	Oil-Water Contact
PDHG	Permanent Dowhnole Gauge
PDO	Plan for Development and Operation
PI	Productivity Index
PLT	Production Logging Tool
RCP	Rate Controlled Production
RE	Reservoir Engineering
SAGD	Steam-Assisted Gravity Drainage
SAS	Stand-Alone Sandscreen
SC	Standard Conditions
SLB	Schlumberger
TD	Target Depth
TFE	Turbulent Flow Element
TPR	Tubing Performance Ratio
VFP	Vertical Flow Performance
WHP	Wellhead Pressure

Introduction

Background

Initially, the operator on Gjøa did not use any ICD technology for the oil producer wells when the field was developed. Characterized by a thin oil column located between a gas cap and an underlying aquifer, the reservoir drainage strategy was based on simple pressure depletion by gas expansion drive and water displacement from below with use of long horizontal producers.

Although a study performed by Reslink indicated improved performance in terms of delayed water breakthrough and enhanced oil recovery, this matter was not further pursued, and the wells were developed with conventional non-ICD completions. Production from the oil wells on the field has proven to be challenging, with excessive water and gas production, ultimately leading to a rapid decline in oil production and short lifetime.

Experience with inflow control from the NCS and globally has proven the technology to be quite beneficial in terms of improved well performance. Several benefits such as delayed gas/water breakthrough, improved well clean-up and sand control robustness, and consequently, improved oil recovery are some of the benefits worth mentioning. In the last decade, autonomous inflow control has presented further advantages, where the technology is able to selectively choke harder on unwanted fluids, consequently prolonging the production of oil after breakthrough.

It would be interesting to see if inflow control could have improved the production performance of the Gjøa wells, and mitigated the challenges faced during production.

Objectives

The main objective of this study is to perform a retrospective evaluation of inflow control technologies on two existing Gjøa wells, to see if an ICT completion could have improved the well performance. By reviewing current inflow control technologies on the market, one can get an indication for which of the technologies that are suitable for further simulations. Furthermore, a NETool simulation model will be established for each well, which includes the existing well designs. By using input from the existing reservoir model, in addition to available production data, the NETool models will be further calibrated to match the historical production behavior of the wells.

Having obtained an adequate match, the well design will be altered to include inflow control. The first simulations will include conventional nozzle-type ICDs. Secondly, the

well models will be simulated with autonomous inflow control valves to see if this can present further benefits in terms of reduced gas/water production after breakthrough.

A well known principle within the world of science and engineering is to learn from the past to predict the future. This evaluation study also aims at improving knowledge about the principles of inflow control within the company, aiding in better decisions in future field developments and well designs.

Structure of report

In the beginning of Part I, an introduction to the Gjøa field and reservoir along with the two candidate oil wells, is provided. The first step of solving any problem is to properly define and address the challenges. Therefore, a focus was laid on accurately defining the production challenges for the two wells. Section 2 explains the principles of inflow control technology and provides a review of currently available inflow control technologies on the market. The end of this section qualitatively discusses the potential benefits of the technologies on Gjøa.

Part II begins by explaining the methodology used for building the simulation models. An overview of the workflow for each well is given, to describe how the reference case models were established in NETool. The calibration of the well models according to production history ensured that the models were set up correctly and that the subsequent simulations with inflow control would be somewhat accurate. Once this was achieved, further simulations could be done to see the effect of ICD and AICV in the wells. This is discussed in Section 4 and 5, respectively.

Part III discusses the results obtained in Part II, and evaluates the benefits of adapting to inflow control for the two oil wells. There are several factors that need to be taken into account when assessing the benefits and disadvantages of the technology. Section 7 discusses the uncertainties related to the simulations and results that we have obtained in the study. The magnitude of these uncertainties is also debated in this section. Lastly, a conclusion for the thesis is formed, considering the observations and learnings from the study and providing future recommendations.

Part I

Theory

1 The Gjøa Field

Operated by Neptune Energy, Gjøa is an oil and gas field located in blocks 35/9 and 36/7 in the North Sea, approximately 50 km North-East of Troll B, see Figure 1. The field assigned to license PL-153 was first discovered in 1989, when an exploration well detected gas and some amounts of oil in the northern part of the field. The well was later followed up by two appraisal wells, one in the southwestern part of the field, and another in the eastern part of the field. Both of these detected the presence of oil and gas [1].

In 2007, the Plan for Development and Operation (PDO) was approved by the Norwegian Ministry of Petroleum and Energy. Recoverable reserves were initially estimated at 39.7 Billion Sm^3 of rich gas, and 9.2 Million Sm^3 of oil [2].

As shown in Figure 1, the field was developed with a semi-submersible platform with production and processing facilities with partial power-supply from shore. four subsea template structures and one satellite well are tied back to the platform, which started production from the field in 2010 [3].

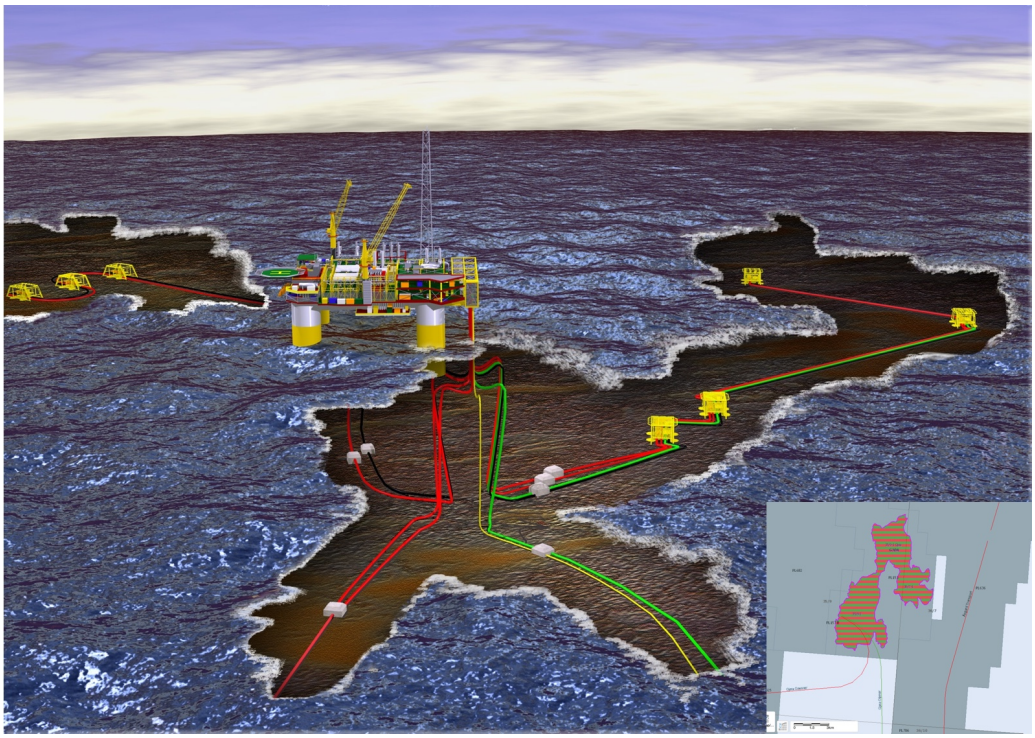

Figure 1: *The Gjøa Field, [2]*

1.1 Reservoir and Geology

The Gjøa reservoir is positioned in a structure of several tilted fault blocks, mainly divided into seven main segments, P1 - P7, see Figure 2. The hydrocarbon bearing column contains a 200 meter thick gas cap with a thin underlying oil rim with a thickness of 30-45 m. The Upper Jurassic sandstones of the Viking Group make up the main reservoir, which consists of the Sognefjord, Fensfjord and Krossfjord formations. The northernmost segment (P1) lies in a Brent/Dunlin reservoir. The P1, P2 and P5 segments have all been proven with an exploration well. Meanwhile, the P3 segment was treated as a proven segment in the PDO documentation, as a results of having the highest discovery probability [4].

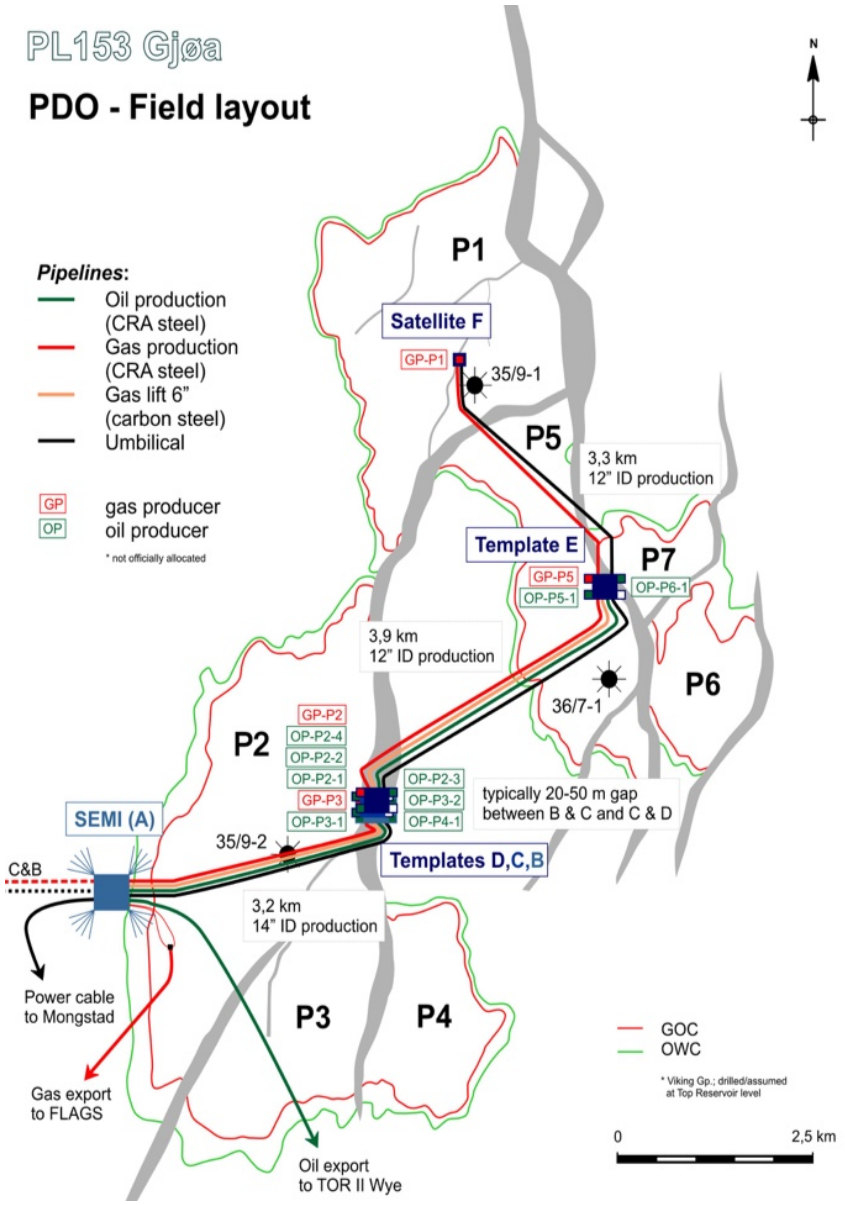

Figure 2: *Field layout with the main segments of the Gjøa reservoir, [2]*

The mean initial reservoir pressure is around 235 bars, at a temperature of 82 ℃. The

reservoir permeability is quite varying through the Viking sands, from some millidarcys to several darcys. While the Krossfjord and Sognefjord formations have great reservoir quality, the former is mostly water-filled on Gjøa. The Fjensfjord sands present rapid vertical variations in both porosity and permeability and is of relatively lower reservoir quality.

Based on various wireline logs, core and fluid analysis results, a petrophysical field evaluation was conducted. This later resulted in a full field geological facies model, see Figure 3. This model incorporated 16 faults and 23 different reservoir zones. Once this grid model was completed, the simulation model was constructed by upscaling reservoir parameters to the Eclipse simulation grid. This dynamic model is a full field model which covers all segments of Gjøa, and was built as a Black oil model with live oil and wet gas [4].

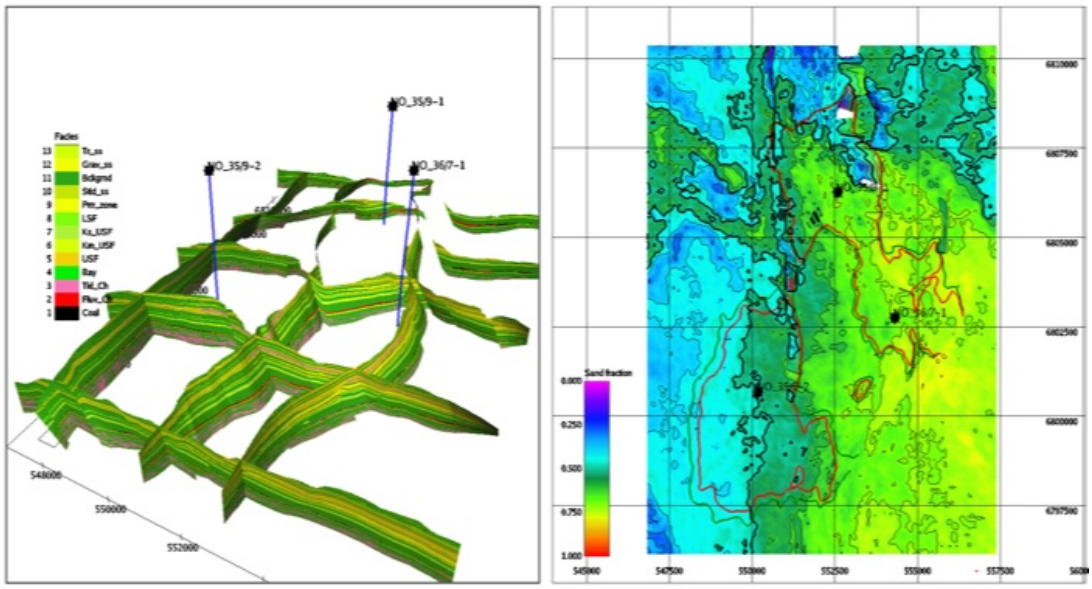

Figure 3: *Gjøa Geological Facies Model, [5]*

Initial reservoir simulations showed that the oil production will suffer from simultaneous production of gas. However, without the gas production there would be no economical incentive to develop the field. The drainage strategy for Gjøa is mainly based on natural pressure depletion. The gas will be recovered with four vertical gas producer wells located high on the segments P1, P2, P3 and P5.

Because of the thin oil rim, the oil recovery strategy involved using long horizontal wells to get a steadily descending Gas-Oil Contact (GOC) and limit excessive gas production. Injection of gas or water was evaluated at an early phase, but was deemed unprofitable in terms of recovery and economy. Experience has also shown that for thin oil columns with an overlying gas cap, the challenge of significant water/gas breakthrough in high

permeable layers is only worsened with application of pressure support by injection. Reservoir simulations showed that a placement of the horizontal producers in the middle of the oil column would give a steady production of oil, approximately 9-10 Million Sm^3. According to the models, the reservoir pressure will not drop much during the main oil production phase, implying that the system has sufficient energy available. The main drainage strategy for the oil rim is therefore displacement of water from below and gas cap expansion from above. The drainage strategy can further be elaborated as follows [4]:

- Simple pressure depletion
- Simultaneous oil and gas production, with some delay of the early gas to enhance oil production.
- Low pressure production of oil from start (20 bar).
- Initial gas production towards 65 bar, with possibility for low pressure production (20 bar) during the decline phase of the production lifetime.
- Oil will be produced through 9 horizontals, 4 of which have two extra branches.
- Zone control devices installed in each multilateral junction to enable branch control.
- Gas production through 4 vertical gas wells located at the crest of the major gas segments (P1, P2, P3 and P5).

1.2 Gjøa Wells - History and Challenges

The Gjøa field was developed with 7 oil wells and 4 gas wells. The horizontal oil producer wells were developed with a reservoir section from 900 to 2800m. Of the 7 oil producers, 4 oil wells were planned as multilateral wells, while 5 wells were planned as single producers. When assessing the type of sand-face completion, the main focus was laid on whether the wellbore would penetrate several sand formations or not. The oil wells that fall under the former category, would be completed with a liner and oriented perforations, i.e. Cased & Perforated (C&P) completion. The oil producers mainly penetrating the Sognefjord sands, were completed with stand-alone screens (SAS). Moreover, the gas wells were completed with an open-hole gravel pack (OHGP) completion [2].

1.2.1 Well B3

Well 35/9-B3 HT2[1] is a single oil producer in the P2 segment that was drilled and completed in during the middle of 2011. The completion consists of stand-alone sandscreen completions and blank pipe sections, which is shown in the well schematic in Appendix G.1, Figure G-24. The horizontal section penetrates approximately 2000 meters of consolidated reservoir rock [6].

As shown in Figure 4, B3 started production in December 2011. The different fluid rates in the chart are tuned rates generated by studying the data from subsea flow meters and adjusting the rates to match export rates according to deduction testing of the wells. The gas rate is the most reliable data with an estimated uncertainty of ±5%. The oil and water rates are linked to a higher degree of uncertainty because of flow meter drifting[2] over time. Thus, several step changes can be observed in the production rates for these fluids. The observed sudden drops in production show the production shut-ins, that are generally caused by well testing, integrity testing, or planned maintenance work [7].

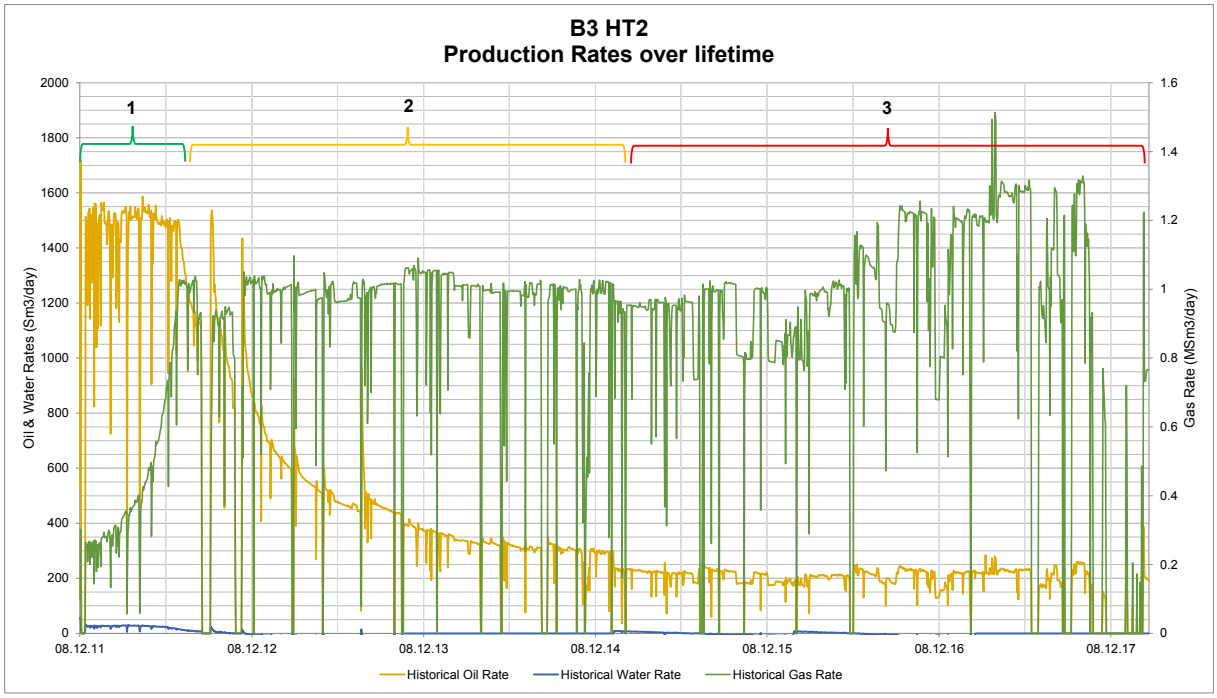

Figure 4: *Production history for well B3-HT2, [8]*

The history of B3 has mainly involved production of oil and gas. The well has produced negligible volumes of water, with a minor water influx at the toe. After the gas breakthrough took place in July 2012, the oil production was severely affected. This is believed to have

[1] Initially called OP-P2-4, see Figure 2

[2] Drifting refers to the slow change in response of a gauge, which can lead to erroneous measurements

held back significant oil volumes. For further evaluation and discussion, the lifetime of the well can be divided into three categories, as displayed in Figure 4:

1. **Early-life (December 2011 - July 2012):** Before gas breakthrough, gas cone developing. Characterized by a somewhat steady oil production and increasing gas production, i.e. a decreasing Gas/Oil Ratio (GOR).
2. **Mid-life (July 2012 - March 2015):** After gas breakthrough. Decreasing oil rate and steady gas production rate, i.e. an increasing GOR.
3. **Late-life (March 2015 - February 2018):** Gas cone is becoming more and more severe, leading to an increase in the gas rate, while the oil production is steadily low (increasing GOR).

For the purpose of this thesis, the main objective for B3 is to see if inflow control technology can help to hold back and delay the gas breakthrough, and thereby increase oil production. Furthermore, if the gas production can be reduced after breakthrough, the gas cap expansion drive could aid in an improved oil sweep [7].

1.2.2 Well B1

Well 35/9-B1 AHT3[3] is a single oil producer in the P4 segment that was drilled and completed in early in 2012. The completion consists of stand-alone sandscreen completions and blank pipe sections, as shown in the well schematic in Appendix G.1, Figure G-25. The horizontal section stretches approximately 1500 meters at a depth of 2300 mTVD [9].

The well started producing in March 2012 with a high oil rate and relatively quick gas breakthrough, as displayed in the production history in Figure 5. The different fluid rates are tuned in the same way as described for B3.

[3]Initially called OP-P4-1, see Figure 2

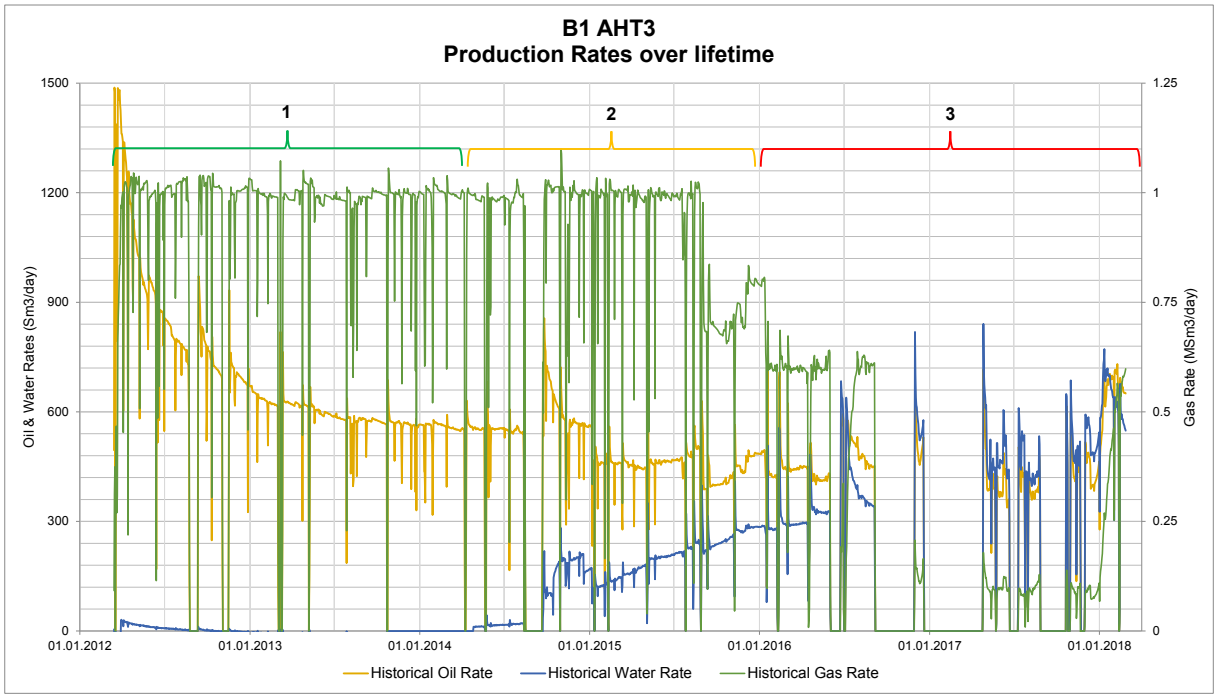

Figure 5: *Production history for well B1-AHT3, [8]*

Reservoir modeling indicated an early water breakthrough that would immobilize the reservoir oil. However, B1 has produced better than anticipated with a relatively high oil production rate and a late water breakthrough in mid 2014 [7].

As displayed in Figure 5, the lifetime of well B3 can be divided into three categories according to the production characteristics:

1. **Early-life (March 2012 - April 2014):** This period is characterized by a decreasing oil rate and steady gas production, i.e. an increasing GOR. No water production.
2. **Mid-life (April 2014 - December 2015):** Relatively stable GOR and increasing water production because of water coning.
3. **Late-life (December 2015 - February 2018):** High water cut after breakthrough. Periods of problems kicking off[4] the well after shut-in because of a high water cut at start-up.

As implied, well B1 has experienced challenges related to high water production in the late-life period. When the well is shut-in, the water mobilizes and floods the near-wellbore area leading to problems with kicking off. The problems occur because of the heavy hydrostatic column which prevents the well from flowing naturally. Usually, gas lift must

[4]When production from a well is initiated after shut-in

to be employed at start-up to make the well flow sufficiently. In the case of long shut-in periods, gas lift is necessary for several months before the well can flow naturally.

Therefore, it would be interesting to see if ICT can aid in delaying the water breakthrough to increase the recovery of oil. Another objective is to see if the water influx can be restricted during start-ups and lessen the need for long gas lift periods, which would present several operational and cost-reducing benefits [7].

1.3 Key Reservoir and Production data

In addition to the production data presented in Figure 4 and 5, the Eclipse reservoir model for Gjøa will play an important role in the simulation work. Table 1 shows some of the important data for the two oil wells on Gjøa. Further input data used in the thesis will be discussed in Section 3.2.

Table 1: *Selected Key Reservoir and Production data, [6, 8, 9, 10]*

Field	**Gjøa**	
Wellbore	**35/9 B3-HT2**	**35/9 B1-AHT3**
Air gap (RKB-MSL)	22 m	22 m
Water depth, m	363 m	363 m
Total depth, mTVD	2332 mTVD	2335 mTVD
Total length, mMD	5845 mMD	4419 mMD
Reservoir Pressure, bar	235 bar	235 bar
Reservoir Temperature, ℃	84℃	84℃
Live Oil Density (g/cc)	0.642 g/cc	0.649 g/cc
Live Gas Density (g/cc)	0.207 g/cc	0.228 g/cc
Live Water Density (g/cc)	1.009 g/cc	1.009 g/cc
Live Oil Viscosities (cp)	0.2650 cP	0.2835 cP
Live Gas Viscosities (cp)	0.0238 cP	0.0270 cP
Live Water Viscosity (cp)	0.384 cP @ Pres	0.384 cP @ Pres
Bo at Reservoir pressure	1.54 Rm3/Sm3	1.528 Rm3/Sm3
Rs at Reservoir pressure	175 Sm3/Sm3	167.3 Sm3/Sm3
Initial reservoir drawdown pressure	0.177 bar	8.837 bar

2 Inflow Control Technology

2.1 Introduction

With the advancements in drilling technology the last decades, various production challenges have followed. Extended reach- (ERD) and horizontal well drilling has allowed operators to achieve high production rates at low drawdown pressures because of increased reservoir contact. As Glaser et al. [11] pointed out, there is a general acceptance within the industry that the well productivity is proportional to the length of the wellbore. This especially applies to reservoirs with thin oil rims, such as the Troll field. However, the drilling of long horizontal wells to utilize thin oil rims has introduced various challenges when it comes to well clean-up, steady layer drainage, and even flow distribution along the well bore [12].

To mitigate these challenges, ICT was introduced in the nineties. The technology is based on integration of flow devices in the well completion to control the inflow behavior at various rates and pressures. The main purpose of this is to delay water or gas breakthrough, but can also have other significant benefits when it comes to improved well performance. In recent years a number of service companies have developed technologies that can hold back unwanted fluids following breakthrough, widely termed as autonomous inflow control technology. This has enabled production from thin oil rims as well as providing an insurance on well performance uncertainty.

Inflow control technology has thus enabled production from previously infeasible reservoirs, as well as enhanced oil recovery from existing fields by improving reservoir and well performance.

This section of the thesis is divided into five subsections. First, an outline of current completion, production and reservoir challenges will be given. The four following subsections consist of a detailed review of various inflow control technologies, and how they may mitigate the presented challenges along with other potential benefits. This includes functionality, flow characteristics and field case studies. A special focus will be laid on two particular technologies; the nozzle type ICD and the RCP valve. The reason for this is that they are considered the current industry standard when it comes to inflow control. Additionally, they will be used in further simulation work, which makes them the most relevant for the purpose of this thesis.

Inflow control technology can be categorized into two primary categories; *active* and *passive* inflow control technology. Active ICT describes flow control that is integrated with surface control. Usually, this involves control lines running from the devices up to the surface. On the other hand, passive inflow control cannot be changed or altered once the well has been completed, and behaves according to the predetermined design of the apparatus.

Table 2 provides an overview of current passive inflow control technologies. This category can further be divided into three classifications; Inflow Control Devices (ICD), Autonomous Inflow Control Devices (AICD) and Autonomous Inflow Control Valves (AICV). Apart from the fact that the two latter types are autonomous, it is common to distinguish between *devices* and *valves*; Devices are fixed fittings with no moving parts, while valves include some moving components. This distinction is important when it comes to the reliability and functionality of the respective technology.

The rightmost column displays a rating in accordance to how many installations there have been with the respective technology. The rating is based on discussions with vendors as well as industry experts within the discipline. There are however some uncertainties linked to the use of the relatively new autonomous inflow control technologies. Therefore the categorization will be as follows:

- Very few: 0 - 10 installations
- Few: 11 - 50 installations
- More: 51 - 100 installations
- Many: 101 - 1000 installations
- A lot: $>$ 1000 installations

The purpose of displaying this characterization is to give an impression of which technologies that are mostly used across the industry. In the ICD category, the nozzle ICD is the most applied technology. This also why most vendors offer to provide this technology. Furthermore, the RCP has been found be the most extensively used autonomous inflow control technology on the market, especially on the Norwegian Continental Shelf (NCS). For this reason, these two technologies will be the main focus in further simulations.

Table 2: *A summary of current Passive Inflow Control Technologies*

Main Group	Subgroup	Section	Mechanical Characteristics	Flow Characteristics	Vendor	Use
Inflow Control Device (ICD)	Nozzle	Section 2.3.2, Page 27	Restrictive orifice	Density dependent pressure drop	Tendeka, SLB, Weatherford, Halliburton	A lot
	Helical Channel	Section 2.3.2, Page 29	Frictional fluid channels	Mostly viscosity dependent pressure drop	Baker Hughes	A lot
	Tubular	Section 2.3.2, Page 30	Mainly restrictive and somewhat frictional tubular flow	Mostly density dependent pressure drop	Halliburton	Few
Autonomous Inflow Control Device (AICD)	Hybrid ICD	Section 2.4.1, Page 35	Restrictive and frictional Combination of channels and restrictions	Flow dependent on the Re number	Baker Hughes	Many
	Fluidic diode	Section 2.4.2, Page 38	Changing flow path based on fluid	Viscosity dependent	Halliburton	More
	Autonomous ICD	Section 2.4.3, Page 42	Fluid is directed tangentially through a circular path	Flow dependent on the Re number	Schlumberger	Very few
Autonomous Inflow Control Valve (AICV)	RCP	Section 2.5.1, Page 44	Restrictive, Levitating Disc	Viscosity dependent	Tendeka, Baker Hughes	Many
	AICV®	Section 2.5.2, Page 50	Pilot flow path determines valve behavior	Flow dependent on the Re number	Inflow Control	Few
	ERV	Section 2.5.3, Page 54	Buoyancy-based design with three fluid chambers	Density dependent	Acona	Very few
	AFD	Section 2.5.4, Page 57	Design with a pilot flow orifice and spring actuated valve	Constant flow rate regardless of flowing BHP	Superior	Very few
	Adaptive ICD	Section 2.5.5, Page 59	Combination of hybrid type ICD and magnetic valves	Viscosity and rate dependent flow	Wormholes	Very few

2.2 Current Challenges

Heel-Toe Effect

One of the early recognitions when it came to production of long horizontals, was the heel-toe effect. In high-permeability reservoirs, the friction along the wellbore can often lead to a phenomenon where the heel of the well is much more productive than the toe. This effect is illustrated in Figure 6. It occurs because the fluid in the toe has to overcome a tubing pressure drop from the toe to the heel, while the fluids at the heel do not experience this resistance. The result is a significant difference in flow rate between the heel and toe of the well, in some cases leading to little or no production from the toe. The consequence is a reduced oil sweep and early gas/water breakthrough, see Figure 6. The challenge of poor oil drainage is only exacerbated once water or gas has broken through, since the production of these fluids will be dominant because of higher mobility. Moreover, the pressure support of the reservoir, previously from the aquifer or overlying gas cap is lost, which can lead to considerable oil reserves at the toe becoming irrecoverable [11, 13, 14].

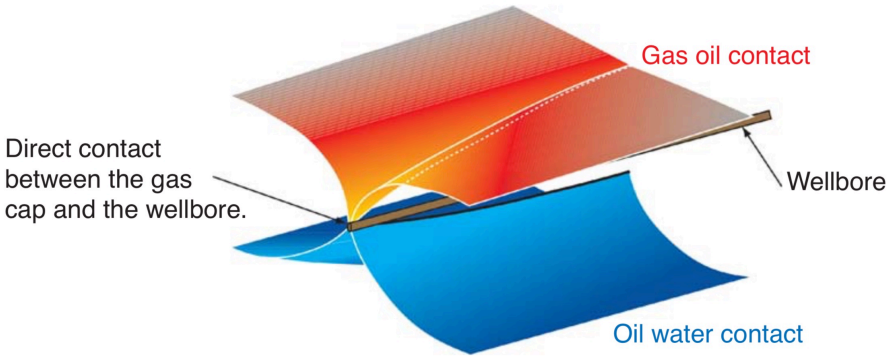

Figure 6: *Coning at the heel of a horizontal well, [13]*

Heterogeneous Reservoirs

Another challenge with long horizontal sections can arise if the reservoir is heterogeneous with varying formation quality along the wellbore. In this case, the permeability is often quite varying, resulting in an uneven flux along the wellbore. Flux is defined as the volumetric flow rate per unit area, and the consequence of uneven flux can be an irregular oil sweep, as illustrated in Figure 7. The high permeability zones will often be dominant when it comes to production, and can lead to early gas/water breakthrough in these respective zones. Additionally, high production in some zones may limit production from the lower permeability zones with lower flux. This can further lead to substantial reserves being left behind [13, 15].

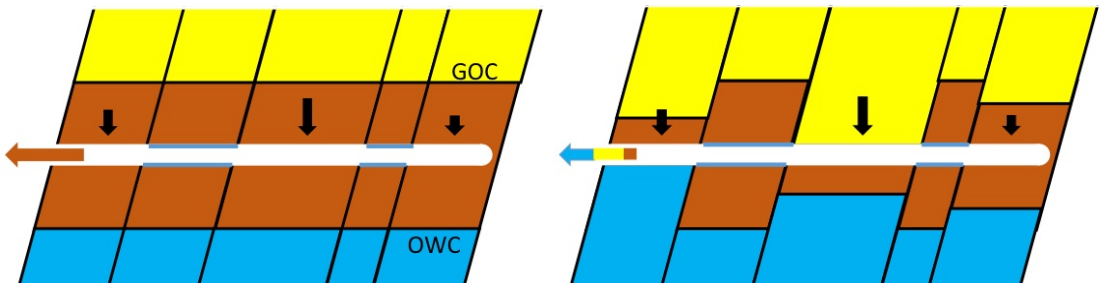

(a) *Start of production* **(b)** *After some time*

Figure 7: *Production from a heterogeneous reservoir with variable permeability, [15]*

Well Clean-Up

Conventionally, an oil well is drilled in static overbalance. This means that hydrostatic pressure of the drilling fluid exceeds the pore pressure of the formation fluids, i.e. the pore pressure. This pressure control is the most important function of the drilling fluids and it is directly related to hole stability and prevention of blow-outs.

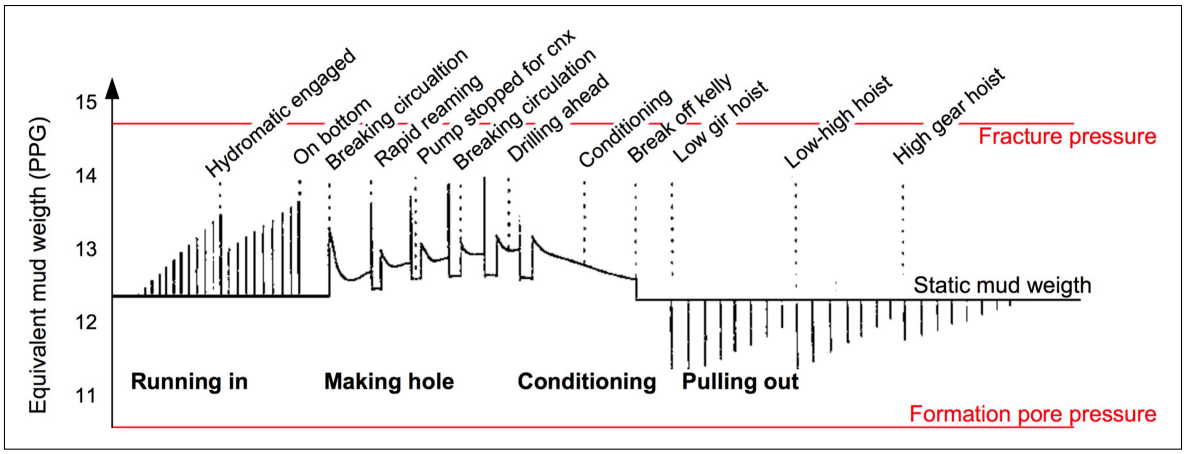

Figure 8: *Demonstration of how different operations affect the ECD, [16]*

Figure 8 illustrates the effects of various drilling related operations on the bottom-hole pressure (BHP). To achieve a sufficiently high hydrostatic pressure, the mud weight (density) must be sufficient. This is achieved by adding various weight elements such as Barite to increase the mixture density. Additionally, clay minerals are added to the drilling fluid to increase the viscosity, and thereby limiting the settling of particles and cuttings. When drilling into the reservoir zone, a filtercake is formed which limits filtrate invasion to the formation.

After a well has been drilled, the lower completion can be run into the well. Based on a number of factors, it can take weeks to months from the lower completion has been run till the well has started to produce, e.g. in pre-drilled wells. If the lower completion is

run in drilling fluid, this can have considerable production consequences later on. It can take a long time before production is started, which can lead to settled particles in the drilling fluid, forming a solid plug at the low-side of the well, as Moen and Asheim [14] demonstrated. If the completion consists of stand-alone sandscreens, the screen can be clogged and inflow may be impaired [14].

A common clean-up method to mitigate this effect is to displace the mud with brine prior to running screens. In practice, this means a longer open-hole time, increasing the risk of having hole-stability issues. Additionally, when the drillpipe is laying at the low-side of the wellbore, the removal of settled solids can be challenging. This can leave the borehole with significant amounts of mud and cuttings even after displacing with brine. These uncertainties have led to the common practice of running screens in properly conditioned mud instead of displacing with brine. Proper sand screen slot opening is also an important consideration, to avoid plugging the screens when back-producing the drilling fluid [14].

Another challenge when it comes to initiating production, is the removal of the filtercake from the borehole sand-face. In some cases, chemical treatments (e.g. breaker fluids) may be applied to dissolve the filtercake. However, in the case of long horizontal wells, it can be challenging to place the breaker fluid accurately because of operational limitations. A common approach is to rely on the back-flow from the reservoir to sufficiently remove the filtercake. The reliability of this approach highly depends on the local drawdown and inflow rate, as illustrated in Figure 9. According to Moen and Asheim [14] and associated sources, a minimum drawdown in the magnitude of 0.15 to 1.6 bar is typically required for filtercake lift-off.

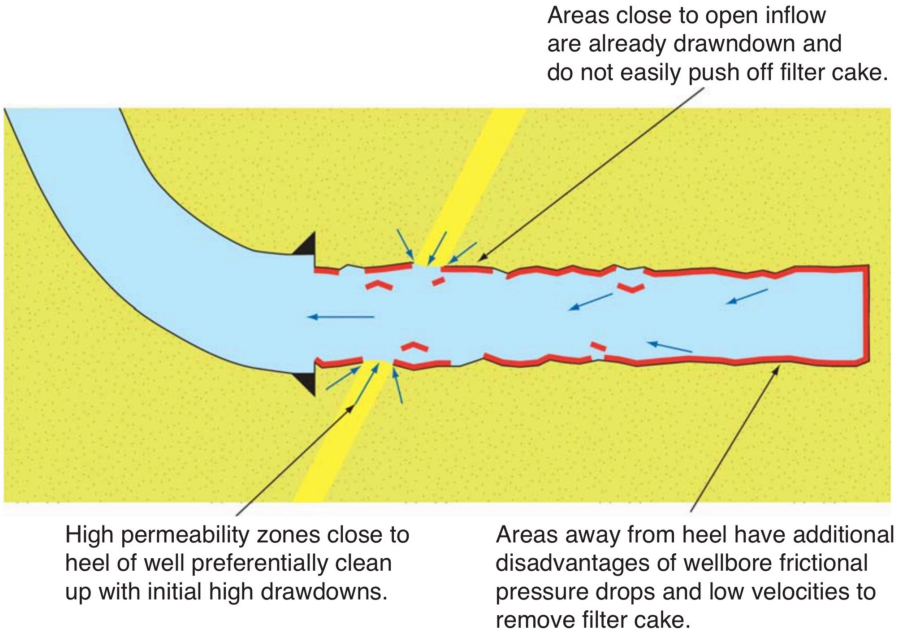

Figure 9: *Irregular clean-up of a horizontal well, [13]*

Put into light of the aforementioned challenges with the heel-toe effect and heterogeneous reservoirs, the challenge of proper well clean-up is only exacerbated. At startup of production when the wellbore pressure is reduced, the filtercake is lifted off the sand-face, allowing inflow at certain sections. However, the reservoir fluids will always choose the paths of least resistance, i.e. high permeability sections and preferentially closer to the heel. Not only does the heel-toe effect reduce the inflow rate closer to the toe, but also the drawdown. In practice, this can leave long sections of the lower well part with an intact filtercake, see Figure 9. It should also be mentioned that poor well clean-up only exasperates the challenges of the heel-toe effect and low producing zones in heterogeneous reservoirs. This is because of the added friction of the filtercake in low productive zones (i.e. higher completion skin) [13, 14].

Sand Control

Stand-alone sandscreens are one of the most commonly used sand-face completions in oil & gas wells, because of their low cost and complexity. Stand-alone screens are often categorized into three categories, see Figure 10:

- Wire-Wrapped screens
- Pre-Packed screens
- Premium screens

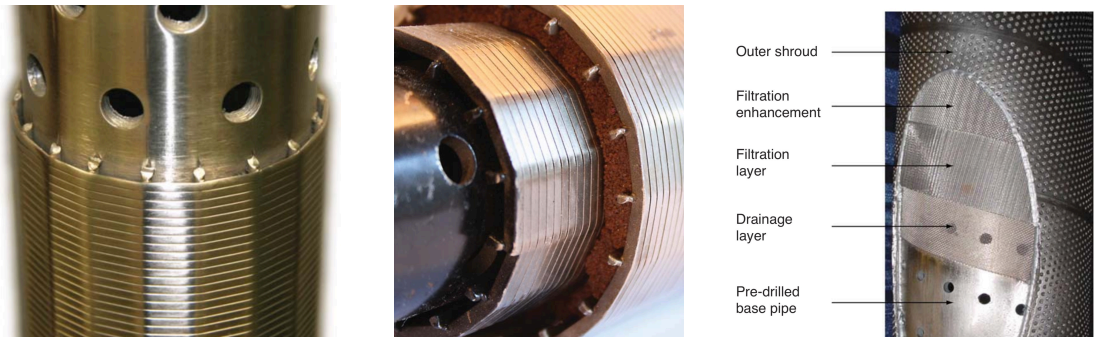

(a) *Wire-Wrapped screen* **(b)** *Pre-Packed screen* **(c)** *Premium screen*

Figure 10: *Stand-alone screen types, [13]*

Wire-wrapped screens are built on a perforated base pipe, longitudinal metal rods and a wire which is wrapped and welded around the rods, see Figure 10a.

Pre-packed screens are built similarly to the wire-wrapped screens, however, they are based on two wire-wrapped layers as pictured in Figure 10b. Between the two layers, gravel is packed to provide an additional sand-control layer.

Premium screens are the most complex screen type when it comes to construction, see Figure 10c. They are constructed with multiple woven layers and an offset layer, making them more robust and resistant to erosion [13].

Completion designs with stand-alone screens often incorporate blank pipe sections as well as swellable elastomer packers. However, due to sand control failures, stand-alone screens have developed a poor reputation. The reliability of SAS has substantially improved in the past couple of decades owing to developments within material selection, screen design and quality control during installation. The main cause of stand-alone screen failure has been screen erosion, exacerbated by plugging. Hot spot is a term that describes areas of focused inflow, which are consequently prone to erosion and sand control failure [13].

A number of operator companies have reported high failure rates when it comes to the use of stand-alone screens, including BP, Chevron and Shell. According to Bellarby [13], there are some common factors that usually cause screen failure:

- Mud plugging (In wells with Oil-Based Mud (OBM) displaced by brine after running the screens)
- Screen plugging because of reactive shales, creating erosion-prone hot spots. An open annulus aggravates this problem
- Large annular areas allowing for annular flow
- Failures caused by insufficient well clean-up because of low drawdown, i.e. partial filtercake removal

- Heterogeneous reservoirs are more prone to failure than homogeneous.
- Wells with high flux and varying flux contribute to failure
- Mechanical failure when running screens into the borehole, because of excessive applied weight and out of gauge boreholes)

Bennett et al. [17] proposed a decision flow chart that addresses these causes, and possible solutions to avoid sandscreen failure. However, operators at the time such as Norsk Hydro[5] challenged these guidelines for being too cautious and proposed a different recommended practice which has been applied in 230 offshore wells [18].

There is clearly a relation between the four challenges related to production of long horizontal wells. The heel-toe effect can lead to a high flux at the heel of the well, significantly increasing the risk of forming hot spots and having sand control failure in this section of the well. Similarly, heterogeneous reservoirs with varying permeability and flux along the wellbore, can lead to concentrated production in certain parts of the well, and screen plugging in low productive zones, leading to screen failure. The issue of poor well clean-up and filtercake removal also has clear consequences for the reliability of sandscreens [13].

Annular Flow

Amongst others, Bennett et al. [17] pointed out how annular flow can be a determinant when it comes to SAS failure and reliability. Firstly, annular flow can prevent particles from accumulating at the point of solids production, i.e. where the formation has failed, see Figure 11. This exposes the screen to excessive sand impact until it packs with sand. Bellarby [13] describes how the annular velocity during production is quite similar to the tubular velocity and more than sufficient for transporting sand along the annular wellbore space. A mitigation for this issue can be to maximize the outer diameter (OD) of the screen, i.e. minimizing the annular to tubular space-ratio, and thereby reducing the solids velocity in the annulus.

[5]Later merged into Statoil Hydro. Now called Equinor.

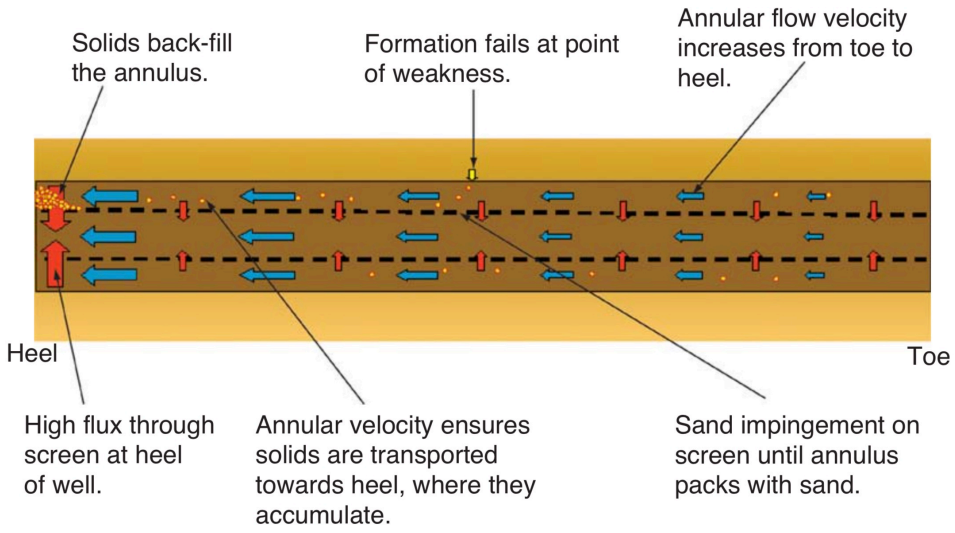

Figure 11: *Annular flow and solids redistribution, [13]*

Secondly, annular flow can transport shale and clay fines from the point of production to points where they can lead to screen plugging. The effect is further exacerbated by natural diversion; once a screen part has been plugged, the annular flow transports fines to the next open screen part, leading to further plugging and forming of hot spots [13, 19].

Various attempts have been made to solve the challenges in this section. This includes [11, 13, 20]:

- **Drilling multilateral (MLT) wells** to shorten the horizontal sections, and thereby avoiding the wellbore friction associated with long horizontal sections. This can be quite costly and operationally demanding.
- **Deploying a stinger** one-third into the horizontal well, to force fluids to flow from the heel and along the wellbore before entering the stinger, see Figure 12. This gives an additional pressure drop which helps even out the inflow profile and thereby reduce the heel-toe effect.

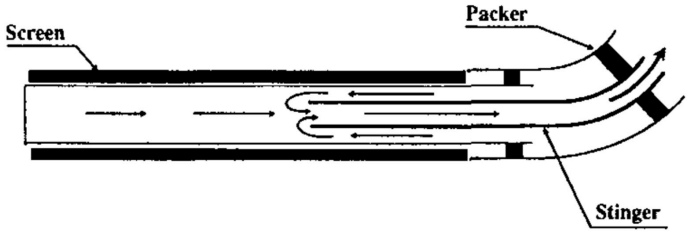

Figure 12: *Stinger completed well, [21]*

- **Incorporating Interval Control Valves (ICV)** to choke or shut off laterals with early gas or water breakthrough with the purpose of prolonging production lifetime. However, this requires hydraulic control lines down to the ICV and there is a limited number of ICVs that can be integrated in the well completion.

- **Varying the perforation intervals** to achieve a more uniform inflow profile, e.g. increase perforation density towards the toe.
- Similar to the previous point, **add blank pipe sections** in SAS completions to achieve a more uniform inflow profile.
- **Increase the screen size** to minimize annular area, and consequently annular flow.
- **Place External Casing Packers** (ECP), e.g. swell packers, at certain sections of the lower screen completion, to minimize annular flow. However, Bellarby [13] noted how an ECP will likely have a minimal effect on this issue, since the flow will probably take a route from the base pipe into the annulus downstream of the packer.

One of the most significant technological breakthroughs in the early nineties was the implementation of inflow control technology as part of the completion. As will be explained later, this technology has helped dramatically reduce the effect of the above-mentioned completion and production issues.

2.3 ICD

An Inflow Control Device is a small choking device installed in each screen joint in the base pipe layer, as illustrated in Figure 13. The device is a solid fitting with no moving parts, meaning that the flow through the device cannot be manually regulated or modified after installation. The ICD introduces an additional pressure drop across the completion, which reduces flow at high producing sections and allows for better inflow in low producing zones, thereby ensuring an even flow distribution along the well. This pressure drop follows a predetermined pressure drop equation, and highly depends on the flow rate through the ICD. It should nonetheless be mentioned that not all ICD completions rely on a sand control completion, which is the case for consolidated formations [22, 23, 24].

From a construction point of view, the ICD screen joint is mostly similar to a non-ICD screen joint, see Figure 13. While a conventional screen joint has a perforated base pipe, the ICD joint has a non-perforated base pipe with a choking device that introduces the additional pressure drop.

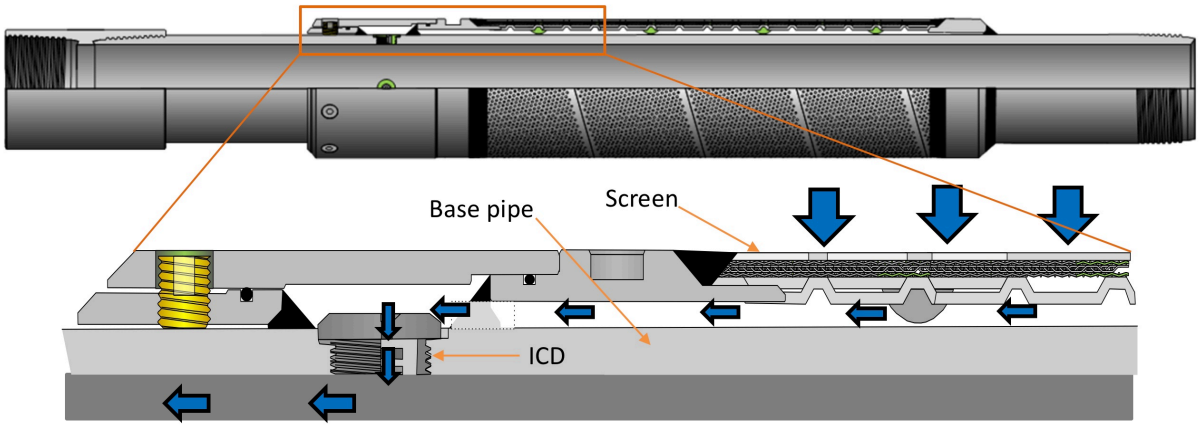

Figure 13: *A typical ICD screen joint, [25]*

During production, fluid is first separated from the sand through various filter media in the screen joint. Subsequently, the fluid flows along the base pipe to the end of the joint, where it enters the inflow control module, see Figure 13. Here, the fluid meets a resistance or restriction in the form of a nozzle, tiny tube, channel or spiral, which introduces a pressure drop. The pressure resistance is consequently propagated out to the reservoir, thereby altering the reservoir dynamics. After passing through the ICD, the fluid enters the base pipe and flows up through to the tubing to the production facilities [26].

An important consideration when it comes to designing an ICD completion is compartmentalization[6]. One of the purposes of installing ICDs in the well is to hold back

[6]In this context, the term refers to separating the annular space along the wellbore into compartments.

zones with high flux, and promote zones with low flux. However, without the proper annular isolation in an ICD completion, highly productive zones will remain dominant, since production from these zones will be diverted through the annulus to other parts of the well. Not only will this deem the lower flux zones unproductive, but annular flow and cross-flow will be further promoted since the fluid chooses the path of least resistance. As explained in Section 2.2, annular flow can present a number of problems related to screen plugging and sand control failure. Poor use of annular compartmentalization will also exacerbate the effect of an early water breakthrough, which is closely associated with high productive zones [12, 27].

The issue can be easily understood by the following analogy. If a ship which is built with one floating compartment suffers a small leak, it will easily flood and sink. On the other hand, if the floating compartment is made up of many smaller individual segments, a small leak will only result in the flooding of one segment, and the ship can stay buoyant. The situation is similar in an oil producing well with water breakthrough; without compartmentalization, the water will flood the whole wellbore and dominate production, severely reducing oil recovery. However, with the proper annular compartmentalization, the high-rate water producing zones will be choked back because of a higher ICD pressure drop, allowing lower flux zones to contribute to production.

The early solutions for compartmentalization was based on mechanical open-hole packers to isolate various well sections. However, this limited the number of possible well segments, involved the risk of not being able to set the packers, and presented a significant expense. In the last decade there has been a shift in the use of open-hole packers, from mechanical packers to swell packers [28].

Pictured in Figure 14, a swellable packer consist of an elastomer rubber element that has been bonded to a blank pipe by molding, and cured to the desired temperature and pressure ratings according to well specifics. When the rubber comes in contact with hydrocarbons or water, it will expand as a result of diffusion of said fluids. The downhole temperature and pressure further affect this swelling. The expansion can more than double the volume of the swell packer, providing a tight seal to the formation, holding up to 350 bars of differential pressure. The pressure rating of the swell packer depends on several factors [13, 29]:

Figure 14: *Swellable packer, courtesy of Tendeka*

- The length of the rubber element
- The thickness of the rubber element
- Percentage volume increase resulting from swelling

From an operational point of view, the swell packer should have a small initial OD to easily be run downhole, before swelling to the borehole inner diameter (ID). Nevertheless, as the swelling percentage increases, the pressure rating decreases, as illustrated in Figure 15. Hence, a compromise must be made between these two engineering aspects. A simple, yet efficient mitigation to this issue, has been to introduce a smaller-diameter blank pipe pup joint for the rubber elements. This will enable the use of a thicker rubber element, decrease the swelling percentage, and thereby allow for a higher differential pressure rating [29, 30].

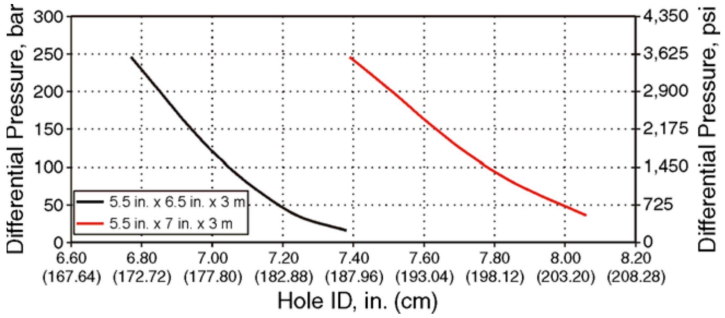

Figure 15: *Differential pressure ratings at different levels of swelling, [29]*

There are numerous advantages when it comes to using swell packers in the completion [31]:

- A design with no moving parts, simplifying installation and use
- Adaptable to irregular wellbore
- Cost-effective
- Reduced rig time for installation
- Intervention-less operation
- No limitation for number of packers in one completion
- No need for pipe manipulation, dropping a ball or applying pressure for activation of packer

Depending on downhole conditions, the completion fluid and a series of other factors, swell packers can take up to 40 days to set. On one hand, it is important to accomplish all

completion operations before the packers have fully set, however, this should not be at the expense of delayed production start. It is therefore important to plan this time delay properly, to save well time and cost [29].

The use of swell packers is not exclusively limited to ICD completions. They can be run in both open-hole completions as well as cased holes, both producers and injectors. Additionally, they can be applied in intelligent well completions, with control lines fed through.

The number of packers in an ICD completion can vary from a few packers to dozens. What primarily determines the number of packers and distribution along the wellbore, is the reservoir heterogeneity and pressure variations - more variations require more packers. From an inflow control point of view, the optimal solution would be to have a swell packer at each screen joint, yielding a "high definition" solution which maximizes compartmentalization. Some engineers argue that this increases the risk of operational problems when running the completion downhole, and lead to increased torque and drag because of premature swelling. However, this is a disputed topic among completion engineers. A typical swell packer joint has a nearby centralizer with a greater OD than the packer, to prevent the packer from being torn apart when running the completion. Furthermore, the swelling time usually takes several days, as previously explained. Hence, the validity of the former argument can be debated [29, 30].

2.3.1 History

Norsk Hydro were one of the first operators to use ICD in their wells in 1993, on the Troll field. Initially planned as a gas field, Troll was found to have a thin but sizable oil rim of 4-27 m. To make the production of this oil profitable, significant measures had to be taken. For the past decades, the field has been a key driver for innovation within drilling, completion and production engineering, including advancements within geo-steering, multilateral well completions, gas-cap gas lift and sand-face completions. The initial motivation for implementing ICD technology was to minimize the Heel-Toe effect to delay the gas breakthrough from the gas cap and water breakthrough from the underlying aquifer [23, 32].

Initially, channel type ICDs were used in the first 200 meters of the well, i.e. in the heel part. The idea of having the fluid flow through channels was to achieve a successive pressure drop through the ICD. Later on, a helical channel type device by Baker Hughes (Figure 16) was applied and the ICD interval was increased to 1000 m of the heel part.

The reason for this transition was to have a continuous pressure drop through the channel while further avoiding erosion and fines plugging by having a larger flow area and thereby lower fluid velocity. In the following years, a methodology was developed in-house to model the ICDs in the reservoir simulator. The simulations showed how gas breakthrough was delayed with longer ICD intervals. Additionally, a significant gain in cumulative oil production and net present value was evident [33].

An early realization with the use of ICD was the importance of annular isolation via packers. Not only would this aid in an increased ICD effect, but it would also mitigate the issues of heterogeneity [22].

Figure 16: *Baker Hughes' Equalizer Helix ICD, [13]*

This sparked the interest for inflow control across the industry, and since then, service companies have developed a series of inflow control technologies. As the technology has matured, the application range of ICDs has been widened. Inflow control is now being applied in different types of completions, both in sandstone and carbonate reservoirs, in producer and injector wells. In recent years, ICDs have been used in Steam-Assisted Gravity Drainage (SAGD) wells to enhance heavy oil reservoir sweep [34, 35].

2.3.2 ICD Types

Today, several service companies offer their version of an ICD, including Baker Hughes, Schlumberger, Weatherford, Halliburton and Tendeka.

Inflow control devices can be categorized into three main categories, based on the method used to generate the pressure drop [36, 37]:

- Nozzle Type (Restrictive)
- Helical Channel Type (Frictional)
- Tubular Type (Frictional and restrictive)

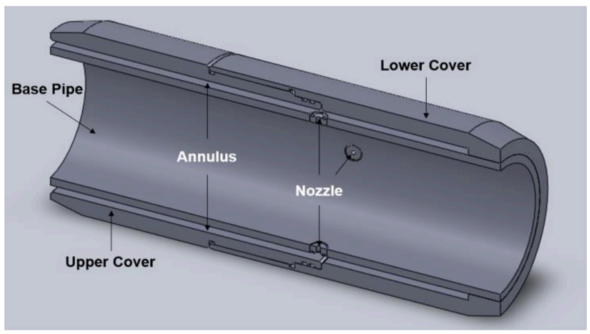

(a) *Nozzle Type ICD*

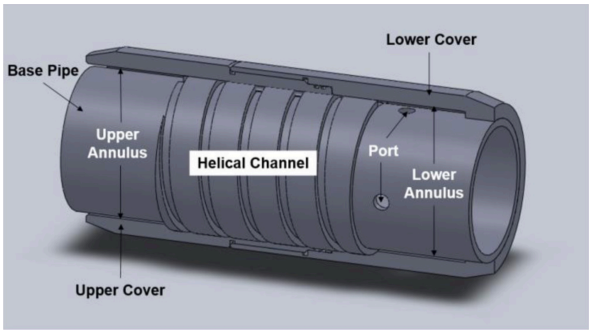

(b) *Helical Channel Type ICD*

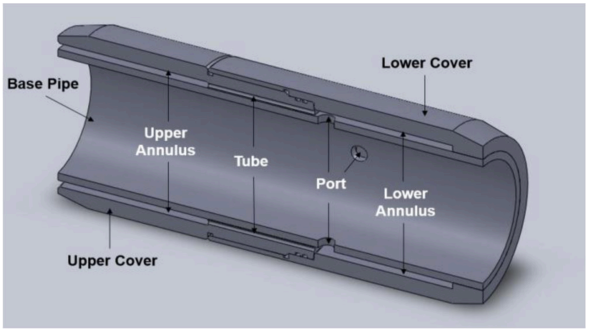

(c) *Tubular Type ICD*

Figure 17: *Types of Passive ICDs, [38]*

Nozzle Type

As the name implies, a nozzle-type ICD completion (Figure 17a) is based on 1 - 4 orifices installed in the base pipe layer. When the fluid flows past the screen layer it is forced through the small nozzles, creating an instant pressure drop across the orifice. The pressure drop utilizes Bernoulli's principle, where as a fluid goes from a large flow area to a smaller flow area, it experiences a higher flow velocity as the pressure decreases. The resulting pressure drop can be found by the fluid flow rate and geometry of the orifice [39]:

Figure 18: *Typical Nozzle ICD, courtesy of Tendeka*

$$Q_r = C_D A_2 \sqrt{\frac{2(P_1 - P_2)}{\rho\left(1 - (A_2/A_1)^2\right)}} \tag{1}$$

where C_D is a discharge coefficient that takes into account the orifice geometry, ρ is the fluid density, A is the flow area, P is the fluid pressure, and subscripts 1 and 2 signify the

parameter at nozzle entry and exit, respectively. The pressure drop can thus be derived:

$$\Delta P_R = \frac{\rho Q^2 \left(1 - (A_2/A_1)^2\right)}{2{C_D}^2 A_2^2} \tag{2}$$

If we neglect the area difference at entry and exit, while assuming a circular nozzle, i.e. $A_1 = A_2 = A = \frac{\pi}{4}D^2$, we can simplify Eq. 2 to the following [39]:

$$\begin{aligned} \Delta P_R &= \frac{\rho Q^2}{2{C_D}^2 A^2} \\ \Delta P_R &= \frac{8\rho Q^2}{\pi^2 D^2 {C_D}^2} \end{aligned} \tag{3}$$

From Equation 3 it is obvious that the restrictive pressure drop is proportional to the flow rate squared, i.e. a doubling of the flow rate gives a pressure drop increase to the factor of four. Further, it is inversely proportional to the nozzle diameter squared, hence a small increase in diameter will yield a great reduction in pressure drop. The diameter is also the main factor when it comes to design and sizing of the nozzle ICD. As previously mentioned, it is further possible to have 1-4 nozzles installed in each screen joint, and an increase in the number of nozzles will yield a lower pressure drop. This is because of the fact that the flow rate through each nozzle depends on the number of nozzles. For instance, four nozzles means that the flow rate through the joint is reduced by the same number, compared to a single nozzle ICD joint.

The simple design of the nozzle ICD makes it easy to manufacture, and should the real-time well data indicate need for a different nozzle-size, it is relatively easy to replace the nozzle prior to running the lower completion (see Figure 18). Because of the relatively small nozzle diameter (typically 1-5 mm), the fluid velocity through the nozzle will be high, making it prone to erosion by fluid-borne fine sands. However, manufacturers are constantly working on material and geometry design to prevent this issue. Another drawback with the small nozzle design is the susceptibility to plugging, especially when flowing back mud. A number of service companies offer their version of a nozzle ICD. This includes Tendeka's *FloMatik*, Schlumberger's *ResFlow*, Weatherford's *FloReg* and Halliburton's *EquiFlow* [15, 37, 40].

Several vendors have also equipped the nozzle ICD with a ball check valve, as illustrated in Figure 19. The check valve enables a series of completion related operations, such as open-hole gravel packing, hydraulic set open-hole packers, well clean-up and fluid

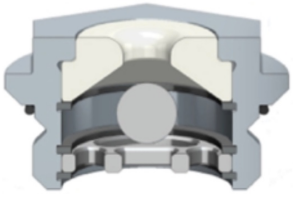

Figure 19: *Resflow Check Valve ICD, [41]*

displacement. For conventional ICD and non-ICD completions, a washpipe is often run to the toe of the well, either for open-hole gravel packing or for fluid displacement, e.g. base oil completion fluid. The washpipe has the function of leading the fluids to the well toe, before they are back-produced through the screen along the well up to the heel. By installing an ICD with a check-valve, the use for washpipe becomes unnecessary. When fluid is injected into the well, the check valves will close, preventing fluid loss to the annulus through the nozzles. Furthermore, this function enables the setting of annular hydraulic packers, by allowing a pressure build-up inside the lower completion. The ball in the check valve is made of various materials. For instance, Schlumberger's Resflow CV can be made with aluminum balls, which is dissolved before production by an acid-based breaker system. Optionally, the ball can also be ceramic, and will be produced with the production fluids once the aluminum ball seat is eroded [41].

Helical Channel Type

The helical channel type ICD (Figure 17b) is based on a channel that goes around the base pipe. When the fluid enters the device, it is forced through this channel, and the surface friction it is subjected to generates a pressure drop across the device. The flow rate through a helical channel is given by the following equation [39]:

$$Q_f = \frac{\pi D^4}{4CL} \cdot \frac{\Delta P}{\mu} \tag{4}$$

where C is a geometrical factor based on the channel shape, L is the channel length and μ is the fluid viscosity. By combining this with the pressure drop equation for laminar flow, and the dynamic pressure, we can find the resulting pressure drop in the helical channel [39]:

$$\Delta P_F = f \cdot \frac{L\rho v^2}{2D} \tag{5}$$

In this equation, f is the friction factor which is dependent on the fluid density and wall roughness, while v is the average fluid velocity. Because of the channel design, the pressure drop is generated over a longer path and the flow area is relatively[7] large. This yields a low fluid velocity, making it more resistant towards erosion, while not being susceptible to plugging. The helical channel type ICD has a disadvantage because of the highly viscosity-dependent pressure drop. This makes it more preferable for water to flow through

[7]Compared to e.g. the nozzle-type ICD flow area

the device in the case of a water breakthrough. Additionally, Visosky et al. [40] pointed out that the helical channel ICD is somewhat reliant on the integrity of the surface finish to maintain the desired pressure drop. The most common helical channel type ICD on the market is the *Equalizer ICD* (Figure 16) by Baker Hughes [15, 37].

Tubular Type

Figure 17c illustrates the tubular type ICD. The device is built up by a number of tubes with a certain diameter. This ICD acts as a restrictive device, but because of the long tubes, friction is also introduced to the picture. After entering the annulus below the screen layer, the fluid is forced through the long tubes, generating a pressure drop. Like the helical channel type ICD, the tubular type ICD has a relatively large cross-sectional flow area, resulting in a low fluid velocity. This gives the tubular ICD similar advantages when it comes to erosion and plugging. However, since the pressure drop mechanism is more based on resistance than friction, the pressure drop through the tubular ICD is less viscosity-dependent compared to the helical channel type ICD. Halliburton is one of the few service companies offering this type of ICD design, and it should be mentioned that this design is rarely used in the industry [37, 42].

2.3.3 ICD Benefits

As previously mentioned, the initial benefits of the ICD were to minimize the heel-toe effect by evening out the flux along the wellbore. However, a review of the literature reveals many secondary benefits, that can exclusively justify the inclusion of ICDs in the well completion. In conjunction with Section 2.2, a focus will now be laid on how inflow control technology mitigates the addressed challenges.

As previously mentioned, the heel-toe effect occurs as a result of friction along the wellbore in high-permeability reservoirs. The fluid would rather choose the path of least resistance, which is through the heel of the well. By installing ICDs in the sand-face completion, the flow towards the heel will meet a greater resistance than the rest of the well. This is because of the ICD's high dependence on flow rate - the higher the flow rate, the higher the pressure drop across the device. This is further evident by the presented mathematical formulas. The result is that the fluid is forced to become evenly distributed along the whole well, significantly increasing production from the toe of the well. This can further be observed in the results from a generic 3300 ft well, modeled by Bellarby [13] in Figure 20, 21 and 22.

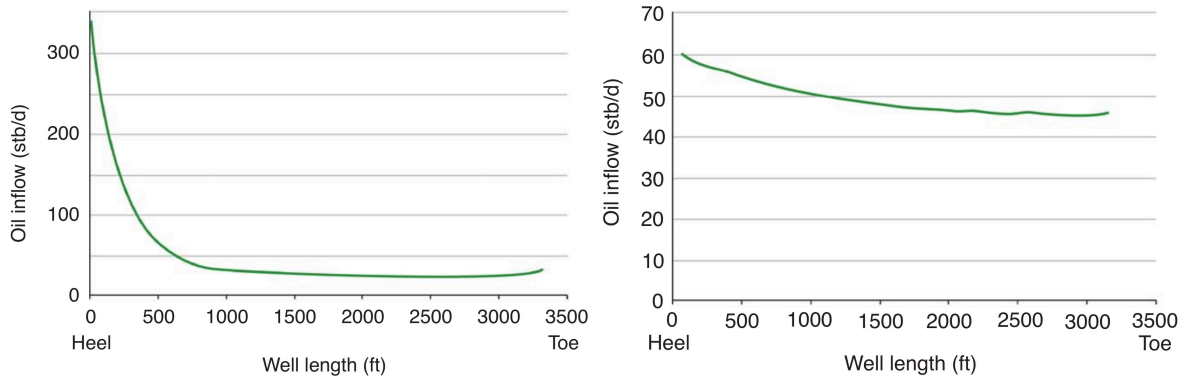

(a) *Screen flux without ICD* **(b)** *Screen flux with ICDs*

Figure 20: *Flux variation along the wellbore in a homogeneous reservoir, [13]*

A similar production challenge is linked to heterogeneous reservoirs producing with varying flux. In zones with high permeability, the fluid will flow more easily into the wellbore, increasing the chance of premature gas or water breakthrough, while preventing production from other low-permeability zones. In the case of the ICD, a higher pressure drop will be imposed on high flux zones, allowing production from low flux zones. This will enable drainage from more of the exposed reservoir and thus increase oil recovery.

As a result of heterogeneity and uneven flux, annular flow can often occur. As explained earlier, annular flow can lead to screen plugging, and creation of hot spots, ultimately leading to sand control failure. Annular isolation, which is an essential part of the ICD completion, prevents annular flow and cross-flow between zones. In Figure 21, this effect is clearly illustrated. Without the ICD, the annular flow is much higher towards the heel, proportional to the base pipe flow and declining towards the end. However, it is drastically minimized with the use of ICDs, as illustrated in Figure 21b. As a result, the risk of screen plugging, hot spots and sand control failure is greatly reduced [13].

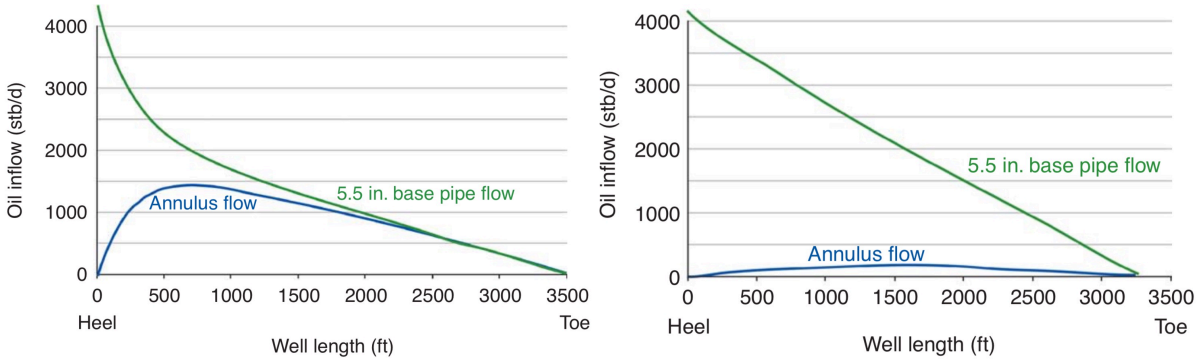

(a) *Without ICD* **(b)** *With ICD*

Figure 21: *Base pipe and annular flow for the same well as in Figure 20, [13]*

Moen and Asheim [14] studied the effects of inflow control devices in the near-wellbore area. As explained in Section 2.2, proper well clean-up is an essential factor for the well

to perform optimally. Because of heterogeneities and the heel-toe effect, the drawdown at certain zones of the well is insufficient for filtercake removal. Additionally, mud and settled particles left behind can impair the inflow of reservoir fluids.

With inflow control, the clean-up performance is significantly altered. Since the ICD generates an added pressure drop, the tubing pressure will be lower, as illustrated in Figure 22b. This additional drawdown aids in filtercake lift off, as well as mud particle removal during flow-back. This further means that a much lower flow rate is required to achieve proper clean-up. The simulations performed in the study indicate that the required flow rate is approximately three times as much for a conventional sandscreen completion compared to the ICD case.

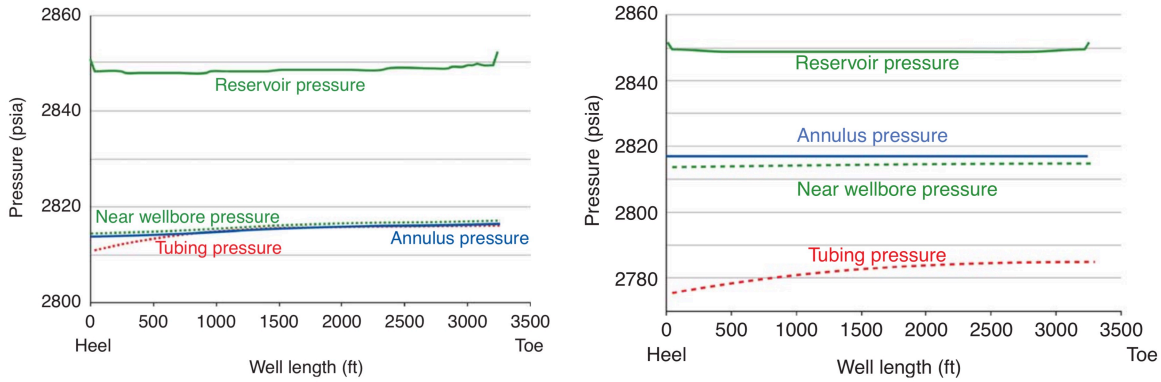

(a) *Without ICD* **(b)** *With ICD*

Figure 22: *Pressure profiles for the same well as in Figure 20, [13]*

Simulations presented at an internal meeting [15], also support this understanding. However, another aspect was considered to quantify the improved well clean-up, that is the maximum clean-up length. As previously mentioned, the filtercake must be subjected to a certain differential pressure to be removed, basically the pressure difference between the near wellbore formation and the tubing pressure, see Figure 23a. At the heel section of the well, this pressure difference is more than sufficient due a higher flux. However, towards the toe, this differential pressure converges towards the critical lift-off pressure. Once it has become lower than the lift-off pressure, the filtercake will not be removed, and this boundary point defines the maximum clean-up length or maximum well length. Because of the added drawdown that the ICD presents, the lift-off pressure is increased along the whole wellbore, also in non-flowing zones, see Figure 23b. This leads to an increase in maximum well length by almost 70% compared to a non-ICD well [15].

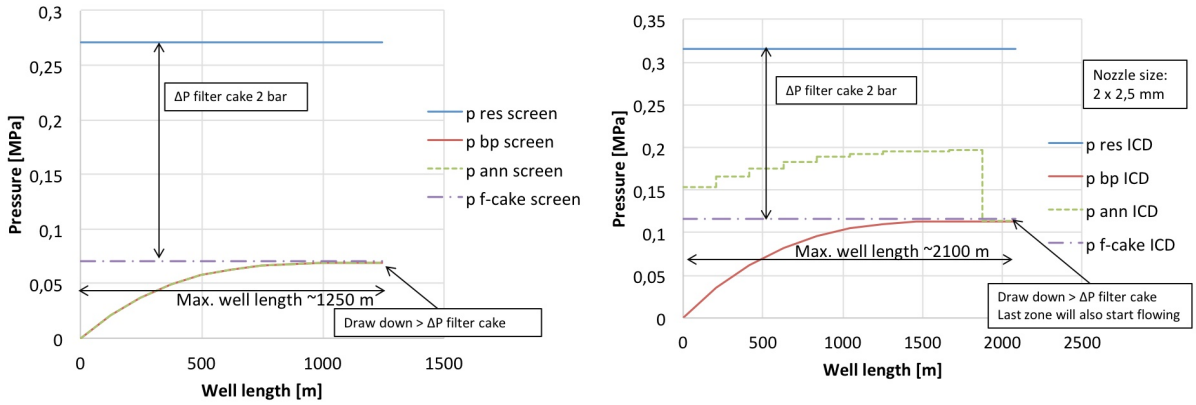

(a) *Without ICDs* **(b)** *With ICDs*

Figure 23: *Comparison of maximum clean-up length, [15]*

As a result, well clean-up performance is significantly improved in sections with low drawdown pressure. Hence, the well will behave in a more predictable manner with better inflow performance. This conclusion is also supported by Henriksen et al. [33] concerning the application of inflow control on the Troll field. A clear effect was observed where ICD wells were more efficiently cleaned up compared to non-ICD wells, representing a significant decrease in completion mud at each sandscreen. This was verified by radioactive tracers [14, 33].

Based on the presented benefits, it is evident that inflow control has a potential of increasing oil recovery. Despite the fact that ICDs lower the oil productivity index (PI), the recovery factor can be significantly increased. The productivity index is measured as volumetric flow rate per pressure drop, e.g. Sm^3/bar. It is a function of the fluids, geology and reservoir quality. Preferably, one would like the PI to be as great as possible, i.e. produce at high rates with a low reservoir drawdown. The rationale behind this is that high PI wells will enable more oil production while still maintaining a high reservoir pressure. From a reservoir and production point of view, this is quite a rational mindset. However, it might not be entirely correct. As formerly mentioned, long horizontal wells in highly permeable (i.e. high PI) reservoirs have a tendency to be dominated by the heel-toe effect, which greatly reduces recovery from the lower part of the well. Because of the fact that the ICDs generate an additional drawdown pressure, the productivity index will be reduced. Nevertheless, the result will be a uniform inflow profile that utilizes oil reserves at the toe, further enhancing oil recovery.

It is not an easy task to quantify an increase in cumulative oil production based on observed production from an ICD completed well. This is because of the fact that it is impossible to know how the well would have behaved had it been developed with a

conventional sand-face completion. However, by looking at analogue non-ICD wells nearby, the effect can be anticipated. A good example of this is the Troll field which has several hundreds of wells drilled in a somewhat similar and predictable formation and reservoir. Simulations performed in the reservoir simulator predicted a clear upside of ICDs in the well, see Figure 24.

Not only did the results show an additional oil production of 200,000 Sm^3, but also a delay in gas breakthrough by 100 days. Moreover, once the gas had broken through, the GOR would be lower for the ICD case. After some time the GOR would be higher and faster increasing compared to the base case, because of the even drainage and lowering of the GOC, leading to a wider spread gas cone being produced. Another paper by Halvorsen et al. [43] supports this conclusion. Here, it is anticipated that on average, the installation of ICD on Troll wells increased oil production by 31% [33, 43].

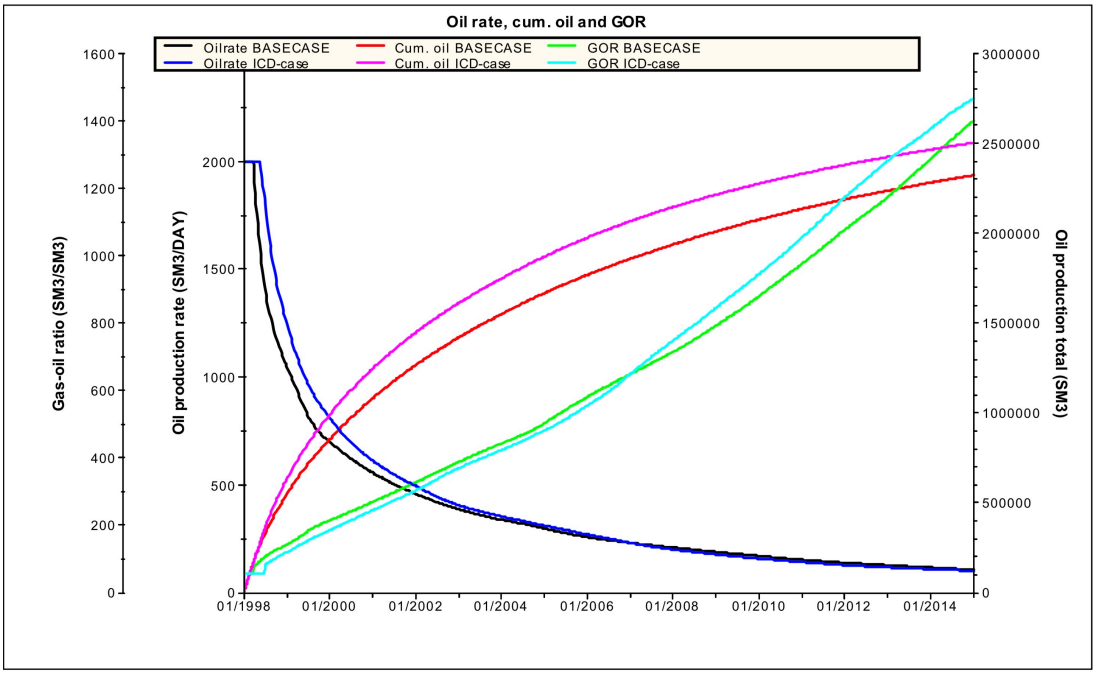

Figure 24: *Comparison of oil production and GOR for an ICD vs. non-ICD well on Troll, [33]*

2.4 AICD

Despite the fact that ICDs have the ability to delay early water or gas breakthrough, they will not stop or reduce the inflow of unwanted fluids once breakthrough has occurred. This may impair production performance, and lead to reduced recovery. Autonomous Inflow Control Technology (AICT) has the aim of mitigating this challenge. It involves self-controlled instruments that adjust the level of restriction based on the fluid properties. The main aim of the technologies is to hold back unwanted fluids such as water or gas, while allowing for production of oil. Hence, they can lead to enhanced oil recovery (EOR) and delay gas or water breakthrough.

As previously mentioned, autonomous inflow control can be characterized by two categories; *devices* and *valves*. While Autonomous Inflow Control Devices are fixed fittings with no moving parts, Autonomous Inflow Control Valves include some moving parts that lead to the restrictive nature of the instrument. This distinction is critical when it comes to the assessment of factors such as robustness, erosion resistance, plugging risk, integration and reliability of the respective technology [44].

2.4.1 Hybrid Type

The three ICD types discussed in Section 2.3.2 have shown both strengths and weaknesses, and manufacturers have worked rigorously to improve their efficiency, to maximize productivity during the whole life of the well. However, none of the previously mentioned ICDs meet all the requirements for optimized function:

- Low risk for plugging
- Mud flow-back assurance
- High erosion resistance
- Negligible viscosity sensitivity

In 2009, Baker Hughes published an IPTC[8] paper on their newly developed hybrid ICD design. The *Baker Equalizer Select* is based on a series of flow passages in a labyrinth path, see Figure 25. When fluid passes through the maze, it meets a series of restrictions while being distributed in the chambers, see Figure 25b. Each of these chambers has one or more slots that represent restrictions, successively generating pressure drops as the fluid passes. The slots are not positioned in a straight line, which means that the fluid has to

[8]International Petroleum Technology Conference

turn direction after each slot, further introducing friction into the pressure drop equation [45].

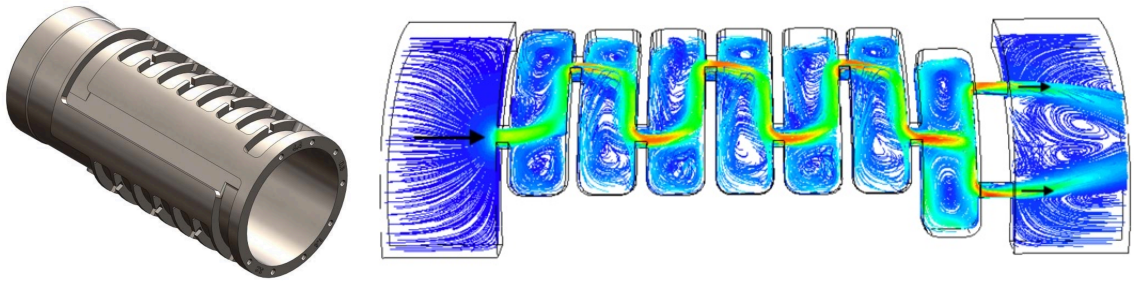

(a) *Adjustable Hybrid ICD*

(b) *CFD flow line velocity plot with water flow*

Figure 25: *Baker Equalizer Select, [45]*

The adjustable design makes it possible to change the flow resistance just before running the completion into the well. Each adjustment has a different number of chambers, more chambers give a higher resistance while fewer chambers yield a lower resistance. It is also possible to run several setting in the open position, for e.g. abnormally high production rates. Because of the fact that the pressure drop is generated in multiple steps, i.e. at multiple restrictions, the risk of erosion and plugging is significantly reduced.

However, when it comes to flow performance characteristics, the hybrid differs from the other restrictive ICD, i.e. the nozzle ICD. The following equations can be used to describe these flow performance characteristics, using seven parameters and Reynolds number (Eq. 6) [45]:

$$\mathrm{Re} = \frac{\rho v L}{\mu} \tag{6}$$

$$K_{highrate} = a_1 \mathrm{Re}^{b1} \tag{7}$$

$$K_{lowrate} = a_2 \mathrm{Re}^{b2} \tag{8}$$

$$K = K_{lowrate} + \frac{K_{highrate} + K_{lowrate}}{\left(1 + \left(\frac{\mathrm{Re}}{t}\right)^c\right)^d} \tag{9}$$

$$\Delta P_{hybrid} = K\rho\left(\frac{v^2}{2g_c \cdot 144}\right) \tag{10}$$

Without going too much into the number-crunching, it can be seen that at higher Reynolds numbers, the hybrid ICD will choke harder than the nozzle type ICD. Fluids with a high Reynolds number are typically dense with low viscosity, which is the case with water (relatively high density) and gas (relatively low viscosity). Moreover, the pressure drop will be low at lower Reynolds numbers, which is the case for oil with relatively low density and high viscosity. The dependency to the Reynolds number is the opposite for the helical-type

ICD, where the device will choke harder at low Reynolds numbers, and choke less at higher Reynolds numbers. This is illustrated in Figure 26, where the pressure loss coefficient (K) is plotted against the Reynolds number.

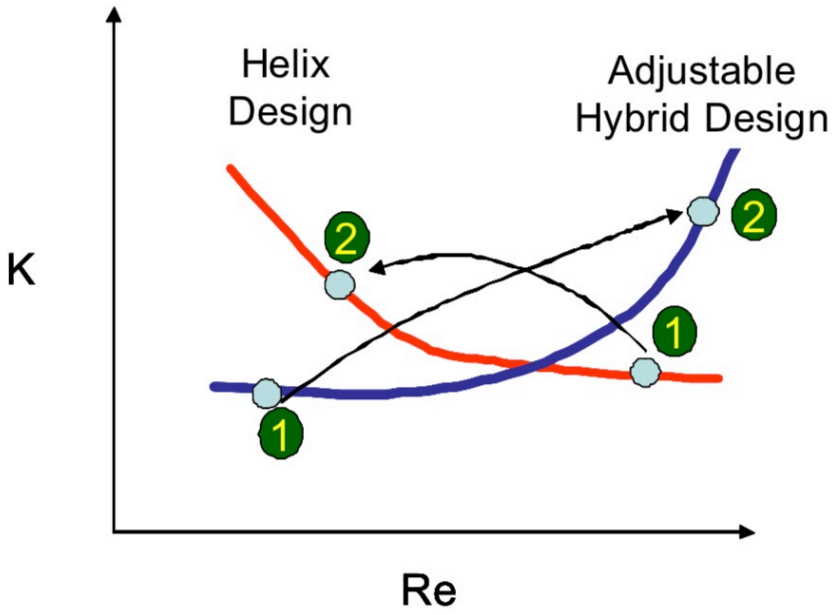

Figure 26: *Theoretical flow performance for Hybrid vs. Helical ICD, [45]*

The theoretical flow performance plot is a result of CFD[9] analyses and laboratory flow experiments. In the initial production phase of the hybrid design (point 1, blue line), there will typically be production of oil and the Reynolds number will be low. The hybrid ICD will impose a lower pressure loss coefficient, as opposed to the helical-type ICD that will generate a greater pressure loss at the same Reynolds number. Later in the well life (point 2, blue line), water and/or gas will typically be produced. In this case, the hybrid ICD will have a greater pressure loss compared to the helical design. In a gas well, the development of the Reynolds number is typically the opposite where gas is initially produced (point 1, red line) before a water breakthrough occurs, and the Reynolds number decreases because of the liquid viscosity (point 2, red line). In this case, it is observed that the helical ICD performs better, since it chokes harder for lower Reynolds numbers, while allowing for production at higher Reynolds numbers, see Figure 26.

Compared to the helical channel ICD, the pressure drop in the adjustable hybrid ICD is more density dependent, and less sensitive to viscosity. Conclusively, this gives the adjustable hybrid ICD better flow characteristics, by holding back water and gas producing zones while promoting oil productive zones [15, 45].

[9]Computational Fluid Dynamics

2.4.2 Fluidic Diode

In 2012, Least et al. [46] presented a fluidic diode type AICD by Halliburton. The device has a geometry that resembles a circular vortex that diverts the fluid into different paths based on its properties. Depending on the path that the fluid takes, it will meet different levels of restriction.

The fluidic diode is mainly dependent on three fluid properties; density, viscosity and flow rate. While the density and flow rate generate an inertial force, the viscosity and flow rate produce a viscous force in the fluid. The balance of these two forces allows the function of the fluidic diode. This functionality can be explained using Figure 27. When the fluid enters the AICD at the entrance, it has to choose between two paths before reaching the exit and flowing up the production tubing. This choice is made based on the balance of the two forces mentioned above. If the inertial forces are the dominant forces, the flow will stay in the initial path and choose the straight pathway. This is typically the case for low viscous fluids such as water and gas. However, if the viscous forces are dominant in the force balance, the flow will have a tendency to spread and become split between the divergent and the straight pathway. This is the case for viscous fluids such as oil. The angular momentum of the fluids taking both pathways will be balanced leading to minimal rotation when entering the vortex bowl. The result is flow going directly towards the exit of the diode, without meeting significant restriction, similar to the performance of a standard nozzle-type ICD.

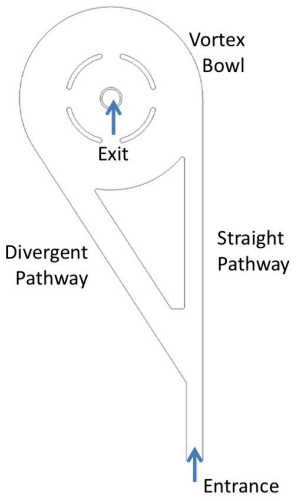

Figure 27: *Simplified illustration of the fluidic diode, [47]*

In the case of water or gas, where the fluid takes the straight pathway the outcome will be quite different. The fluid will enter the circular vortex bowl with a high angular momentum, and start spinning at high speeds before it gets to the exit. Similar to when driving a car at high speeds in a roundabout, the fluid will lose considerable energy in the form of pressure, as it circles the vortex. This follows from Bernoulli's principle that relates the dynamic pressure of a moving fluid to the fluid velocity. The following equation can be derived from Bernoulli's principle when neglecting gravity effects[47]:

$$\Delta P = P_2 - P_1 = \frac{1}{2}\rho v_2^2 - \frac{1}{2}\rho v_1^2 \tag{11}$$

From Equation 11 can be understood that the restriction of flow across the AICD, that

is the ΔP, is proportional linked to the velocity change that the fluid experiences when entering and exiting the fluidic diode. Furthermore, when more fluids take the straight pathway, the local spinning velocity increases, resulting in a larger pressure drop. Hence, fluids with low viscosity and high inertia will meet a greater restriction in the AICD compared to viscous fluids with relatively low inertia. This is how the fluidic diode manages to preferentially produce oil, while holding back water and gas [47].

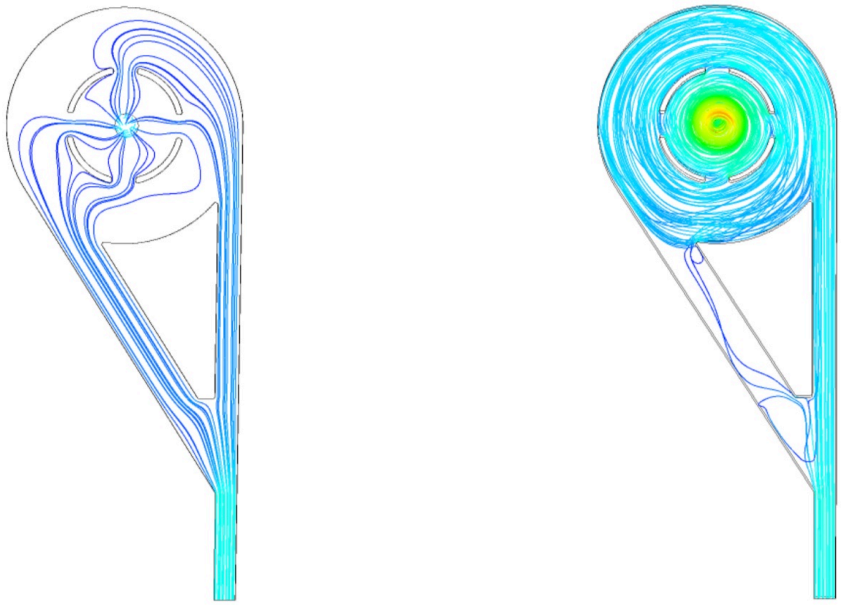

(a) *Oil flow* **(b)** *Water flow*

Figure 28: *CFD Velocity Streamline plot of the simplified AICD Principle, [47]*

The aforementioned phenomenon can clearly be observed in Figure 28, where the CFD plots show the velocity streamlines for two fluids. When oil flows through the fluidic diode (Figure 28a), the flow is split between the straight and the divergent pathway. The fluid takes the most direct path towards the exit without going into a spinning motion. Another observation from Figure 28a is that the fluid velocity is nearly constant, as is evident by the blue flow lines. On the other hand, a different observation can be made from Figure 28b where water flow is simulated. The water will take almost exclusively the straight path into the vortex bowl where it starts spinning. This creates a back pressure that restricts the water from passing through the AICD [47] .

Fripp et al. [47] also points out how the restriction of the AICD is proportional to the fraction of fluid flowing the straight pathway versus the divergent pathway. Moreover, the amount of fluid flowing in the divergent pathway is linked to the fluid viscosity; a higher viscosity will typically increase this amount, see Figure 29. Hence, a fluid with higher viscosity will be less restricted in the AICD. Additionally, a higher contrast between the oil and water viscosity will give a better effect when it comes to promoting oil production and holding back water.

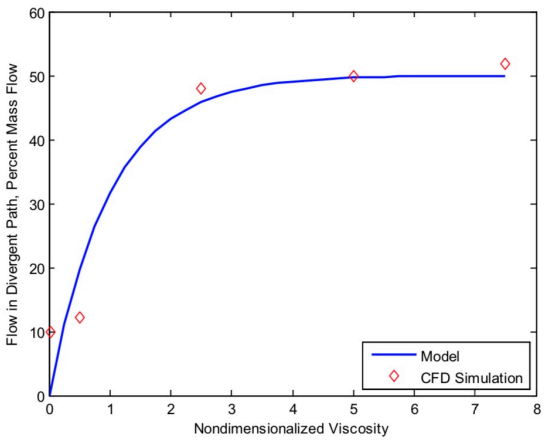

Figure 29: *Percentage of divergent flow as a function of viscosity, [47]*

The Equiflow AICD by Halliburton has been proven in a series of qualification tests for risk of plugging, erosion, shock, torque, bending, tensile burst and collapse. Further, numerous flow tests , both single-phase and multi-phase, have been conducted to develop a way of modeling the flow characteristics of the AICD. Currently, the device comes in four different versions, or so-called "Ranges". Table 3 provides an overview for these ranges. Based on the viscosity range, the design of the pathways in the fluidic diode varies [48].

Table 3: *The different versions (ranges) of the Equiflow AICD, [49]*

Fluidic diode AICD	**Viscosity Range**	**Oil Type**	**Fluid Restricted**
Range 1	0.3 - 1.5 cP	Very Light	Gas
Range 2	1.5 - 10 cP	Light, Medium	Gas and Water
Range 3	3 - 200 cP	Light, Medium, Heavy	Gas and Water
Range 4	+150 cP	Heavy, Very Heavy	Gas and Water

Figure 30 shows how the Range 3 AICD responds to water and oil with different viscosities, in terms of pressure drop. Despite the viscosity being relatively low, it is clear how the AICD favors production of the oil by inducing a lower pressure drop on the fluid, compared to the water. Even for the lightest oil (3cP) the pressure drop across the device is approximately half that of the water. Figure 31 shows the flow lines in the Range 3 AICD for oil and water flow, respectively [47].

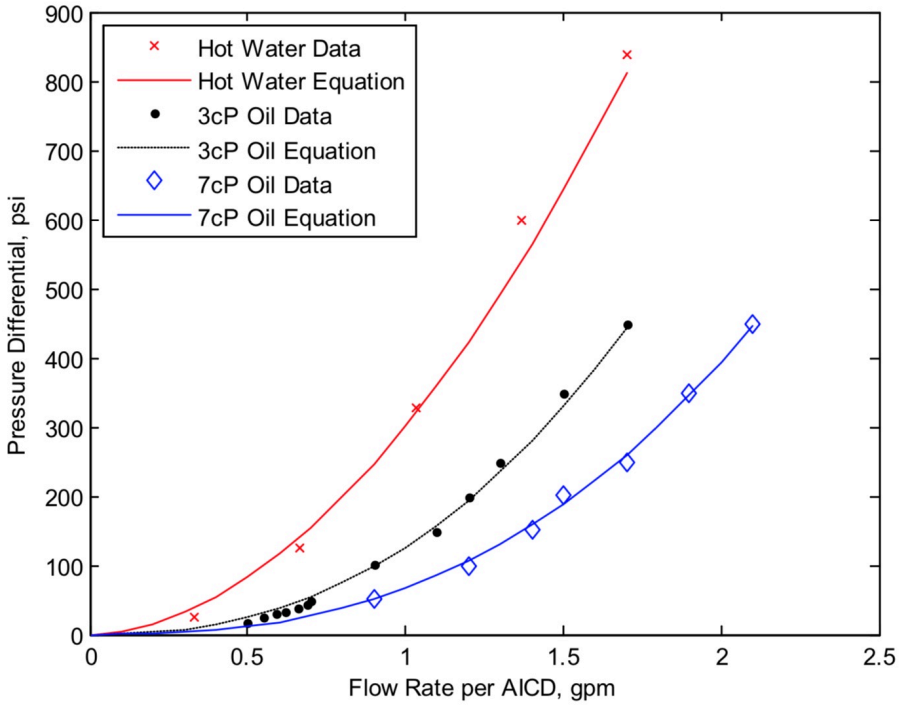

Figure 30: *Single phase flow characteristics for the Range 3 AICD, [47]*

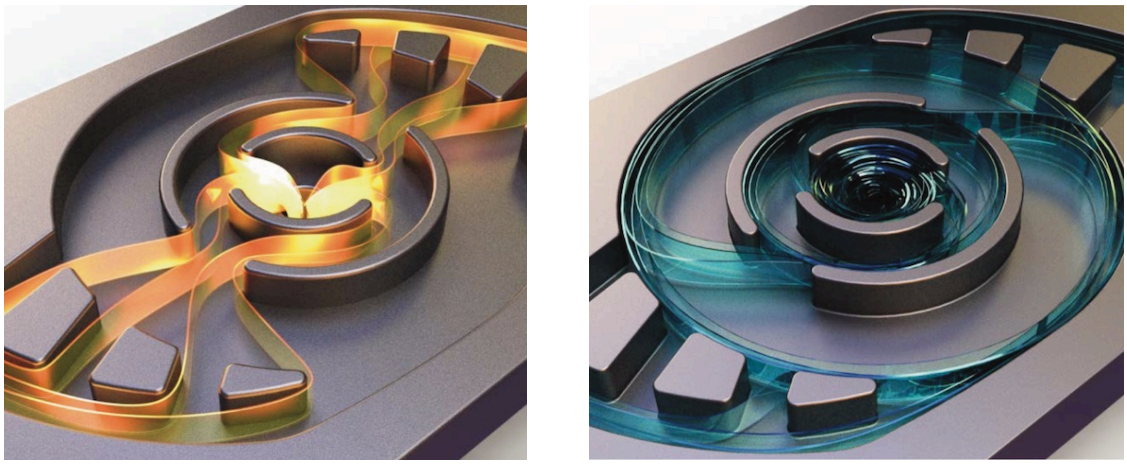

(a) *Oil flow* **(b)** *Water flow*

Figure 31: *Halliburton Equiflow Range 3 AICD, [50]*

According to the current literature, [48, 49, 51], the Equiflow AICD has a successful track-record in both the Middle-East and Latin-America. In a light-oil carbonate reservoir in the United Arab Emirates, the deployment of the Equiflow AICD increased oil production by five times, while decreasing water-cut by 50%. In Ecuador, the installation of the Equiflow in a heavy-oil field increased oil recovery by 16% while decreasing water production by 34%. Additionally, the technology has been deployed in Columbia and Saudi Arabia with successful results. The fluidic diode AICD has also been shown to reduce production of unwanted gas by more than 30% compared to a standard nozzle-type ICD.

2.4.3 Autonomous ICD

The Autonomous ICD by Schlumberger (SLB) is a similar technology to the Equiflow AICD. The device has two entry ports at which the fluids are directed tangentially into a cylindrical chamber, see Figure 32b. Because of a lower Reynolds number[10], oil entering the device will spin at a low velocity and immediately exit through the nozzle (point 54) with only a minor pressure drop. When water or gas with a significantly higher Reynolds number[11] enter the Autonomous ICD, it will spin at much higher velocities in a circular path (point 56). In this manner the fluid will lose much of its momentum and thus dynamic pressure to the spinning motion. As a result, water and gas is held back, while oil flow is promoted. In addition to the selective fluid functionality, the Autonomous ICD also offers the same choking feature as a standard nozzle-type ICD, by including a constriction (point 54). Furthermore, the device features a modular design that can be adjusted the wellsite to tune restriction [52].

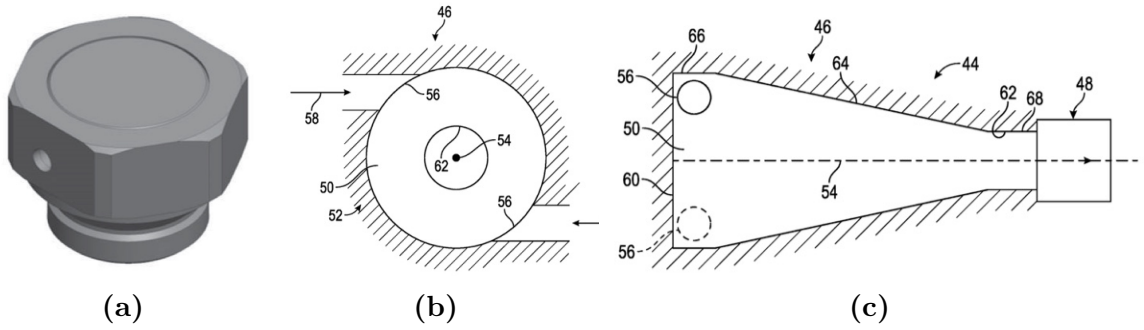

Figure 32: *Schlumberger Autonomous ICD actual design(a) and schematics viewed from the top (b) and side (c), [52, 53]*

The flow performance of the SLB Autonomous ICD varies for different oil viscosities, as shown in Figure 33. In all cases, the flow performance for oil flow is quite similar to a standard nozzle-type ICD. However, when gas flows through the device, the pressure drop will be higher than for the ICD, regardless of flow rate. Similar to the previously discussed autonomous technologies, the selective choking effect becomes better when the viscosity difference between the fluids widens. A search in available literature found no field tests of the SLB Autonomous ICD. The technology has however been patented [53].

[10] A low Reynolds number is caused by a high viscosity and/or low density, see Equation 6
[11] A high Reynolds number is caused by a low viscosity and/or high density

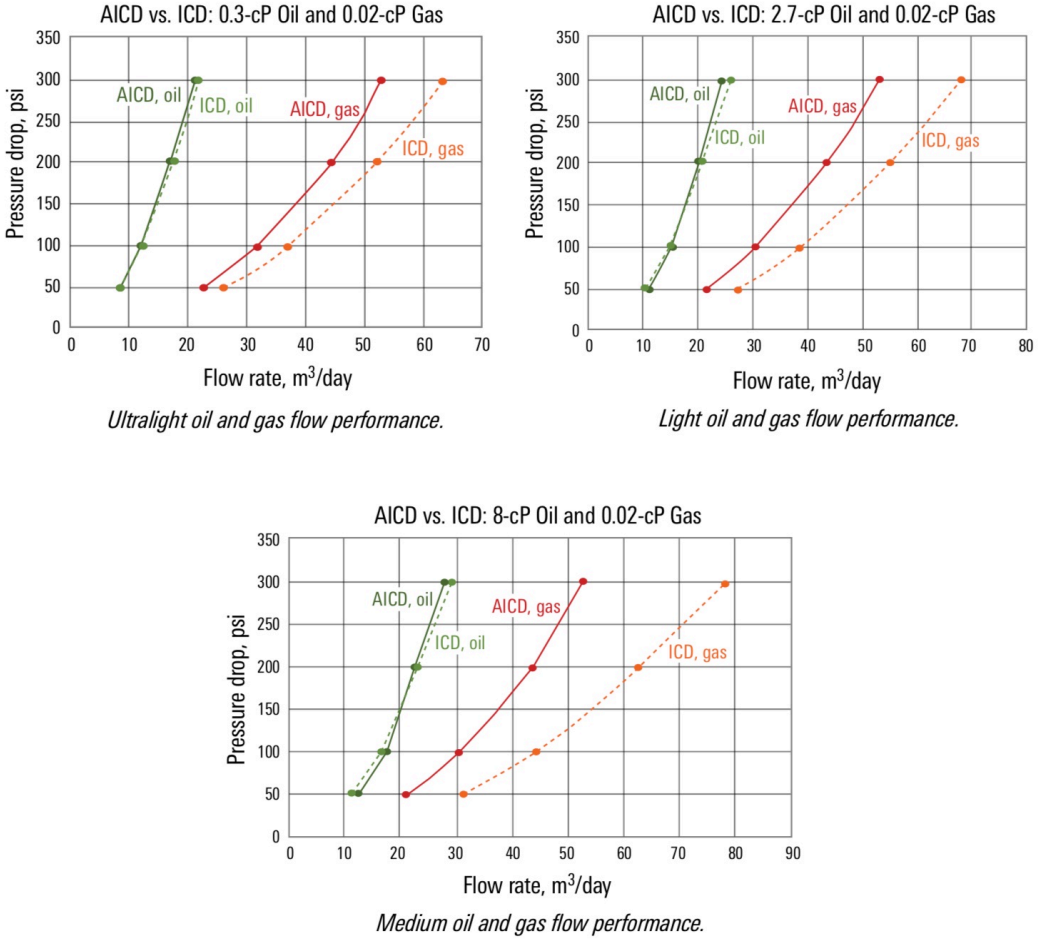

Figure 33: *Single phase flow characteristics of the SLB Autonomous ICD vs. Standard ICD for different oil types, [52]*

2.5 AICV

Autonomous Inflow Control Valves serve a similar purpose to AICD, with the main difference being that they include moving parts that enable the selective choking of fluids. There are various types of AICV currently on the market, including the Tendeka FloSure TR7, InflowControl AICV®, Wormholes Adaptive ICD, Acona ERC and the Superior AFD. The following sections provide an overview over these solutions where their functionality, flow characteristics and field deployment will be discussed.

2.5.1 The Rate Controlled Production (RCP) Valve

The Rate Controlled Production (RCP) valve is a development that was patented by Statoil[12] in 2011. The main driver for the technology was the Troll field, where production of gas was the main challenge. Despite the fact that the integration of ICDs helped with delaying the gas breakthrough in the wells, they had a minimal effect once the coning of gas had started. This would critically impair oil production and leave significant oil volumes unrecoverable.

First installed on Troll in 2008, Statoil' RCP valve was unique in that it could choke harder on low-viscous fluids while favoring high-viscous fluids, in addition to having the nozzle-ICD functionality. Figure 34 illustrates the autonomous valve. Considerably larger than the nozzle ICD, the valve has a freely moving disk (orange colored) in the core, which levitates when low-viscous fluids flow through the valve. This levitation causes a restriction between the disc and inner seat, choking back the respective fluids [23].

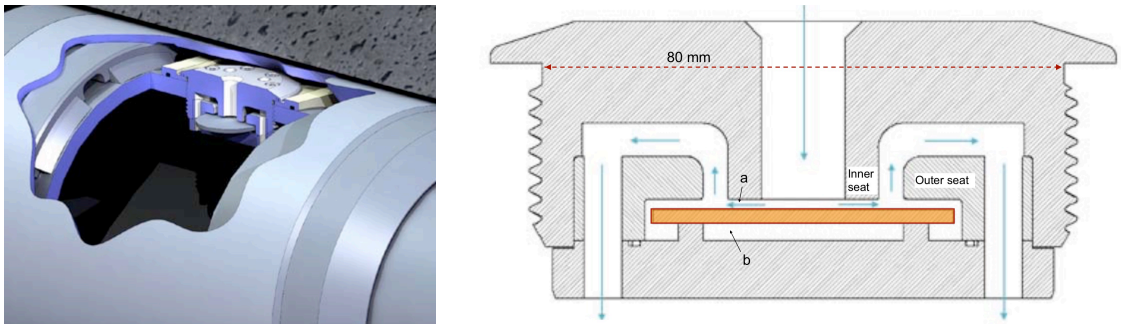

(a) *The RCP mounted in the base pipe of a screen joint* **(b)** *Schematic showing the fluid flow path through the valve*

Figure 34: *The first generation Statoil RCP Valve, [23]*

The mechanism of the RCP valve is mainly based on Bernoulli's principle, which states that the speed of a fluid is inversely proportional to its pressure (or potential energy); an

[12]Now called Equinor.

increase in the fluid's velocity will decrease its pressure. It is the principle that allows planes with several hundred tons of weight to take off in the air. If fluid compressibility and hydrostatic pressure is neglected, Bernoulli's principle can be stated as follows [23]:

$$P_1 + \frac{1}{2}\rho v_1^2 = P_2 + \frac{1}{2}\rho v_2^2 + \Delta P_{friction} \tag{12}$$

Equation 12 states that the sum of static and dynamic pressure at the inlet is equal to the static, dynamic and frictional pressure at the outlet.

There are three forces acting on the disc when fluid is flowing through the RCP, see Figure 35:

- F_{mom} - Force due to transfer of momentum from the fluids to the disc, pushing it down.
- F_{lift} - Force due to hydraulic lift, pushing the disc upwards.
- F_{drag} - Force due to viscous drag, corresponding to the frictional pressure loss (Eq. 12) pushing the disc down.

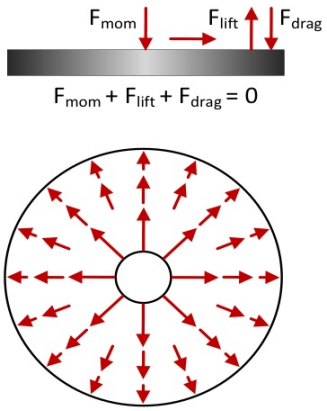

Figure 35: *Forces acting on the RCP disc, [25]*

The hydraulic lift principle may be a bit hard to grasp, therefore it will be explained in more detail. It is the same principle that airplane wings utilize to stay airborne The fluids will enter the RCP valve with a high static pressure, before the velocity is increased because of the restriction it meets. When the velocity increases, the static fluid pressure will be lowered, see Eq. 12. This corresponds to the pressure at point a, Figure 34b. However, for the fluid below the disc at point b, the static pressure is higher because of stagnation. The pressure difference between point a and b, creates a force on the surface below the disc. This is what generates a hydraulic lift. If the lift force is greater than the momentum and drag force combined, the disc will start to levitate, restricting inflow at point a.

The viscous drag force is highly dependent on fluid viscosity, a higher viscosity yields a greater drag force. Moreover, the force because of fluid momentum is proportional to the fluid density. In the case of a relatively dense and viscous fluid, e.g. heavy oil, the sum of these two forces will push the disc downwards, allowing for open flow through the valve.

On the contrary, for fluids with low density and viscosity, the hydraulic lift force will dominate the force balance, leading to disc levitation and a restriction of flow [23, 25].

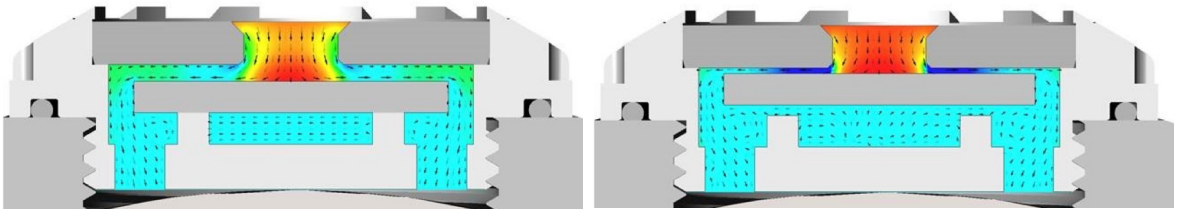

(a) *100% oil flow* **(b)** *25% oil and 75% water flow*

Figure 36: *CFD pressure plot showing fluid flow through the RCP, [25]*

Figure 36a shows the behavior of the RCP valve when oil flows through the valve. In this case the disc is pushed down, allowing flow. When a lower viscosity mixture of water and oil is introduced, the drag becomes too small and the lift force pushes the disc upwards, restricting flow. The levitation effect is intensified in the case of gas flow because of the lower momentum and drag. Note that in order for the disc to levitate, it is essential that a small amount of fluid is flowing through the valve, to maintain hydraulic lift. Another result of this is that heavier oils flow more easily through the valve compared to lighter oils, a behaviour opposite of fixed inflow control devices.

Considering the design of the RCP, it also includes the restrictive choking effect seen in nozzle ICDs, thus providing the benefits seen in fixed inflow control devices. However, the main advantage of the valve is the selective choking feature. As previously mentioned, the ability of holding back unwanted fluids such as gas or water is crucial after breakthrough. In the case of gas breakthrough in light oil reservoirs, the RCP will favor production of oil while preventing inflow of gas. The valve will operate similarly in heavy oil reservoirs with water production, and the design of the valve can be customized to field specifications.

The RCP valve has been subjected to a series of qualification tests to understand its behavior and durability. The first generation RCP involved some uncertainties when it comes to erosion resistance, which have been addressed and resolved in later years. Experiments have been conducted to model the valve's behavior. By examining the flow of gas, water and oil with various densities and viscosities, and observing rate and pressure drop through the valve, an empirical formula was developed to describe the flow characteristics [23]:

$$\Delta P = f(\rho, \mu) \cdot a_{AICD} \cdot q^x \tag{13}$$

where the first factor of the equation is directly linked to the fluids properties. a_{AICD} is the user-input strength parameter, while q designates the flow rate through the valve. x is

also a user input factor. The function of $f(\rho, \mu)$ can be expressed as follows:

$$f(\rho, \mu) = \left(\frac{\rho_{mix}{}^2}{\rho_{cal}}\right)\left(\frac{\mu_{cal}}{\mu_{mix}}\right)^y \tag{14}$$

where subscript *cal* designates the calibration fluid properties, while *mix* designates the properties of the fluid mixture expected to flow through the valve. The mixture properties can be found by calculating the weighted average based on volume fractions:

$$\rho_{mix} = \alpha_{oil}\rho_{oil} + \alpha_{water}\rho_{water} + \alpha_{gas}\rho_{gas} \tag{15}$$

$$\mu_{mix} = \alpha_{oil}\mu_{oil} + \alpha_{water}\mu_{water} + \alpha_{gas}\mu_{gas} \tag{16}$$

Furthermore, these functions were validated against several fluid types and viscosity ranges. An example of the RCP flow characteristics is given in Figure 37.

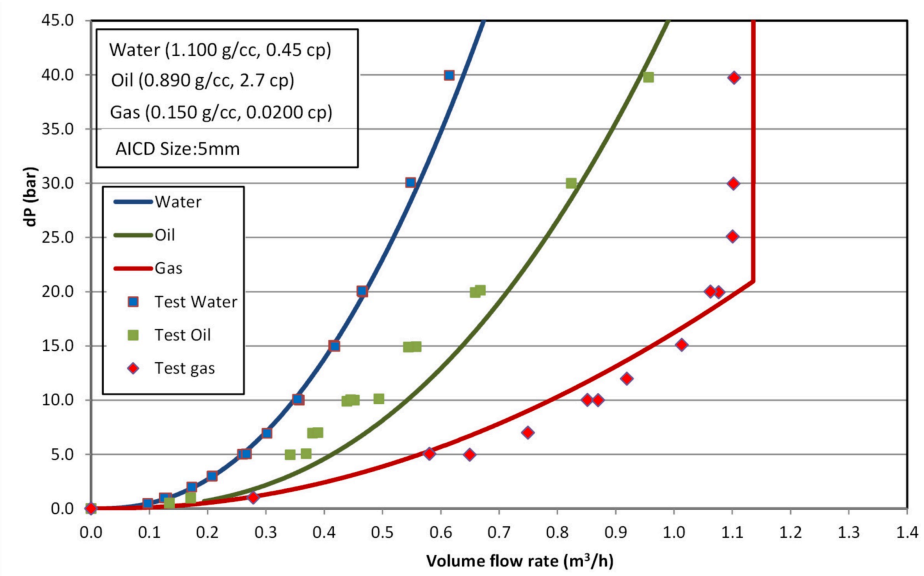

Figure 37: *Modelled and tested Single Phase Flow characteristics of light oil, [43]*

Several observations can be made from this chart. Firstly, at lower flow rates, the valve will choke harder on the water compared to the other fluids. This is because of the restrictive mechanism which depends on the fluid density, similar to the behaviour of the nozzle-type ICD. Since the RCP is sensitive to low viscosities as well, it will choke even harder, as the disc will start levitating (see Figure 36b). Because of the oils high viscosity, the main choking mechanism is based on restriction and the oil will flow more easily compared to water, see Figure 36a. In heavy oil reservoirs, the viscosity contrast between water and oil will be more significant, leading to an easier flow of the oil through the valve. At low flow rates, the RCP will choke minimally on the gas, because of its low density. However,

when approaching rates of 1.1 m^3/h, the pressure drop will increase with a vertical slope. This is because of the hydraulic lift force acting on the disc, shutting off gas flow. This is a similar but more severe case of the levitation illustrated in Figure 36b [43].

Following the trial and patenting of the RCP valve, several vendors bought a license to the technology, including Baker Hughes, Weatherford and Tendeka.In recent years, Tendeka has become the main provider of this technology, and has further developed the valve to improve functionality, reliability and applicability. The first generation RCP, the AR2, was bulky and incompatible with smaller ID screen housings because of its wideness. Additionally, its protrusion through the base pipe could prevent intervention tools from entering the lower completion, as well as deployment of stinger completions later in the life of the well. The most up-to-date version of the RCP is the Tendeka FloSure TR7 valve, pictured to the right in Figure 38. It is small enough to be integrated in standard ICD housings, enabling the installation of the valve in screens originally manufactured for standard nozzle-ICDs. To achieve this small size, a focus has been laid on simplification of the fluid path through the device, in addition to optimizing the manufacturing process. To improve stability and erosion resistance, the disk and nozzle of the valve have been thickened and upgraded to tungsten carbide [43].

Figure 38: *Design evolution of the RCP, [43]*

Halvorsen et al. [54] evaluated the performance of the RCP valve on three different Troll wells. One of the wells, P-13 BYH, was completed with two lateral branches. The first branch was run with conventonal ICDs while the other was equipped with RCP technology. The well was chosen as a candidate because of the similarity in the geology that the branches penetrated. Figure 39 shows the GOR development of the two branches of time. Prior to gas breakthrough the performance of the branches is similar up to June 2011. By evening out the inflow profile along the wellbore, the gas breakthrough is delayed up to this point. After this date, branch Y1 started to produce considerably higher gas volumes than branch Y2. It should also be mentioned that the two branches were producing at

approximately the same liquid rates. In this time period, it is clearly observable how the RCP manages to hold back the gas after breakthrough, while maintaining a similar or higher oil production. Evaluation of cumulative production showed that the RCP-fitted branch produced approximately 20% more oil compared to the ICD-fitted branch [54].

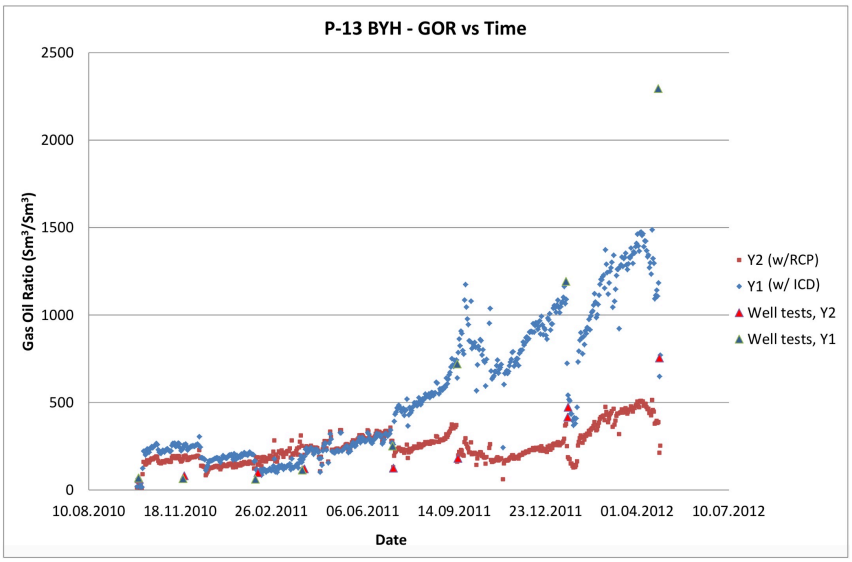

Figure 39: *Troll P-13 BYH – GOR development over time, [54]*

Another well that was evaluated in the respective study was P-21 BYH. Fitted with the RCP, it produced better than expected, when compared to other Troll wells. After 10 months it had produced the equivalent oil production that a typical Troll well is expected to produce during its entire lifetime. A comparison of the actual production with the simulated production in the reservoir simulator, revealed that the well performed even better than expected, see Figure 40. Also shown in the plot, is the simulated production with a 3.2 bar ICD, which shows a lower oil production compared to the RCP case. In 2012, the RCP valve became part of the standard sand-face completion for Troll wells [11].

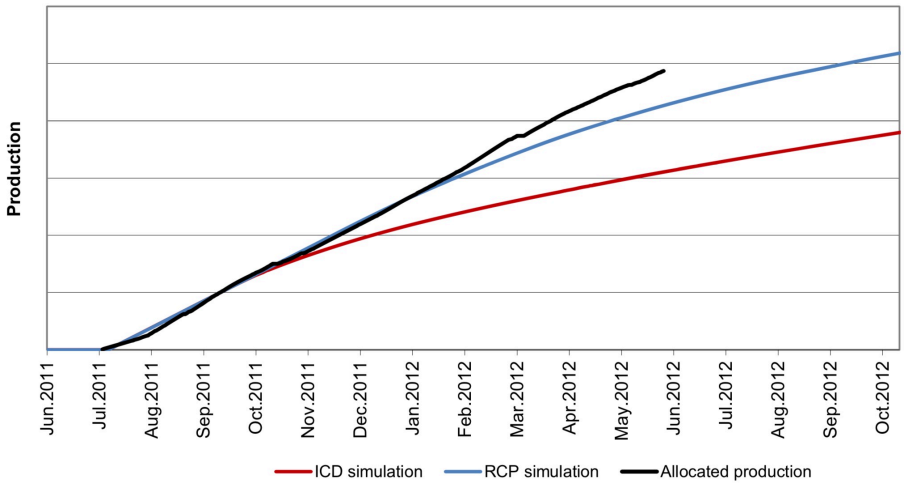

Figure 40: *Troll P-21 BYH Simulated and actual production, [54]*

The topic of improved recovery on Troll by implementation of inflow control was revisited four years later, by Halvorsen et al. [43]. Here it is concluded that on average, the simulated increased oil production with the RCP is approximately 46%. Moreover, the wells equipped with RCP valves typically produced better than expected.

The RCP valve also has a great track record globally. The current provider, Tendeka, reports that the Flosure TR7 (Previously RCP) valve has been installed over 20,000 times in over 100 wells, with no reported failures [25].

2.5.2 The InflowControl AICV®

In 2011, the inventors of the RCP valve joined together and founded the company InflowControl in Porsgrunn. With more than 15 years of experience in passive inflow control, they invented the AICV®, pictured in Figure 41.

(a) *The AICV core* **(b)** *The AICV with the pilot flow tube*

Figure 41: *The InflowControl AICV, [23]*

The InflowControl AICV utilizes the flow behavior of fluid in the laminar and turbulent regime. To achieve this the valve has two different flow elements integrated in the valve for these respective flow types.

When a Newtonian fluid is flowing through a pipe in the laminar flow regime, it moves along defined paths and the pressure drop along the pipe can be determined by the following equation [55]:

$$\Delta P_f = f \cdot \frac{L\rho v^2}{2D} = \frac{64}{\mathrm{Re}} \cdot \frac{L\rho v^2}{2D} = \frac{32\mu v L}{D^2} \tag{17}$$

On the contrary, a fluid flowing through a restriction in a turbulent flow regime will act in a chaotic manner, and the pressure drop can be found as described in Section 2.3.2 and Equation 3. A simplified form of this equation can written as follows [55]:

$$\Delta P_R = \frac{1}{2}\frac{\rho v^2}{C_D} \tag{18}$$

Aadnøy [56] pointed out how the pressure drop in a laminar flow regime is mainly viscosity and rate dependent, which is evident from Equation 17. For turbulent flow, the pressure drop is dependent on the density and rate squared, see Equation 18.

These two principles are incorporated in the InflowControl AICV, by use of a pipe element and a thin plate orifice, respectively. Figure 42 illustrates how this can be achieved in a series of flow restrictions. The fluid enters the flow conduit at the inlet (A). Initially, it meets a laminar flow restriction. This will induce a pressure drop ($P_1 - P_2$), according to Equation 17. Further, the fluid flows through a turbulent flow element that induces an additional pressure drop ($P_2 - P_3$). As previously mentioned, this pressure drop will be proportional to the fluid density and rate squared, according to Equation 18. In the plot in Figure 42 it is shown how three different fluids will react when flowing through the flow conduit. At the laminar flow element, the heavy oil will undergo a relatively large pressure drop because of its high viscosity. The equivalent pressure drop for water and gas, on the other hand, is low because of the low fluid viscosity. The additional pressure in the case of water and gas can be utilized to perform work, such as triggering an actuator and moving a piston or valve [57].

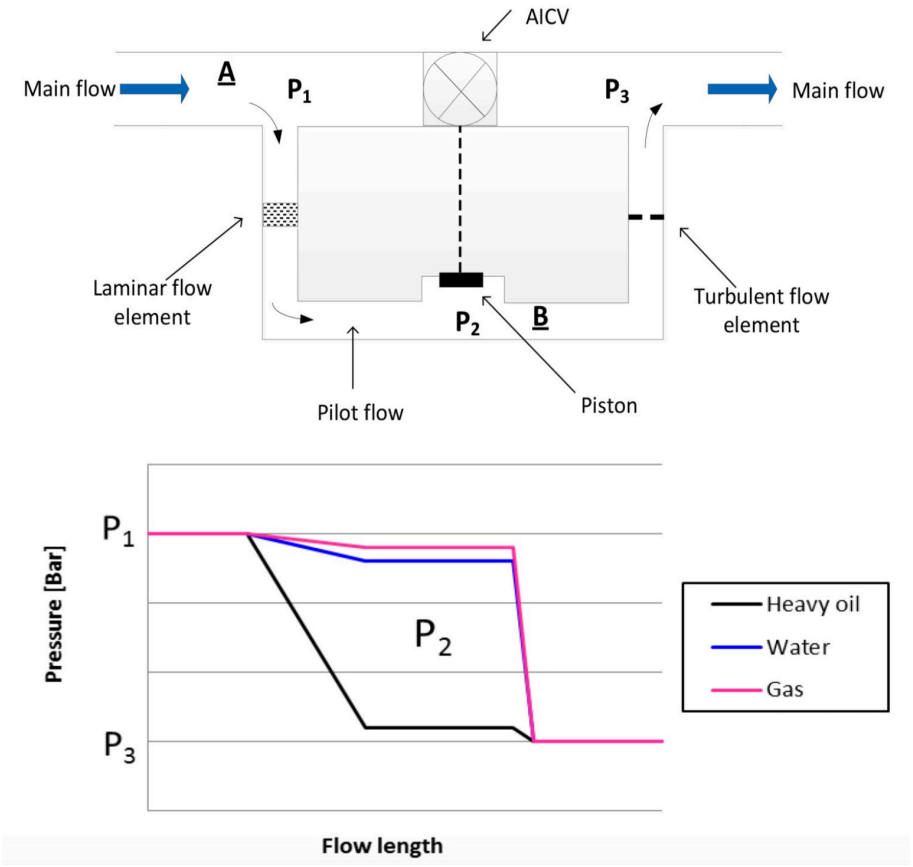

Figure 42: *Combination of laminar and turbulent flow elements in series, [58]*

In the AICV, a pilot flow tube is used to induce the initial laminar flow pressure drop

and utilize this pressure. In Figure 43 it is shown how this can be be achieved in practice. The pressure P_2 at the end of the pilot flow is used to actuate a piston (yellow) with a force F_2. Moreover, there is a force F_1 resulting from fluid flow at the main inlet. If the area A_1 is smaller than A_2, a lower pressure P_2 is required in order for $F_2 > F_1$. This will push the piston upwards and close the valve, restricting fluid inflow, see the plot in Figure 42. If the pressure drop $P_1 - P_2$ is significant, the pressure P_2 will not be high enough to push the valve upwards (i.e. $F_2 < F_1$), leaving the valve open for flow. This is typically the case with viscous fluids such as oil, which also increase the force F_1 because of the additional viscous drag. The flow is subsequently led through the turbulent flow element (TFE) before it exits the valve with a pressure P_3.

In open position, the AICV can be designed with different strength to include the ICD-functionality that evens out the inflow profile. This pressure drop is induced at the small channel between the yellow piston and the pink colored seat. The ratio between the areas A_1 and A_2 is also a design parameter depending on the fluid properties [57, 59, 60].

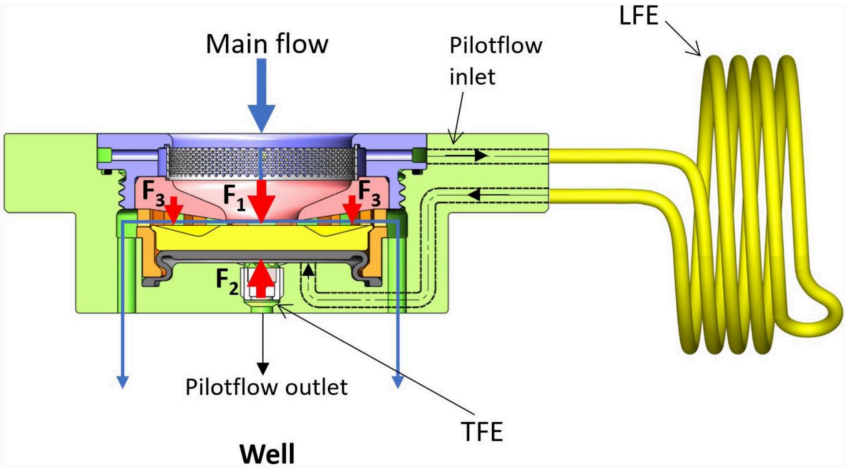

Figure 43: *Forces acting on the AICV, [59]*

For the valve to function as intended, there needs to be a flow through the pilot flow tube, even when the gas or water is being produced. However, the pilot flow represents only a fraction of the total flow, approximately 1%. The AICV is also reversible, if the valve has been previously closed because of production of water or gas, it will be autonomously opened upon seeing oil again. The AICV has been subject to numerous experiments to qualify its use in the oilfield. This includes [61]:

- LFE and TFE tests in a flow element test rig to find the most suitable flow elements for the valve
- Single phase and multiphase tests to validate the valves functionality
- Tests in a multiphase flow loop test rig in real reservoir conditions

- Erosion test with particles
- Clean-up test with mud and completion fluid
- Long-time longevity test

Based on these tests, a series of flow characteristics curves were developed. Figure 44 shows the behavior of the AICV for gas, water, light oil and heavy oil. It is clear how water and gas undergo a much higher pressure drop at low flow rates compared to the oil. Moreover, the heavy oil will undergo less choking compared to the light oil, because of its high viscosity.

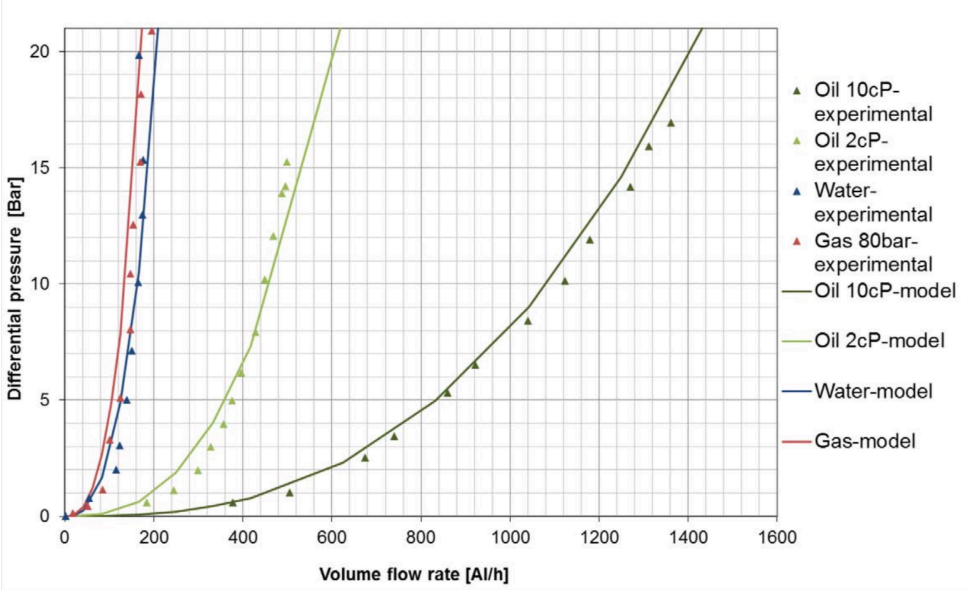

Figure 44: *Comparison of experimental and modelled flow characteristics of the AICV, [62]*

To be able to model the AICV behavior in static near-well simulators such as Landmark NETool, it is possible to use the same functions as the ones for the RCP valve, see Equations 13 - 16. In retrospect, a slightly different version of Equation 16 has been developed by request from Statoil, to improve correlation:

$$\mu_{mix} = \alpha_{oil}^{d}\mu_{oil} + \alpha_{water}^{f}\mu_{water} + \alpha_{gas}^{e}\mu_{gas} \tag{19}$$

Similar to the RCP, the input parameters for the AICV are $a_{AICD}, \rho_{cal}, \mu_{cal}, x, y, e$ and f. These values should be experimentally estimated for each field, and tuned to fit the flow performance of the AICV. The solid lines in Figure 44 show the tuned RCP-functions, and there is obviously a good correlation with the experimental data [62].

The AICV has been successfully deployed in 11 wells to date, according to the CEO of InflowControl, Vidar Mathiesen [63]. Nugraha et al. [61] described the first field installation of the AICV. Despite being an overall successful installation, some key learnings were

highlighted with regards to the initial operations. After running the liner down to target depth (TD), the well was displaced with breaker fluid in the liner interval, and completion brine above the liner packer. Some viscous brine was also added to this section to prevent the AICV from closing off the back-flow. To ease the back-flow process, nitrogen was pumped down with coiled tubing to lighten the fluid column in the well. It was observed that back-flow time was much longer than expected. The authors' reasoning for this is that the AICV was choking down on the water, allowing flow only through the pilot tube. Based on these observations a special procedure is recommended during back-flow of the well, where a sleeve is installed in the completion to enable circulation and bypassing the AICV. Additionally, it is recommended to use a high viscosity completion fluid to keep the AICV open during back-flow.

2.5.3 The Enchanced Recovery Valve (ERV)

All autonomous inflow control designs discussed until now have been dependent on both fluid density and viscosity. In 2017, some engineers from Acona Flow Technology came up with a new autonomous inflow control valve that addressed several of the challenges linked to the existing technologies. The new design is buoyancy-based and is called the Enhanced Recovery Valve (ERV).

The focus and objectives of designing this new technology were as follows [64]:

- There should be a minimal number of design parameters for each field to simplify design and planning. Additionally, the operational window should be broader to improve function during the whole lifetime of the well.
- Reliable design and functionality, with negligible risk of plugging and erosion.
- Easy integration into the lower completion.
- Efficient well clean-up. As previously mentioned, proper clean-up in long horizontals can be challenging, and the ERV should be able to improve the removal of completion fluids and filtercake for enhanced well performance.
- Allows for easy back-flow of fluids, in the case of bullheading stimulation fluids, tracers or temporary solvents. Additionally, this feature is also important for well integrity instances where bullheading or well killing may be necessary.
- Viscosity independent design. In situations where the difference between the oil and water viscosity is minimal, existing autonomous technologies struggle to differentiate

between the two fluids, and end up producing high amounts of water. The new generation AICV will function independently of both viscosity and production rate.

- Negligible pressure drop across the valve during production of desired fluids. Unless an ICD effect is desired, an ideal inflow control system should have a minimal pressure drop in open position.
- In the case of water or gas production, only unfavorable amounts of these fluids should be held back. When producing water with oil, a certain water cut is necessary to ensure proper reservoir drainage. When gas is produced with oil, it can aid in providing lift and improving the Tubing Performance Ratio (TPR). Because of these factors, the new ERV will only choke back very high volume fractions of unwanted fluids.

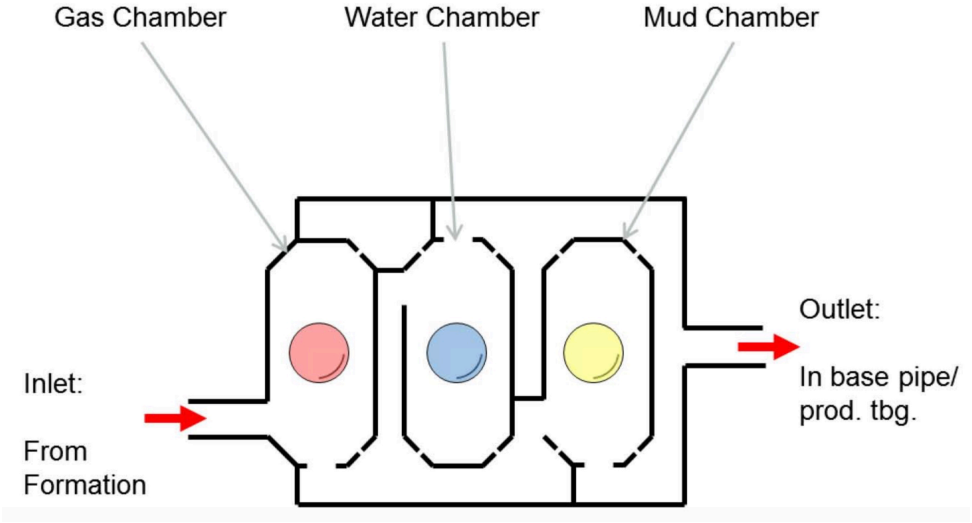

Figure 45: *The main principle of the ERV, [64]*

Figure 45 illustrates the new proposed design for the ERV. A mathematical approach was used to find a mechanism that was both robust and operationally versatile. The optimal solution was found to be a buoyancy-based system.

The design includes three fluid chambers with floating elements that react on different fluid densities. The relation between the flow elements can be summarized as follows:

$$\rho_{gas} < \rho_{red} < \rho_{oil} < \rho_{blue} < \rho_{water} < \rho_{yellow} < \rho_{mud} \tag{20}$$

For fluid to flow through the valve, it has to pass through all three chambers. Illustrated as balls in Figure 45, the red ball floats when the chamber contains oil, but sinks in gas. If the red ball sinks, it will choke the main chamber outlet preventing the fluid from continuing to the next chamber. Similarly, the blue ball floats in water, but sinks when the chamber is filled with oil. The main outlet for the water chamber is at the top, and

when the ball floats it will prevent fluid flow through this chamber. However, fluid may bypass this chamber and flow directly to the third, mud chamber. Lastly, the yellow ball in the third chamber will sink in water but float in mud or completion fluid (that is heavier than water). Hence, if oil (which is lighter than water) was to enter this chamber it would be prevented, and forced to flow from the second chamber and above the mud chamber, see Figure 45. Each fluid chamber also has some small outlet channels, these will allow a negligible amount of unwanted fluid production to keep the system stable during production. These channels make the ERV reversible; if the valve sees oil after some time, the existing water or gas in the chambers will be replaced by oil and the valve will open for flow.

Figure 46 shows the different operational modes of the ERV along a long horizontal well. In the toe of the well, the clean-up of mud is typically incomplete as explained in Section 2.2. The ERV enables better clean-up of sections as it will stay open to these respective zones, as long as mud is being produced. When the valve sees oil it will switch to a closed position, thus inducing a greater drawdown pressure on insufficiently cleaned zones. This is done by having a "differential stick" function in the middle chamber. In zones with coning of water or gas, the valve will effectively exclude these zones from production [64].

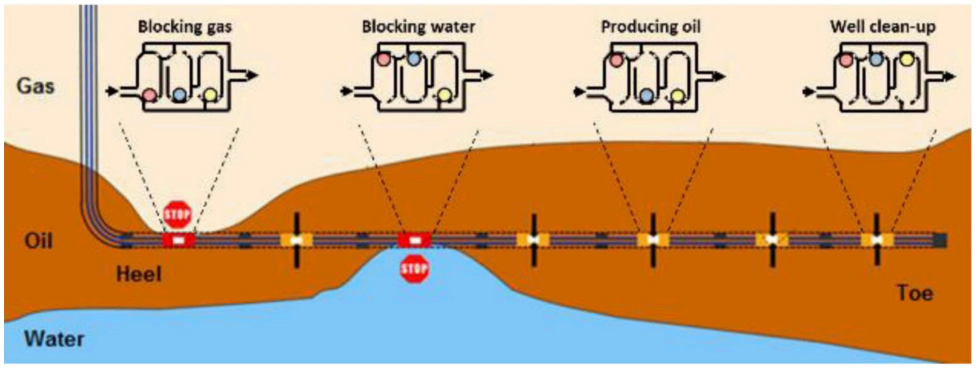

Figure 46: *The mode of the ERV in different situations, [64]*

There are some challenges related to the functionality and design of the ERV. Firstly, the orientation of the system is quite important in order for the floating elements to function as intended. Multiple systems in parallel may be necessary to keep the valve independent of orientation. Additionally, solids found in mud can settle in the chambers and lead to plugging or entrapment of the floating elements. Moreover, the system should be tuned to balance the forces acting on the floating elements caused by a variable flow rate. For instance, viscous drag forces can become a challenge that prevents the floating elements from moving around properly. Lastly, the balls used in the ERV must be designed with the correct density and robustness to ensure reliability and accuracy in the system [15].

A review of current literature found no field deployments of the ERV technology, but the solution has been patented [64].

2.5.4 Autonomous Flowcontroller Device

In 2014, Bowen and Aadnoy [65] published a paper describing a new type of autonomous inflow control valve. The Uniflo Autonomous Flowcontroller Device (AFD) is a constant flow regulator valve that is based on hydraulic feedback and Bernoulli's principle. The main aim of the technology is to maintain a constant flow rate through the valve regardless of flowing inlet pressure. A pre-determined flow rate through each unit is the only input parameter needed to design the AFD valve.

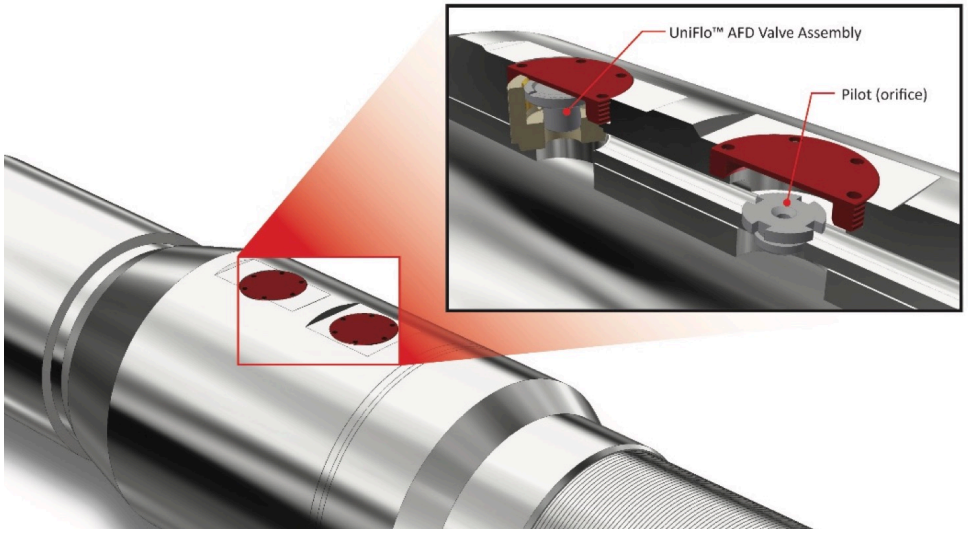

Figure 47: *The Uniflo Autonomous Flowcontroller Device, [15]*

Figure 47 shows how the AFD valve can be integrated in the lower completion screen joints, in a similar was as the previously described inflow control technologies. The patented AFD technology is simple but effective; it consists of a valve and valve body, which can be applied for both production and injection purposes depending on the orientation of the valve. The schematic in Figure 48 shows how the fluid enters the valve in a production scenario. After passing through the screen layers and a pilot orifice with a flowing BHP equal to P_1, the fluid can flow into two paths. At the top of the valve, there is a larger flow area compared to underneath the valve. From below, the valve is pushed upwards by a spring with a force following Hooke's law. Hence, there are three forces controlling the valve's behavior:

1. Pressure-area force above the valve, acting downwards.

2. Pressure-area force below the valve, acting upwards. For the same flowing BHP this force will always be lower than the previous force, due to a smaller area.
3. Spring force acting with a known spring constant k, acting upwards.

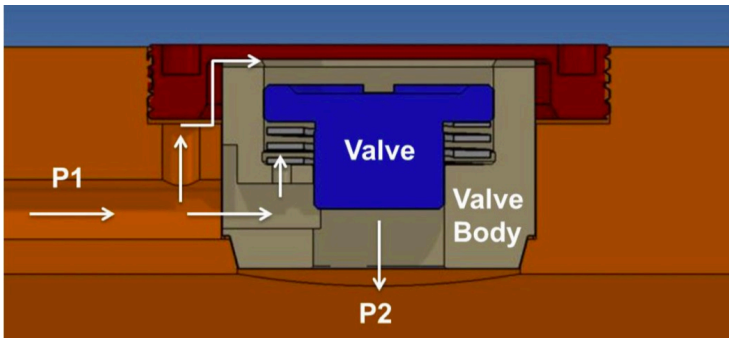

Figure 48: *Schematic of the AFD valve, [65]*

For fluid to flow through the valve, the upwards force must exceed the downwards force, i.e. the difference in the two pressure-area forces must be overcome by the spring force. At an early production stage, P_1 will be relatively high, making the valve choke harder. As the reservoir is drained, this pressure will decrease, consequently leading to a greater opening in the valve and lower pressure drop through the AFD while still maintaining a constant flow rate through the unit. This makes the AFD technology adaptive to the different phases of the production lifetime. The same principle can be applied for water injection purposes, aiding in a distributed flow with a constant injection rate along the whole length of the injector.

A series of simulations and flow experiments have been performed with the AFD. The results from drainage analysis and comparison with nozzle-type ICDs show that the time needed to drain the same reservoir was almost half for the AFD compared to the conventional ICDs. Draining the field in 5.2 years, instead of 9 has significant economical and operational benefits which justify the implementation of the AFD in the lower completion.

Figure 49 shows the flow characteristics of the AFD valve at different fluid viscosities. At an approximate flowrate of 4.5 gpm, the flow through the valve stays constant despite an increasing pressure drop. It is clear how the AFD valve's flow characteristics are nearly unaffected by different fluid viscosities. The constant flow behavior is a contrast to the flow characteristics of conventional ICDs, where the pressure drop is generally proportional to the square of the flow rate[13] [65]. A literature review did not find any documented field

[13]See Equation 3

deployments with the Uniflo AFD. Discussions with Professor Bernt Aadnøy revealed that the valve is going through various experiments to qualify its use in the oilfield [66].

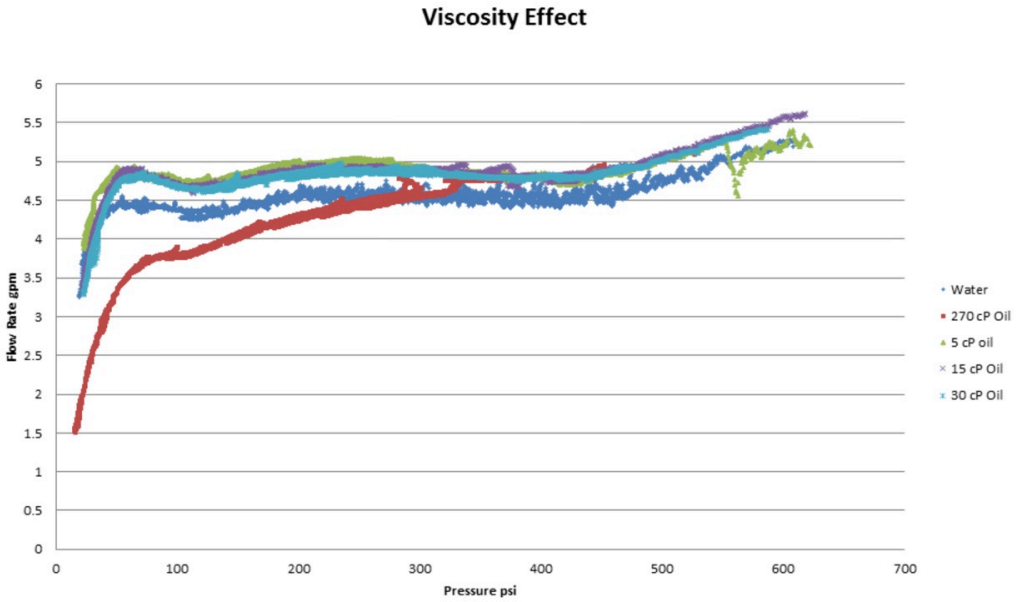

Figure 49: *Flow characteristics of the AFD valve, [15]*

2.5.5 Adaptive Inflow Control Device

WORMHOLES is a Russian-based service company that was established about a decade ago. Initially, they developed a hybrid-type inflow control device, with a similar functionality as the Baker Equalizer Select (Figure 25). The device consists of a labyrinth shaped channel reminiscent of the trail of wormholes in a tree, see Figure 50. Subsequent development of this inflow control device led to the creation of the Adaptive ICD. The Adaptive ICD consist of a series of coupled ICD units with multiple valves, see Figure 51.

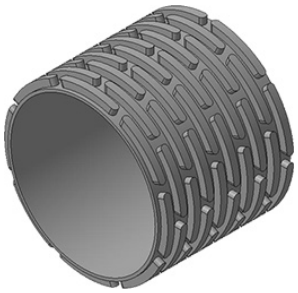

Figure 50: *The first generation Wormholes ICD, [67]*

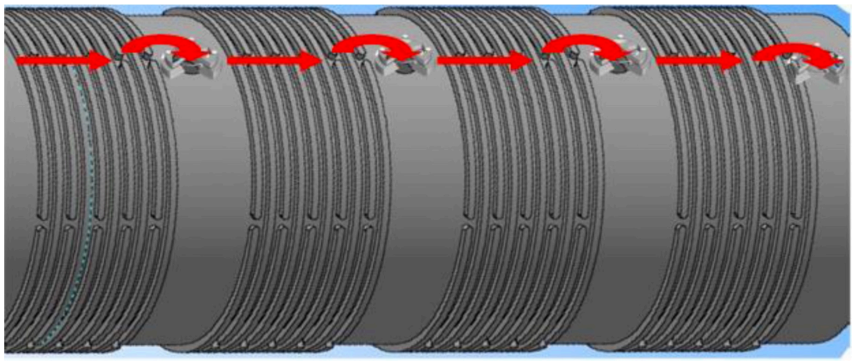

Figure 51: *Schematic of the Adaptive ICD, [68]*

As explained Section 2.4.1, the hybrid-type of ICD induces a combination of frictional and restrictive pressure drop by leading the fluid through several channels and restrictions. The Adaptive ICD has a similar design, but also includes valves along the device that can open and close based on fluid properties. The valves contain throttle rings that control the gate position of the valve (open or closed). Illustrated in Figure 52, the valve consists of three main parts; the valve saddle (1), valve cap (2) and a ball of magnetic material (3). Inside the valve cap there are also permanent magnets (4).

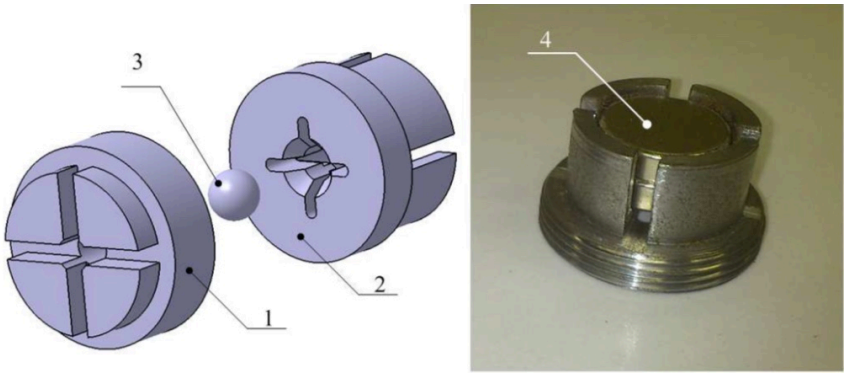

Figure 52: *The Adaptive ICD valve design, [67]*

The operation of the valve is based on two physical principles; magnetism and hydrodynamics. When fluid flows into the valve, the hydrodynamic force of the fluid will push the valve gate from the side of inflow. At the opposite side, the permanent magnet pushes gate with a magnetic force to keep the valve open. If the flow rate exceeds a certain limit, the hydrodynamic force will overcome the magnetic force, lowering the gate to the saddle and consequently closing the valve [67].

When the completion integrated with the Adaptive ICD is run downhole, all the valves are in an open setting. At start of production, fluids will pass the sand-control layer before being led into the first maze where a pressure drop will be generated. Subsequently, the fluids will enter the first valve and. If the localized flow rate exceeds a certain preset, the first valve will close, and flow is diverted to the next valve. This results in another pressure drop being generated as the fluid meets another ICD unit. If the flow rate at the second valve still exceeds the limit, flow will continue to the third valve, and so on. In this way the flow rate can be limited to a certain limit, independent of the inflow rate [68].

Delia et al. [68] also presented the flow characteristics of the Adaptive ICD, after a series flow tests. In Figure 53 the results of tests performed with liquid and gas respectively, are shown.

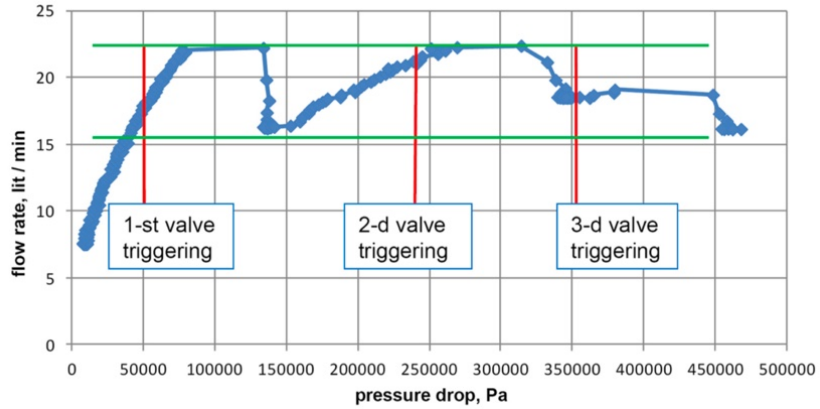

(a) *Liquid flow*

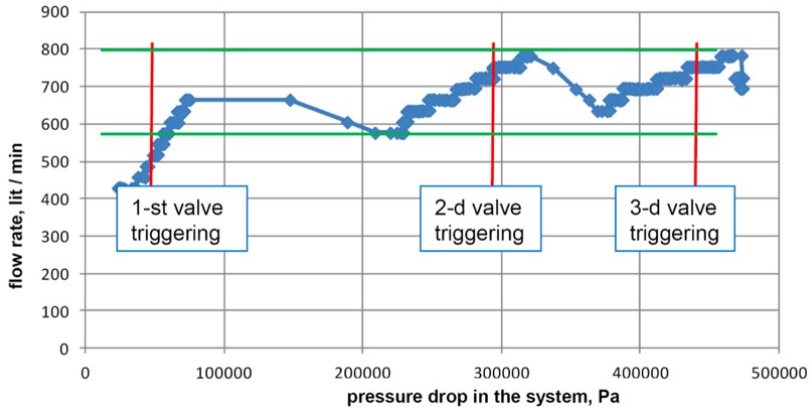

(b) *Gas flow*

Figure 53: *Adaptive ICD: Flow rate as a function of pressure drop. Green lines signify flow rate range while the red lines show each valve activation, [68]*

As each of the valves is triggered, the pressure drop in the system increases, and the flow rate is kept within the desired limits for both fluids. It should also be noted that the flow performance varies based on fluid properties, as these determine the magnitude of the hydrodynamic force. The Adaptive ICD can be customized for different applications by altering the valve saddle cross-section and gate plate rigidity to deliver the desired pressure drop and flow rate range. According to available literature, the Adaptive ICD has been field proven in the Caspian sea with successful results [68].

However, the Wormholes system does have some shortcomings. Firstly, the channels in the labyrinth unit is susceptible to settling of solids, which can lead to reduced performance or plugging. Secondly, the reliability of the permanent magnets can also be questioned. Furthermore, documentation of erosion testing have not been published, thus the risk of eroding the valve components is unknown [15].

2.6 The potential upside for ICT on Gjøa

Based on the discussed technologies, several potential benefits for the two Gjøa oil producers can be anticipated.

When it comes to well B3 which presented the challenge of excessive gas production and immobilized oil reserves, the main objective is to delay and hold back gas. To understand the dynamics leading to this challenge, a good indicator can be the permeability profile along the wellbore. In Appendix G.2, Figure G-26, the B3 well log is shown. A clear observation is the consistently high permeability along the open production zones.

One can draw a parallel to the Troll wells which seem to have the same characteristics with regards to the high permeability and overlying gas cap. As explained in Section 2.2, such wells can suffer from the heel-toe effect. Having a relatively long horizontal section, well B3 might have experienced an early gas breakthrough at the heel of the well. Another indication that supports this theory can be seen from Figure 54. While the red color signifies gas saturated layers, the green gridblocks are oil-filled. Blue, water filled zones are insignificant since they have been excluded from production by using blank pipe sections in the respective zones. As the major portion of the oil filled layers lie in the lower (toe) part of the well, this part is most likely the main contributor to oil production. This further exacerbates the severity of the heel-toe effect, as production from the heel will be encouraged, leaving the substantial oil reserves behind in the toe.

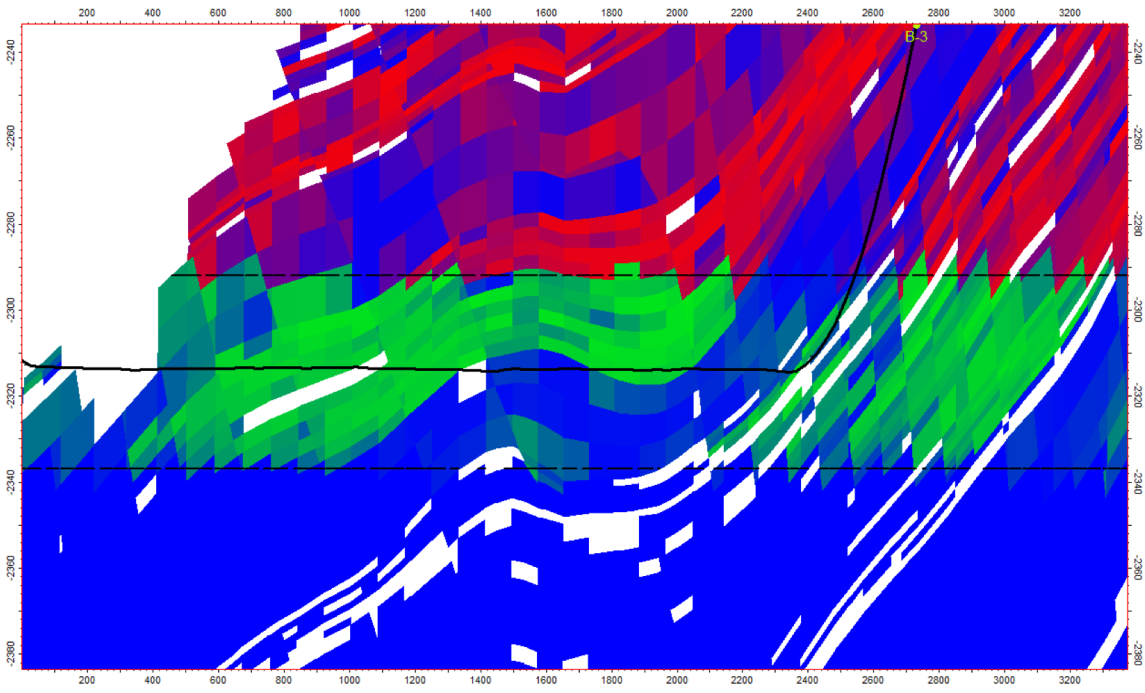

Figure 54: *B3 Well placement in the reservoir showing the initial saturations according the the reservoir model, [10]*

For the purpose of mitigating the heel-toe effect, inclusion of inflow control devices can help distribute inflow along the whole well, and promote production from the toe. This will further delay any potential early gas breakthrough in the heel. However, once the gas breakthrough has started, the gas mobility will be the determinant factor for inflow, and the ICD effect will be insufficient. Perhaps the use of autonomous inflow control will assist in this manner. Several autonomous inflow control technologies presented in Section 2.4 and 2.5 have proven to be able to hold back gas and drastically improve oil recovery, while also including the choking effect of the ICD. This matter will be further investigated in Part II

Well B1 has experienced different production challenges. An important difference from B3 is the production of water, which has presented further problems after long shut-in periods. Two objectives were discusses regarding this issue; to delay the water breakthrough, and to help with restricting water influx at start-up and thereby lessen the need for extended gas lift periods.

In Figure G-27, the permeability log for B1 can be viewed. In contrast to B3, B1 has quite a heterogeneous permeability profile which can indicate an uneven flux along the well during production. As discussed in Section 2.2, an uneven flux will lead to preferential production from high permeable compartments, and limit production from lower flux zones. This can also be a cause of early gas/water breakthrough. In the case of B1, the heterogeneity along the wellbore could cause the observed water breakthrough.

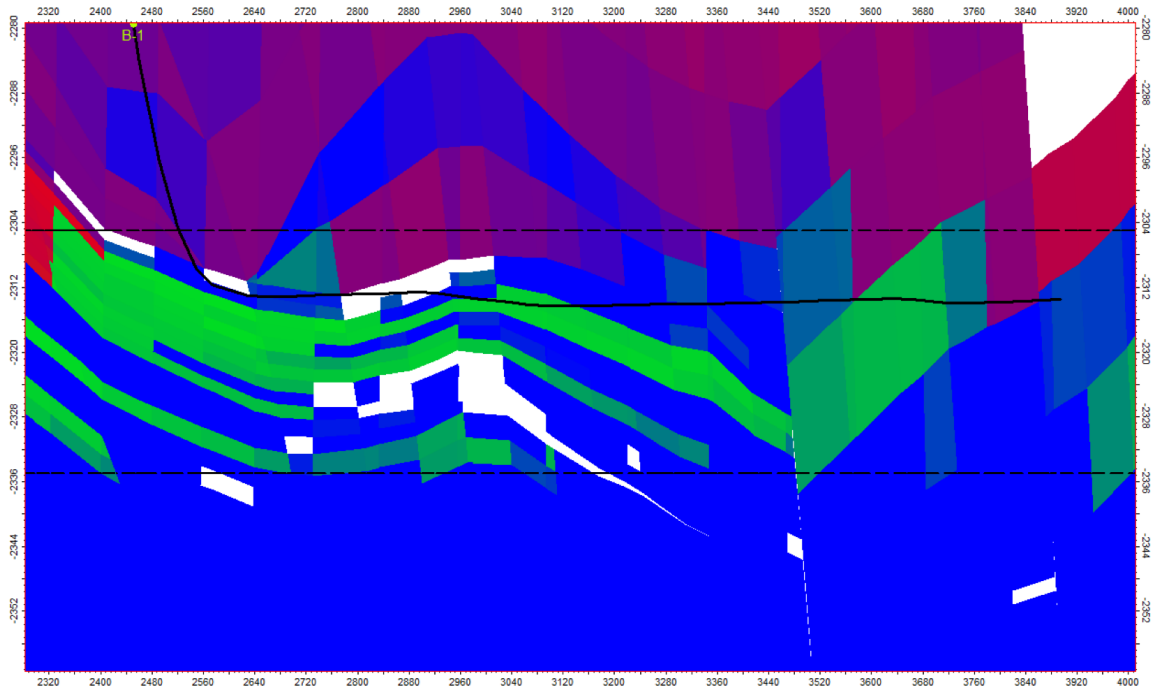

Figure 55: *B1 Well placement in the reservoir showing the initial saturations according the the reservoir model, [10]*

With the use of ICDs in B1, flow from the high permeable zones will theoretically meet a higher resistance in the form of a higher pressure drop. This will aid drainage from low flux zones, and potentially increase the time to breakthrough.

Once the water breakthrough has taken place, ICDs will no longer serve a critical purpose. However, the placement of annular isolation packers, e.g. swell packers, can help reduce the severity of the breakthrough. As previously discussed with regards to compartmentalization, water flooding the annular space and spreading throughout the whole well length, can severely exacerbate the breakthrough, and deem the well economically nonviable. Therefore, using annular packers can help minimize the consequences of the breakthrough and help retain the breakthrough within certain well segments. This can significantly mitigate the well start-up challenges previously described.

Theoretically, it could be anticipated that autonomous inflow control could prevent water production. This is because of the viscosity sensitivity integrated in the various autonomous technologies, and the generally positive viscosity difference between oil and water. However, by examining the fluid properties presented in Section 1.3, it can be seen how the oil viscosity is lower than the water viscosity. Consequently, this could in some cases lead to the AICT to preferentially produce water in favor of oil. This is an important detail, which will be discussed later in the thesis.

In 2007, Reslink performed an study which investigated the use of ICDs on Gjøa, [5]. The study considered the preliminary reservoir model with various permeability profiles. B3 and B1 were part of this study, which considered the dynamic and cumulative effect of ICD inclusion in the wells. In the simulations performed, an annular packer per well segment was assumed, i.e. every 12 - 38 screen joint. For well B1, the results indicated a delayed water breakthrough by 1 year, and an increased oil production of 42 000 Sm^3/day or approximately 260 000 bbl. For B3, the results indicated an accelerated production of oil, i.e. higher oil production rate in the early well life. Moreover, the gas rate was considerably reduced. For both wells, the optimal configuration was found to be 3 x 4mm nozzle ICDs. Although the technology was not implemented in the two wells, the results from this study has significant indications with regards to the performance with inflow control.

Part II

Simulations: Method and Results

Introduction

To see the effect of various inflow control technologies on the Gjøa reservoir, a simulation software called Landmark NETool was used. The simulation models were developed by use of the existing reservoir model for Gjøa, in addition to relevant completion and production data. The aim of the initial simulations was to calibrate the simulation model and thereby achieve a match between simulation results and production history. This would ensure that the model is set up correctly and that the subsequent simulations with inflow control were somewhat accurate. Section 3 will provide an overview of the approach that was taken to develop the reference case models for the two wells. Once this was achieved, further simulations could be done to see the effect of ICD and AICV in the wells. This will be discussed in Section 4 and 5, respectively.

3 Base Case Model

3.1 Landmark NETool

Halliburton's Landmark NETool™is a steady-state near-wellbore simulator that is based on reservoir properties and completion setup. It is one of the most widely used simulation softwares in the industry for modeling advanced well completions. The simulator has a simple graphic user interface that makes it convenient to assess the effect of different completions in terms of reservoir influx and drawdown pressure in the vicinity of the wellbore. The fact that the simulator is steady-state means that it can only assess well productivity at a certain timestep, i.e. it is a static simulator. On one hand, this means much faster computing time and faster results, when compared to dynamic simulators such as Eclipse™. However, it also represents a series of limitations when it comes to assessment of the overall effect of various completion equipment, e.g. development of pressures and rates over time.

The numerical model in NETool is based on a discretized network system comprising a series of micro-nodes interconnected through fluid flow, as illustrated in Figure 56. The network also combines several completion layers, which enables the user to see the interaction between e.g. the reservoir, the sandscreen and the inflow control layer. Hence, the tool will provide a better understanding of the well performance and behavior. In Figure 56, an illustration of the micro-nodal software model is shown [62, 69].

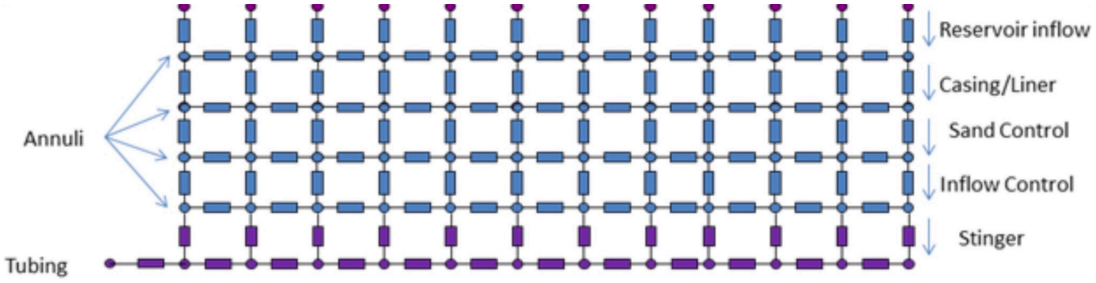

Figure 56: *The general node configuration in NETool, [69]*

The NETool software enables a number of benefits when it comes to completion engineering [69]:

- It analyzes the flow in the near wellbore area in a quick and efficient manner.
- It allows for advanced well completion configurations, which is usually not possible in other simulators.
- It provides a graphical user interface that clearly shows the various completion layers, both in the input data and output results.

- It allows for inclusion of various effects such as completion skin and filter cake.
- It enables quick and easy modeling of the most widely used inflow control technologies.
- It allows for importation of the reservoir model from Eclipse, enabling development of very accurate wellbore models.

3.2 Building the Model

As mentioned, NETool allows tuning of a great number of parameters, enabling accurate modeling of the well. The workflow for developing models for the two candidate wells will be presented.

The models were initially developed by importing the full-field Gjøa Reservoir model from Eclipse. Seeing as NETool is a static simulator, it is only possible to simulate at certain timesteps, and not through time. Each timestep (date) reflects the reservoir condition as defined in the Eclipse-model at the respective time. This includes, for instance, the remaining in-place fluid volumes, pressure and fluid contacts. To obtain an accurate and detailed history-match it was important to simulate at many time-stamps, and therefore necessary that the Eclipse-model imported included these time-stamps.

The initial Eclipse files from the Reservoir Engineering (RE) team contained several time-stamps for the first production year, but less frequent time-stamps in the later years, from 2013 to 2018. For the purpose of this thesis, more frequent time steps were requested, and Table 4 shows the main time-stamps that were used for the simulations of B1 and B3. At a later stage in the work process, further intermediate time-stamps were acquired. These were not used for all the simulation cases presented, and will thus not be listed.

Table 4: *Eclipse time-stamps used for simulations*

Wells	B1-AHT3	B3-HT2
		01.01.2012
	10.05.2012	10.05.2012
	21.05.2012	21.05.2012
	01.06.2012	01.06.2012
	17.06.2012	17.06.2012
	29.06.2012	29.06.2012
	01.01.2013	01.01.2013
Timestamps	01.01.2014	01.01.2014
(Date)	01.01.2015	01.01.2015
	01.01.2016	01.01.2016
	01.01.2017	01.01.2017
	01.01.2018	01.01.2018

Before the simulation work was initiated, the production data based on Eclipse simulations were acquired from the RE team. The reason for this was to compare Eclipse results with the observed production data presented in Figure 4 and 5. If the two statistics deviate significantly, it indicates the Eclipse model does not reflect the actual reservoir conditions. Seeing as the major part of the NETool models is based on Eclipse input, this potential deviation would consequently propagate towards NETool simulation results. Hence, this detail could possibly be decisive for the feasibility of the calibration work.

We will now have a look at the production profiles for the two wells. Well 35/9 B3-HT2 will be discussed initially, as it was the first well to be drilled and completed. In Figure 57 the solid lines represent the actual production rates for oil (yellow), gas (green) and water (blue). Additionally, the simulated production rates from Eclipse were plotted as points through time. There is a good conformity between the simulated[14] and actual rates, especially for the gas production. Figure 58 shows the corresponding production history of well B1-AHT3, which started production in March 2012. The actual production rates and simulated Eclipse fluid rates were plotted with the same coloring as for the previous well. An important difference can be observed between the two wells when it comes to the conformity between actual and simulated production data. For well B1-AHT3, a large deviation can be seen between the two oil rates, as well as the water rates. This will be

[14]Eclipse-simulations

discussed later in the thesis, as it will play a critical role in the subsequent work. The actual/observed production was used as a basis for calibration of the base case models in NETool.

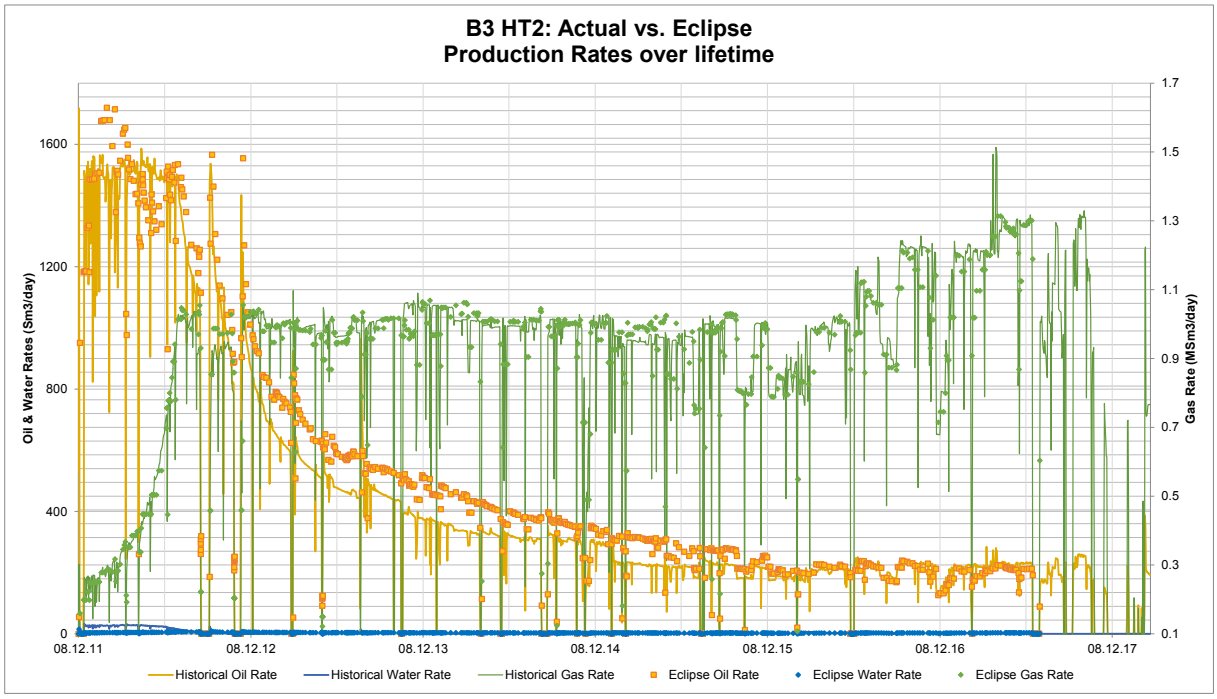

Figure 57: *Actual production and Eclipse-simulated production for well B3-HT2*

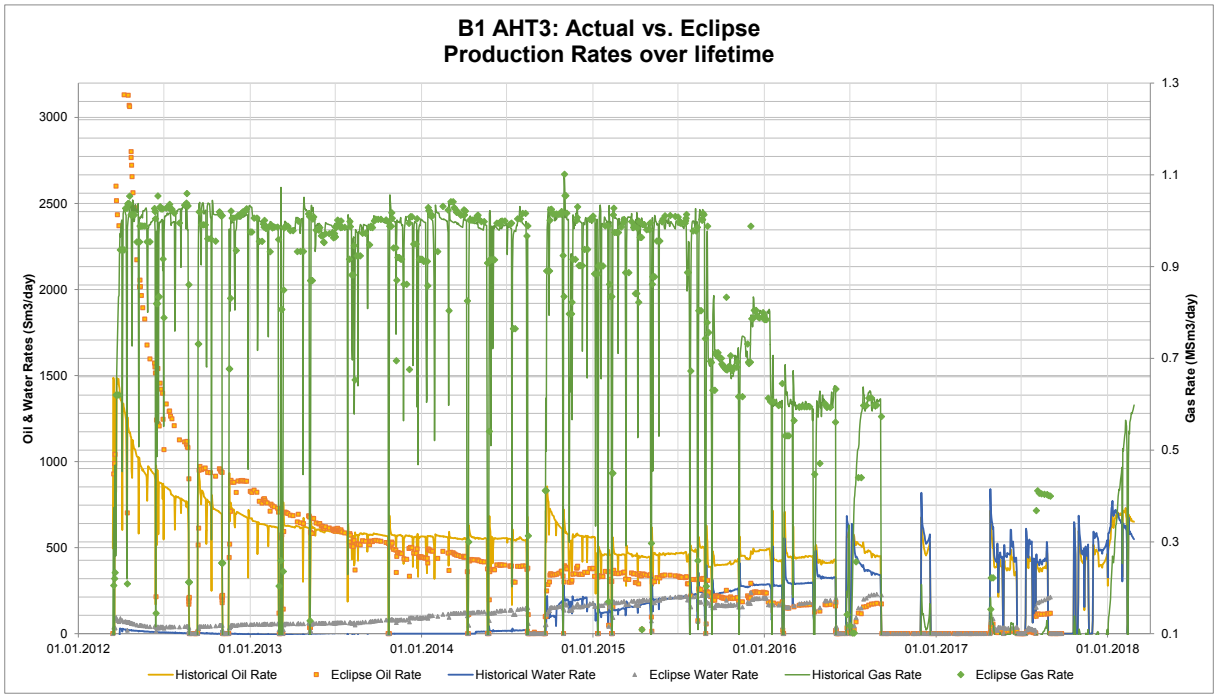

Figure 58: *Actual production and Eclipse-simulated production for well B1-AHT3*

The next step of the work was to acquire information about the well trajectory and completion so that the well design could be developed in Eclipse. The directional surveys

from the drilling engineer were acquired and entered into NETool. It is important that this trajectory corresponds with the well path that was applied in the Eclipse models, otherwise the modeled wellbore could technically produce from the wrong reservoir zones. Therefore, the trajectory used in Eclipse was requested for comparison. A negligible systematic difference was found between the two datasets, and to be on the safe side, the Eclipse well path was entered into NETool.

Moreover, the final well reports were acquired for the completion tallies. The schematic for the final well design for the wells can be found in Appendix G.1. In accordance to the completion running tally, the well designs for B3 and B1 were set up in NETool. The process of calibrating the base case models for the two wells could now be initiated. To understand NETool and its many functions, the manual was reviewed thoroughly, before the process of trial and error followed. Many cases were run for both wells to achieve an adequate match, and the process will now be explained individually for each well.

3.2.1 Well B3

To present the process of calibration in NETool, a convenient table will be presented. Table 5 shows the most important cases and the features that were tweaked to obtain the final base case.

Originally, around 45 cases were run with different input parameters. Some cases lead to a divergence from the actual production rates, while others only lead to insignificant improvements. Only the alterations that yielded considerable improvements are presented in the listed cases. Parameter(s) changed from one case to the other are emphasized in bold font.

In the top row of Table 5, various categories are listed. These presented the most significant changes, and were experimented with during the calibration. However, NETool allows for a wide range for customization with many other features. Through trial and error, these were deemed insufficient for our objective. The rightmost column in Table 5 gives a brief explanation of the reasoning behind the changes that were made for each new case. This will be discussed in detail below.

Table 5: *Overview of history matching workflow in NETool for Well B3*

Case	Results	Well part simulated	Well Design	End-point Scaling	Rel.Perm Model	Perme -ability	Node dist.	PI Model	Skin	Rationale
Case 1	Figure B-1	Complete	As run	From Nearest blocks	Default Eclipse model	Use Grid Upscaling	6	Joshi	10	Joshi was chosen as the PI model, and skin was set to 10, according to recommendations from the production engineers.
Case 2	Figure B-2	Complete	As run	**No scaling (as in RelPerm table /correlation)**	**Stone's 2nd**	Use Grid Upscaling	6	Joshi	**0**	End-Point scaling was changed to the latter, as this will directly apply the input specified in Eclipse, with no further scaling. Stone's 2nd RelPerm model was applied as an attempt to converge towards better results.
Case 3	Figure B-3	Complete	As run	No scaling (as in RelPerm table /correlation)	Stone's 2nd	**From Nearest blocks**	**1**	Joshi	0	Instead of upscaling the permeability values according to the Joshi PI model, the values are taken directly from the reservoir gridblock. The node distance was decreased to increase calculation accuracy.
Case 4	Figure B-4	Complete	As run	No scaling (as in RelPerm table /correlation)	**Default Eclipse model**	From Nearest blocks	1	Joshi	0	The relperm model used in the Eclipse reservoir model seems to be the default one, therefore it will be used.
Case 5	Figure B-5	Complete	As run	No scaling (as in RelPerm table /correlation)	Default Eclipse model	From Nearest blocks	1	**Use gridblock connection factors**	0	When gridblock connection factors are used for the PI modeling, the inflow performance is calculated according to the specifications in the reservoir grid.
Case 6	Figure B-6	Complete	**Packers around blank pipe**	No scaling (as in RelPerm table /correlation)	Default Eclipse model	From Nearest blocks	1	Use gridblock connection factors	0	Since blank pipe sections were modeled with a cemented annulus in the reservoir model, the same effect should be replicated in the NETool model. Setting packers around the blank pipes achieves this objective.
Case 7	Figure B-7 to B-11	**Production Zone only**	Packers around blank pipe	No scaling (as in RelPerm table /correlation)	Default Eclipse model	From Nearest blocks	1	Use gridblock connection factors	0	When simulating the complete well, NETool is not the best tool to model the flow behavior up through the tubing to surface. As recommended in the software itself, the top node MD should be at the top of the production section of the well. From the top node and up to surface, the program applies user specified VFP curves to simulate flow behavior.

1. The first parameter in the table describes which part of the well that was simulated. Initially, the whole well design was specified in the model, from TD up to the wellhead. This would simulate the production from the bottom of the well all the way up through the production tubing, by use of various specified multiphase flow models built-in to the software. An alternative is to simulate from TD up to a certain point, from which the NETool applies user-input Vertical Flow Performance (VFP) curves to calculate the pressure and flow rate along the production tubing. Such VFP curves were acquired from the RE team at a later stage in the work process.
2. How the well is designed in the NETool model is a critical factor that determines the inflow of reservoir fluids as well as annular flow along the well. Initially, the well was simulated according to the completion running tally. However, an important detail was later implemented when it comes to the modeling of blank pipe sections.

In talks with one of the reservoir engineers [70], it was revealed that the stand-alone sandscreen completions were modeled as a cased and perforated completion in Eclipse, with perforations in the sandscreen intervals and cemented annulus at the blank pipe intervals. This is shown in Figure 59 where the well schematic was exported from the reservoir simulator. To replicate this setup in NETool, the blank pipe sections were modeled with packers to isolate the annulus. Running the model with cemented casing instead yielded identical results.

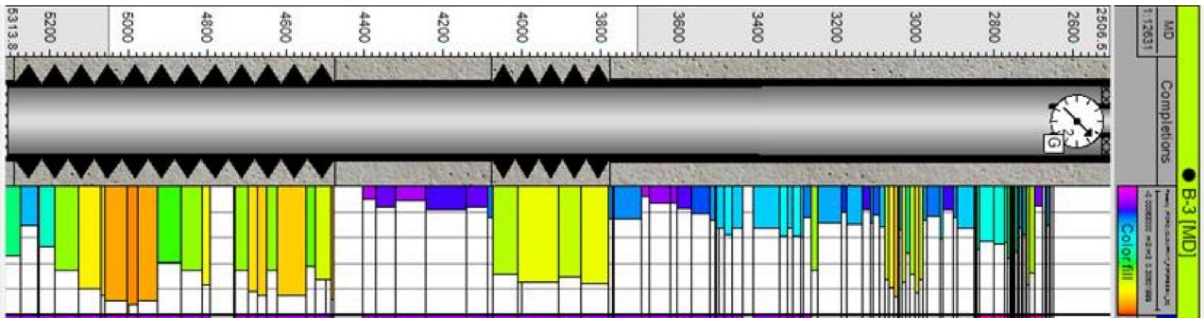

Figure 59: *B3 Eclipse Well Schematic, [70]*

3. The end-point saturations designate the connate, critical and maximum saturations in the relative permeability calculations. There are three options for this input category:

   - *No scaling (as in RelPerm table/correlation)* - The end-points are not scaled, and the value of each end-point is acquired from the relative permeability tables in the Eclipse reservoir model.
   - *From Nearest blocks* - The end-point values are extracted from the reservoir grid-blocks of which the well penetrates, and scaled either by Two End-Points Scaling or Three End-Points Scaling methods. This procedure is further explained in the Technical Manual of NETool, [71].
   - Manual entry of each end-point saturation.

4. The relative permeability model (sixth column) determines how the relative permeability values are chosen. The relative permeability profiles determine how easily the three fluids flow at different fluid saturations. Usually, such curves are determined by core sample testing as well as application of correlation approximations, e.g. Corey's correlation or the LET correlation. It is essential that such curves represent the reservoir rock as they will determine the resulting production and drainage of the reservoir. The options for this entry are as follows:

- *Default Eclipse model*, this is the default method applied in the Eclipse reservoir simulator
- Stone's first model
- Stone's first model modified by Fayers and Matthews
- Stone's second model

A detailed description of these alternatives can be found in [71].

5. When it comes to the permeability, there are three options to choose from. This option is closely related to the choice of PI model, as will be explained later.

   - *Use Grid Upscaling* - The software will use the permeability values as they are defined in the reservoir grid, and run an upscaling procedure based on the inflow model (PI Model). More information of this procedure can be found in [71].
   - *From Nearest blocks* - The permeability values are taken directly from the gridblocks that the well penetrates.
   - Manual entry of permeability values along the wellbore.

6. The node distance defines the number of computational nodes along the wellbore. In practice, this determines the accuracy of the simulations. Increasing the number of nodes along the well, will lead to more accurate results. Initially, the intermediate node distance was set to 6 meters. It was later concluded that 1 m node distance yielded better results. Decreasing the distance further did not significantly improve the results.

7. The PI model describes the characteristics of fluid flow from the reservoir to the wellbore. There are four models that can be used within NETool in this category:

   - *Radial Inflow Model* - The inflow is determined by use of an apparent permeability based on the wellbore inclination. The model assumes either a steady inflow where there is a constant pressure boundary at the drainage radius of the well, or a semi-steady inflow where the flow rate is constant at the drainage radius.
   - *Use gridblock connection factors* - Assumes a radial inflow where the drainage radius of the well is determined by the formula from Peaceman, in accordance with the reservoir grid.

- *Joshi* - The model assumes a constant pressure boundary and a reservoir centered wellbore.
- *Babu and Odeh* - Assumes a close volume and pressure depletion. Allows for specification of the reservoir geometry and well position within the reservoir.

It should be mentioned that if the second option is used, the permeability values are automatically limited to the option "From Nearest Gridblocks".

8. Skin is a factor that describes an impairment of flow in the form of a pressure drop. An additional skin may be specified in the model to represent e.g. perforation skin, near wellbore damage skin or non-darcy skin. Production inflow models received from the production engineer at Neptune Energy assumed an additional skin of 10, to calculate inflow performance. An additional skin factor was later deemed unnecessary in our NETool model.

When using NETool to simulate production performance of the well, it is necessary to specify the value for a boundary condition. There are several categories for the boundary condition, as listed below:

- Tubing pressure at reference MD
- Total downhole flow rate
- Total liquid rate at standard/surface conditions (SC)
- Oil flow rate (at SC)
- Gas flow rate (at SC)
- Water flow rate (at SC)
- Wellhead / tubing-head pressure (WHP)

Although not presented in the case overview (Table 5), all the above listed categories were tested, to see if a better match could be achieved. Considering our input, it was clear that the simulator could handle the gas flow rate with the highest accuracy. Therefore all presented cases featured this boundary condition as a basis for simulation.

When simulating production at several timesteps, NETool offers a series of output results. The main results from the summary are as follows:

- Pressure at first node, i.e. pressure at depth of the downhole pressure and temperature gauge. Hence, this can be regarded as the Permanent Downhole Gauge (PDHG) pressure.

- Oil rate
- Gas rate
- Water rate
- Liquid rate at surface conditions
- WHP
- GOR
- Water cut (%)
- Total downhole production rate at reservoir conditions
- Oil PI
- Gas PI
- Water PI

The listed parameters serve as different ways of quantifying and evaluating production performance. For the purpose of the our work, the main focus was laid on the production rates of the respective fluids as well as the pressures. A consistent conformity of the oil, water and gas production rate through all timesteps is regarded as an adequate match. The software also presents a number of plots that illustrate the inflow performance along the wellbore, these will be investigated as well.

The result of the cases with respect to production rates are presented in Appendix B.1 according to the second column listing in Table 5. The featured results are compared to the observed production to illustrate the conformities. Case 7 was considered to yield a satisfactory match, and was thus used as the reference case for further simulations with inflow control technologies. For this case, the production rates are presented in Figure 60.

A comparison of the corresponding WHP and PDHG-pressures are presented in Figure B-8. This served as an additional "quality control" of the reference case results (i.e. Case 7). A significant match can be observed for the different pressures, further verifying the validity of the calibration results.

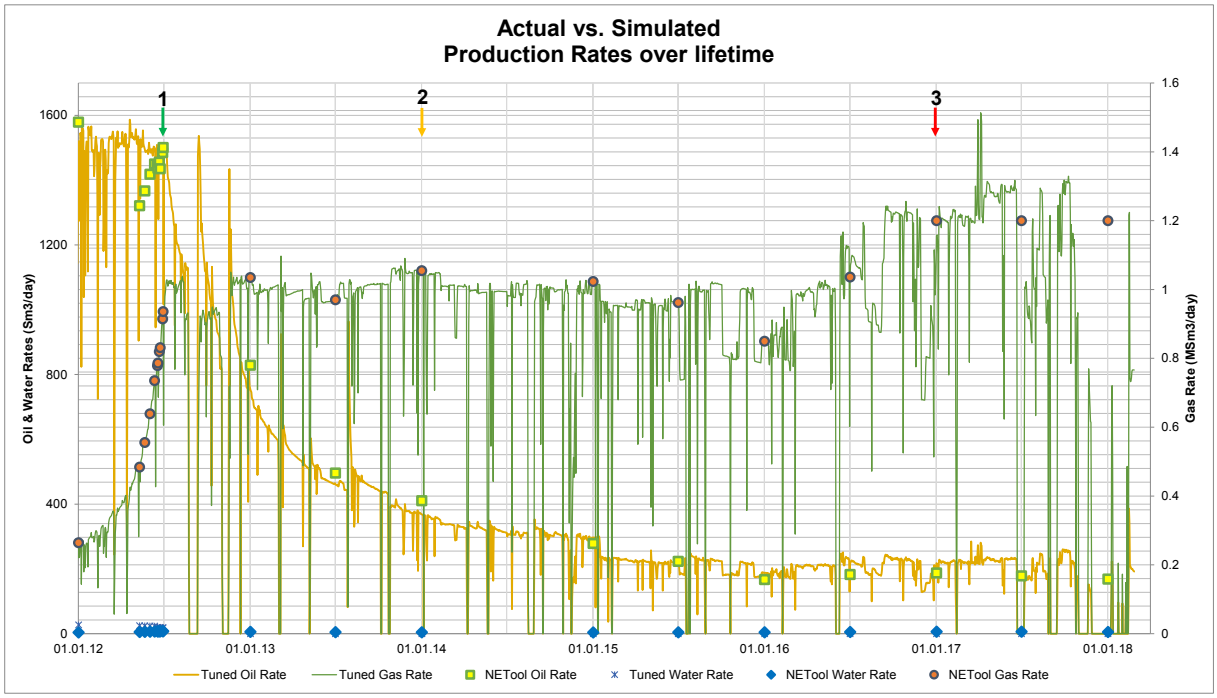

Figure 60: *B3-HT2 Case 7: Actual vs. Simulated Production. This will be the reference case (base case) for further simulations*

With reference to the aforementioned details regarding the boundary conditions, it can be observed how the simulated gas rate is identical to the actual gas rate. However, in the last three timesteps (01.01.17 - 01.01.18) it can be observed that the target gas flow rate does not correspond to the actual rate. This is because of the irregular gas rate during this period. After some discussions with the production engineer, it was advised that an average rate of 1200 kSm^3/day could be used as a basis for simulation. Further deviations and uncertainties will be discussed at a later stage of the thesis.

In Section 1.2.1 the production lifetime of the well was divided into three distinct periods, according to the production characteristics. We will now have a look at the inflow characteristics along the well during these respective periods. To do this, three representative timesteps were chosen for further analysis. As shown in Figure 60, there are plenty of timesteps to be chosen for this purpose, however the main criterion used was the accuracy of the simulated oil- and gas-rate at the respective timestep. The following timesteps were selected, as indicated by vertical arrows in Figure 60:

1. Early-life: 29.06.2012
2. Mid-life: 01.01.2014
3. Late-life: 01.01.2017

Figure 61 to 63 shows the downhole flux along the well at the three timesteps.

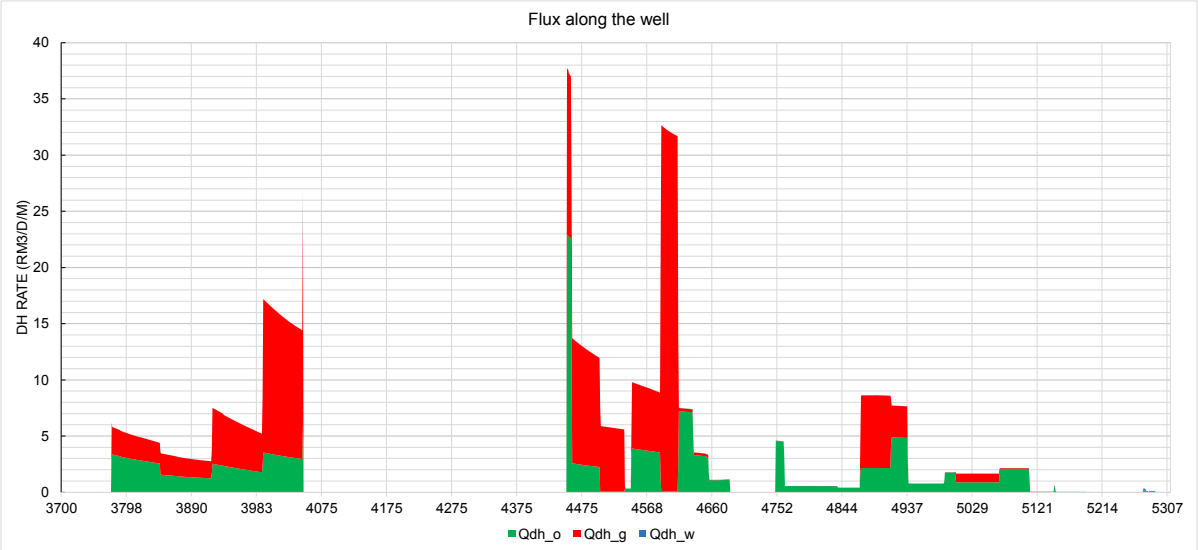

Figure 61: *B3-HT2 Case 7: Flux along the well at early-life*

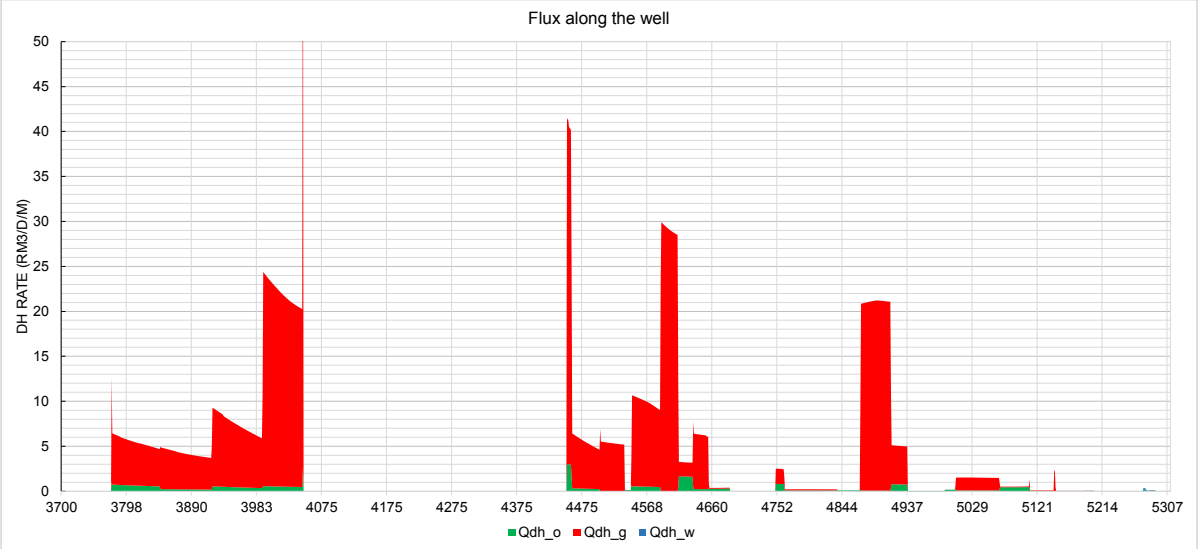

Figure 62: *B3-HT2 Case 7: Flux along the well at mid-life*

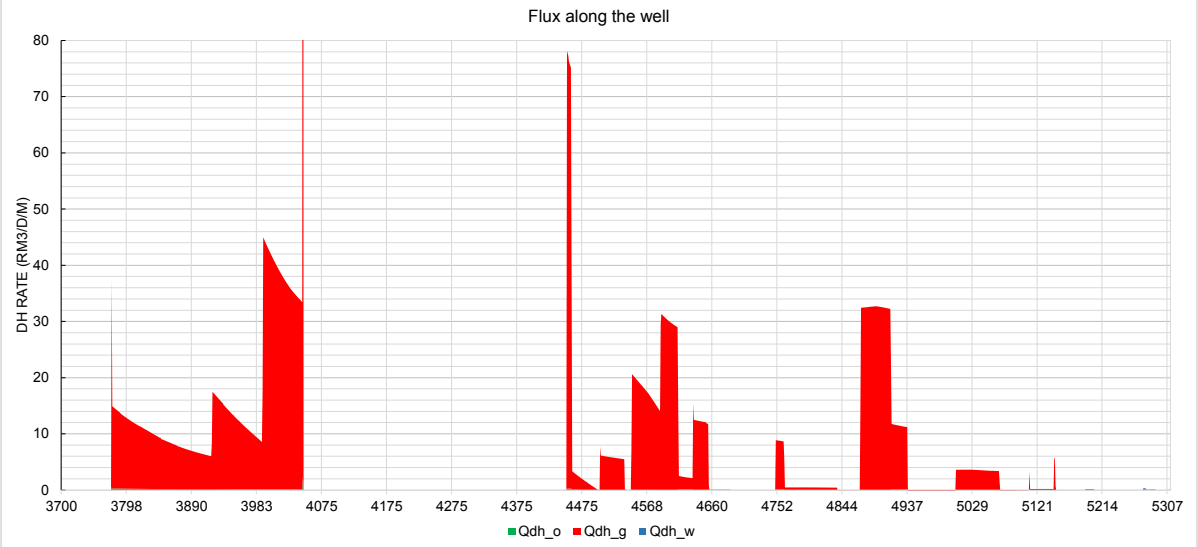

Figure 63: *B3-HT2 Case 7: Flux along the well at late-life*

At an early stage, the well produces significant amounts of oil, as seen by the green profile in Figure 61. However, after some years, the majority of the flux is assigned to the gas (red color). An important observation that can be made for all the phases, is the uneven flux along, with some high spikes at approximately 4000, 4450, 4600 and 4900 meters MD. During early-life, these spikes present significant oil and gas production. However, during mid-life and late-life it is obvious that these spikes are dominated by gas production, clearly implying that the gas influx is mainly entering the wellbore at these respective areas.

Another observation is the minimal production from the toe of the well. From approximately 4930 mMD to 5300 mMD there is minimal inflow. This is particularly evident during mid-life and late-life. Seeing as this interval contributes considerably to the oil production in the early-life, it is an indication that significant oil production has been impeded as a result of the heel-toe effect in later years.

Simulations with inflow control technology will yield similar downhole flux diagrams, which will make it more convenient to analyze the changes in well performance.

3.2.2 Well B1

For well B3, a conformity between the Eclipse production and the actual production could be observed in Figure 57. This is because of the fact that the reservoir model was run through a history matching software called ResX. The software optimizes the reservoir model to correspond with observed production, to enhance reservoir understanding and management.

Well B1 was not included as part of this service, and as a result, the corresponding conformity between modeled and observed data could not be observed in Figure 58. Consequently, this made it quite a rigorous process to calibrate well B1 with respect to actual production data. Furthermore, well B1 has produced significant water volumes through its lifetime. To calibrate the NETool model with regards to three fluids is more complicated compared to two fluids rates. As a result of these factors, over 50 cases were originally attempted before achieving acceptable results.

Table 6 shows the summarized workflow that was pursued to obtain a suitable match for well B1. By using the learnings from B3, the same alterations were implemented in B1 to see if the aim of calibration could be achieved. The results are presented in Appendix B.2 according to the second column listing in the table. Similar to well B3, various boundary conditions were tested. None other than the gas rate boundary condition

gave reasonable results.

Table 6: *Overview of history matching workflow in NETool for Well B1*

Case	Results	Well part simulated	Well Design	Rel.Perm values	Perme-ability	Node dist.	PI Model	Skin	Rationale / Other comments
Case 1	Figure B-12	Complete	As run	from Nearest Gridblocks	From Grid Upscaling	6	Joshi	10	
Case 2	Figure B-13	Complete	As run	from Nearest Gridblocks	**From Nearest blocks**	**1**	**Based on Gridblock connection factors**	**0**	Joshi was chosen as the PI model, and skin was set to 10, according to recommendations from the production engineers.
Case 3	Figure B-14	**Production Zone only**	As run	**Based on sat.reg#2**	From Nearest blocks	1	Based on Gridblock connection factors	**10**	The top node MD should be at the top of the production section of the well, and the remaining well section is simulated using VFP. Sat.reg#2 was applied by recommendation from the reservoir engineer.
Case 4	Figure B-15	Production Zone only	**Packers around blank pipe**	**Based on sat.reg#2, see rationale**	From Nearest blocks	1	Based on Gridblock connection factors	**0**	Since blank pipe sections were modeled with a cemented annulus in the reservoir model, the same input should be replicated in the NETool model. Setting packers around the blank pipes achieves this objective. K_row curve was increased by a factor of 1.5.
Case 5	Figure B-16	Production Zone only	Packers around blank pipe	**Based on sat.reg#2, see Figure 65, case 5**	From Nearest blocks	1	Based on Gridblock connection factors	0	
Case 6	Figure B-17	Production Zone only	Packers around blank pipe	**Based on sat.reg#2, see Figure 65, case 6**	From Nearest blocks	1	Based on Gridblock connection factors	0	
Case 7	Figure B-18	Production Zone only	Packers around blank pipe	**Based on sat.reg#2, see Figure 65, case 7**	From Nearest blocks	1	Based on Gridblock connection factors	0	Higher target gas rate for the three last timesteps.
Case 8	Figure B-19	Production Zone only	Packers around blank pipe	**Based on sat.reg#2, see Figure 65, case 8**	From Nearest blocks	1	Based on Gridblock connection factors	0	
Case 9	Figure B-20	Production Zone only	Packers around blank pipe	**Based on sat.reg#2, see Figure 65, case 9**	From Nearest blocks	1	Based on Gridblock connection factors	0	
Case 10	Figure B-20 to B-25	Production Zone only	Packers around blank pipe	**Based on sat.reg#2, see Figure 65, case 10**	From Nearest blocks	1	Based on Gridblock connection factors	0	

Although the Eclipse data in Figure 58 indicate a somewhat conformity for the water production, this fluid proved to be the most erroneous in the simulation results. In Figure B-12 and B-13 it is evident how the water rate is overly exaggerated. After many

trials with poor results, it was suspected that the input data from Eclipse were to blame. Investigations were made to find which factor that could affect the results in the way that was observed. Discussions with the RE team suggested that the relative permeability curves could be a potential determinant.

Initially, the relative permeability curves used for well B1 in Eclipse were requested from the RE team. In the reservoir model, well B1 penetrates two so-called saturation regions, namely region 2 and 4. Assessment of the two relative permeability curves showed identical input. A closer look at how the well penetrates the two zones revealed that the majority of the well goes through region 2, as shown in Figure 64. The relative permeability data for this region were therefore entered manually as an input in the NETool model, instead of the data from Eclipse.

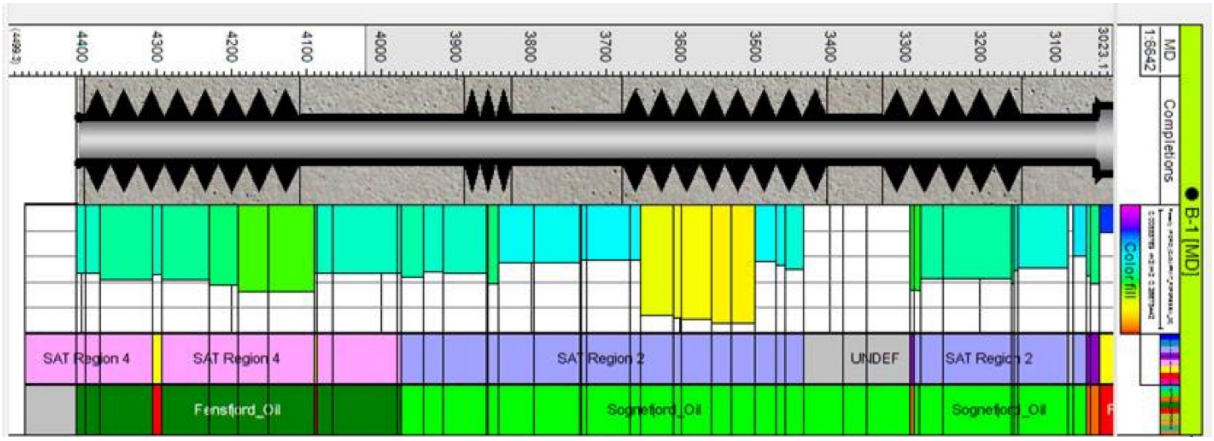

Figure 64: *B1 Eclipse Well schematic with the saturation regions designated by pink and blue intervals, [70]*

Case 3 shows the results of this implementation, including other minor alterations. As a consequence, a significant change can be observed from Case 1 and 2 (Figure B-12 & B-13) to Case 3 (Figure B-14). This was a clear indication that the relative permeability input could drastically affect the simulation results.

Further investigations of the matter were made. A review of the PDO support documentation from the subsurface department indicated that the relative permeability data for the segment penetrated by well B1 was linked to several uncertainties. It was therefore decided to experiment with these curves further, to see if satisfactory results could be achieved. The relative permeability data are usually presented using two charts. In Appendix G.3 the relevant charts for B1 are presented, these charts are representative of saturation region 2 and 4.

Figure G-28 shows the Oil-Gas relative permeability curves. The leftmost curve (purple)

represents the relative oil-gas permeability (K_{rog}) as a function of the gas saturation[15]. At a lower gas saturation, the K_{rog} will be higher, leading to a higher absolute oil permeability. The rightmost curve (blue), shows the gas-relative permeability (K_{rg}) as a function of the gas saturation. In contrast to K_{rog}, the K_{rg} increases with the gas saturation, allowing for easier gas flow. A general observation for the two curves is that they are inversely proportional. For an increasing gas saturation, the gas relative permeability will increase while the oil-gas relative permeability decreases. At a gas saturation of approximately 0.36, the two curves intersect, and K_{rg} becomes higher than K_{rog}.

Figure G-29 shows the Oil-Water relative permeability curves. The leftmost curve (purple) represents the relative oil-gas permeability (K_{row}) as a function of the water saturation (S_w). At a lower S_w, the K_{row} will be higher, leading to a higher absolute oil permeability, and hence an easier flow of oil. The rightmost curve (blue), shows the water-relative permeability (K_{rw}) as a function of the S_w. For an increasing S_w, the water relative permeability will increase while the oil-water relative permeability decreases, consequently leading to a higher water mobility and lower oil mobility. At a water saturation of approximately 0.52, the two curves intersect, and K_{rw} becomes higher than K_{row}.

Typically, the relative permeability curves are quite smooth, as they are a result of correlation models. However, in our case, it can be observed how the curves are linear at some intervals while exponential at other saturations. This was pointed out by a PhD fellow at the International Research Institute of Stavanger. This could indicate some degree of error as well. Discussions were made on how various alterations could affect the results, these were used as a basis for further curve alterations [72].

Figure B-14 shows the results before any changes were made to the relative permeability charts. Several observations can be made for this case:

- Throughout the first part of the timeline up to 2016, the water production rate is too high, and relatively constant compared to the actual rate. We would like to lower this profile while also shaping it to imitate the actual production profile.
- For the same time period, the oil rate is consistently too low, but with the correct development (shape). The goal for this curve is to elevate its profile, i.e. increase the oil rate for all timesteps.
- During the second part of the production lifetime, the water production is too low, and decreasing. On the other hand, the observed development is a somewhat

[15] at the connate water saturation, S_{wco}

increasing water rate, as the water breakthrough becomes more severe. Increasing the water rate for the respective timesteps would yield satisfactory results.

- The oil rate can be argued to be too low, and decreasing in the same manner as the water production. In reality, the oil rate is somewhat constant.

Generally speaking it can be seen that the second part of the production period is affected by long shut-down periods. This makes it more complex to anticipate the reservoir behavior. A special focus will therefore be laid on the first part of the production period.

From Case 4 to 10 various changes were done to the relative permeability charts to achieve the objective. Changing the Oil-Gas relative permeability functions did not yield converging results, therefore this chart was left unchanged for all the cases. When it comes to the Oil-Water relative permeability curves, several changes were made, as shown in Figure 65. For Case 4, the relative oil-water permeability was simply multiplied by a factor of 1.5^{16}, this is not showed in the figure.

The alterations done in the respective cases are mostly based on trial and error. Hence, the rationale has not been specified in Table 6. Rather, the changes can be observed from Figure 65. The thick long-dashed curves represent the initial curves, which are the same as in Figure G-29. The thinner short-dashed lines represent the input used for Case 10, which is the final base case.

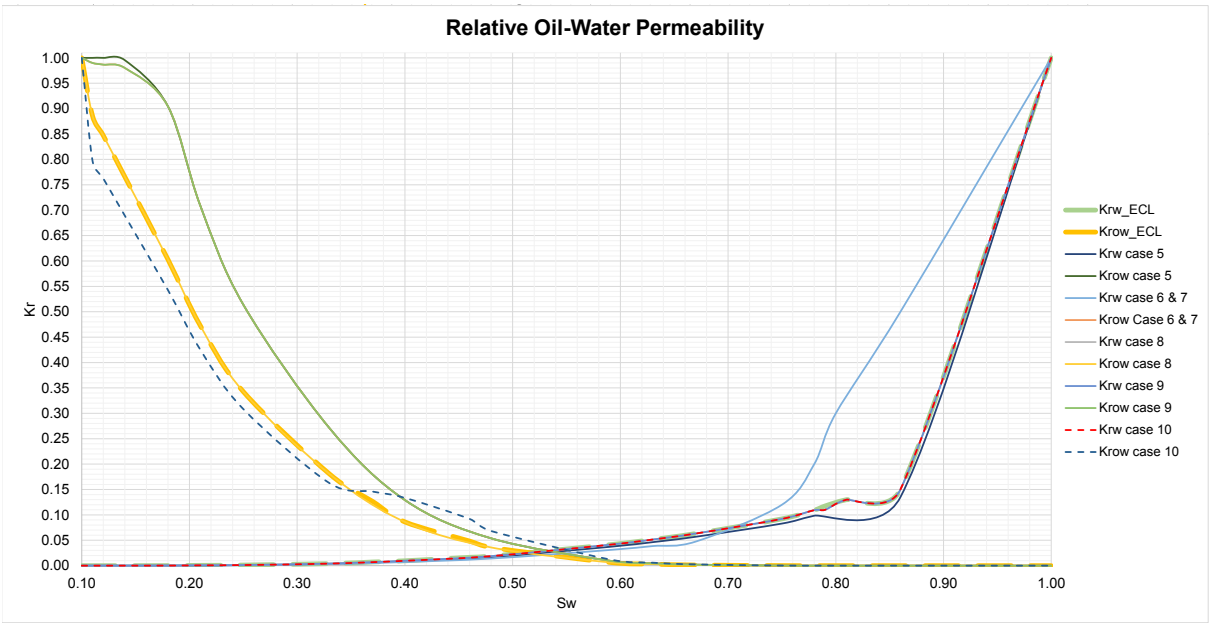

Figure 65: *Oil-Water Relative Permeability changes for well B1*

The learnings from the alterations made from Case 4 to Case 10 can be concluded as follows:

[16]Except for the end points, which were not changed

1. K_{row} at $S_w < 0.37$: At lower pore water saturations in the producing reservoir grid, the K_{row} was decreased to achieve the base case results.
2. K_{row} at $0.87^{17} > S_w > 0.37$: The relative oil-water permeability was increased for this saturation interval as it helped raise the oil production profile, throughout the whole lifetime. Moreover, it lead to a decrease in water production.
3. K_{rw}**:** Changes to the relative water permeability did not show changes that was sought after.

The results obtained for Case 10 are presented in Figure 66. An important detail that should be mentioned is the almost constant gas rate target at 1000 kSm^3/day, which does not match the actual rate for the three last timesteps (01.01.2016 - 01.01.2018). Discussions with the production engineer revealed that the well is generally choked/regulated by a gas rate of 1000 kSm^3/day, which justifies this implementation. Moreover, for the purpose of our work, it helped achieve a better match [7].

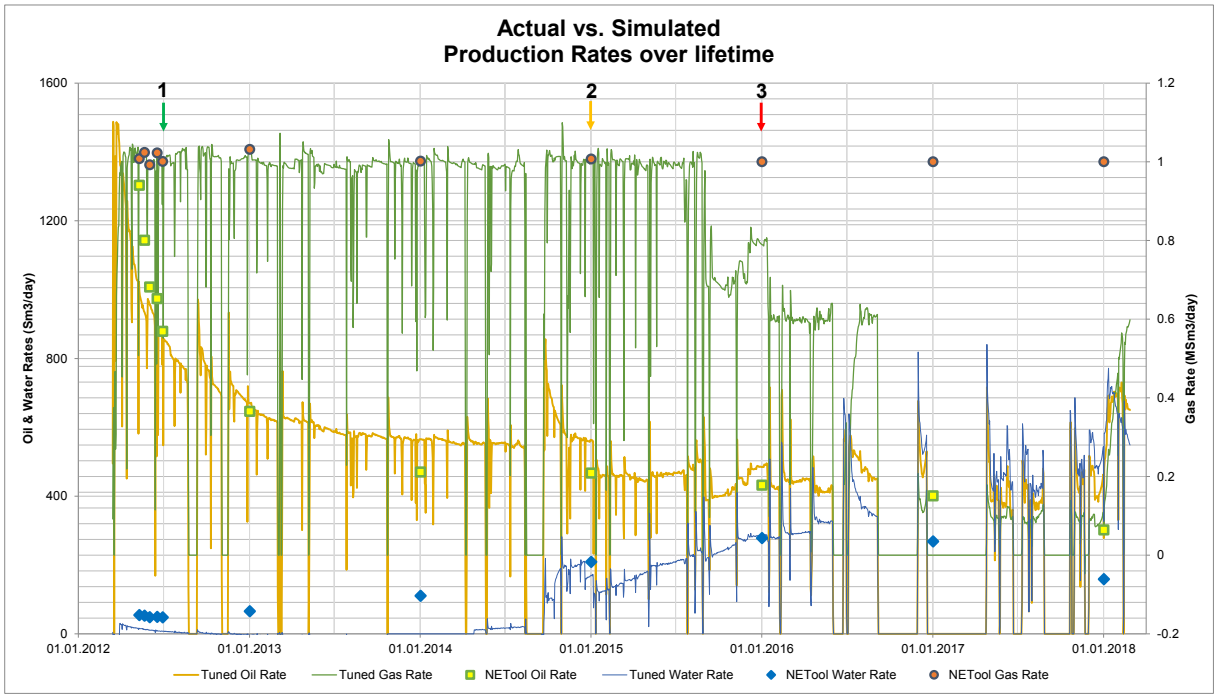

Figure 66: *B1-AHT3 Case 10: Actual vs. Simulated Production. This will be the reference case (base case) for further simulations*

In Figure B-22 the pressures are plotted. This shows an adequate match which further validates the results. Further deviations and uncertainties in the results will be discussed at a later stage of the thesis.

Figure 67 to 69 shows the downhole flux along the well at three different timesteps.

[17] $1 - S_{orw} = 0.87$, above this water saturation oil is immobile.

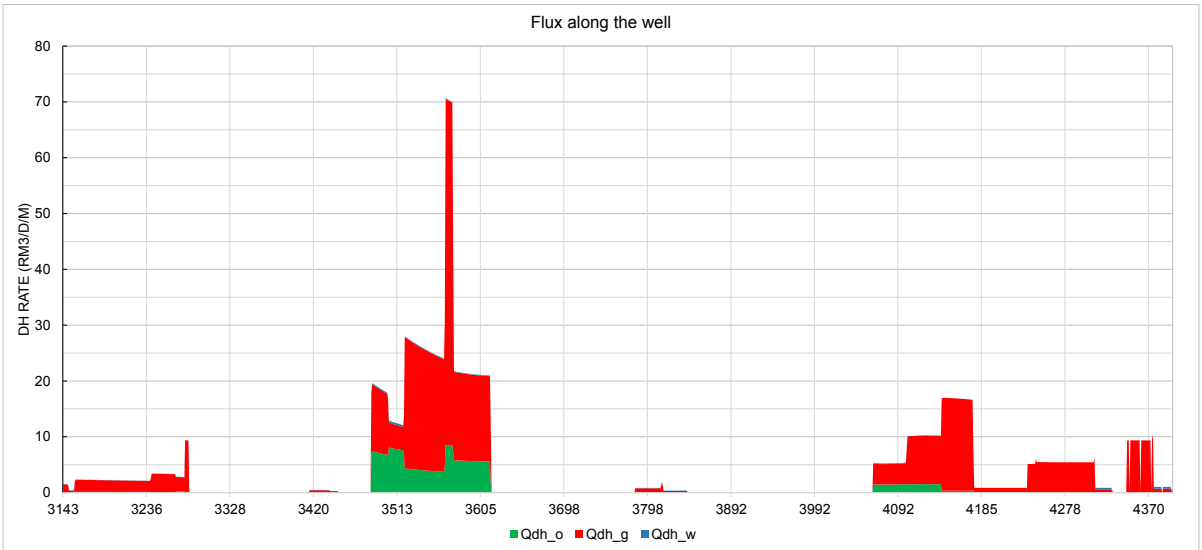

Figure 67: *B1-AHT3 Case 10: Flux along the well at early-life*

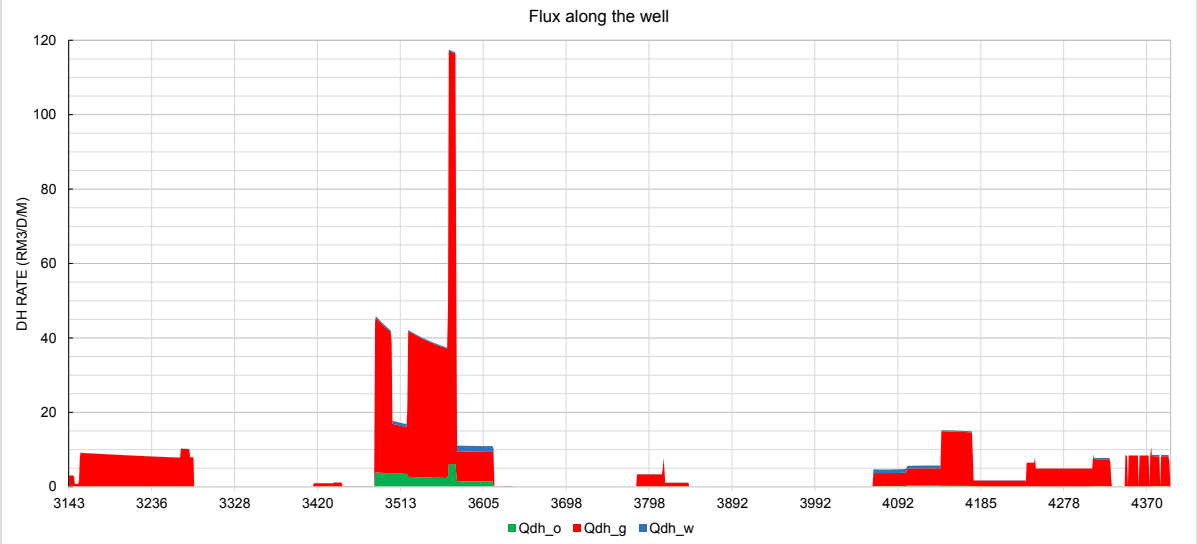

Figure 68: *B1-AHT3 Case 10: Flux along the well at mid-life*

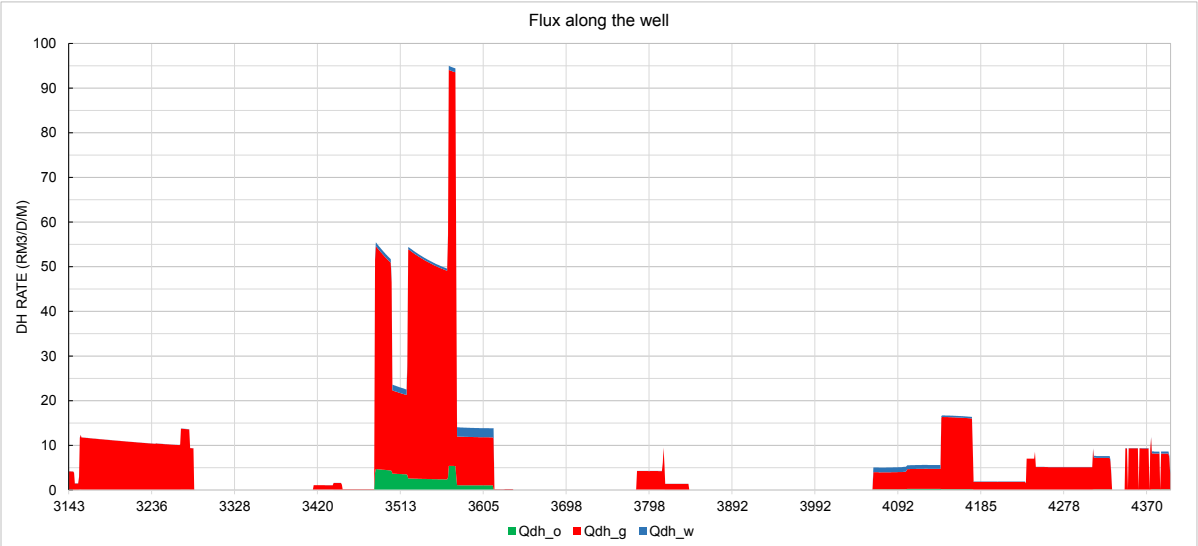

Figure 69: *B1-AHT3 Case 10: Flux along the well at late-life*

As previously explained in Section 1.2.2, the production lifetime of the well was divided into three periods, according to the production characteristics. The inflow characteristics shown above, are taken at some point of time during these periods. Similar to the case for B3, the main criterion for chosen each representative timestep was the accuracy of the simulated rates. The following timesteps were selected, as indicated by vertical arrows in Figure 66:

1. Early-life: 29.06.2012
2. Mid-life: 01.01.2015
3. Late-life: 01.01.2016

It could be argued that the late-life timestep is too close to the mid-life timestep. However as previously mentioned, the main goal is to choose timesteps that are accurate and representative. Of the three last timesteps in the late-life period, the first one (01.01.2016) is considered to be have the best match.

During the early-life, the main oil influx is located at 3480 to 3620 meters MD. There is also considerable gas coning at this interval, which increases through mid-life and late-life. At the later time periods, water influx can be observed in the same interval, indicating a high-permeable layer in this zone which allows for easier inflow of fluids. A similar behavior can be seen in the interval 4050 - 4170 mMD, which produces some oil at early-life. At mid-life and late-life, this zone starts producing water.

The uneven flux in B1 is more critical compared to well B3, where a very high gas flux can be observed from 3480 to 3620 mMD. The high flux spikes seen along the well, are dominated by gas production through all life periods. Unlike the conditions for B3, the heel-toe effect is not so obvious in B1. In fact, the inflow at the toe-end is somewhat higher than at the heel during early-life. In the following years, a shift can be seen, where production from the heel becomes dominant.

4 ICD

We will now have a look at the same wells, and their behavior when equipped with inflow control devices. To integrate this in the existing well designs in NETool, the screen joints will be equipped with standard nozzle-type ICDs. As discussed in Section 2.3, the importance of compartmentalization is critical when it comes to achieving optimal effects with inflow control. Furthermore, it was argued that the best results with inflow control

could be achieved by having a maximum number of swell packers along the well, that is, one swell packer at each screen joint. For the NETool well designs, a 0.3m packer was set at each screen joint[18].

Another important detail regarding the inflow control simulations is the choice of ICD configuration along the well. Some operators prefer to have a tailored ICD configuration with various strengths, according to the modeled inflow and permeability profiles. However, the majority of vendors do recommend a homogeneous configuration along the whole well path for a number of reasons. This will be further discussed in Part III. For our simulations, the latter approach was followed.

A key consideration when it comes to designing an ICT completion is the determination of the resulting pressure drop. Initially, the main rule of thumb was to try and match the expected initial reservoir drawdown and the IC pressure drop. The intention behind this idea was to prevent the reservoir of having the main control of the inflow performance. Moreover, the IC pressure drop should not be so high that significant drainage energy (pressure) is lost. However, in the recent decades, operators have started to challenge this approach by imposing a larger IC pressure drop. Experience has shown that there is a positive correlation between an increasing IC pressure drop and improved well performance, and consequently higher oil recovery. In the following simulations, we will investigate this matter further, to see what is the most suitable methodology [73, 74].

4.1 Well B3

Appendix C.1 shows the input data for well B3. The main difference when it comes to the completion setup (Figure C-1 to C-4) is the inclusion of the inflow control layer. To include this layer, the diameters of the inflow control layer must be specified, as shown in Figure C-5.

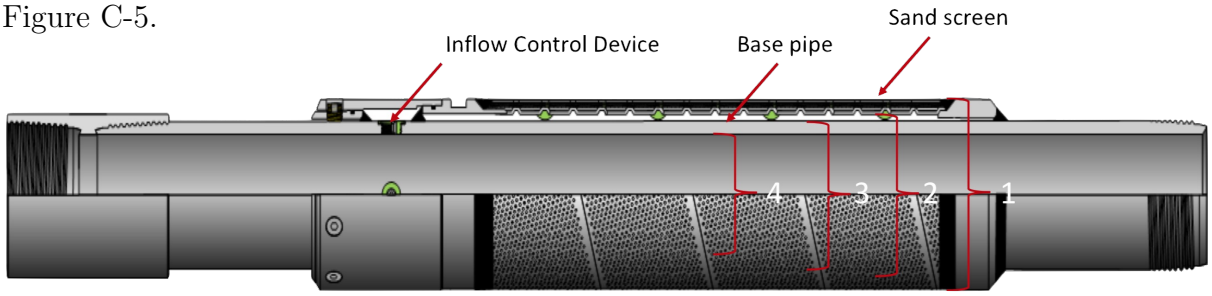

Figure 70: *Explanation of inflow control diameters, adapted after [25]*

It might be tricky to understand what the different diameters describe. Therefore a schematic has been developed in Figure 70, that illustrates the four different dimensions

[18]With the exception of a few joints

that should be entered in NETool:

1. Sand control OD, i.e. Screen OD
2. Sand control ID, i.e. Screen Wrapping ID
3. Inflow Control OD, i.e. Base pipe OD
4. Inflow Control ID, i.e. Base Pipe ID

The most important detail when it comes to the ICD well design is the configuration of nozzle size and number of nozzles per joint. Discussions with one of the leading industry experts when it comes to ICD and Sandscreens, Terje Moen [74], provided some suggestions that were pursued. The configurations used to simulate ICD completions in B3 are shown in Table 7. Case 8 - 10 include ICD configurations that are typically offered by vendors. However, other sizes may be manufactured according to the demand. Case 15 and 16 include a special nozzle size used for comparing the performance of ICD to the performance of AICV, which will be discussed later in Section 5.

Table 7: *ICD Simulation Input for well B3*

Case	Results	ICD Type	Configuration	Simulation target
Case 8	Figure D-1 to D-5	Nozzle-Type ICD	3 x 2.5 mm	Base Case (BC) Gas Rate
Case 9	Figure D-6 to D-10	Nozzle-Type ICD	3 x 5 mm	BC Gas Rate
Case 10	Figure D-10 to D-15	Nozzle-Type ICD	3 x 4 mm	BC Gas Rate
Case 15	Figure D-16 to D-20	Nozzle-Type ICD	3 x 2.65 mm	0.5 x BC Gas Rate
Case 16	Figure D-21 & D-22	Nozzle-Type ICD	3 x 2.65 mm	BC Gas Rate

To demonstrate the effect of ICD in the simulations, the boundary condition was a critical factor. As previously mentioned, the production engineer informed that the wells were controlled by a gas rate of 1 Million Sm^3/day. It could be argued that the well would perform and behave in a different way with the inclusion of ICDs, which would possibly change this measure. Using the base case oil rate could also be another boundary condition, which we will have a look at later. Nevertheless, both alternatives are valid for the purpose of evaluating the well performance. In the following ICD case, the main question we would like to have answered is as follows:

If the well had been equipped with ICDs and produced at the same gas rate[19]*, how would this affect the production of oil?*

The results from the respective simulations are shown in Appendix D.1, according to the listing in the second column of Table 7. For each case, two result charts are shown. Firstly, the production rates are plotted in comparison to the actual history of the well. The second chart shows the base case WHP and PDHG-pressure compared to the pressures generated by the ICD simulations. As previously mentioned, the inclusion of inflow control in the sand-face completion comes at the expense of an additional drawdown pressure, i.e. lost energy. Comparing the resulting downhole and surface pressures to the reference case is therefore an important evaluation factor.

Furthermore, the flux and IC pressure drop plots for the three life phases are presented for each case in the same appendix. Although NETool offers convenient output plots for this purpose, the data was rather applied in Excel to obtain more illustrative plots. Case 8-10 will be primarily evaluated in this manner, as they include the most typical configurations.

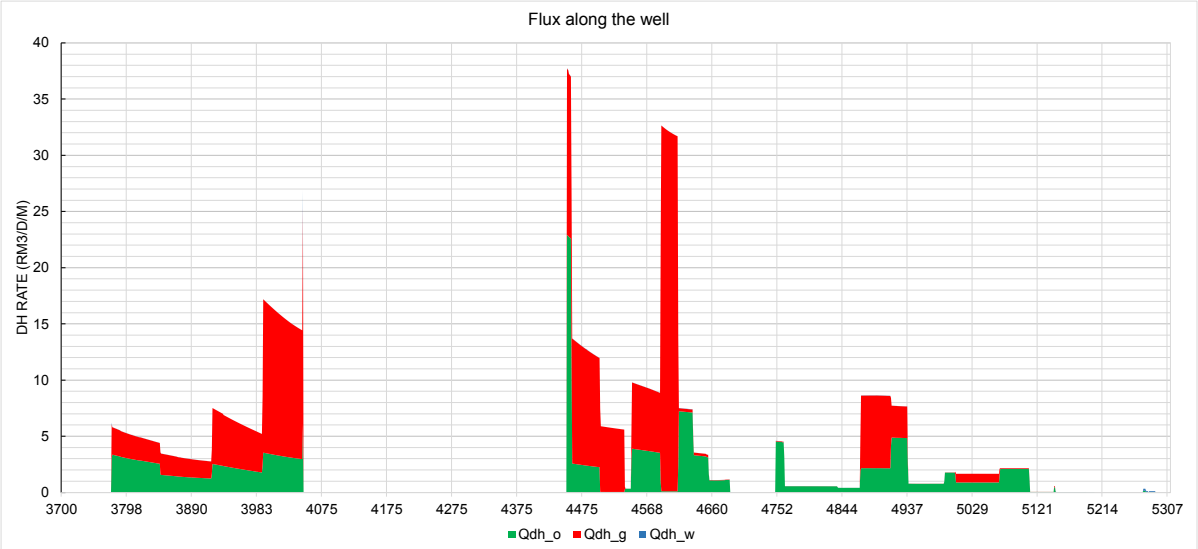

Figure 71: *B3-HT2 Case 7: Flux along the well at early-life*

[19]I.e. the base case gas rate

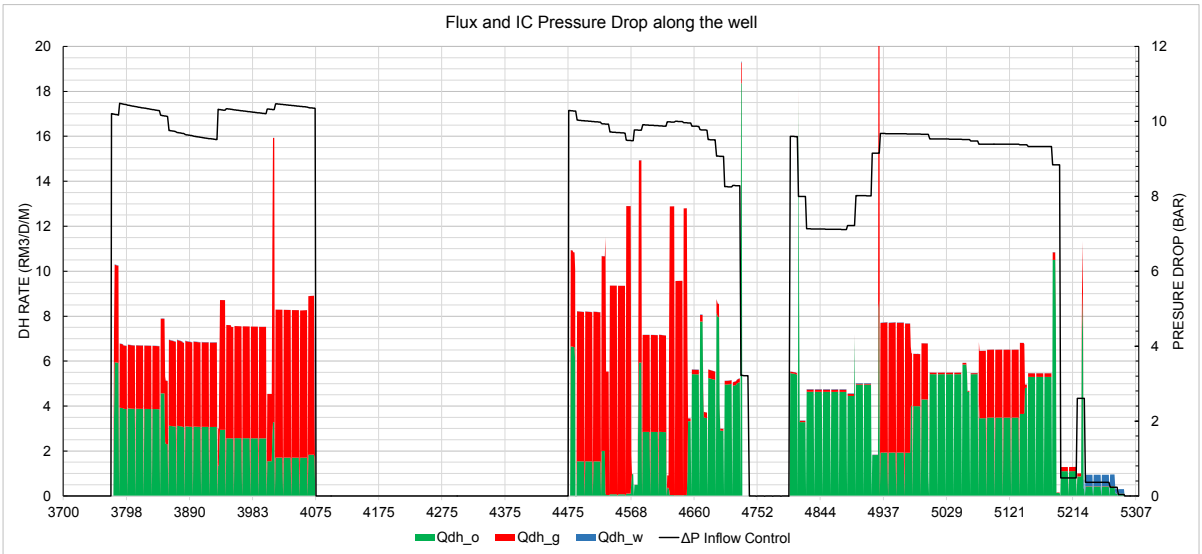

Figure 72: *B3-HT2 Case 8: Flux and IC pressure drop along the well at early-life*

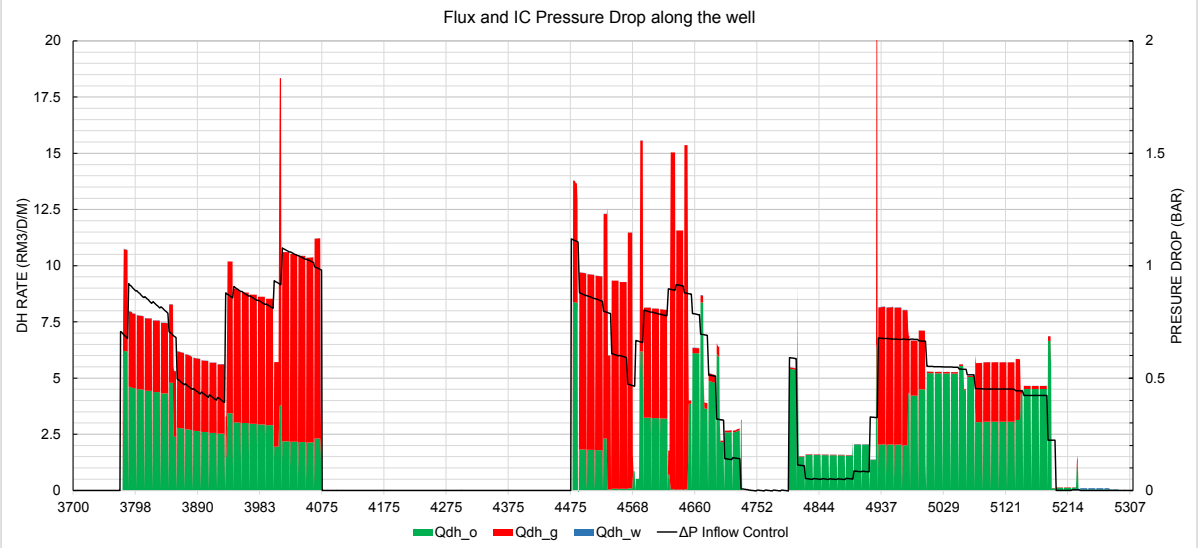

Figure 73: *B3-HT2 Case 9: Flux and IC pressure drop along the well at early-life*

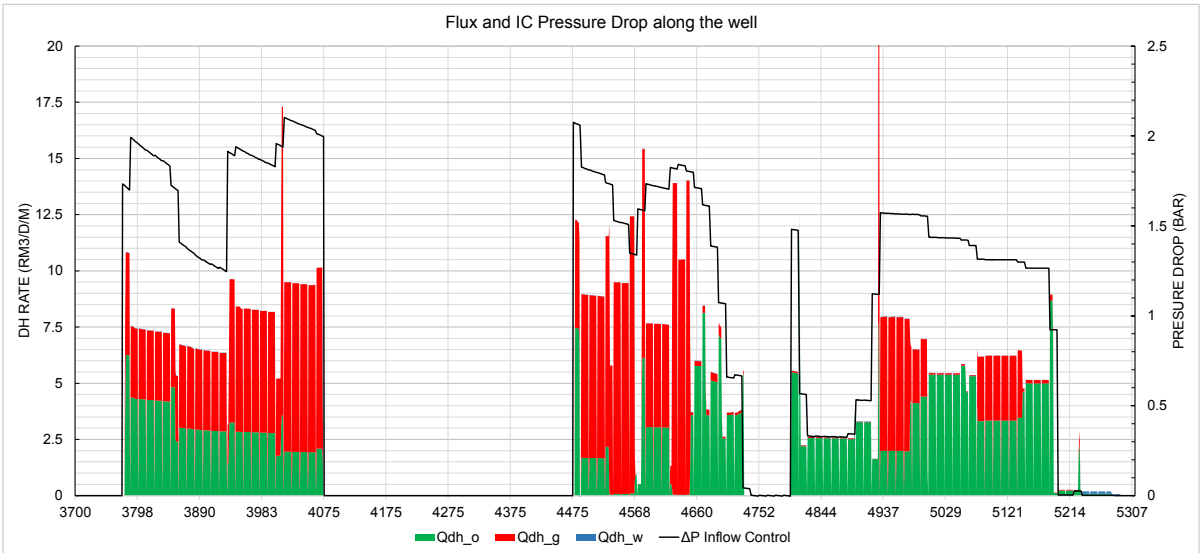

Figure 74: *B3-HT2 Case 10: Flux and IC pressure drop along the well at early-life*

Figure 72 to 74 show the downhole flux along with the pressure drop generated by the inflow control devices for Case 8 - 10. For easier comparison, all plots are taken at the same timestep, which represents the early-life stage. Moreover, the reference case flux results are presented in Figure 71, which makes it more convenient to see the ICD effect in the subsequent figures.

In Case 8, the flux was evened out significantly at an approximate average value of 6 - 8 Rm^3/day/meter. On the contrary, the plot presented for the base case (Figure 61) had high spikes reaching 15 - 35 Rm^3/day/meter. These were previously observed at approximately 4000, 4450, 4600 and 4900 meters MD. In Figure 72 a higher pressure drop was been generated in these respective zones, consequently reducing the high flux. Moreover, the values in the previously low-producing intervals at e.g. 3800 - 3980 mMD and 4750 - 5300mMD were increased considerably. Further, it can be seen that a higher pressure drop is generally imposed at the heel, which mitigates the previously observed heel-toe effect. An important remark can be made for the lower interval of the well, where the majority of the oil is being produced along with minor gas production.

Case 8 included a small nozzle size of 2.5mm for each ICD fitting, which resulted in a relatively high pressure drop of 8 - 10 bar. By using a greater nozzle, the resulting pressure drop will decrease, as indicated in Equation 3. Figure 73 shows the results when using a nozzle size of 5mm. Several differences can be observed to the previous case. Firstly, the pressure drop has been decreased by an approximate factor of 10, at 0.5 - 1 bar. This resulted in a more variable flux along the well, with values in the range of 4 - 10 Rm^3/day/meter. There is still significant improvement in performance compared to the base case, in the sense that the toe and heel of the well are more oil productive. However, the oil influx in the toe is reduced when compared to Case 8.

The third case includes the nozzle size that was found to be the most applicable, yielding the early-life results in Figure 74. In this case, the ICDs have an average pressure drop of approximately 1.2 bars. At the expense of a insignificant pressure drop, the oil production from the toe is higher than in Case 9. Furthermore, the gas spikes in the heel and mid section of the well are lowered.

Although much lower than in Case 8, the IC pressure drop in Case 10 was sufficient for achieving comparable results with regards to evening out the flux, and reducing the heel-toe effect.

By assessing the corresponding mid-life and late-life plots for the respective cases, a better impression can be made. During these two life stages, the gas breakthrough has taken place, and it is therefore interesting to see how the ICDs perform in retrospect of

the breakthrough. Considering the reference case result for the mid-life downhole flux, an increase in gas production could be observed, where the high gas spikes were severely upscaled. Additionally, the oil production dropped to a minimum. For all three cases[20], an interesting observation can be made during the mid-life, where the flux is more equalized compared to the early-life. In all cases, the oil production comes primarily from the toe end of the well, and declines towards the heel. During the late-life, the oil inflow can be exclusively observed at the lower middle part of the well, predominantly from 5000 to 5070 mMD[21]. Although the IC pressure drop for this oil peak considerable differs for the three cases, the magnitude of the oil peak is quite similar. However, the configuration in Case 8 manages to promote greater oil inflow at 4700mMD and 4900mMD compared to the two latter cases.

Table 8: *ICD Results for B3*

Case	ICD Nozzle configuration	Early-life		Mid-life		Late-life	
		Average IC pressure drop (bar)	Increase in oil production rate (%)	Average IC pressure drop (bar)	Increase in oil production rate (%)	Average IC pressure drop (bar)	Increase in oil production rate (%)
Case 8	**3 x 2.5 mm**	8,18	56 %	5,53	156 %	7,67	256 %
Case 9	**3 x 5 mm**	0,51	32 %	0,36	83 %	0,52	138 %
Case 10	**3 x 4 mm**	1,23	41 %	0,85	113 %	1,22	193 %

Table 8 shows a summary of the results for Case 8 to 10. The average IC pressure drop is tabulated together with the relative increase in oil rate. The comparison shows how the increase in production comes at the expense of reduced reservoir pressure. When comparing the three cases, it can be seen that a higher IC pressure drop results in an oil rate increase. This is valid for all three life periods. However, while the pressure drop in Case 10 is about 6 times lower than in Case 8 during early-life, the resulting oil rate decrease is only 15%. A similar observation can be made for the two later life periods. This further validates the choice of Case 10 as the most applicable ICD configuration for well B3.

Since the base case gas rate was used as the target for the simulations, this is kept constant, and not listed in Table 8. An increase in water production could also be seen in the results, but the absolute values were still negligible. It should however be mentioned that the greatest increase in water rate was observed for the smallest nozzle size[22]. This is

[20] See Figure D-4, D-9 and D-14
[21] See Figure D-5, D-10 and D-15
[22] I.e. Case 8

because the water influx is mainly located at the very end of the well, and only when the heel-toe effect is mitigated to the utmost, the water will be produced.

To answer the main question formulated in the beginning of this section, there is a clear positive effect of including ICDs ás part of the completion for B3. Simulations conducted with the same gas rate as in the base case, showed a considerable increase in oil production through all time-periods. This is an important finding which will be further discussed in Part III, along with the associated uncertainties.

4.2 Well B1

The ICD input data for well B1 are shown in Appendix C.2. The configurations used to simulate ICD completions in the well are summarized in Table 9. Compared to B3, different nozzle sizes were simulated for well B1.

Table 9: *ICD Simulation Input for well B1*

Case	Results	ICD Type	Configuration	Simulation target
Case 11	Figure D-23 to D-27	Nozzle-Type ICD	3 x 4 mm	BC Gas Rate
Case 12	Figure D-28 to D-32	Nozzle-Type ICD	3 x 3 mm	BC Gas Rate
Case 13	Figure D-33 to D-37	Nozzle-Type ICD	3 x 2.5 mm	BC Gas Rate

The results from the respective simulations are shown in Appendix D.2, according to the listing in the second column of the table. Each case includes five figures; simulated production, pressures, and flux plots at the three life stages.

Figures D-23, D-28 and D-33 show the simulated production rates compared to the historical production. In contrast to the equivalently presented results for B3, the first ICD case includes the largest ICD nozzle size (4mm), while the subsequent cases include smaller nozzle sizes of 3mm and 2.5mm, respectively.

When compared to the reference case results in Figure B-21, several remarks can be made. For Case 11, the oil production has been slightly increased, at some timesteps. This applies especially to the last timestep (01.01.18). The magnitude does however not compare to the significant increase in water production. While the water production in the reference case has a drop at the last couple of years, Figure D-23 shows that the water production is increasing more towards the end. Although it is not correct to regard this as the dynamic behavior of the well, it still gives an idea of the effect of the ICDs. We will

have a further look into this later.

When it comes to the observed increase in water production rate, Case 12 shows worse tendencies in this manner. While the change in oil production is negligible, the water rates are generally more elevated, and rising with a steeper slope compared to Case 11. Case 13 which involved the smallest nozzle size shows a similar behavior.

We will now have a closer look at the downhole flux, to further investigate the reason for the observed effects. Since the late-life behavior of the ICDs was the most remarkable, this period will be mainly looked into.

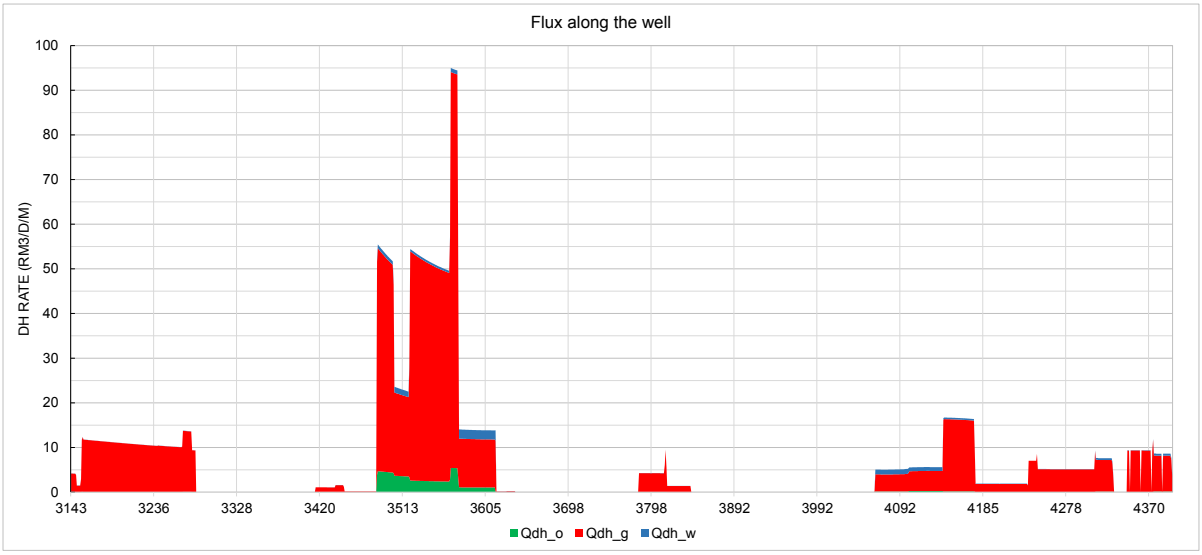

Figure 75: *B1-AHT3 Case 10: Flux along the well at late-life*

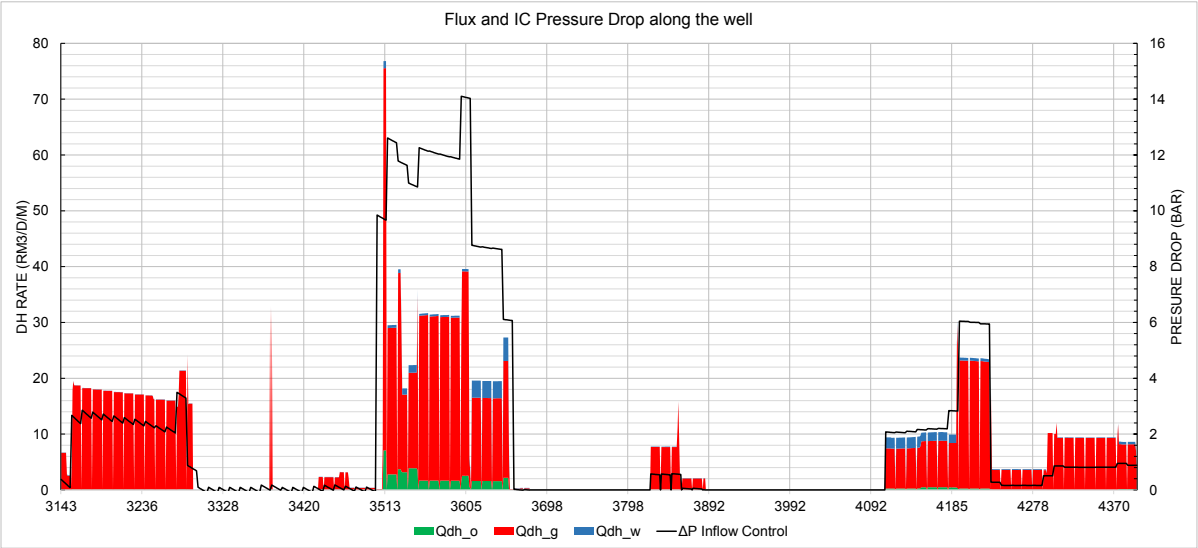

Figure 76: *B1-AHT3 Case 11: Flux and IC pressure drop along the well at late-life*

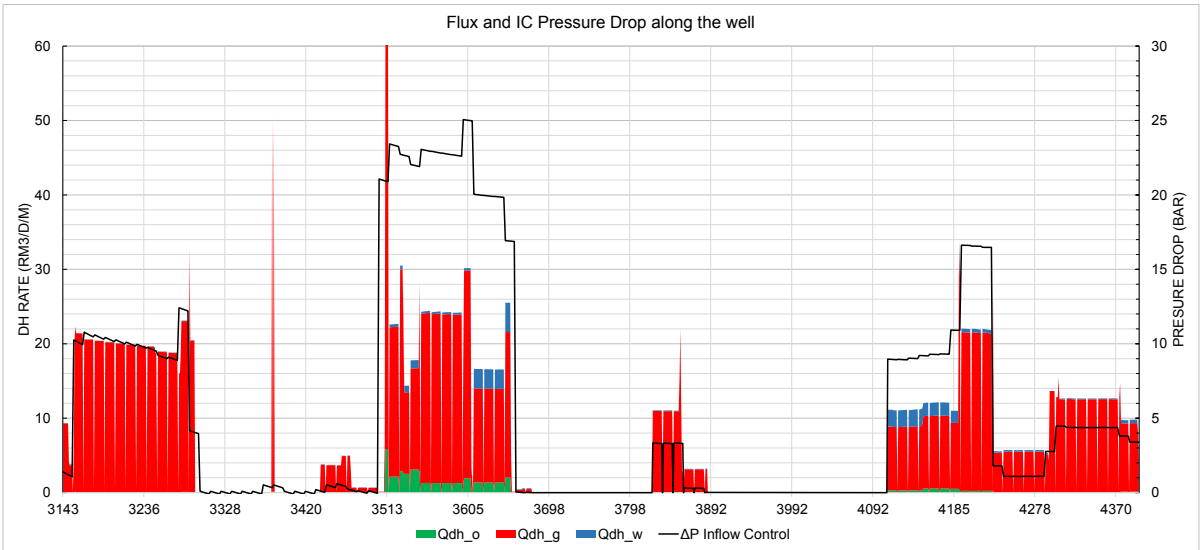

Figure 77: *B1-AHT3 Case 12: Flux and IC pressure drop along the well at late-life*

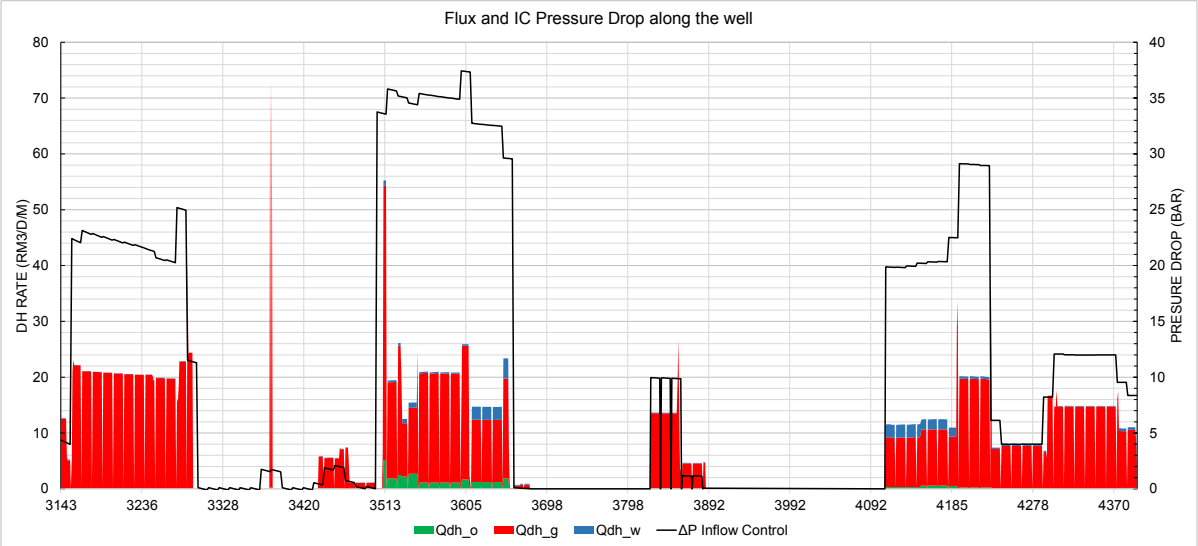

Figure 78: *B1-AHT3 Case 13: Flux and IC pressure drop along the well at late-life*

Figure 75 to 78 shows the resulting late-life flux plots for Case 10 to Case 13.

In Case 11, the gas peak previously observed in the reference case from 3480 to 3620 mMD, has been significantly reduced. This is because of the high IC pressure drop of around 12 bars in the respective interval. On the contrary, the low gas flux values previously seen at 3150 - 3280 mMD, 3800mMD and 4000 - 4400mMD have been increased, and a lower IC pressure drop has been generated at these intervals. This comes as a result of the known equalizing effect of inflow control devices, which helps mitigate the heel-toe effect. Another observation that can be made is with regards to the water influx at approximately 3600 mMD and 4100mMD. A lower pressure drop has been imposed on these zones, which promotes the production of water. This effect has been further intensified in Case 12 and 13, where the flux is more equalized compared to Case 11. This

is the reason for the increased water production seen in Figures D-23, D-28 and D-33. The oil production at this life stage is somewhat constant as a result of the high pressure drop imposed at the interval 3480 - 3620 mMD, where the main oil influx is situated. This observation applies for all the three cases.

During the early-life and mid-life, similar effects are present, as shown in Appendix D.2.

Table 10: *ICD Results for B1*

Case	ICD Nozzle configuration	Early-life			Mid-life			Late-life		
		Average IC pressure drop (bar)	Change in oil production rate (%)	Change in water production rate (%)	Average IC pressure drop (bar)	Change in oil production rate (%)	Change in water production rate (%)	Average IC pressure drop (bar)	Change in oil production rate (%)	Change in water production rate (%)
Case 11	**3 x 4mm**	2,15	-5 %	35 %	2,46	-9 %	48 %	2,88	-12 %	38 %
Case 12	**3 x 3mm**	5,65	-9 %	57 %	6,58	-16 %	51 %	7,72	-22 %	38 %
Case 13	**3 x 2.5mm**	10,50	-12 %	64 %	12,57	-19 %	58 %	14,84	-28 %	40 %

Table 10 shows a summary of the results for Case 11 to 13. The IC pressure drop along with the relative changes in oil and water production are listed for each of the life periods. As previously observed, the water production increases drastically with the the use of ICDs. With a smaller nozzle size, there is a greater increase. From observing the production rate plots in Appendix D.2, the oil rate was considered to be somewhat similar to the reference case results. However, the values in Table 10 show that the oil production at the three timesteps has decreased. The smallest nozzle size gave the greatest decrease in oil production.

5 AICV

The inclusion of autonomous inflow control valves was done in a similar way as for the ICDs. Two technologies were applied for the simulations in this section. The first technology was the Tendeka FloSure TR7[23] which was described in Section 2.5.1. As explained in the section, a number of parameters must be defined to model the valve in simulators such as Eclipse and NETool. These parameters are dependent on the fluid properties, reservoir characteristics and flowing data. Voll et al. [75] described the typical workflow for determining the parameters needed for modeling the flow characteristics of the FloSure TR7 valve. For the purpose of this thesis, Tendeka was contacted to acquire the suitable parameters for our two wells. The data presented in Table 1 were provided to the vendor.

In addition to the FloSure TR7 valve, the InflowControl AICV®was included in the simulations. As mentioned in Section 2.5.2, the AICV can be modeled in the same way

[23]Previously termed the RCP valve

as the RCP valve. To aqcuire the AICV®parameters for our wells, InflowControl were contacted and provided with the same data as Tendeka. The simulations and input for each well will now be discussed individually.

5.1 Well B3

The NETool input for well B3 is presented in Appendix E.1. The input for the five AICV cases can be further summarized as shown in Table 11. For the previous simulations presented for B3, the gas rate has been an adequate boundary condition. However, when simulating AICV, this target produced a series of errors, and it was therefore necessary to try with other boundary conditions. The reason for this is suspected to be related to the main intention of autonomous inflow control, that is, to hold back production of gas and water. The high target gas rate is a result of a breakthrough that has taken place. If NETool was to simulate with this boundary condition, the AICV would in theory generate a very high pressure drop that would severely impede production. It is therefore suspected that the simulator cannot handle such a high gas rate.

Table 11: *AICV Simulation Input for well B3*

Case	Results	AICV Technology	Configuration	Simulation target
Case 11	Figure F-1 to F-5	Tendeka FloSure TR7	4 x 7.5mm	BC Oil Rate
Case 12	Figure F-6 to F-10	Tendeka FloSure TR7	4 x 7.5mm	0.5 x BC Gas Rate
Case 13	Figure F-11 & F-12	Tendeka FloSure TR7	4 x 7.5mm	BC Downhole rate
Case 14	Figure F-13 & F-14	Tendeka FloSure TR7	2 x 7.5mm	0.5 x BC Gas Rate
Case 17	Figure F-15 to F-19	InflowControl AICV®	2 x AICV®	BC Oil Rate

In the rightmost column, the simulation targets for the AICV cases are listed. The rationale behind these boundary conditions can be further explained with the following theoretical questions:

- Case 11 and 17: *If the well had been equipped with AICVs and produced at the same historical oil production rate, how would the gas production be affected?*
- Case 12 and 14: *If the well had been equipped with AICVs and produced at half of the historical gas rate, that is, if the well had been regulated by* $\sim 500\text{kSm}^3/\text{day}$*, how*

would the oil production look like?

- Case 13: *If the well had been equipped with AICVs and produced at the same downhole fluid rate, how would the production of oil and gas be affected?*

In a way, these are all equivalent ways of evaluating the performance of the AICVs. To further study the answer to the questions, it is necessary to analyze the simulation results. These can be found in Appendix F.1, according to the second column listing in Table 11. Figure F-1 shows the overall results for Case 11 compared to the actual production. The first observation that can be made is the lowered gas rate at all of the timesteps. Although this is somewhat expected from the autonomous technology of the FloSure TR7, it would be interesting to look further into the effects that are taking place downhole. Figure F-3 to F-5 show the downhole flux at the three different life stages of B3. During early-life, a relatively high pressure drop of approximately 4 bars can be seen. Zones that are producing oil experience a lower pressure drop, e.g. at 4820 - 4900 mMD. This observation can be further applied in the mid-life and late-life flux plots. However, a lower IC pressure drop is generally created for these periods, at around 1 bar and 0.5 bars, respectively. The reason for this is suspected to be the secondary functionality of the AICV, that is, the restrictive choking through the initial passage in the valve, see Figure 36a.

As mentioned in Section 2.4, the unique feature of autonomous inflow control is to reduce production of unwanted fluids after a breakthrough has taken place. It is therefore appropriate to evaluate the performance of the AICV cases at mid-life and late-life since this could illustrate the main difference between AICV and ICD technology.

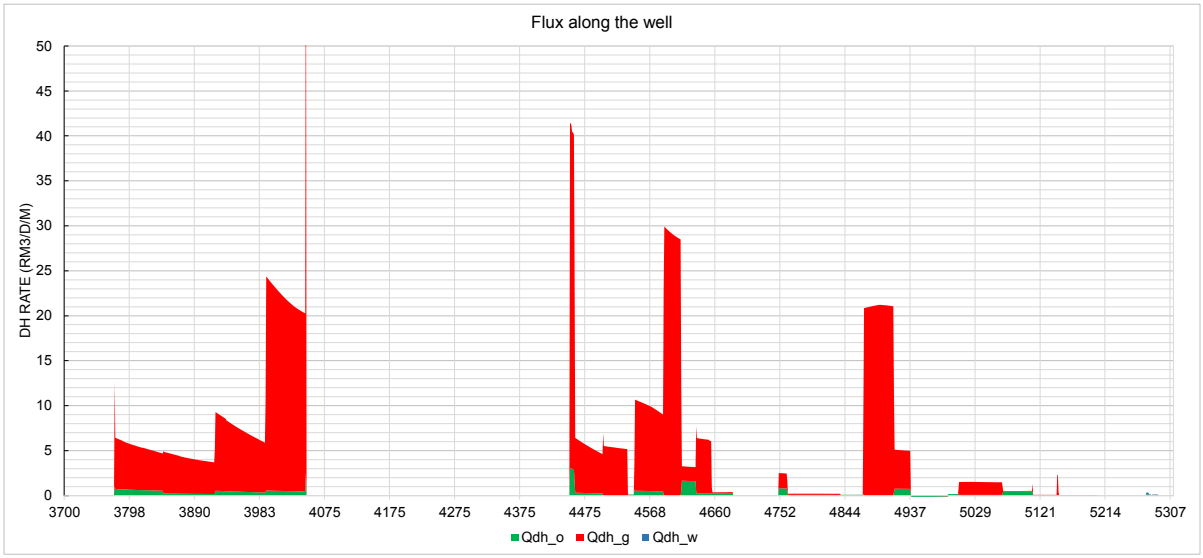

Figure 79: *B3-HT2 Case 7: Flux along the well at mid-life*

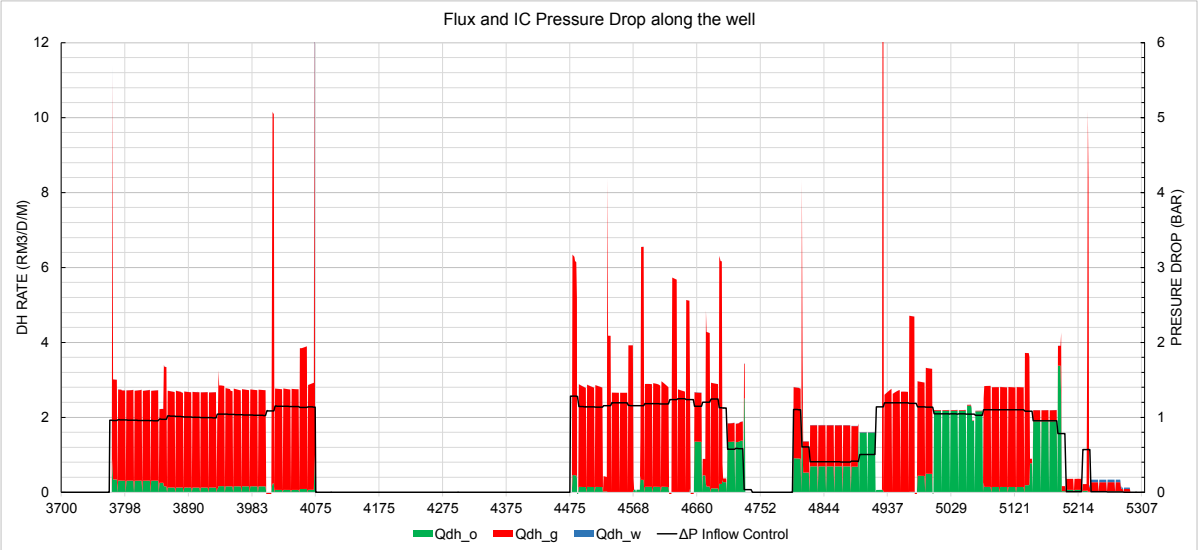

Figure 80: *B3-HT2 Case 11: Flux and IC pressure drop along the well at mid-life*

Figure 79 and 80 shows the downhole flux for the reference case compared to Case 11. While the oil production resulting in the two results is identical, a clear reduction in gas rate can be seen for Case 11. It is also important to note the different axis ranges for the two plots with regards to the downhole rate. The reference case gas peaks seen at 4000, 4450, 4600 and 4900 meters MD were drastically reduced down to a minimum level of 3 Rm^3/day/meter. While the same tendencies could be observed for the optimally chosen ICD case in Figure D-14, the effect was not as good as in Figure 80. Similar to the results in the ICD case results, the flux has been equalized along the wellbore, effectively promoting oil inflow from the toe.

A similar impression can be perceived in Case 12, which featured the same AICV configuration. With half of the base case gas rate as target, the results in Figure F-6 show a slight increase in oil production. It would be interesting to see how a comparable nozzle-ICD would perform in this case. To find a comparable ICD configuration, the initial pressure drop through the TR7 valve was looked into. The argument was that, to be able to compare the two technologies, they had to have the same initial IC pressure drop. The average initial pressure drop through the TR7 valve was found to be 1.39 bars. Through iteration with various nozzle-sizes, the configuration in Case 15 and 16 in Table 7 was found to have a comparable pressure drop of 1.42 bars. Case 15 was run with the same boundary condition as Case 12, and the results are shown in Figure D-16.

We will now have a closer look at the downhole flux for the two cases, to see the similarities and differences between the two types of inflow control. Figure 81 and 82 show the downhole flux plots for Case 12 and 15 at the late-life timestep, respectively. Generally, it can be observed that the AICV generates an average IC pressure drop nearly twice of

the ICD, at around 1.83 bars vs. 1.07 bars respectively. This demonstrates the selective fluid choking feature of the AICV; Initially when oil is mostly produced, the same pressure drop was generated. After the gas breakthrough, the TR7 valve will autonomously choke harder than the ICD. When compared to the ICD case, the oil flux levels at the toe are generally more elevated in the AICV case, while the gas flux is better equalized. This indicates that the AICV promotes production of oil in favor of the gas.

Although not as distinct as in the presented plots, the early-life[24] and mid-life[25] plots show similar tendencies. During the early-life, the AICV manages to lower the gas flux peaks in a better way than the ICD. Furthermore, the ICD generates an average pressure drop around 1.84 while the AICV shows a pressure drop of 2.43 bars.

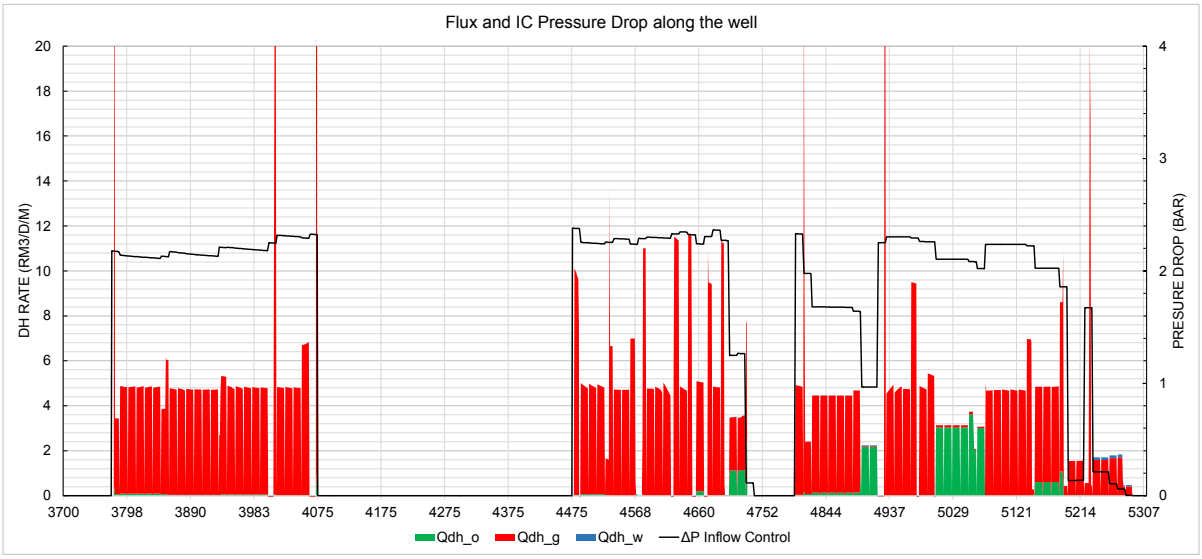

Figure 81: *B3-HT2 Case 12: Flux and IC pressure drop along the well at late-life*

[24]See Figure F-8 (Case 12) and Figure D-18 (Case 15)
[25]See Figure F-9 (Case 12) and Figure D-19 (Case 15)

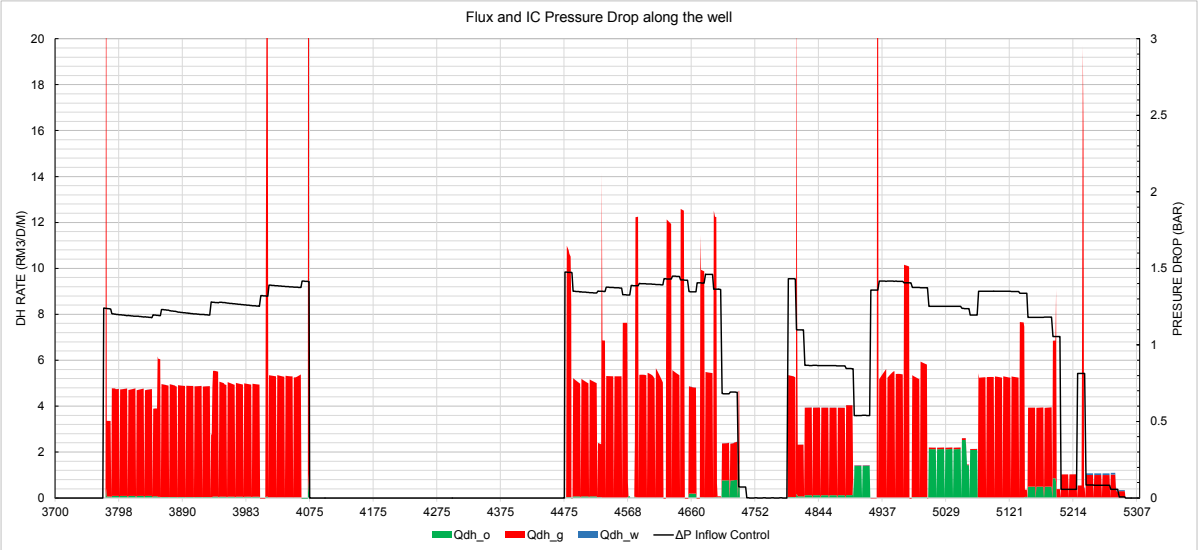

Figure 82: *B3-HT2 Case 15: Flux and IC pressure drop along the well at late-life*

Table 12: *Comparison of AICV vs. ICD Results for B3*

Case	Configuration	Early-life		Mid-life		Late-life	
		Average IC pressure drop (bar)	Increase in oil production rate (%)	Average IC pressure drop (bar)	Increase in oil production rate (%)	Average IC pressure drop (bar)	Increase in oil production rate (%)
Case 12	**4 x 7.5 mm FloSure TR7**	2,43	-14 %	1,62	33 %	1,83	75 %
Case 15	**3 x 2.65mm Nozzle ICD**	1,84	-20 %	0,99	12 %	1,07	36 %

Table 12 shows a summary of the discussed observations for the comparison between the AICV and ICD cases. Despite the fact that the AICV has a higher IC pressure drop through all three life phases, it manages to produce higher oil rates at the same gas rate. This is an important finding as it demonstrates the benefits of adapting to autonomous inflow control technology in favor of conventional ICT, and is consistent with the experience from the Troll field[26].

[26] See Section 2.5.1

Table 13: *A summary of AICV and ICD results for B3*

Case	Configuration	Simulation Target	Early-life			Mid-life			Late-life		
			Average IC pressure drop (bar)	Change in oil production rate (%)	Change in gas production rate (%)	Average IC pressure drop (bar)	Change in oil production rate (%)	Change in gas production rate (%)	Average IC pressure drop (bar)	Change in oil production rate (%)	Change in gas production rate (%)
Case 11	4 x 7.5 mm FloSure TR7	BC Oil Rate	3,42	0 %	-38 %	0,86	0 %	-64 %	0,53	0 %	-76 %
Case 12	4 x 7.5 mm FloSure TR7	0.5 x BC Gas Rate	2,43	-14 %	-47 %	1,62	33 %	-53 %	1,83	75 %	-58 %
Case 13	4 x 7.5 mm FloSure TR7	BC DH Rate	-	42 %	-14 %	-	156 %	-13 %	-	276 %	-14 %
Case 14	2 x 7.5 mm FloSure TR7	0.5 x BC Gas Rate	13,81	-10 %	-47 %	8,21	39 %	-53 %	9,30	82 %	-58 %
Case 15	3 x 2.65mm Nozzle ICD	0.5 x BC Gas Rate	1,84	-20 %	-47 %	0,99	12 %	-53 %	1,07	36 %	-58 %
Case 16	3 x 2.65mm Nozzle ICD	BC Gas Rate	-	52 %	0 %	-	143 %	0 %	-	235 %	0 %
Case 17	2 x AICV®	BC Oil Rate	22,91	0 %	-52 %	6,21	0 %	-80 %	2,72	0 %	-91 %

Table 13 shows a summary of the results obtained for all the AICV cases along with the two comparable ICD cases (Case 15 & 16). Case 13 and 14 were not further looked into in terms of downhole flux. However, by examining the simulated production in Appendix F.1, together with the observations made from Case 11 and 12, the downhole behavior can be anticipated. For Case 13, the results in Figure F-11 and Table 13 indicate an increase in oil production and a decrease in the gas production. This further supports the impressions from the inclusion of AICVs in the well completion, that is, better control of the gas production and lower restriction in oil productive zones.

Case 14 was run with only two TR7 valves per screen joint, and simulated with the same target as in Case 12. The results from these simulations, in Figure F-13 show a slight increase in oil production when compared to Case 12. However, as is evident by the pressure plot in Figure F-14, this small increase in oil production comes at the expense of a greatly reduced downhole pressure, because of the high IC pressure drop. Therefore it is rather recommended to use the first configuration of the TR7 completion with four valves per joint.

In Case 17, the coefficients for the InflowControl AICV®was entered in NETool. In discussions with Vidar Mathiesen at InflowControl, it was informed that it is possible to include a maximum of two AICV valves per joint. The same target as in Case 11 was applied for the simulations, and the results are shown in Figure F-15 and in Table 13. In terms of production, a strong reduction in the gas rate can be observed, with an approximate 90% decrease at the late-life period. However, this comes at the expense of a relatively large IC pressure drop. We will look further into the downhole behavior

for this case, to get a better understanding of the difference between the InflowControl AICV®and the FloSure TR7 valve.

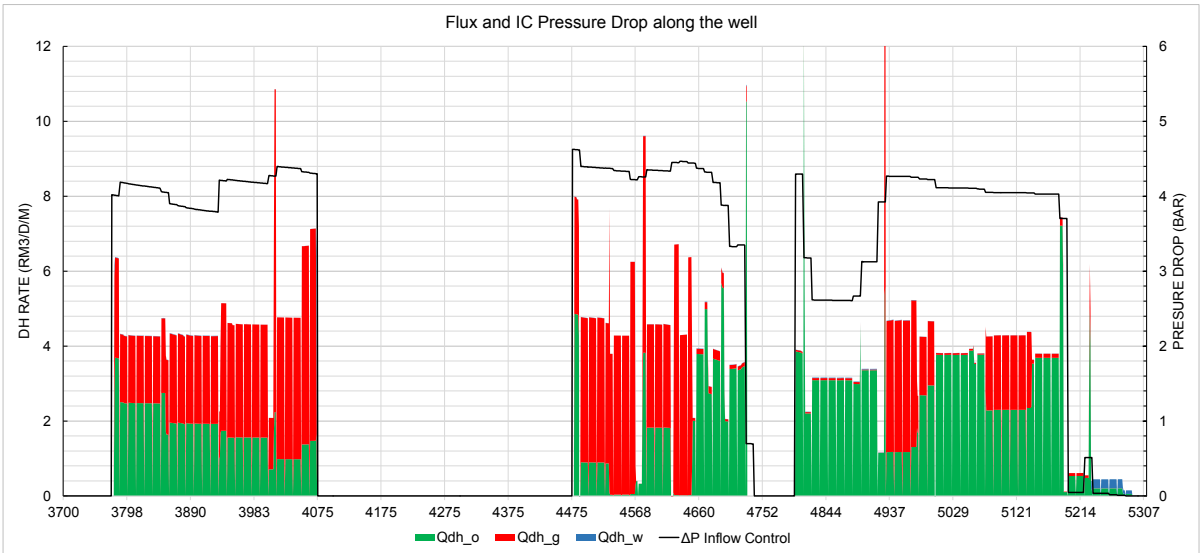

Figure 83: *B3-HT2 Case 11: Flux and IC pressure drop along the well at early-life*

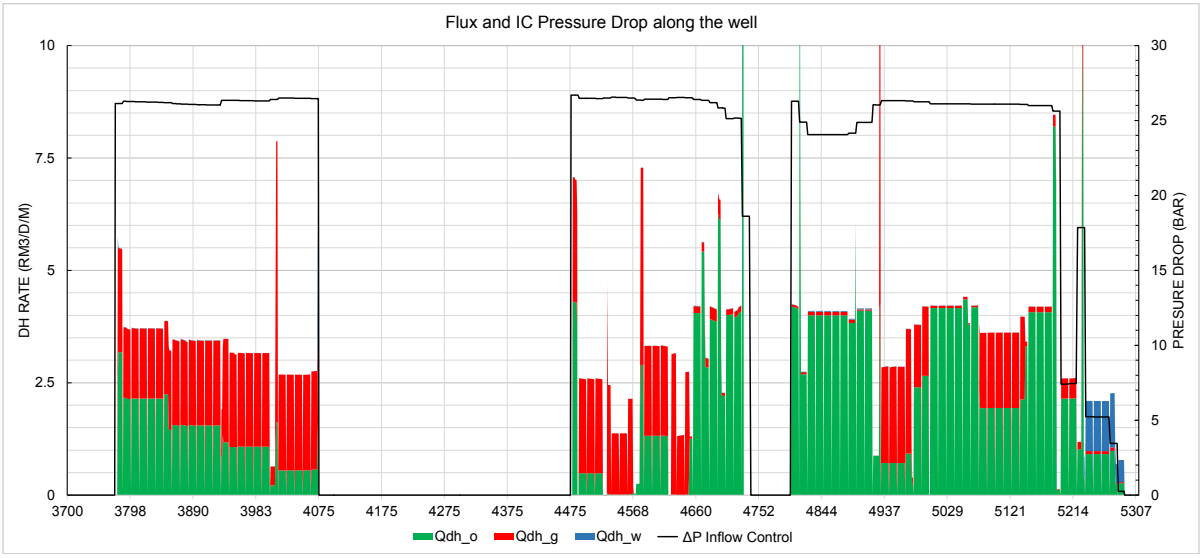

Figure 84: *B3-HT2 Case 17: Flux and IC pressure drop along the well at early-life*

Figure 83 and 84 compares the downhole behavior in Case 11 and 17 during late-life. Firstly, there is a clear difference in the IC pressure drop between the two cases. While the FloSure TR7 creates an average pressure drop of 2.4 bars, the AICV®generates an IC pressure drop almost ten times greater. Although the oil inflow is somewhat similar for the two cases, the gas influx is greatly reduced in the heel section for Case 17. Moreover, the gas peaks observed from 4000 - 4080 mMD and 4500 - 4650 mMD are noticeably lower for the AICV®. As previously observed with the smallest nozzle ICD configuration in Figure 72, the water influx at the toe is promoted as a result of the strong equalization of

the flux. Generally, the same performance of the AICV®can be observed in the mid-life and late-life plots in Figure F-18 and F-19, with respect to the drastic reduction of gas influx.

5.2 Well B1

For well B1, the simulations with AICV included only one case, which involved four FloSure TR7 valves per joint. The coefficients received from Tendeka were entered into NETool as shown in Appendix E.2.

Although only one AICV case for B1 will be reviewed, it should be mentioned that simulations with the InflowControl AICV®were attempted. The simulator gave several errors and did not yield any results. Attempting to run simulations with four valves, instead of the maximum number of two valves per joint, gave some results. It is therefore suspected that the errors in the simulator are related to the high pressure drop through the valve. Since it is not possible to include four AICV®in a screen joint, the results for this configuration will not be further reviewed.

The results for the FloSure TR7 simulations for B1 are presented in Figure 85 as well as in Appendix F.2. The use of the FloSure TR7 valve critically lowers the downhole pressure and the WHP through the lifetime of the well, as shown in Figure F-21. As a consequence, the last three timesteps gave a wellhead pressure below the minimum limit of 30 bar. The simulated rates in Figure 85 show that the water production is increased, while the oil rate is somewhat reduced.

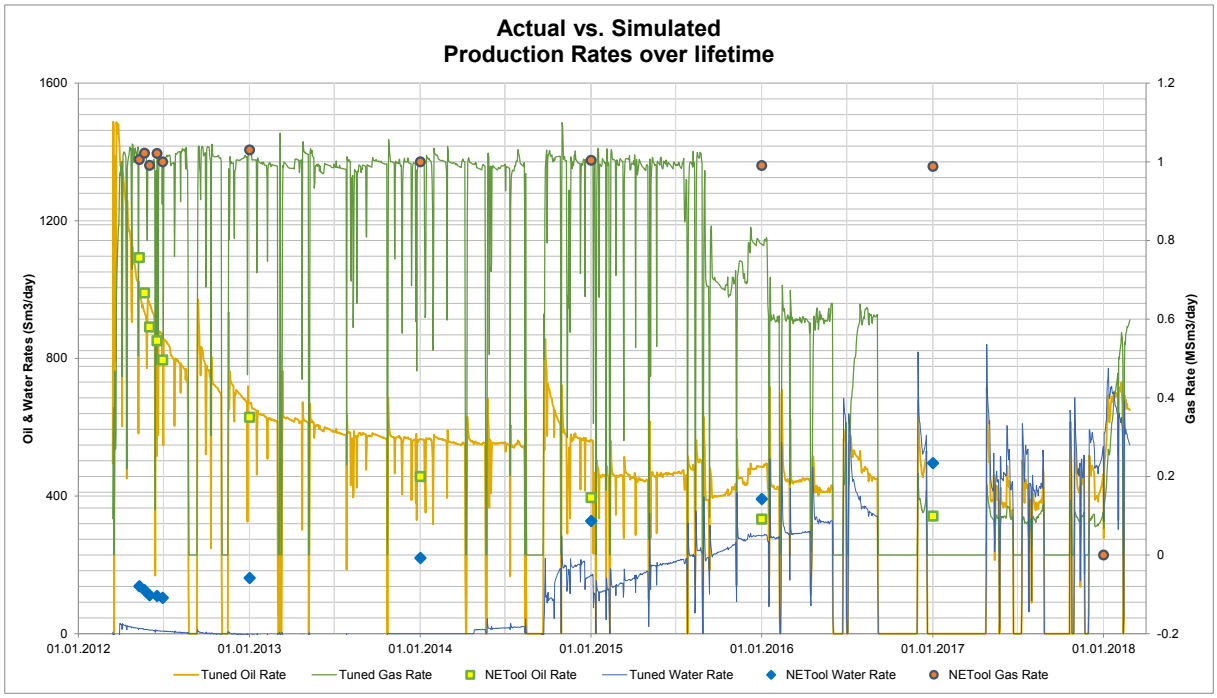

Figure 85: *B1-AHT3 Case 14: Actual vs. Simulated Production*

To understand the reason for this behavior, we will have a closer look at the downhole flux through the three life phases. Because of the deficient WHP at the late-life timestep, the downhole flux at this respective date will not be considered.

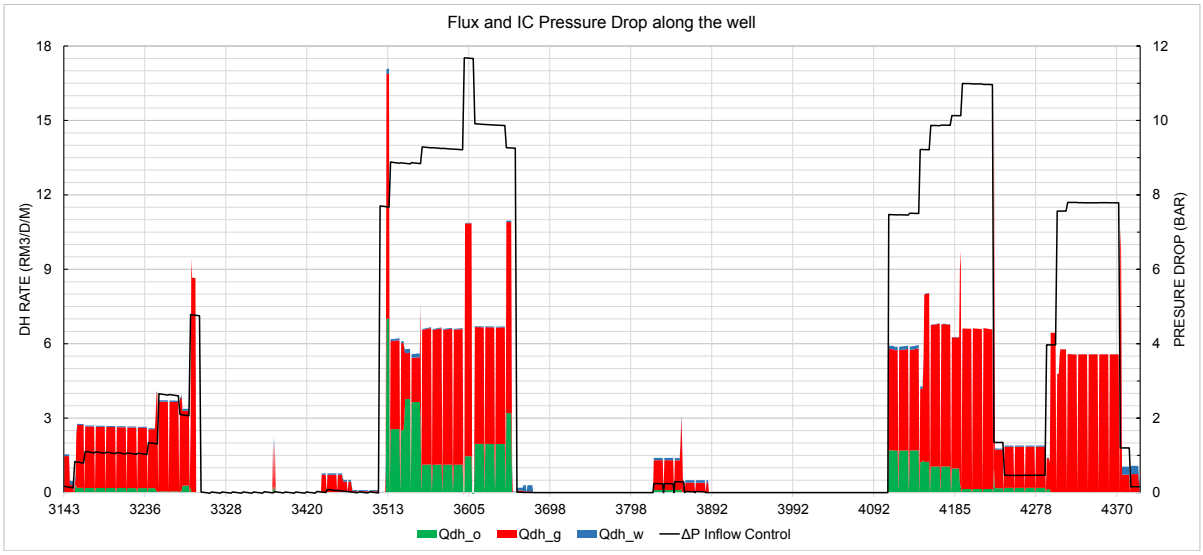

Figure 86: *B1-AHT3 Case 14: Flux and IC pressure drop along the well at early-life*

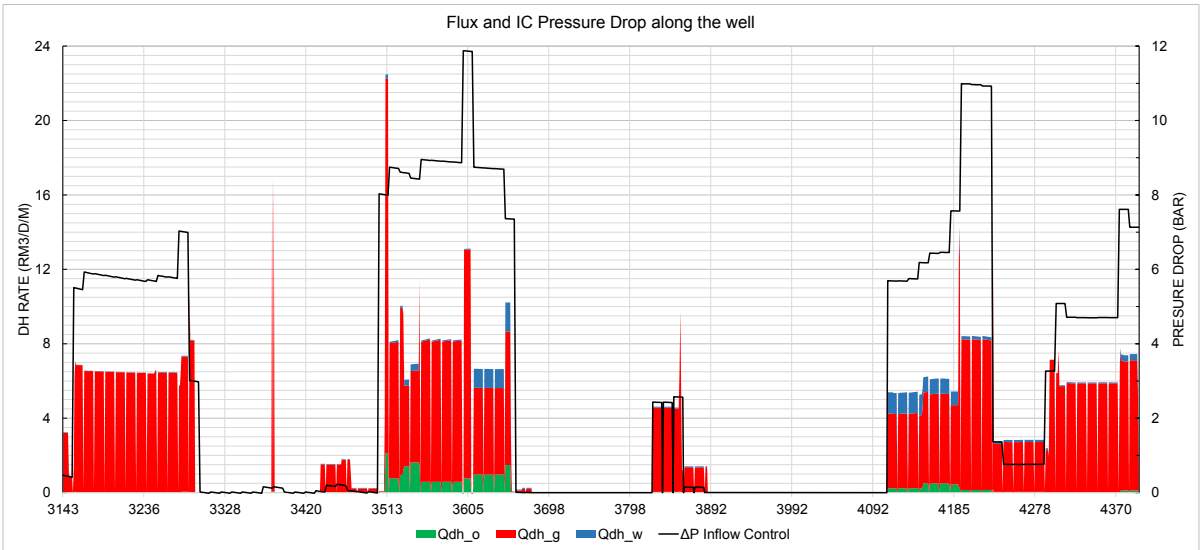

Figure 87: *B1-AHT3 Case 14: Flux and IC pressure drop along the well at mid-life*

During the early-life, it can be seen that the gas peak observed in the reference case from 3480 to 3620 mMD, has been greatly equalized, in proportion to the high pressure drop that is applied at this interval. While the previous flux peak reached a magnitude of 70 Rm^3/day/meter, it has been reduced by a factor of ten, with the inclusion of the AICV valve. The same observation can be made for the interval from 4000 to 4400mMD, where the highest gas peak was reduced from approximately 17 to 6 Rm^3/day/meter.

Assessment of the mid-life shows improvements in the gas control, in similarity to the early-life observations. However, higher water rates can be observed at approximately 3610 mMD and 4100 mMD, when compared to the reference case results. Furthermore, because of the high pressure drop in the intervals 3500 - 3650 mMD and 4100 - 4200 mMD, the oil flux has been decreased. Although the late-life behavior could not be simulated, it can be anticipated that the indications of higher water production and lower oil production are further exacerbated. Thus, it can be concluded that the performance of AICV technology in well B1 did not yield beneficial results. Uncertainties and the reasons for this results will be further discussed in Part III.

Part III

Discussion and Conclusions

6 Evaluation of IC technologies on Gjøa

Simulations performed for the two oil wells on Gjøa have given different impressions for the use of inflow control technology.

6.1 Well B3

In Section 1.2.1 the production challenges in B3 were discussed. The main issues were related to excessive gas production and immobilization of oil reserves. When it comes to the integration of conventional nozzle ICDs, the early-life results in Figure 74 showed that the heel-toe effect is reduced, which further promoted oil production from the toe. During the mid-life and late-life periods, which were dominated by gas coning, the downhole flux plots showed that the main oil influx was located at the lower part of the well. At the same time periods, the behavior in the reference case showed almost no production of oil at this part of the well, see Figure 62 and 63. This indicates that the use of ICDs could potentially enhance oil recovery for B3, by improving the oil inflow at the toe. This impression is supported by the observations made from Figure 54, which displayed the placement of B3 within the reservoir model along with the fluid saturations. Here, it was observed that a major part of the oil saturated reservoir layers were located at the lower part of the well. Utilizing these reserves by use of ICDs could increase oil production significantly.

The use of autonomous inflow control valves was also evaluated for B3, as shown in Section 5.1. Three different configurations were run, which yielded promising results. For the FloSure TR7, the configuration with four valves per joint was found to be the optimal solution. The valve managed to control the gas in a better way compared to what the ICD results were indicating. Moreover, it could be observed that the oil producing zones had a lower restriction (pressure drop). To further compare the FloSure TR7 with conventional ICD technology, nozzle ICD configuration with the same initial pressure drop was simulated. From production start, the performance of the two technologies was similar in terms of pressure drop and oil production. However, through the mid-life and late-life periods, significant differences started to show, where the AICV imposed twice the

pressure drop on the produced fluids, and showed better gas control. This demonstrates the autonomous functionality of the valve, where the levitating disc will choke harder for low viscosity fluids compared to the nozzle-ICD.

The performance of the InflowControl AICV®was also assessed in Section 5.1. As described in Section 2.5.2, the principle of the technology is based on a pilot flow tube which determines the restrictive setting in the valve. As a result of this principle, insignificant amounts of gas need to flow through the valve for it to function as intended. The same cannot be said for the FloSure valve, which needs higher gas rates for the disc levitation principle to work properly. It is speculated that this is the reason behind the results observed in Figure 84 for the InflowControl valve. The results showed lower gas rates when compared to the performance of the FloSure TR7 valve in Figure 83. However, considering the pressure drop through the AICV®which was approximately ten times that of the FloSure valve, it can be argued that the 15% decrease in gas rate cannot be justified for the adaption of the AICV®in favor of the FloSure TR7 valve.

It is important to consider the lost pressure energy against the added oil production when assessing the results we have obtained. Alternatively, the reduction in gas production may offer the same benefits, as the gas will stay in the reservoir and provide pressure support for increased oil drainage. Having said this, and taking into account the results presented in Table 8 and 13, there is a clear benefit of adapting to inflow control in B3. The optimal technology is considered to be the FloSure TR7 configuration in Case 11, which added most value in terms increased oil production and reduced gas production per generated pressure drop.

6.2 Well B1

For B1, the results were puzzling as they showed an increase in water production in all cases with ICDs and AICVs.

With reference to the results presented in Section 4.2 and Appendix D.2, it can be argued that the inclusion of ICDs in well B1 gave poor/worse results. Table 10 indicated that the smallest nozzle size gave the highest increase in water rate and the highest decrease in oil rate. This conclusion is not consistent with the ICD study described in Section 2.6, which concluded that the use of ICDs on B1 would defer the water breakthrough by 1 year, and increase oil production by 260 000 oil barrels. There are several potential reasons for this contradiction. Firstly, the possibility of uncertainties in the reservoir model and established reference case model should not disregarded. The uncertainties will be

discussed in detail in Section 7, but one of the main uncertainties linked to the results for B1 is the initially high water production rate in the reference case, see Figure B-21. Although the simulations show a considerable water rate from the first timestep, the actual water breakthrough did not start to develop until mid-2014. This source of error can be the reason for the increased water rate observed in the ICD simulations, and it can be argued that no water production at the early-life timestep could result in increased oil rate by equalization of the flux.

The fact that NETool cannot capture the dynamic behavior of the well, means that the delayed water breakthrough could not have been shown in the simulation results. However, the reservoir simulations in [5] did indicate this outcome. Conclusively, it is therefore anticipated that ICDs could have deferred the water breakthrough, contrary to the indications from our simulation results. In that case, the configuration with 3 x 4mm ICDs would be the most appropriate with respect to a reasonable pressure drop.

Simulations with AICV showed an unexpected behavior where the production of water was increased. According to the described behavior of the FloSure TR7 valve in Section 2.5.1, it could be expected that the opposite would have been the case. While not disregarding the abovementioned uncertainties in the model, one should also consider the fluid properties listed in Table 1. For B1, the live water viscosity is 0.384cP while the live oil viscosity is 0.284cP. The principle of the FloSure valve is based on the positive difference between the oil and water viscosity, where the restriction is minimized for the more viscous oil. However, for the ultralight oil in B1 the opposite might be the case, where water is preferentially produced in favor of the oil.

When Tendeka provided the AICV coefficient for the FloSure valve, a flow characteristics chart was also attached. Figure 88 shows the flow characteristics of the simulated AICV including the characteristics of a comparable nozzle type ICD. Considering this performance, a different conclusion can be made regarding the viscosity difference just discussed. In the chart it can be observed that the single phase flow of water (blue) through the valve experiences a higher pressure drop compared to the oil (green). This means that the valve will preferentially produce oil in favor of the water. The observed results in Section 5.2 may however be attributed to the fact that the oil producing zones are located within the intervals with very high gas production. When the AICV generates a high pressure drop as a result of the gas influx, it also impedes oil production at these zones. On the contrary, the water producing zones do not include a high gas production, as shown in Figure 75. As a results, the IC pressure drop in these respective zones is relatively low, which allows the influx of water as shown in Figure 87.

Moreover, the use of AICV on B1 may reduce the gas production in the well, which is not desired, as the gas aids in the vertical lift of production fluids to the surface.

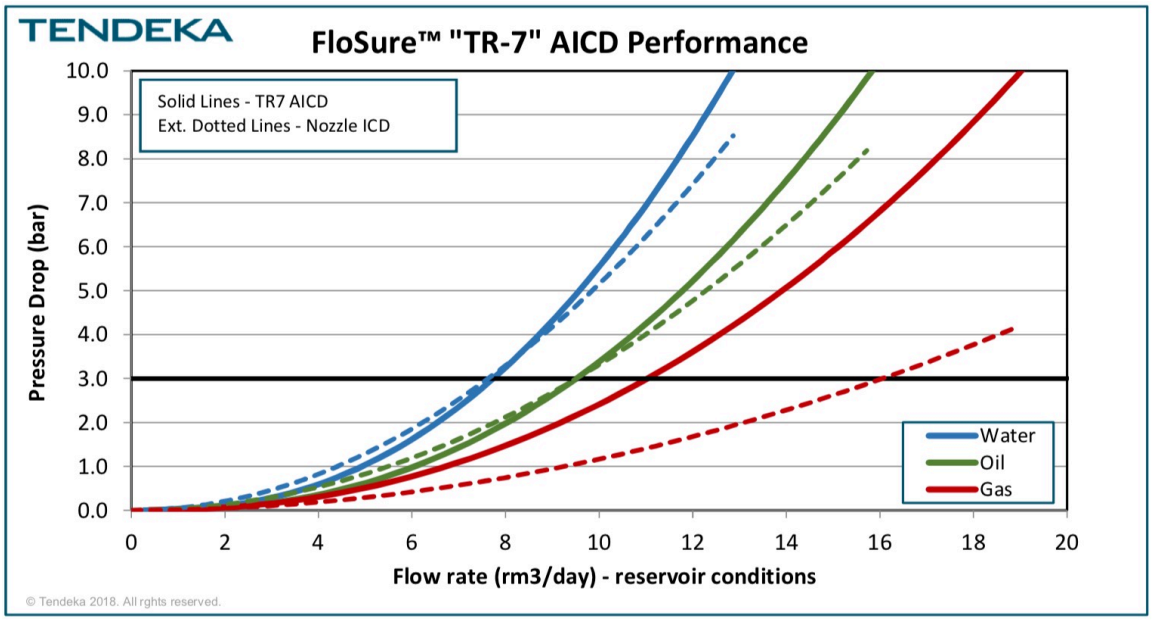

Figure 88: *Tendeka FloSure TR7 and Flow Characterstics for well B1, [73]*

Another objective of evaluating B1 in this study, was to see if the water influx during the shut in periods could be restricted during start-ups and lessen the need for long gas lift periods. Considering the technologies we have reviewed in this thesis, it is not expected that this issue can be solved by the use of ICT. However, it is possible to have Interval Control Valves together with multiphase flow meters to selectively shut off zones with higher water rates during start-ups. This can introduce further operational complexities including running hydraulic control lines up to the surface, as well as requiring an inner string with a smaller ID which introduces a higher tubing pressure drop. Moreover, the valves tend to be operationally unstable, and have in some cases gotten stuck in one position due to scale build-up. The cost of incorporating ICVs as part of the completion is also very high compared to passive inflow control technology [11].

6.3 Secondary benefits of IC technology

In Section 2.3.3 the benefits of including ICDs were discussed. Secondary benefits with ICD include reduced risk of sand control failure, minimized annular flow and cross-flow, improved clean-up. Well clean-up simulations done by Moen [15] and Bellarby [13] showed significant improvements in well clean-up performance. Experience has shown that a majority of conventional horizontal wells on the NCS suffer from some degree of poor well clean-up, and the two Gjøa wells are not exceptions to this. Including horizontal sections

of 1500 - 2000 meters, the probability of poor well clean-up in B3 and B1 is significantly high. This can critically impair production by reducing the productivity index as a result of certain well segments being plugged. As shown in Figure 22, the ICD will generate an additional pressure drop which can aid in filtercake lift off and mud particle removal during flow-back. As a result, the required flow rate for proper clean-up is drastically reduced. For B3 and B1, the improved clean-up resulting from ICD inclusion can greatly increase the PI and subsequent oil production in the wells. This can further justify the inclusion of ICT on the two oil wells.

6.4 Cost

An important part of the discussion when it comes to adapting any new technology is the aspect related to cost, and ICT is no exception. In discussions with Lasse Hermansson and Terje Moen, [74, 76], it was concluded that the typical cost of integrating inflow control as part of a typical horizontal well completion could be expected to be in the interval of 1 - 10 Million NOK. Typically the higher cost range can be assigned to adaption of autonomous inflow control technologies such as the FloSure TR7 valve, while the lowest cost can be expected for conventional nozzle-ICD configurations. While this might seem as a considerable expense, it would be logical to compare it against the added value of the technology.

If a typical oil well produces around 1000 Sm^3/day, this is the equivalent of around 6300 bbl of oil per day. At an average oil price of 70 USD/bbl and currency conversion rate of 8 NOK per USD, the price of an oil barrel can be estimated at 560 NOK. Consequently, a days production of oil will have a value of 3.5 Million NOK. Thus, three days of added oil production can make up for the cost of ICT inclusion in the well.

This does not take into account the added value of delayed gas/water breakthrough which presents a large cost saving aspect in terms of handling unwanted fluid production in addition to prolonged oil production resulting from the delayed breakthrough. Moreover, the reduced risk of potential interventions resulting from sand control failure or poor well clean-up presents significant cost-saving benefits. Conclusively, it can be understood how the cost of ICT integration is insignificant when compared to the contrary alternative.

7 Uncertainties

As with all computational simulators, there will always be uncertainties related to the results that we obtain, and NETool is no exception. The software simulates at a certain timestep, with a limited number of parameters at static conditions, while the reality is much more advanced and dynamic. In this thesis, we have attempted to limit these uncertainties by calibrating the well models to actual production performance. Through extensive trial and error, we have achieved reference case models that were adequate for subsequent simulations. The rationale between each alteration was explained Table 5 and 6 and the results were presented in the appendices. Still, there are several uncertainties that cannot be completely mitigated. These will now be explained along with the potential impact they may have for the results.

7.1 Limitations with NETool

As explained in Section 3.1, Landmark NETool is a software which serves as an simple yet effective tool for modeling advanced well completions. However, the software is based on a series of basic assumptions that may limit its reliability. There are several limitations that can be discussed which can influence the certainties in our results:

- The flow within and around the wellbore is one-dimensional, and the flow between two adjacent nodes along the well is averaged over the cross-section within the annular space or inside the tubing.
- The reservoir flow performance is based on PI models and phase fractions. Furthermore, the permeabilities can be averaged along the trajectory.
- NETool does not apply single phase fluid flow. The inflow in one compartment is averaged with respect to the fluid properties. This can have significant consequences for the modeling of AICVs which are reactive and dependent on the fluid properties. In many cases, the inflow of water or gas is not commingled when produced with the oil, and it can therefore be speculated that NETool does not manage to capture this behavior.
- When simulating with annular packers, NETool assumes a radial isolation out into the reservoir. In reality this is not the case, and fluids can potentially cross-flow between reservoir layers if the pressure difference is sufficient.

One of the critical uncertainties in the results from NETool is the question of whether or not the resulting downhole flux profile is correct. This is not necessarily exclusively related to NETool but is also a result of the input from the reservoir model. Although the history matching shows a match in surface production rates and pressures, it does not ensure that the downhole flux behavior is correct. Production from one zone could be mistaken for another zone etc.

The only possible way of knowing the contribution from each interval is either by use of a Production Logging Tool (PLT), downhole flow meters or tracer technology. PLT is usually run downhole by wireline to measure and monitor the productivity along the wellbore. There have not been any PLT surveys on the two Gjøa wells. The inflow performance resulting from the NETool simulations are merely based on the PI model, phase fractions and permeability data from Eclipse, which can present a significant uncertainty in the results.

Static vs. Dynamic behavior

The fact that NETool is a static simulator is an important topic for discussion. The way the results were presented does not show the dynamic well behavior of the IC-completed wells. To simulate such behavior, the use of dynamic reservoir simulators such as Eclipse is necessary.

The main focus for the two oil wells was to see the behavior of inflow control technologies at different life periods. As mentioned in Section 2, a central part of evaluating the application of various IC technologies, is to find a technology that can perform optimally during the whole life of the well. Some technologies typically perform well at an early-life, while others prove beneficial in the late-life. The objective of our simulations was to capture this behavior.

The way of understanding our simulation results at the different timesteps is to ask the following theoretical question:
If the well had been equipped with inflow control at the respective timestep, how would the performance look like?
To elaborate on this question, this means that the well was completed without ICT up until the respective date. This is an important limitation of our simulation work that one should be aware of.

7.2 Reservoir model

The two well models established in NETool are closely linked to the input from the Eclipse reservoir model. The full-field reservoir model for Gjøa was developed as a black oil model, and further optimized following the drilling of exploration and appraisal wells in the field. Using the keywords for history matching in Eclipse, the model has been optimized to fit observed production from the various wells. Some of the wells, including B3 have also been part of a service called ResX, which aimed at calibrating the reservoir model more accurately with respect to historical production. This is based on the assumption that the measured production data are somewhat accurate.

A significant uncertainty can be assigned to the way of modeling the well completion in the reservoir model. As explained in Section 3.2.1, the sandscreen completions for B3 and B1 are modeled as cased and perforated liners with cemented annulus in the blank pipe sections. Whether or not this is a fair assumption can be argued. Placement of blank pipe sections without any further annular isolation cannot ensure that there will not be any fluid inflow from these respective intervals. One could assume a collapsed annulus if the surrounding formation consists of unconsolidated sands, but it would not ensure complete annular isolation. During the well design phase, the intention of placing blank pipe sections in the two wells was to prevent inflow from highly water-saturated zones.

In Section 3.2.2, it was shown how the modeling of blank pipes in the NETool model could affect the results. Conclusively, this detail does not represent the actual conditions downhole, but was necessary for the NETool models to work as intended. It can be regarded as an uncertainty in the reservoir model.

There is fairly high confidence that the reservoir model for B3 is applicable for the purpose of our work. For B1, this cannot be said with the same certainty, as the reservoir model for the well has not been through the ResX service. However, apart from the details regarding the relative permeability data, the reservoir model for B1 can be regarded as applicable for our simulations.

7.3 Quality of history matching

The accuracy of the history matching results is a key factor for the quality of the subsequent simulations with inflow control. A major part of the work during this study was therefore assigned to this task.

For well B3, the final results showed a fairly good match for the major part of the wells lifetime, see Figure 60. Initially, the increase in gas production due to the development

of the gas cone was not captured optimally by the simulator. By having a closer look at Figure 57, it can be understood why that is the case. From May to June 2012, the Eclipse results show an increase in oil rate together with the increase in gas rate. The history indicates a constant oil rate in this time interval. It could be argued if the measurement of the oil rate is accurate in this case, or if the Eclipse model is at fault. This will be further discussed more in Section 7.4.

Furthermore, the last timesteps in the production lifetime were simulated with a higher gas rate than the actual rate. For the dates 01.06.17 and 01.01.18, the same rate as the previous timestep was used to achieve a proper match. The reason for this is that the well was shut in at these dates. The purpose of running simulations with a gas rate of 1.2 Million Sm^3/day was to see if we could achieve the correct production profile for the oil. As these two timesteps were not the main focus in subsequent simulations with ICT, there is not much concern related to the deviation in the gas rate values at these points. Otherwise, the accuracy of the match shown in Figure 60 is adequate from point 1 to 3, assuming that the production data are accurate. Furthermore, the pressure plots presented in the respective appendix showed a very accurate match between the simulated and measured pressure data, which further validates the results from the history matching.

Well B1 was not as easy to calibrate with regards to production history. It was not part of the previously described ResX service, which clearly showed in the Eclipse results in Figure 58. After implementation of the learnings from B3, the well clearly did not yield results in accordance with observed production. It was only after the relative permeability curves were changed, that any reasonable conformity could be achieved. Figure 65 shows the relative permeability changes that were made to achieve the results in the reference case (Case 10). Due to their shape, it could be argued that the resulting Rel.Perm curves are non-physical. However, in discussions with a PhD fellow at IRIS [72] who has worked with the topic, it was revealed that the relative permeability data for any reservoir rock is generally linked to a high degree of uncertainty. This is because of the methods that are used to determine this type of information. Typically, the data are also a result of correlation models. In our case, the initial Rel.perm values from Eclipse did not quite follow this description, something that was pointed out by [72] as well. A review of the PDO support documentation from the subsurface department indicated that the relative permeability data for the segment penetrated by well B1 was linked to several uncertainties. In conclusion, it can therefore not be said with any certainty whether or not our customizations were erroneous. What is certain, though, is that the customizations yielded converging results which conformed with the production rates, as

shown in Figure 66. This implies that the changes done to the relative permeability values were somewhat correct.

The results obtained for B1 did show some considerable deviations. For the last three timesteps, the target gas rate was set to 1 Million Sm^3/day, which does not match the actual rates in this time interval. Discussing the matter with the production engineer concluded that the observed rates during this time period is not representative of the reservoir behavior, but rather that it is a result of frequent shut-ins. Moreover, as long as the same targets were used for subsequent ICT simulations, this discrepancy can be neglected. The main focus of our simulations was on the points 1, 2 and 3, which were all fairly accurate in terms of production rates. Further, the pressure plots presented in the respective appendix showed a good match between the simulated and measured pressure data [7].

An emphasis should be laid on the raised value of history matching. Typically, when wells are simulated with advanced completions in NETool, the well has not been drilled nor completed. Consequently the uncertainties are significantly larger in such wells. The process of retrospective history matching of the wells eliminates a great number of these uncertainties. To mention a few, this applies to uncertainties in well placement, permeability distribution, production forecasts and time to gas/water breakthrough.

7.4 Production measurements

The validity of the history matching and accuracy of our two well models is all based on the fact that the acquired production data are correct. However, as mentioned in Section 1.2.1, there are uncertainties related to the presented production rates for B3 and B1 in Figure 4 and Figure 5, respectively. According to the production engineer, the gas rate had an estimated uncertainty of $\pm 5\%$, while the oil and water rates were linked to a higher degree of uncertainty because of flow meter drifting. This does not lower the credibility of the data significantly, but should be kept in mind when assessing the accuracy of our reference case results.

In Figure 5, it can be seen that the water rate is quite irregular, something that can be explained by the aforementioned measurement uncertainty. This can explain why the results in the reference case did not match accurately with the production data. Additionally, the precision of the fluid rates in the late-life period for B1 can be questioned due to the rapid changes in fluid rates.

The same inaccuracies are related to the pressure measurements shown in Figure B-7

and Figure B-22. Pressure gauge drifting is a well known phenomenon, and varies a lot depending on the gauge manufacturer. This detail should be kept in mind when evaluating the accuracy of the reference case [76].

7.5 Choice of boundary condition

The choice of simulation target will greatly affect the results obtained from NETool. The software produces results which converge towards the value of the target, and it is therefore important to choose this parameter with great care. Experience from the reference case calibrations showed that the gas rate gave the most accurate results when it comes to achieving a match with the historical production. For an ICD- or AICV-equipped well, however, it cannot be expected that the well will perform in the same way. For instance, the simulations in Section 4 used the base case gas rate as a basis for simulating ICDs in the well. The rationale behind this was that the wells were generally regulated by an approximate gas rate of 1 Million Sm^3/day. Whether or not this would be the case with ICDs installed can be argued. However, the ICD simulations gave an impression of the production behavior of the well, which was the main objective.

For the AICV cases, various boundary conditions were tested to see how the results differed. These include the BC oil rate, half the BC gas rate and the BC downhole rate. As evident in Table 13, the results for all three alternatives imply the same behavior in terms of reduced gas production and/or increased oil production. It can therefore be expected that the results and conclusions from these simulation are quite reliable.

However, there should exist a rationale behind the choice of boundary condition, and the presumptions should be made clear, as to not cause any confusions about the results.

7.6 Inflow Control Well Design

There are three main uncertainties related to the implementation of inflow control in the two well designs.

A widely debated topic in the industry is the choice of a tailored vs. a uniform ICD configuration along the whole well length. Some operators prefer to have a tailored ICD configuration with various strengths, in accordance to the modeled inflow and permeability profiles. However, the majority of vendors providing the ICDs do not recommend this approach due to a number of reasons. Firstly, the uncertainty regarding the permeability profile in new wells is quite high. Even with well logs, it cannot be said with confidence that the logged permeability at a certain depth is radially representative throughout the

reservoir. Heterogeneities throughout the reservoir is generally fair to assume, and logs do not demonstrate this picture. Therefore, unless extensive knowledge and experience indicate high heterogeneities in reservoir quality and permeability, it is not recommended to go for a tailored ICD configuration. In the case of a tailored ICD with the wrong assumptions, the solution can actually worsen the production performance.

Moreover, failing to reach TD when running an ICD completion with customized strengths (restrictions), will deem the ICD customization pointless. In many cases, it could counteract its purpose, where e.g. low productive oil zones are greatly restricted, while highly productive gas/water compartments meet minimal restriction.

A common misconception among some completion engineers is that the placement of ICDs with identical configurations along the whole well implies the same restrictive choking for the entire well length. However, as discussed in Section 2.3.2 the restrictive nature of all inflow control devices is rate-dependent, meaning that the choking is dependent on the inflow behavior at each respective zone. Put in other words, the ICD completion can be considered to be self customizing, by "reading" the inflow performance along the wellbore and restricting the inflow accordingly. For the sake of operational robustness and engineering simplicity it is therefore generally recommended to use a uniform ICD configuration. All ICT simulations in this thesis featured a uniform configuration, and it is not expected that a customized configuration would have significantly improved the obtained results.

The choice of ICD nozzle size is also an important detail in the design process, which depends on the intention of the integration of ICT in the completion. In the case where it is necessary to hold back gas, a small nozzle diameter is recommended. This was demonstrated in Table 8 and Figure 72 to 74 where the smallest nozzle size showed better gas control and improved oil production. On the contrary, if the reason for using ICDs is to hold back water, it is recommended to rather use a relatively larger nozzle size. As shown in Table 10 for B1, a smaller nozzle size showed an increase in water production.

The third consideration when it comes to IC well design, is the number of annular packers. As emphasized in Section 2.3, the importance of annular compartmentalization is essential for the proper functionality of ICDs and reduction of annular flow and screen erosion risk. In our simulations, one swell packer per screen joint was defined in the models. From an engineering perspective, this is the optimal solution. However, from a practical and operational point of view, running the completion with fewer swell packers is more attainable, and reduces the risk of getting stuck while running the completion into the wellbore. It is rather typical to place one swell packer per fifth or tenth screen joint. For

our simulations, this is expected to give a poorer ICD performance. In terms of holding back high flux zones and equalizing the inflow rate, fewer swell packers can lead to a poorer equalization effect and in some cases also crossflow between high- and low-pressure zones. As previously discussed, poor use of annular compartmentalization will also exacerbate the effect of an early water breakthrough.

With the use of AICVs in the well, the importance of compartmentalization becomes greater. With a high number of swell packers along the completion, the AICV will better manage gas producing zones, while opening for production in oil producing zones. In the case with few annular isolation packers, the production of oil and gas will be commingled, which keeps the AICV in a semi-closed position; Impeding oil production but without completely preventing gas influx. Conclusively, a worse performance could be expected from ICDs and AICVs with fewer annular packers along the well.

7.7 Number of effective inflow control units

When a borehole has been drilled, settled particles and drilling mud with fine particles can be expected to stay present in the horizontal section of the well. Consequently, when the lower completion is run into the well, the screens and inflow control devices may be plugged with mud or fine particles. This can typically occur at the low-side of the borehole where the particles have settled. The consequence of this is a lower number of effective ICDs/AICVs, and a smaller effective flow area for fluid to enter the tubing. Hence, it would be similar to having a smaller nozzle size, i.e. give a higher IC pressure drop. For well B3, it was observed that a smaller nozzle size yielded better results, at the expense of a higher IC pressure drop, see Table 8.

For well B1, it is anticipated that the plugging of inflow control units, would increase the production of water and reduce oil production as a result of a smaller flow area per joint, see Table 10.

In NETool, there is no other way to simulate the effect of plugging than to alter the nozzle size or number of ICDs per joint. For AICVs it could be possible to acquire coefficients for a valve with higher restriction, or to lower the number of valves per joint. However, to quantify this risk is not an easy task, since it is impossible to predict how many units that will be plugged.

Table 14: *Summary of uncertainties*

Uncertainty	Explanation	Final level of impact
Limitations with NETool	The basic assumptions within the software can limit the accuracy of the results, potentially leading to wrong conclusions. The downhole behavior shown in the simulations is a result of estimated permeability profiles and phase fractions along the wellbore. Additionally, NETool is a static simulator which cannot capture the dynamic production behavior of the wells.	High
Reservoir model	The accuracy of any reservoir model can always be questionned, as it is a result of numerous assumptions and estimations. The fact that the reservoir model has been run through ResX limits this uncertainty to some degree for B3. Furthermore, an uncertainty is linked to the modelling of blank pipe sections as cemented annulus in Eclipse.	Medium
Quality of history matching	Although a fairly adequate match was obtained for both wells, there were some deviations that could not be eradicated. These uncertainties should be kept in mind when assessing the quality of our work.	Low
Production measurements	While a fairly high certainty is linked to the gas rate measurements in the production profile, the same cannot be said for the water and oil rates. Consequently, this uncertainty can play an important role in the accuracy of our history matching results.	Low
Choice of boundary condition	The software will always try and achieve results in accordance to the boundary condition provided by the user. It is therefore of utmost importance that the choice of boundary condition is done with great care and awareness.	Low
Inflow Control Well Design	Three topics that are always up for debate when it comes to IC well design, are the choice of number of annular packers, choice of ICD nozzle (size) and lastly the use of a tailored vs. Uniform IC configuration along the well length. The work in our thesis was based on maintaining simplicity while optimizing the well design. This involved using the maximum number of annular packers along with a uniform configuration along the well. Consequently, the nozzle size / restriction could be optimized by iterative methods.	Low
Number of effective IC units.	It is not easy to predict whether or not all IC units installed in the well will function as intended. In some cases they can be plugged by settled particles left in the wellbore after drilling. Consequently, this can lead to a smaller effective flow area and show similar behavior as a smaller ICD nozzle size configuration with a higher restriction. For AICVs, it is not as easy to predict this behavior.	Low

Table 14 shows a summary of the uncertainties discussed in Section 7. In the rightmost column, an attempt has been made to quantify the impact, with basis in the discussion of each respective uncertainty. Considering the discussions above, it can be concluded that a majority of the uncertainties listed have been greatly reduced as a result of the reference case history matching. Ultimately, some degree of uncertainty must be recognized, as is the case with the majority of simulation studies.

8 Conclusions

The objectives of this thesis were extensively pursued, starting with a description of the Gjøa field and the two candidate wells. The production history and challenges for the two oil wells were closely addressed, before an in-depth review of current inflow control technologies followed. A great number scientific papers were assessed to gain extensive knowledge about the functionality and experience of each technology. Generally speaking, all technologies proved to be beneficial in terms of improved recovery, under the correct circumstances.

To further investigate the benefits of the technologies, simulations within NETool were performed. The first part of the simulation work was assigned to the calibration of the models with respect to production history. This improved the accuracy of the models and ensured some degree of confidence in the subsequent simulations with ICT. It also allowed us to see a clear difference in performance between the conventional (existing) completions and alternative ICT-completions, in terms of flow behaviour, pressures and production rates. Several inflow control technologies and configurations were evaluated, providing a better understanding of the functionality and effect of the respective designs.

The results for the two oil wells showed different behaviors with the inclusion of inflow control. The first candidate, B3, was a long horizontal well with challenges linked to excessive gas production and immobilized oil reserves. Results from the simulations were promising with both standard nozzle-ICDs and AICVs. The final recommendation for the well involves the use of the FloSure TR7 AICV, which proved to be the optimal solution for holding back gas and promoting oil production at a relatively low pressure drop, throughout the lifetime of the well.

The second candidate well, B1, has previously suffered from a water breakthrough which has dominated production in the last couple of years. Calibrating this well to match with the production history was a long and challenging process which resulted in alterations of the relative permeability data. The results from the IC simulations did not show significant improvements in the performance. In fact, the they indicated a higher water rate as a result of the downhole flux equalization. There are however, limitations and uncertainties to these results which indicate that the opposite effect can be expected, with a delayed water breakthrough and increased oil rate at an early-life period. A previous ICD study examining the use of ICDs on B1, supports this conclusion. The recommended design for B1 includes a nozzle-ICD configuration with a 3 x 4mm ICD configuration.

There are other benefits related to the adaption of ICT which can improve well

performance and justify the inclusion of the technology in the well design, including improved well clean-up and increased PI values. However, these benefits can only be quantified by assessing previous experiences in analogue wells, and cannot be demonstrated with simulations.

The are a number of limitations and uncertainties related to the simulations and results that we have obtained. The history matching aspect of our work helped reduce the impact of these uncertainties to the minimum. The biggest uncertainty was associated with the limitations of the NETool software. Realizing this, the indications and conclusions from the results are still valid.

8.1 Future recommendations

There are a number recommendations that follow the findings in this study. By using the configurations resulting from this study, modeling the proposed configurations in Eclipse could be the next step to obtain more conclusive results in terms of cumulative production and dynamic behavior. It would be interesting to see if the results regarding delayed water breakthrough and increased oil recovery from the 2007 Reslink ICD study could be verified with the updated reservoir model.

Retrospective evaluations of well performance is a key for improving knowledge and completing the learning cycle. As previously mentioned, we have to learn from the past to better predict the future. The learnings will hopefully aid in expanding the knowledge on inflow control within Neptune Energy, and can improve future decision making when planning new in-fill well designs. It is recommended to do similar studies for other wells on Gjøa, that may be facing other production challenges.

When designing new wells with inflow control, the first approach should be to use Landmark NETool. The software allows for fast and simple simulations, so that the optimal IC technology and configuration can be found. Sensitivity analyses towards the number of necessary swell packers, restrictive setting, type of ICT and number of units per joint should be conducted to find the optimal solution.

Following this optimization, subsequent simulations with ICT should be performed in dynamic reservoir simulators such as Eclipse, to see the cumulative behavior. It is not an easy task to model an inflow control completion in Eclipse and incompetence with such modeling can quickly lead to inaccurate results and false conclusions. It is therefore suggested that this task is handed over to ICD experts, as they have the knowledge and experience in doing such reservoir modeling.

For the NETool simulations performed in this study, the software license at the university computers was used. Admittedly, this proved to be quite time-consuming. For future studies, it is recommended to purchase a NETool software license to perform in-house simulations. The user manual and simple user interface makes it easy to get into the software and learn how to use it.

An important key when it comes to incorporating inflow control in new well designs, is the close cooperation and communication between the subsurface and well engineering department. A good understanding of the formation and reservoir challenges establishes a solid foundation for selecting the appropriate inflow control design.

References

[1] Statoil. *Plan for development and operation of Gjøa - Part I.* Technical Report PL 153, Statoil ASA, Desember 2006.

[2] Halvard Bjørkesett Cesar Alvarez Harald Mortensen, Gisle Kvevik. *Plan for development and operation of Gjøa - Drilling, completion and production Support document.* Internal RE-GJO-0004, Statoil ASA, 12 2006.

[3] *NPD Factpages - The Gjøa Field.* URL `https://goo.gl/qXk3qm`.

[4] Karin Ask, Merete Eikemo, Torunn Haugvallstad, Roar Heggland, Eric Haller, Eva Holand, Pamela Kaiser, Ole Petter Lødøen, Inger Kloster Osmundsen, Jon Helge Rasmussen, and Rini Verbruggen. *Plan for development and operation of Gjøa - Subsurface support document.* Technical Report RE-GJO-0002, Statoil ASA, Desember 2006.

[5] Torunn Haugvaldstad and Jon Helge Rasmussen. *Gjøa Reslink ICD Study.* Internal Presentation, December 2007.

[6] Steffen Kristiansen and Cor de Boer. *Final Well Report, Drilling and Completion Well NO 35/9-B-3 H/HT2.* Internal, January 2010.

[7] Beder Mohammad Al Furati. *Discussions with Production Engineer Neal Hewitt at Neptune Energy*, 2018.

[8] Beder Mohammad Al Furati. *Data received from Production Engineer Neal Hewitt at Neptune Energy.* Internal, 2018.

[9] Steen Tino Svenningsen, Alf Kjetil Vølstad, Cor de Boer, and Per Brekke Foldøy. *Final Well Report, Drilling and Completion Well NO 35/9-B-1 AHT3.* Internal, December 2012.

[10] Beder Mohammad Al Furati. *Data received from the Reservoir Engineering department at Neptune Energy.* Internal, 2018.

[11] Mark Glaser, Ben Butler, and Gorm Liland. *Reducing Well Costs and Extending Field Life with Intelligently Controlled Trilateral and Quadrilateral TAML Level-5 Multilaterals.* Society of Petroleum Engineers, 2017. doi: 10.2118/184608-MS.

[12] Ayesha A. Rahman Al Marzouqi, Hamdy Helmy, Ashraf Al-Saiid Keshka, Magdi Elasmar, and Shaiful Shafia. *Wellbore segmentation using Inflow Control Devices: Design & Optimization Process.* Society of Petroleum Engineers, 2010. doi: 10.2118/137992-MS.

[13] Jonathan Bellarby. *Well completion design*, volume vol. 56 of *Developments in petroleum science.* Elsevier, Oxford, 2009. ISBN 9780444532107.

[14] Terje Moen and Harald Arne Asheim. *Inflow Control Device and Near-Wellbore Interaction.* Society of Petroleum Engineers, 2008. doi: 10.2118/112471-MS.

[15] Terje Moen. *ICD / AICD Technology.* Internal Presentation, December 2017.

[16] Pål Skalle. *Drilling Fluid Engineering.* Pål Skalle and Ventus Publishing ApS, 4. edition, 2013. ISBN 9788740305821.

[17] C. Bennett, J. M. Gilchrist, E. Pitoni, R. C. Burton, R. M. Hodge, J. Troncoso, S. A. Ali, R. Dickerson, C. Price-Smith, and M. Parlar. *Design Methodology for Selection of Horizontal Open-Hole Sand Control Completions Supported by Field Case Histories.* Society of Petroleum Engineers, 2000. doi: 10.2118/65140-MS.

[18] Anne Mette Mathisen, Gry Lien Aastveit, and Eva Alteraas. *Successful Installation of Stand Alone Sand Screen in more than 200 Wells - the Importance of Screen Selection Process and Fluid Qualification.* Society of Petroleum Engineers, 2007. doi: 10.2118/107539-MS.

[19] E. E. Ratterman, B. A. Voll, and J. R. Augustine. *New Technology Applications to Extend Field Economic Life by Creating Uniform Flow Profiles in Horizontal Wells: Case Study and Technology Overview.* Offshore Technology Conference, 2005. doi: 10.4043/17548-MS.

[20] Harald Asheim and Piet Oudeman. *Determination of Perforation Schemes To Control Production and Injection Profiles Along Horizontal Wells*. Society of Petroleum Engineers, 1997. doi: 10.2118/29275-PA.

[21] Kristian Brekke and S. C. Lien. *New and Simple Completion Methods for Horizontal Wells Improve the Production Performance in High-Permeability, Thin Oil Zones*. Society of Petroleum Engineers, 1994. doi: 10.2118/24762-PA.

[22] A. Haaland, G. Rundgren, and Ø. Johannessen. *Completion Technology On Troll-Innovation And Simplicity*. Offshore Technology Conference, 2005. doi: 10.4043/17113-MS.

[23] Vidar Mathiesen, Bjernar Werswick, Haavard Aakre, and Geir Elseth. *Autonomous Valve, A Game Changer Of Inflow Control In Horizontal Wells*. Society of Petroleum Engineers, 2011. doi: 10.2118/145737-MS.

[24] Bernt Sigve Aadnoy and Geir Hareland. *Analysis of Inflow Control Devices*. Society of Petroleum Engineers, 2009. doi: 10.2118/122824-MS.

[25] Ismail Isma Mohd. *Tendeka AICD Presentation Engie 19th Jan*. Internal Presentation, January 2018.

[26] Edwin Felipe Rios Fuentes. *Clean-up of horizontal well using ICD*. Master's thesis, University of Stavanger, 2016. URL `http://hdl.handle.net/11250/2409318`.

[27] Kieran Joseph Neylon, Edel Reiso, Jonathan Anthony Holmes, and Ole Bernt Nesse. *Modeling Well Inflow Control with Flow in Both Annulus and Tubing*. Society of Petroleum Engineers, 2009. doi: 10.2118/118909-MS.

[28] Peter Elliot Smith, Dustin A. Young, Noman Shahreyar, Jon Eric Lauritzen, and Mohd Zaki Bin Awang. *The Bulkhead Principle - Delaying Water Cut and Improving Horizontal Well Productivity through Compartmentalization Using Short Swellable Packers*. Society of Petroleum Engineers, 2011. doi: 10.2118/147877-MS.

[29] Henry Eugene Rogers, David Allison, and Earl Don Webb. *New Equipment Designs Enable Swellable Technology in Cementless Completions*. Society of Petroleum Engineers, 2008. doi: 10.2118/112302-MS.

[30] Toni Ezeukwu, Horace Awi, Tim Martinson, Bruno Stenger, and Frederic Guinot. *Successful Installation of Elastomeric Packers/Expandable Sand Screen in Subsea Openhole Completions Offshore Nigeria*. Society of Petroleum Engineers, 2007. doi: 10.2118/111885-MS.

[31] Anil K. Sadana, Greg Badke, Christopher Cook, and Xiao Wang. *Water Swell Packers with High Salinity Tolerance and Increased Performance Envelope*. Society of Petroleum Engineers, 2017. doi: 10.2118/183834-MS.

[32] Rolf Prydz. *Troll Oil Development Concept*. Offshore Technology Conference, 1993. doi: 10.4043/7171-MS.

[33] Knut Herman Henriksen, Eli Iren Gule, and Jody R. Augustine. *Case Study: The Application of Inflow Control Devices in the Troll Field*. Society of Petroleum Engineers, 2006. doi: 10.2118/100308-MS.

[34] Eltazy Mohammed Khalid Eltaher. *Modelling and applications of Autonomous Flow Control Devices*. PhD thesis, Heriot-Watt University, February 2017.

[35] Saeed Shad and Mehdi Majdi Yazdi. *Wellbore Modeling and Design of Nozzle-Based Inflow Control Device (ICD) for SAGD Wells*. Society of Petroleum Engineers, 2014. doi: 10.2118/170145-MS.

[36] P. et al. Gavioli. *Evaluating Four Types of Passive Inflow Control Devices*. Presentation at ICT Network. Perth, Australia, 2008.

[37] Quanshu Zeng, Zhiming Wang, and Gang Yang. *Comparative Study on Passive Inflow Control Devices by Numerival Simulation*. Tech Science Press, 2013. URL `www.techscience.com/doi/10.3970/sl.2013.009.169.pdf`.

[38] Quanshu Zeng, Zhiming Wang, Xiaoqiu Wang, Yiwei Li, Weilin Zou, Jingnan Xiao, Tian Chen, Gang Yang, and Quan Zhang. *Selection of Passive Inflow Control Devices Based on Dynamic Weight Fuzzy Evaluation*, 01 2014.

[39] Bruce R Munson. *Fundamentals of fluid mechanics*. Wiley, Hoboken, N.J, 5th ed. edition, 2006. ISBN 9780471675822.

[40] Jason Matthew Visosky, Nicholas Jacob Clem, Martin P. Coronado, and Elmer Richard Peterson. *Examining Erosion Potential of Various Inflow Control Devices To Determine Duration of Performance*. Society of Petroleum Engineers, 2007. doi: 10.2118/110667-MS.

[41] Schlumberger. *Product Sheet: ResFlow Inflow Control Device*. URL `https://goo.gl/EN5iXr`.

[42] Kim Sam Youl, Harkomoyo Harkomoyo, Widayat Suhana, Rhandy Espinosa Regulacion, and Thomas Jorgensen. *Passive Inflow Control Devices and Swellable Packers Prove to Control Water Production in Fractured Carbonate Reservoir: A Comparison with Slotted Liner Completions*. Society of Petroleum Engineers, 2011. doi: 10.2118/140010-MS.

[43] Martin Halvorsen, Martin Madsen, Mathias Vikøren Mo, Ismail Isma Mohd, and Annabel Green. *Enhanced Oil Recovery On Troll Field By Implementing Autonomous Inflow Control Device*. Society of Petroleum Engineers, 2016. doi: 10.2118/180037-MS.

[44] E. J. James and M. M. Hossain. *Evaluation of Factors Influencing the Effectiveness of Passive and Autonomous Inflow Control Devices*. Society of Petroleum Engineers, 2017. doi: 10.2118/186926-MS.

[45] Luis Garcia, Martin P. Coronado, Ronnie D. Russell, Gonzalo Alberto Garcia, and Elmer Richard Peterson. *The First Passive Inflow Control Device That Maximizes Productivity During Every Phase of a Well's Life*. International Petroleum Technology Conference, 2009. doi: 10.2523/IPTC-13863-MS.

[46] Brandon Least, Stephen Greci, Russell Conway Burkey, Adam Ufford, and Angel Wilemon. *Autonomous ICD Single Phase Testing*. Society of Petroleum Engineers, 2012. doi: 10.2118/160165-MS.

[47] Michael Fripp, Liang Zhao, and Brandon Least. *The Theory of a Fluidic Diode Autonomous Inflow Control Device*. Society of Petroleum Engineers, 2013. doi: 10.2118/167415-MS.

[48] Georgina Corona, Michael Fripp, and Weiqi Yin. *Fluidic Diode Autonomous ICD Multiphase Performance in Light-Oil Reservoirs*. Society of Petroleum Engineers, 2017. doi: 10.2118/183863-MS.

[49] Georgina Corona, Stephen Greci, Brandon Least, Weiqi Yin, and Jacqueline Plumlee. *Fluidic Diode Autonomous ICD Single-Phase Testing*. Society of Petroleum Engineers, 2016. doi: 10.2118/180303-MS.

[50] Halliburton. *Product Sheet: Halliburton Equiflow Autonomous Inflow Control Device*, April 2017. URL `https://goo.gl/F41LWf`.

[51] Georgina Corona, Michael Fripp, Tejas Kalyani, and Weiqi Yin. *Fluidic Diode Autonomous Inflow Control Device for Heavy Oil Application*. Society of Petroleum Engineers, 2016. doi: 10.2118/184094-MS.

[52] Schlumberger. *Product Sheet: Autonomous ICD*, April 2018. URL `https://goo.gl/CxhpSR`.

[53] Terje Moen and Aleksandar Rudic. *System and methodology utilizing inflow control device assembly*. Patent, March 2017. URL `https://goo.gl/utF4GM`.

[54] Martin Halvorsen, Geir Elseth, and Olav Magne Naevdal. *Increased oil production at Troll by autonomous inflow control with RCP valves*. Society of Petroleum Engineers, 2012. doi: 10.2118/159634-MS.

[55] Haavard Aakre, Britt Halvorsen, Bjornar Werswick, and Vidar Mathiesen. *Autonomous Inflow Control Valve for Heavy and Extra-Heavy Oil*. Society of Petroleum Engineers, 2014. doi: 10.2118/171141-MS.

[56] Bernt Sigve Aadnøy. *Modern well design*. CRC Press/Balkema, Boca Raton, 2010. ISBN 9780415884679.

[57] Vidar Mathiesen, Bjornar Werswick, and Haavard Aakre. *The Next Generation Inflow Control, the Next Step to Increase Oil Recovery on the Norwegian Continental Shelf*. Society of Petroleum Engineers, 2014. doi: 10.2118/169233-MS.

[58] Haavard Aakre, Britt Halvorsen, Bjørnar Werswick, and Vidar Mathiesen. *Smart Well With Autonomous Inflow Control Valve Technology*. Society of Petroleum Engineers, 2013. doi: 10.2118/164348-MS.

[59] Anita B. Elverhøy, Haavard Aakre, and Vidar Mathiesen. *Autonomous Inflow Control for Maximizing Oil Recovery and Minimizing Water/Steam Production*. Society of Petroleum Engineers, 2018. doi: 10.2118/190016-MS.

[60] Ransis Kais, Vidar Mathiesen, Haavard Aakre, Glenn Woiceshyn, Amr Elarabi, and Ricardo Hernandez. *First Autonomous Inflow Control Valve AICV Well Completion Deployed in a Field Under an EOR Water & CO2 Injection Scheme*. Society of Petroleum Engineers, 2016. doi: 10.2118/181552-MS.

[61] Ikhsan Nugraha, Terki K AlBassam, Alessandro Gallelli, and Vidar Mathiesen. *Optimizing Reservoir Performance through Utilization of Autonomous Inflow Control Valve –Lessons Learnt from the World's First Installation*. Society of Petroleum Engineers, 2016. doi: 10.2118/182755-MS.

[62] Anita B. Elverhøy, Haavard Aakre, and Vidar Mathiesen. *Autonomous Inflow Control for Reduced Water Cut and/or Gas Oil Ratio*. Offshore Technology Conference, 2018. doi: 10.4043/28860-MS.

[63] Vidar Mathiesen and Beder Al Furati. *Discussions with Vidar Mathiesen, CEO of Inflow-Control*, June 2018.

[64] Trygve Rinde, Rune Killie, Totte Lager, Tron Solberg, Mikkel Bakli, and Vegar Grüner. *Design of a New and Viscosity Independent Autonomous Inflow Control System*. Society of Petroleum Engineers, 2017. doi: 10.2118/183930-MS.

[65] Eddie G Bowen and Bernt Sigve Aadnoy. *A Quasi Intelligent Flow Control Device for Water Injectors*. Society of Petroleum Engineers, 2014. doi: 10.2118/170463-MS.

[66] Beder Mohammad Al Furati. *Discussions with Proffesor at UiS & NTNU Bernt S. Aadnoy*, 2018.

[67] V. Y. Volkov, A. P. Skibin, O. N. Zhuravlev, M. T. Nukhaev, and R. V. Shchelushkin. *Adaptive Inflow Control System*. ArXiv e-prints, August 2014. URL `http://adsabs.harvard.edu/abs/2014arXiv1408.5251V`.

[68] S. V. Delia, M. V. Chertenkov, A. V. Zhakovschikov, V. V. Matsashik, O. N. Zhuravlev, and R. V. Shchelushkin. *Field Tests of a New Generation of Flow Control Unit Able to Prevent the Gas Breakthrough in Oil Wells*. Society of Petroleum Engineers, 2015. doi: 10.2118/178417-MS.

[69] Halliburton. *Landmark NETool 5000.0.4.1*. Software, 2015.

[70] Beder Mohammad Al Furati. *Discussions with Reservoir Engineer Claire Le Maitre at Neptune Energy*, 2018.

[71] *NETool 5000.0.4.x Technical Manual*. Halliburton, December 2014.

[72] Beder Mohammad Al Furati. *Discussions with IRIS PhD Fellow Reza Azkarineshad*, 2018.

[73] Beder Mohammad Al Furati. *Discussions and input from Reservoir Engineer at Tendeka, Jon Endre Mjos*, 2018.

[74] Beder Mohammad Al Furati. *Discussions with ICD & Screen Advisor at Ridge, Terje Moen*, 2018.

[75] Benn A. Voll, Ismarullizam Mohd Ismail, and Iko Oguche. *Sustaining Production by Limiting Water Cut and Gas Break Through With Autonomous Inflow Control Technology.* Society of Petroleum Engineers, 2014. doi: 10.2118/171149-MS.

[76] Beder Mohammad Al Furati. *Discussions with Senior Completion Engineer at Neptune Energy and Ridge, Lasse Hermansson*, 2018.

Appendices

All data used and obtained from the simulation work are presented here. It should be mentioned that some of the results figures shown in the appendices are also included in Part II, if they are necessary for the discussions. The appendices consists of:

A Input Data for the Base Case model

A.1 Well B3 NETool Well Design

Hole & Completion

#	Top MD [m]	Seg. Length [m]	Top TVD(SS) [m]	Casing/Liner	Sand Control	User Notes
1	2613.00	38.48	2040.07	Cemented Blank Pipe	-	5.5" 23lbs/ft Vam Top tubing
2	2651.48	3.05	2062.24	Cemented Blank Pipe	-	5.5" 23lbs/ft Vam Top Pup Joint
3	2654.53	0.76	2063.97	Cemented Blank Pipe	-	5.5 x 7" X-over
4	2655.29	1.97	2064.40	Cemented Blank Pipe	-	7" 29lbs/ft Vam Top Pup Joint
5	2657.26	22.40	2065.51	Cemented Blank Pipe	-	7" 29lbs/ft Vam Top Tubing
6	2679.66	4.08	2077.97	Cemented Blank Pipe	-	7" 29lbs/ft Vam Top Pup Joint
7	2683.74	1.28	2080.16	Cemented Blank Pipe	-	7" Single Cycle Tool (SCT)
8	2685.02	3.59	2080.85	Cemented Blank Pipe	-	7" Baker Full Bore Isolation Valve (FBIV)
9	2688.61	1.94	2082.75	Cemented Blank Pipe	-	7" 29lbs/ft Vam Top Pup Joint
10	2690.55	696.44	2083.77	Cemented Blank Pipe	-	7" 29lbs/ft Vam Top Tubing
11	3386.99	2.55	2309.48	Cemented Blank Pipe	-	7" 29lbs/ft Seal Stem w/ shearable No-go
12	3389.54	2.20	2309.73	Cemented Blank Pipe	-	7" Self Aligning Mule Shoe
13	3391.74	8.01	2309.94	Cemented Blank Pipe	-	7 x 9 5/8" Uniflex Liner Hanger Packer w/ PBR
14	3399.75	0.75	2310.68	Cemented Blank Pipe	Packer	7 x 6 5/8" X-over
15	3400.50	1.56	2310.75	Cemented Blank Pipe	Packer	6 5/8" 24lbs/ft Pup Joint
16	3402.06	38.44	2310.88	Cemented Blank Pipe	Packer	6 5/8" 24lbs/ft Vam Top Tubing
17	3440.50	335.07	2313.48	-	Packer	Csg shoe
18	3775.57	302.44	2313.67	-	Screen	6 5/8" 24lbs/ft Ultra grip ww-screen (250micron)
19	4078.01	397.72	2313.84	-	Packer	6 5/8" 24lbs/ft Vam Top Tubing
20	4475.73	813.15	2313.87	-	Screen	6 5/8" 24lbs/ft Ultra grip ww-screen (250micron)
21	5288.88	46.92	2313.58	-	Packer	6 5/8" 24lbs/ft Vam Top Tubing
22	5335.80	12.12	2313.63	-	Packer	Swell Packer 6 5/8"
23	5347.92	11.75	2313.66	-	Packer	6 5/8" 24lbs/ft Vam Top Tubing
24	5359.67	0.47	2313.68	-	Packer	6 5/8" Bull Nose

Figure A-1: *B3-HT2 Completion setup in NETool. The upper completion was entered as cemented blank pipe, since there is no inflow contribution here. Also, all blank pipe sections in the lower completion were entered as packers since they were modeled accordingly in Eclipse.*

Diameters

#	Top MD [m]	Seg. Length [m]	Top TVD(SS) [m]	Wellbore Diameter [in]	Casing/Liner ID [in]	Sand Control OD [in]	Sand Control ID [in]
1	2613.00	38.48	2040.07	10.5	4.67	-	-
2	2651.48	3.05	2062.24	10.5	4.67	-	-
3	2654.53	0.76	2063.97	10.5	4.67	-	-
4	2655.29	1.97	2064.40	10.5	6.184	-	-
5	2657.26	22.40	2065.51	10.5	6.184	-	-
6	2679.66	4.08	2077.97	10.5	6.184	-	-
7	2683.74	1.28	2080.16	10.5	5.75	-	-
8	2685.02	3.59	2080.85	10.5	5.75	-	-
9	2688.61	1.94	2082.75	10.5	6.184	-	-
10	2690.55	696.44	2083.77	10.5	6.184	-	-
11	3386.99	2.55	2309.48	10.5	5.891	-	-
12	3389.54	2.20	2309.73	10.5	5.75	-	-
13	3391.74	8.01	2309.94	10.5	8.553	-	-
14	3399.75	0.75	2310.68	10.5	8.553	-	5.921
15	3400.50	1.56	2310.75	10.5	8.553	-	5.921
16	3402.06	38.44	2310.88	10.5	8.553	-	5.921
17	3440.50	335.07	2313.48	8.5	-	-	5.921
18	3775.57	302.44	2313.67	8.5	-	7.299	5.921
19	4078.01	397.72	2313.84	8.5	-	-	5.921
20	4475.73	813.15	2313.87	8.5	-	7.299	5.921
21	5288.88	46.92	2313.58	8.5	-	-	5.921
22	5335.80	12.12	2313.63	8.5	-	-	5.921
23	5347.92	11.75	2313.66	8.5	-	-	5.921
24	5359.67	0.47	2313.68	8.5	-	-	5.921

Figure A-2: *B3-HT2 Completion diameters in NETool. In this case, the Sand Control ID and OD refer to the base pipe ID and OD, respectively.*

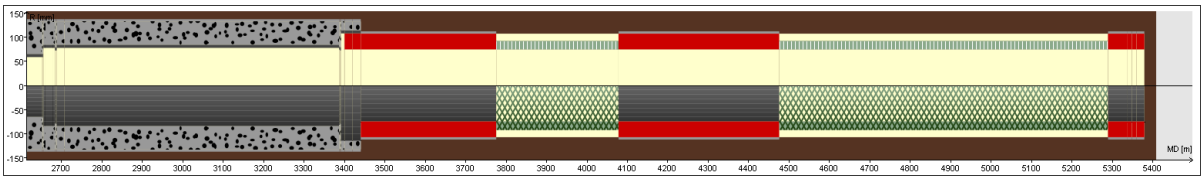

Figure A-3: *B3-HT2 Base Case Completion schematic in NETool.*

A.2 Well B1 NETool Well Design

Hole & Completion

#	Top MD	Seg. Length	Top TVD(SS)	Casing/Liner	Sand Control	User Notes
	[m]	[m]	[m]			
1	2607.00	1.83	2061.70	Cemented Blank Pipe	-	7" 29lbs/ft Vam Top Pup Joint
2	2608.83	3.05	2062.94	Cemented Blank Pipe	-	7" 29lbs/ft Vam Top Pup Joint
3	2611.88	1.45	2064.99	Cemented Blank Pipe	-	7" Gauge Carrier
4	2613.33	2.06	2065.97	Cemented Blank Pipe	-	7" 29lbs/ft Vam Top Pup Joint
5	2615.39	22.00	2067.36	Cemented Blank Pipe	-	7" 29lbs/ft Vam Top Tubing
6	2637.39	3.05	2082.21	Cemented Blank Pipe	-	7" 29lbs/ft Vam Top Pup Joint
7	2640.44	3.66	2084.27	Cemented Blank Pipe	-	9.625 x 7" Production Packer
8	2644.10	0.58	2086.73	Cemented Blank Pipe	-	7x5.5" X-over
9	2644.68	2.00	2087.13	Cemented Blank Pipe	-	5.5" 23lbs/ft Pup, Vam Top B X P
10	2646.68	0.70	2088.47	Cemented Blank Pipe	-	5.5" Landing Nipple
11	2647.38	2.00	2088.95	Cemented Blank Pipe	-	5.5" 23lbs/ft Pup, Vam Top B X P
12	2649.38	25.00	2090.29	Cemented Blank Pipe	-	5.5" 23lbs/ft L80 Vam Top Tubing
13	2674.38	3.00	2107.15	Cemented Blank Pipe	-	5.5" 23lbs/ft Pup, Vam Top B X P
14	2677.38	0.60	2109.18	Cemented Blank Pipe	-	5.5 x 7" X-over
15	2677.98	2.00	2109.58	Cemented Blank Pipe	-	7" 29lbs/ft Vam Top Pup Joint
16	2679.98	2.05	2110.94	Cemented Blank Pipe	-	7" 29lbs/ft Vam Top Pup Joint
17	2682.03	1.15	2112.32	Cemented Blank Pipe	-	7" Single Cycle Tool (SCT)
18	2683.18	3.74	2113.10	Cemented Blank Pipe	-	7" Baker Full Bore Isolation Valve (FBIV)
19	2686.92	2.09	2115.62	Cemented Blank Pipe	-	7" 29lbs/ft Vam Top Pup Joint
20	2689.01	3.00	2117.03	Cemented Blank Pipe	-	7" 29lbs/ft Vam Top Pup Joint
21	2692.01	4.75	2119.05	Cemented Blank Pipe	-	Locator Ring 8"
22	2696.76	49.22	2122.24	Cemented Blank Pipe	-	7" Self Aligning Mule Shoe
23	2745.98	294.02	2154.25	Cemented Blank Pipe	-	7" Liner
24	3040.00	6.00	2306.10	Cemented Blank Pipe	-	Seal Bore Receptacle
25	3046.00	1.90	2307.21	Cemented Blank Pipe	-	5" 15lbs/ft Hydraulic Flex Lock
26	3047.90	3.00	2307.54	Cemented Blank Pipe	-	5" 15lbs/ft Pup Joint
27	3050.90	3.00	2308.03	Cemented Blank Pipe	-	5" 15lbs/ft Pup Joint
28	3053.90	0.57	2308.49	Cemented Blank Pipe	-	5" x 4.5" X-over
29	3054.47	2.58	2308.58	Cemented Blank Pipe	-	4.5" 12.6lbs/ft Vam Top Box X pin
30	3057.05	48.93	2308.94	Cemented Blank Pipe	Packer	4.5" 12.6lbs/ft Vam Top Tubing (Blank pipe)
31	3105.98	25.28	2312.47	Cemented Blank Pipe	Blank Pipe	4.5" 12.6lbs/ft Vam Top Tubing (Blank pipe)
32	3131.26	12.05	2312.97	Cemented Blank Pipe	Packer	Swell Packer B
33	3143.31	186.51	2313.04	-	Screen	4.5" 12.6" Excluder 2000 (250micron)
34	3329.82	73.45	2312.84	-	Packer	4.5" 12.6lbs/ft Vam Top Tubing (Blank pipe)
35	3403.27	274.21	2312.60	-	Screen	4.5" 12.6" Excluder 2000 (250micron)
36	3677.48	148.44	2314.25	-	Packer	4.5" 12.6lbs/ft Vam Top Tubing (Blank pipe)
37	3825.92	62.59	2314.04	-	Screen	4.5" 12.6" Excluder 2000 (250micron)
38	3888.51	221.05	2313.98	-	Packer	4.5" 12.6lbs/ft Vam Top Tubing (Blank pipe)
39	4109.56	287.97	2313.46	-	Screen	4.5" 12.6" Excluder 2000 (250micron)
40	4397.53	12.37	2313.49	-	Packer	4.5" 12.6lbs/ft Vam Top Tubing (Blank pipe)
41	4409.90	0.24	2313.44	-	Packer	4.5" Bull Nose

Figure A-4: *B1-AHT3 Completion setup in NETool. The upper completion was entered as cemented blank pipe, since there is no inflow contribution here. Also, all blank pipe sections in the lower completion were entered as packers since they were modeled accordingly in Eclipse.*

Diameters

#	Top MD	Seg. Length	Top TVD(SS)	Wellbore Diameter	Casing/Liner ID	Sand Control OD	Sand Control ID
	[m]	[m]	[m]	[in]	[in]	[in]	[in]
1	2607.00	1.83	2061.70	8.5	6.18	-	-
2	2608.83	3.05	2062.94	8.5	6.184	-	-
3	2611.88	1.45	2064.99	8.5	6.072	-	-
4	2613.33	2.06	2065.97	8.5	6.184	-	-
5	2615.39	22.00	2067.36	8.5	6.184	-	-
6	2637.39	3.05	2082.21	8.5	6.184	-	-
7	2640.44	3.66	2084.27	8.5	5.8	-	-
8	2644.10	0.58	2086.73	8.5	4.758	-	-
9	2644.68	2.00	2087.13	8.5	4.67	-	-
10	2646.68	0.70	2088.47	8.5	4.588	-	-
11	2647.38	2.00	2088.95	8.5	4.67	-	-
12	2649.38	25.00	2090.29	8.5	4.67	-	-
13	2674.38	3.00	2107.15	8.5	4.67	-	-
14	2677.38	0.60	2109.18	8.5	4.778	-	-
15	2677.98	2.00	2109.58	8.5	6.184	-	-
16	2679.98	2.05	2110.94	8.5	6.184	-	-
17	2682.03	1.15	2112.32	8.5	5.75	-	-
18	2683.18	3.74	2113.10	8.5	5.75	-	-
19	2686.92	2.09	2115.62	8.5	6.184	-	-
20	2689.01	3.00	2117.03	8.5	6.184	-	-
21	2692.01	4.75	2119.05	8.5	6.094	-	-
22	2696.76	49.22	2122.24	8.5	5.75	-	-
23	2745.98	294.02	2154.25	8.5	6.184	-	-
24	3040.00	6.00	2306.10	8.5	6.184	-	-
25	3046.00	1.90	2307.21	8.5	6.184	-	-
26	3047.90	3.00	2307.54	8.5	6.184	-	-
27	3050.90	3.00	2308.03	8.5	6.184	-	-
28	3053.90	0.57	2308.49	8.5	6.184	-	-
29	3054.47	2.58	2308.58	8.5	6.184	-	-
30	3057.05	48.93	2308.94	8.5	6.184	-	3.96
31	3105.98	25.28	2312.47	8.5	6.184	4.967	4.408
32	3131.26	12.05	2312.97	8.5	6.184	-	3.913
33	3143.31	186.51	2313.04	6.0	-	5.31	3.913
34	3329.82	73.45	2312.84	6.0	-	-	3.913
35	3403.27	274.21	2312.60	6.0	-	5.31	3.96
36	3677.48	148.44	2314.25	6.0	-	-	3.913
37	3825.92	62.59	2314.04	6.0	-	4.967	3.96
38	3888.51	221.05	2313.98	6.0	-	-	3.913
39	4109.56	287.97	2313.46	6.0	-	5.31	3.96
40	4397.53	12.37	2313.49	6.0	-	-	3.913
41	4409.90	0.24	2313.44	6.0	-	-	3.96

Figure A-5: *B1-AHT3 Completion diameters in NETool. In this case, the Sand Control ID and OD refer to the base pipe ID and OD, respectively.*

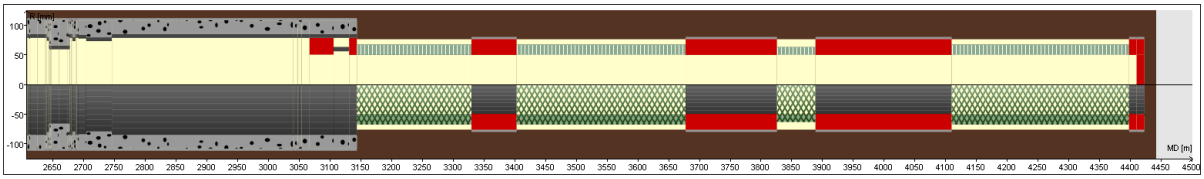

Figure A-6: *B1-AHT3 Base Case Completion schematic in NETool.*

B Results from Base Case simulations

B.1 Well B3 Base Case Results

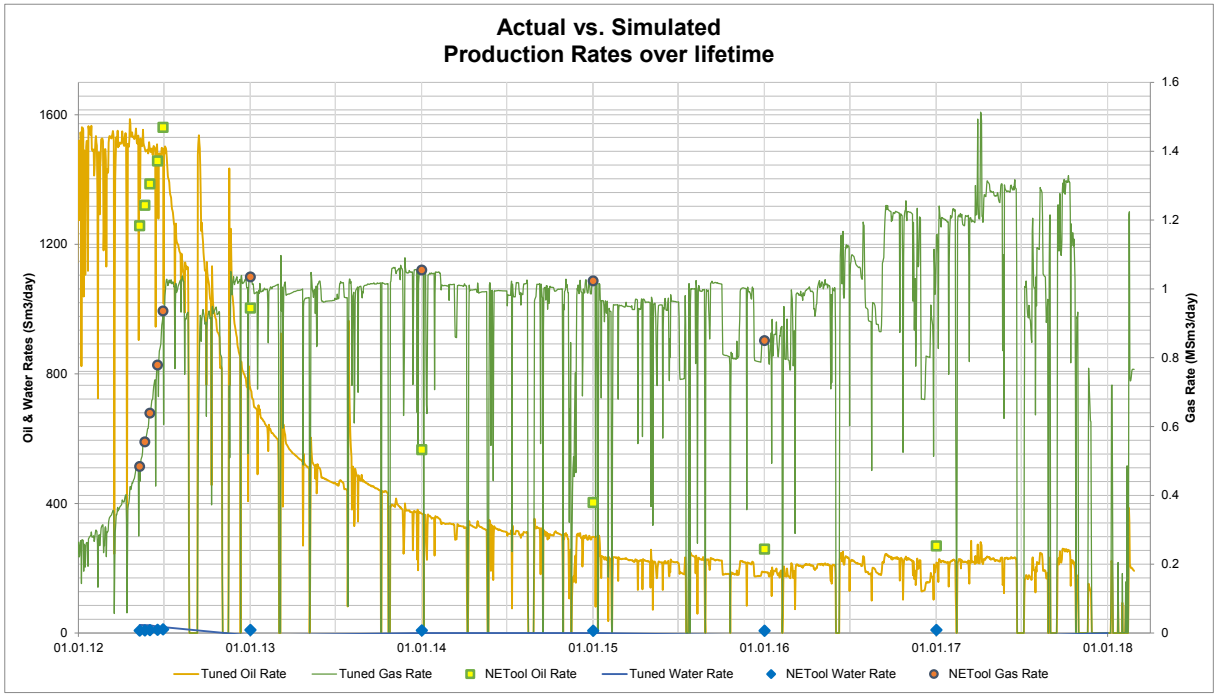

Figure B-1: *B3-HT2 Case 1: Actual vs. Simulated Production*

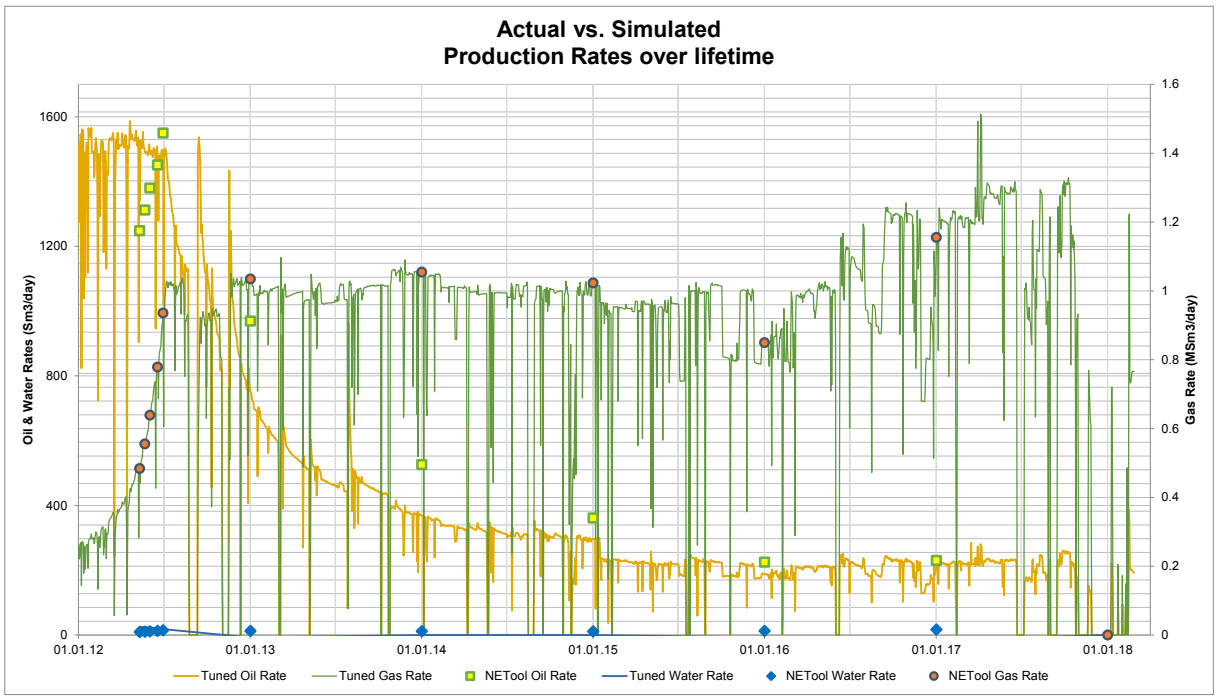

Figure B-2: *B3-HT2 Case 2: Actual vs. Simulated Production*

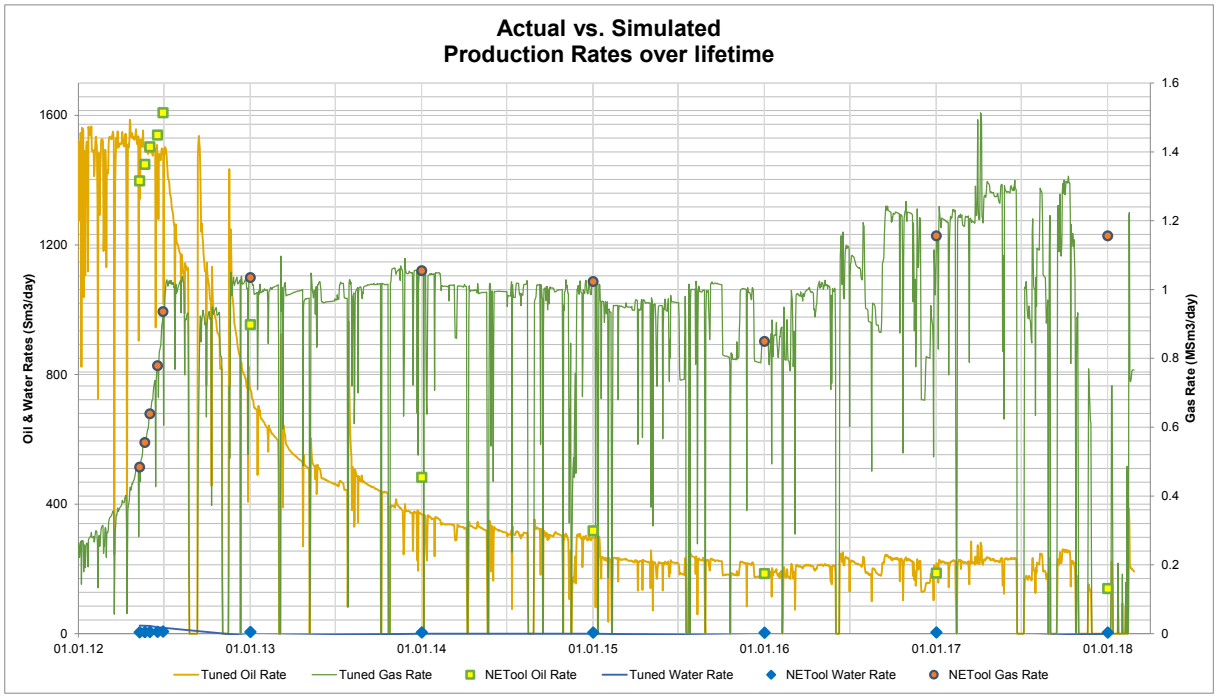

Figure B-3: *B3-HT2 Case 3: Actual vs. Simulated Production*

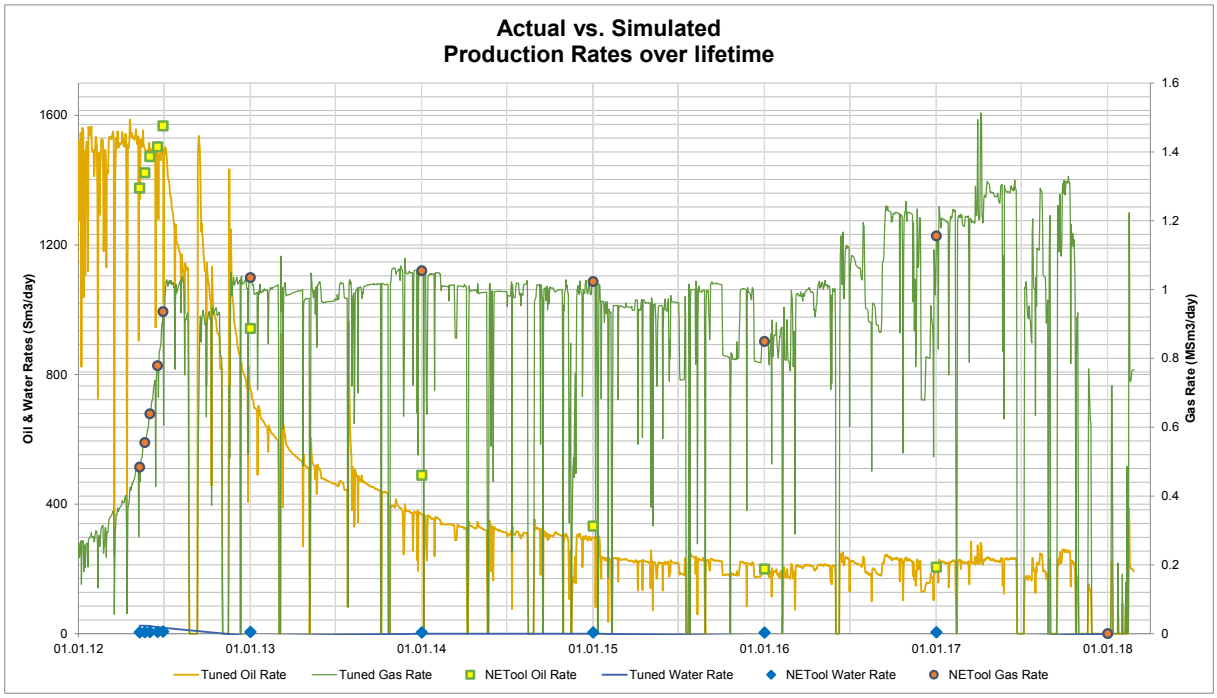

Figure B-4: *B3-HT2 Case 4: Actual vs. Simulated Production*

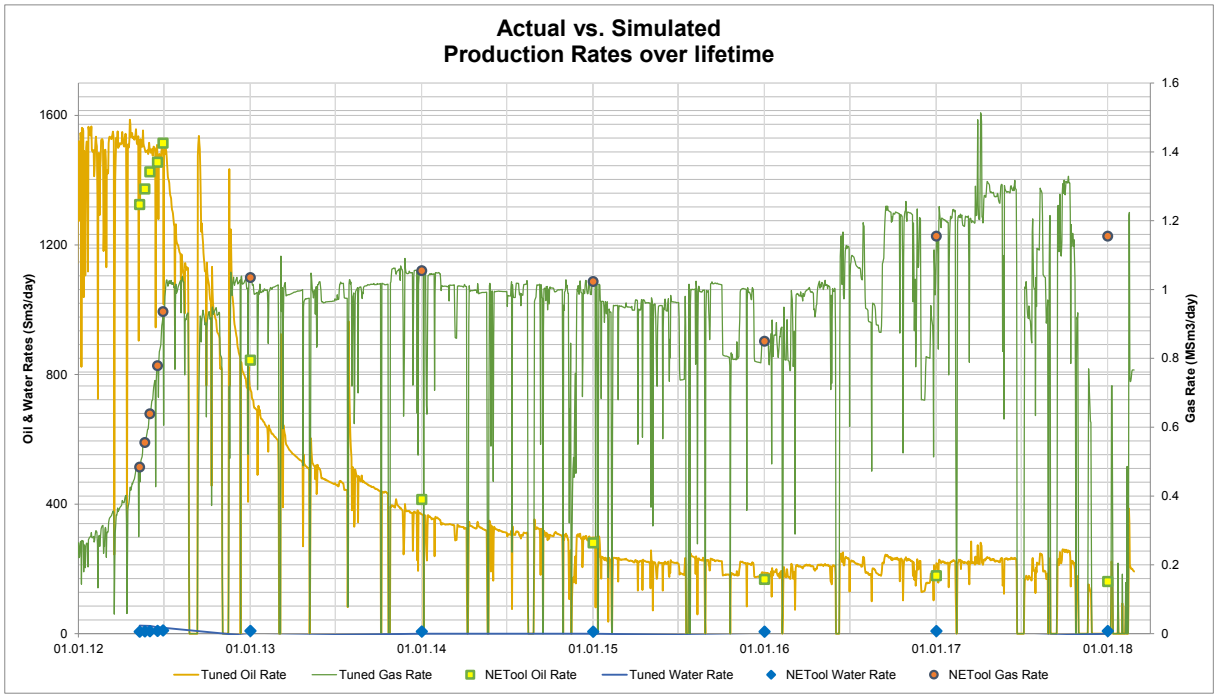

Figure B-5: *B3-HT2 Case 5: Actual vs. Simulated Production*

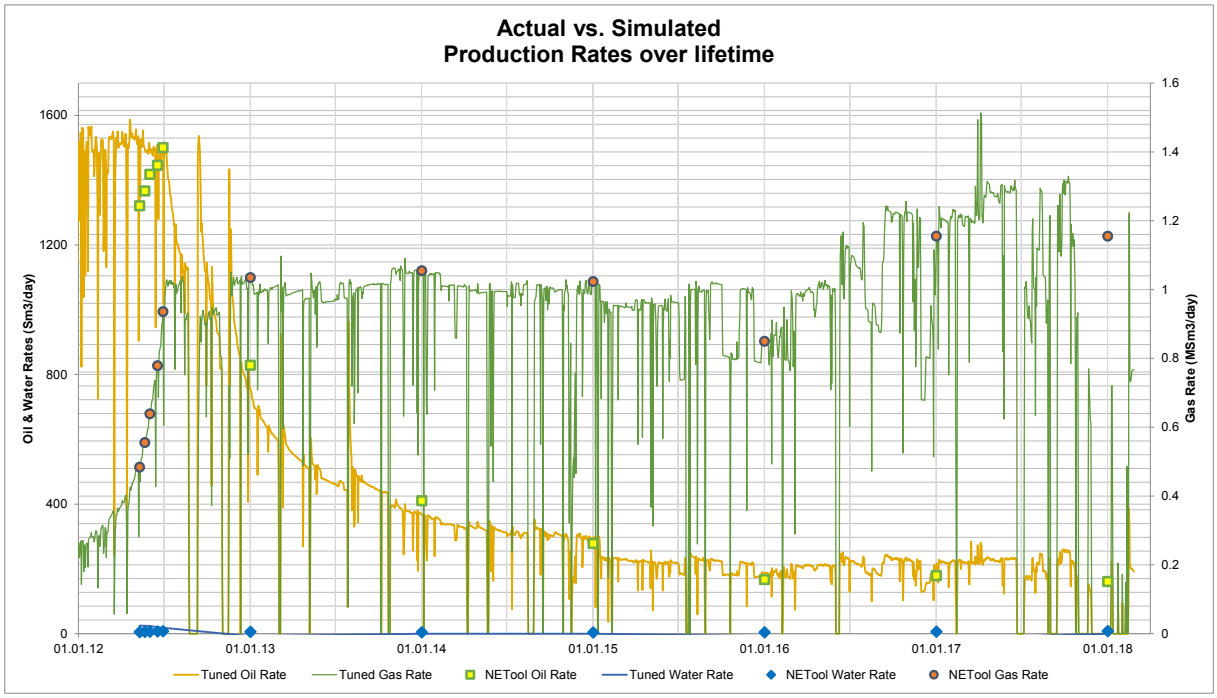

Figure B-6: *B3-HT2 Case 6: Actual vs. Simulated Production*

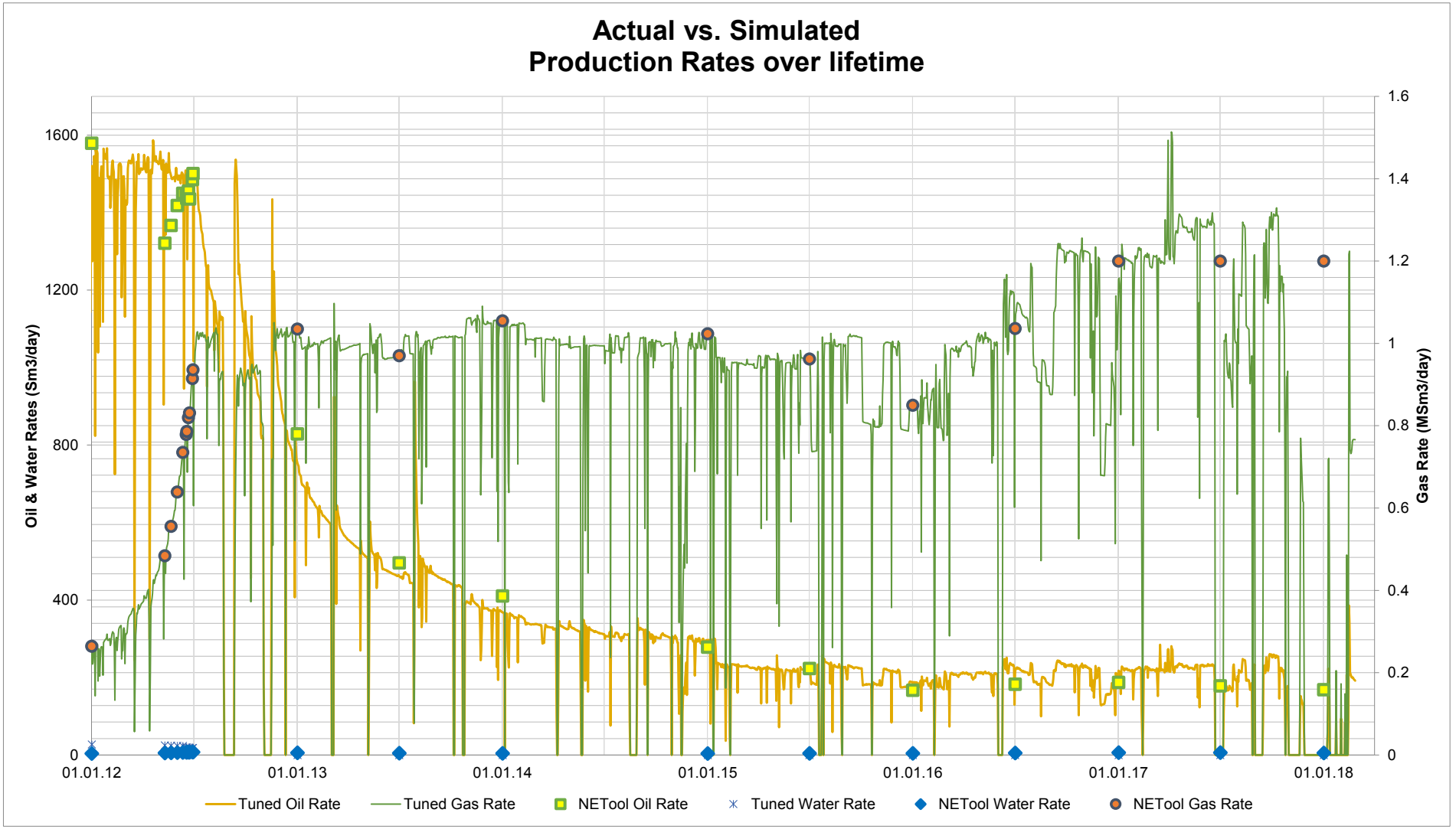

Figure B-7: *B3-HT2 Case 7: Actual vs. Simulated Production. This will be the reference case (base case) for further simulations*

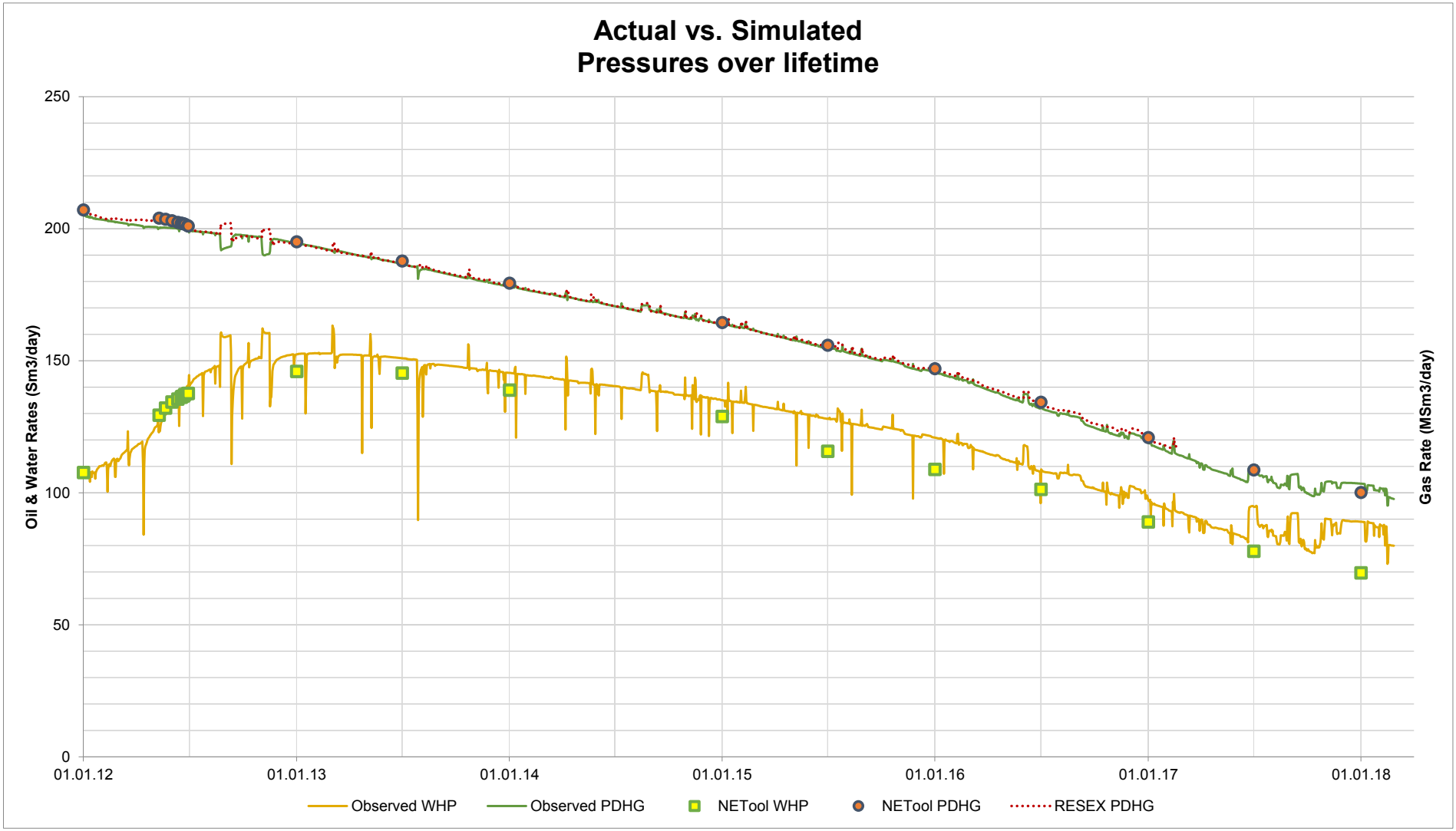

Figure B-8: *B3-HT2 Case 7: Actual vs. Simulated Pressures. This will be the reference case (base case) for further simulations*

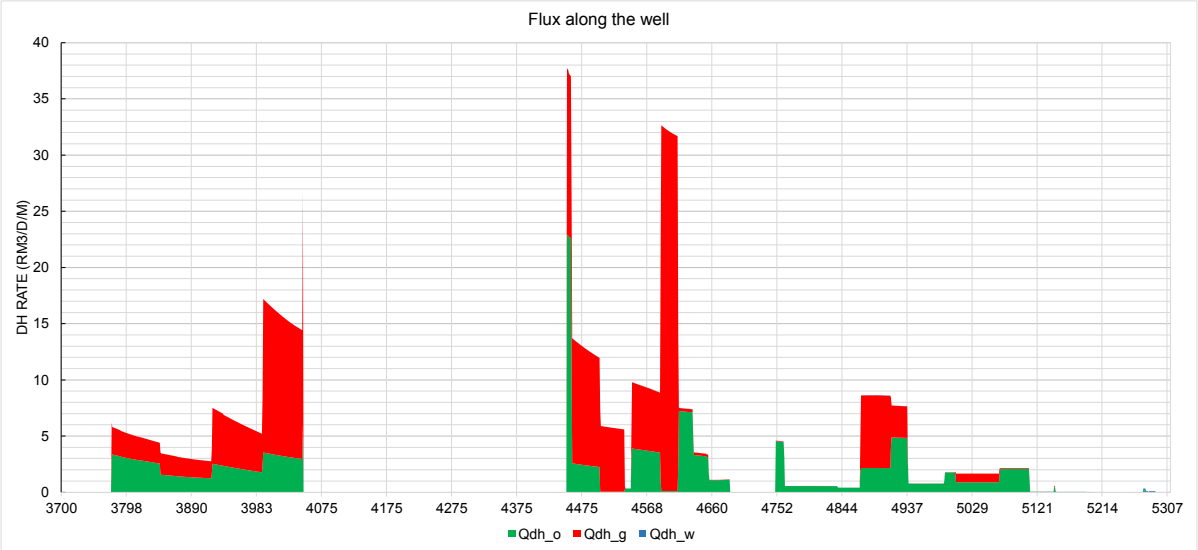

Figure B-9: *B3-HT2 Case 7: Flux along the well at early-life*

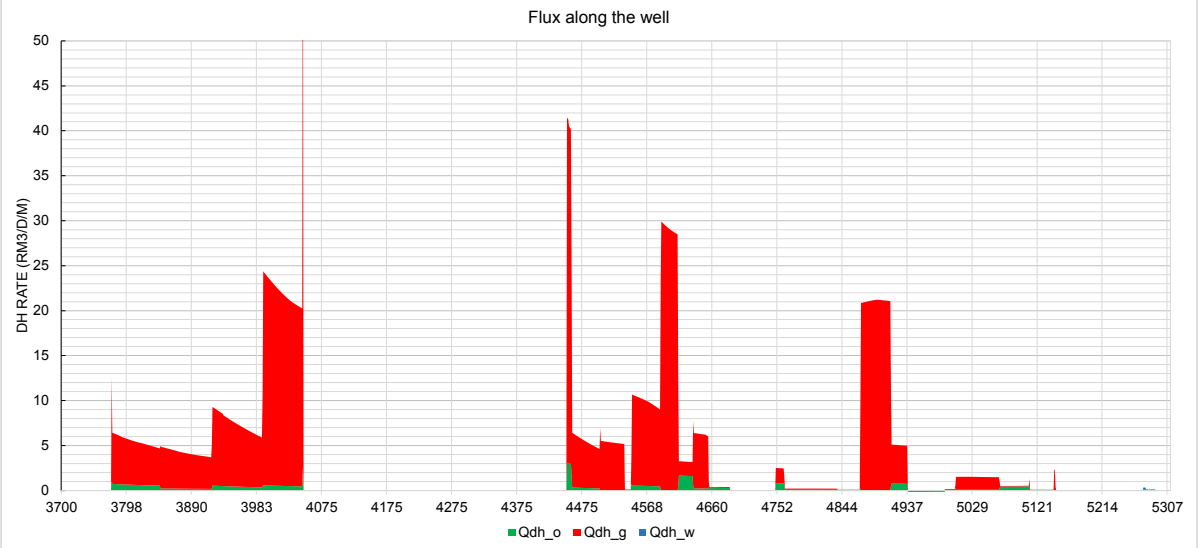

Figure B-10: *B3-HT2 Case 7: Flux along the well at mid-life*

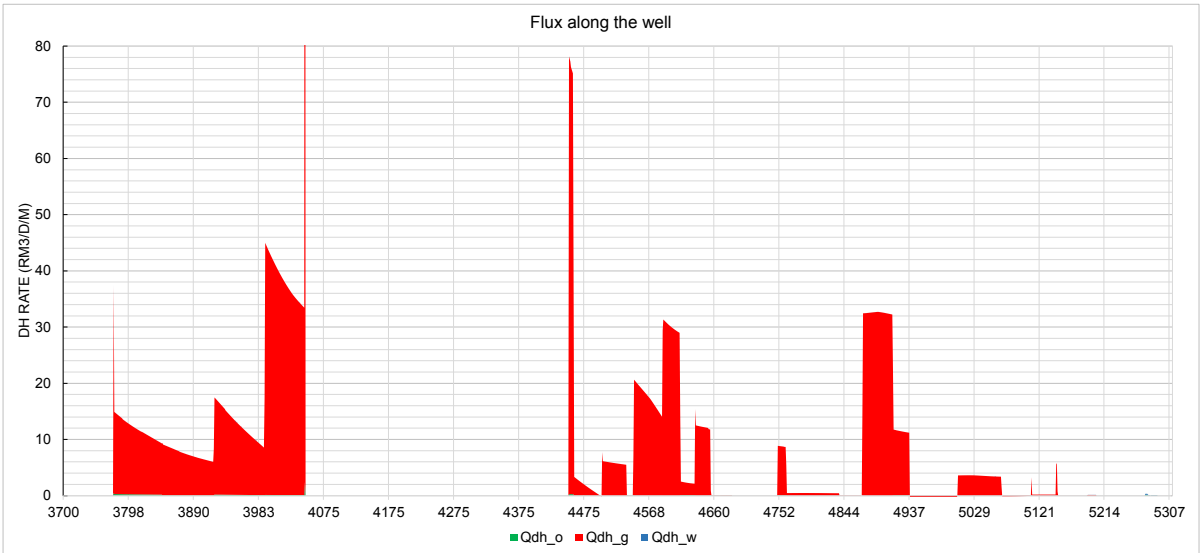

Figure B-11: *B3-HT2 Case 7: Flux along the well at late-life*

B.2 Well B1 Base Case Results

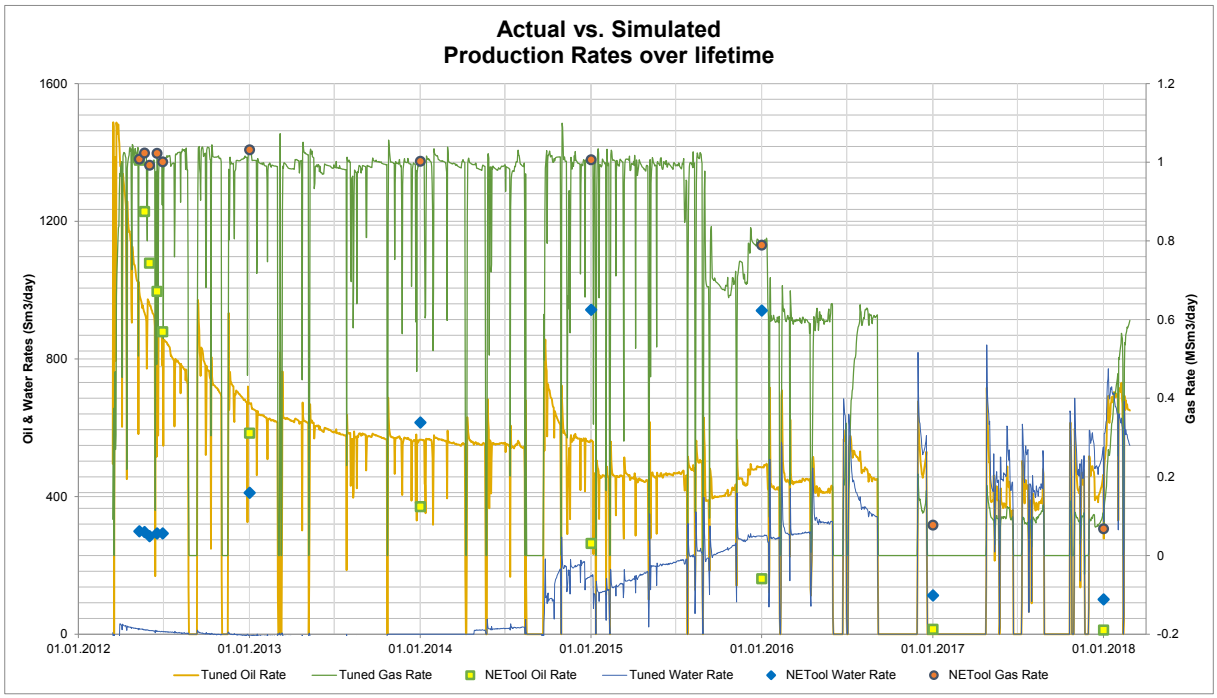

Figure B-12: *B1-HT2 Case 1: Actual vs. Simulated Production*

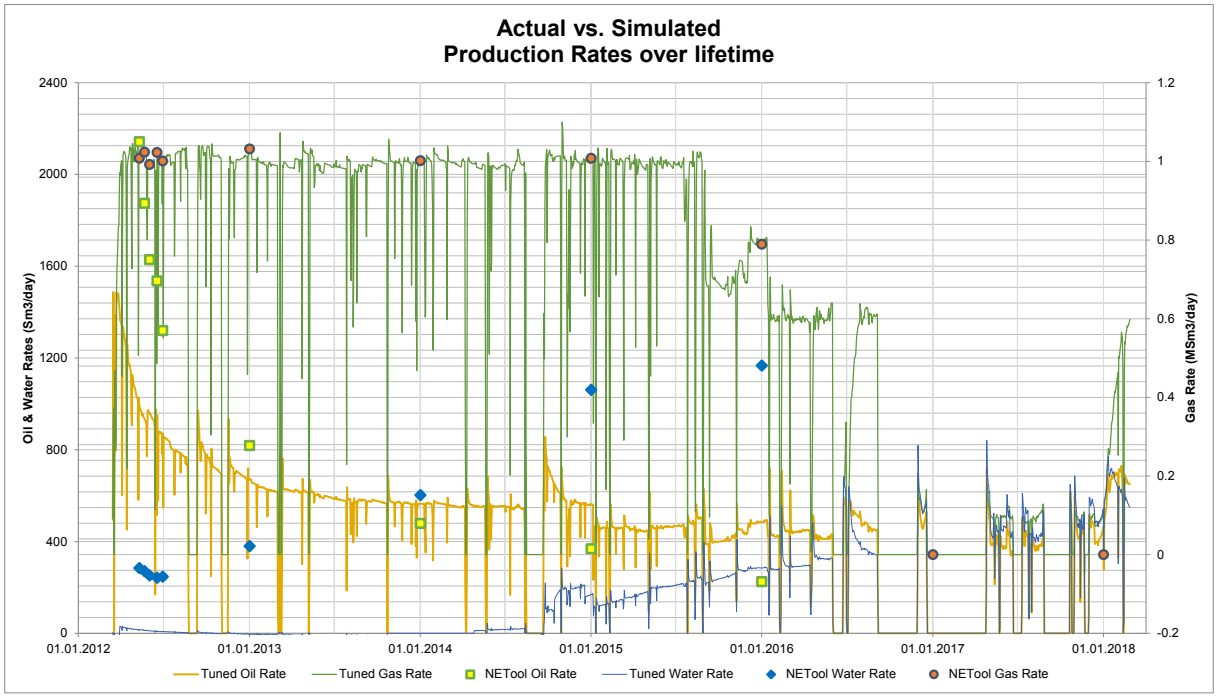

Figure B-13: *B1-AHT3 Case 2: Actual vs. Simulated Production*

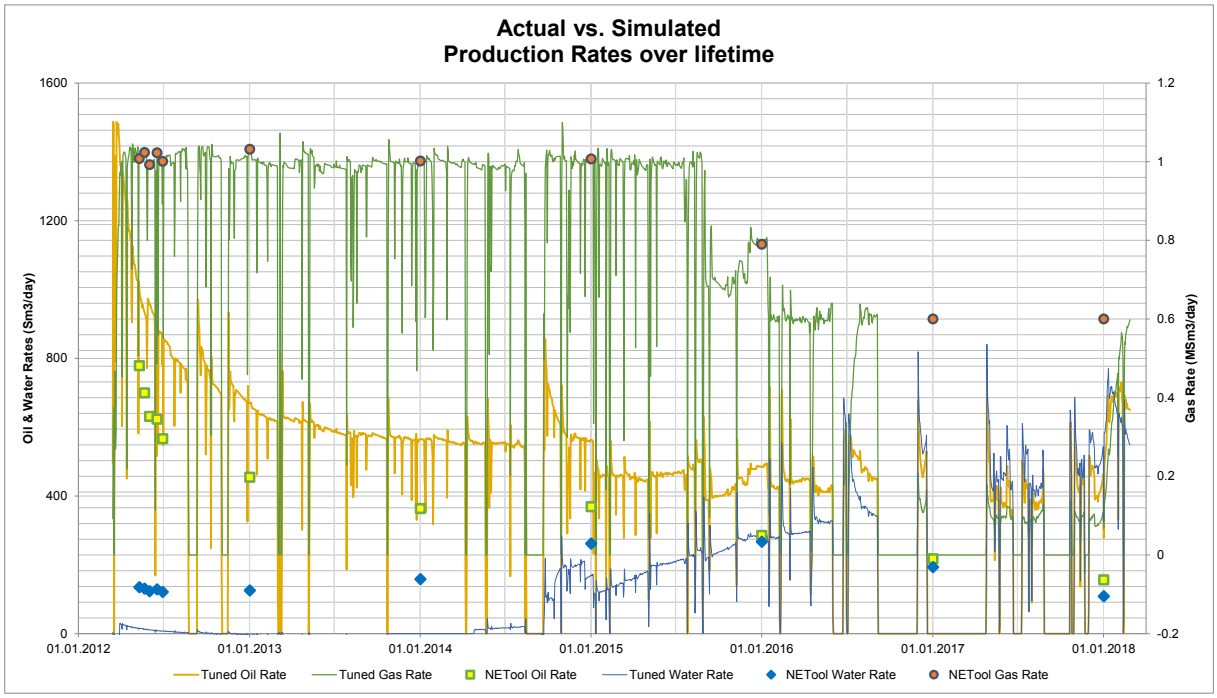

Figure B-14: *B1-AHT3 Case 3: Actual vs. Simulated Production*

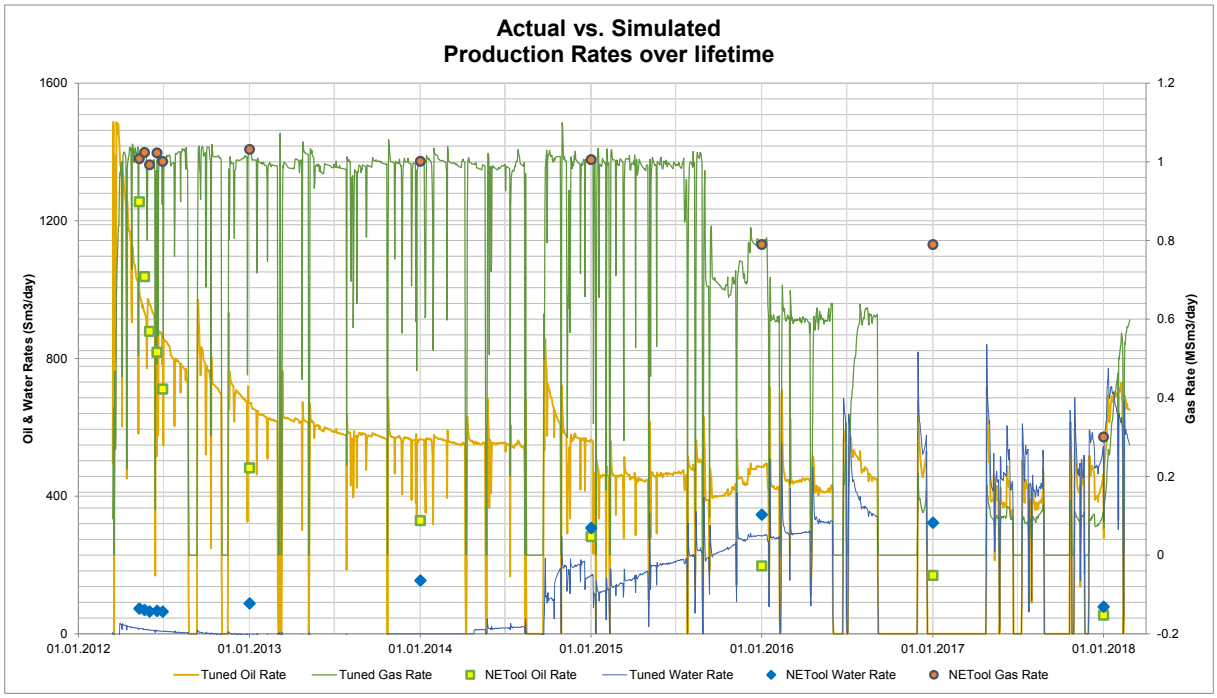

Figure B-15: *B1-AHT3 Case 4: Actual vs. Simulated Production*

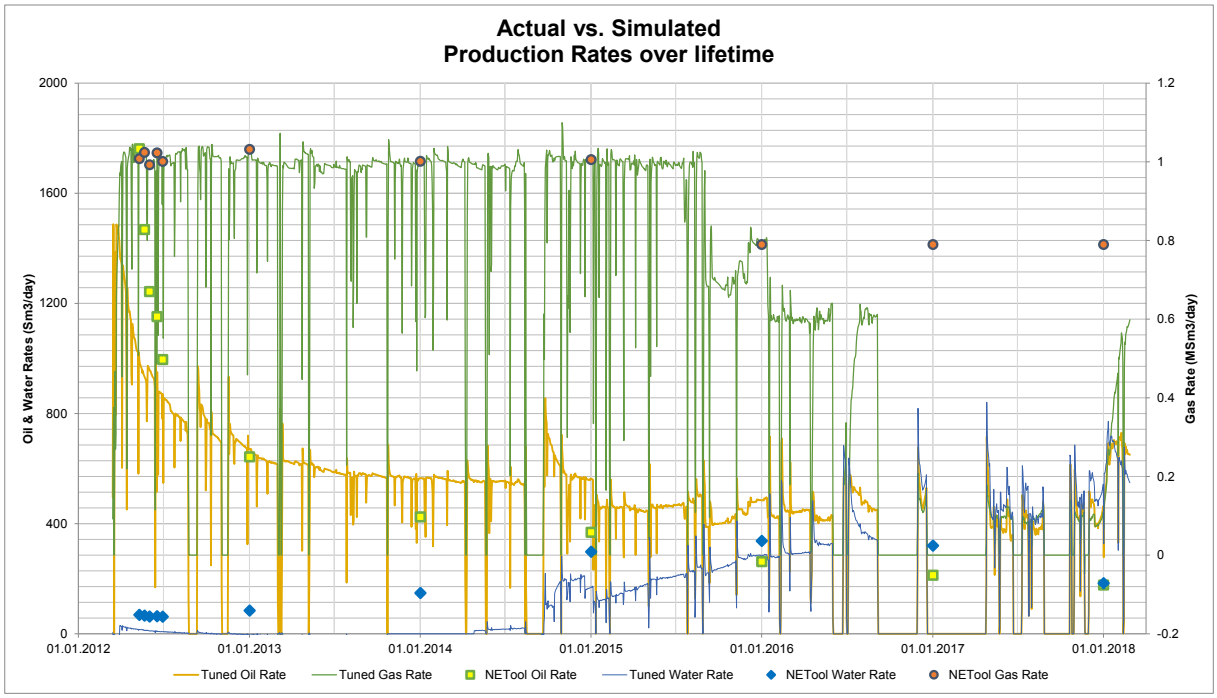

Figure B-16: *B1-AHT3 Case 5: Actual vs. Simulated Production*

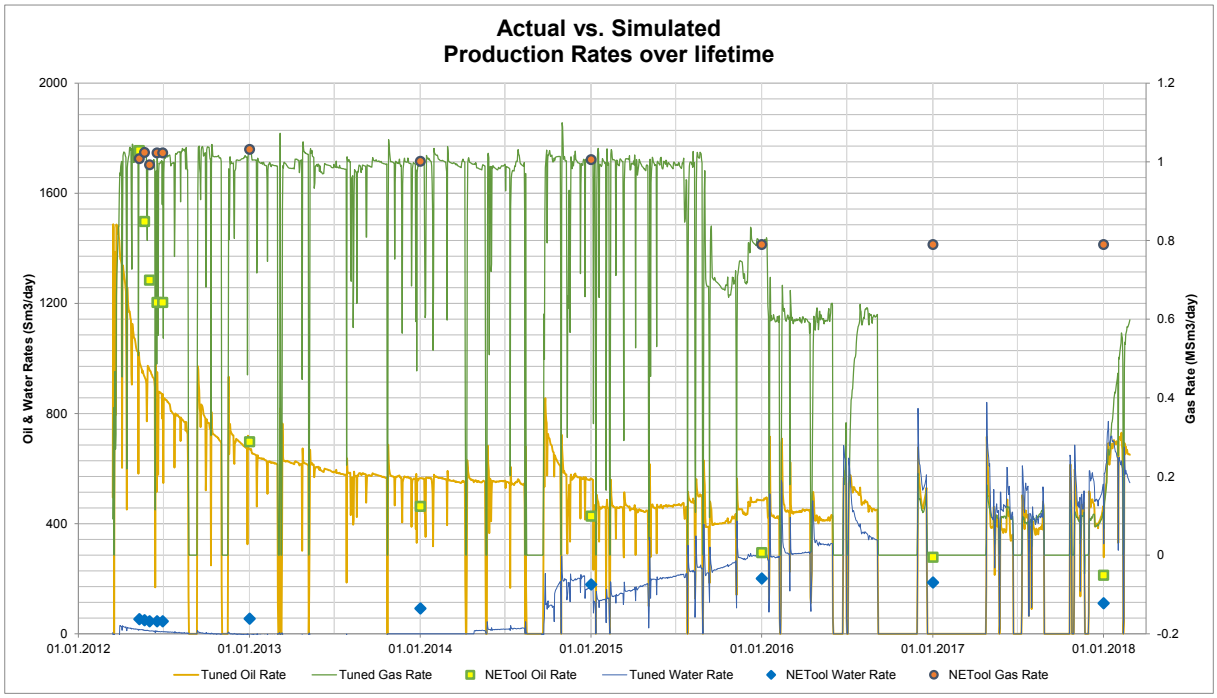

Figure B-17: *B1-AHT3 Case 6: Actual vs. Simulated Production*

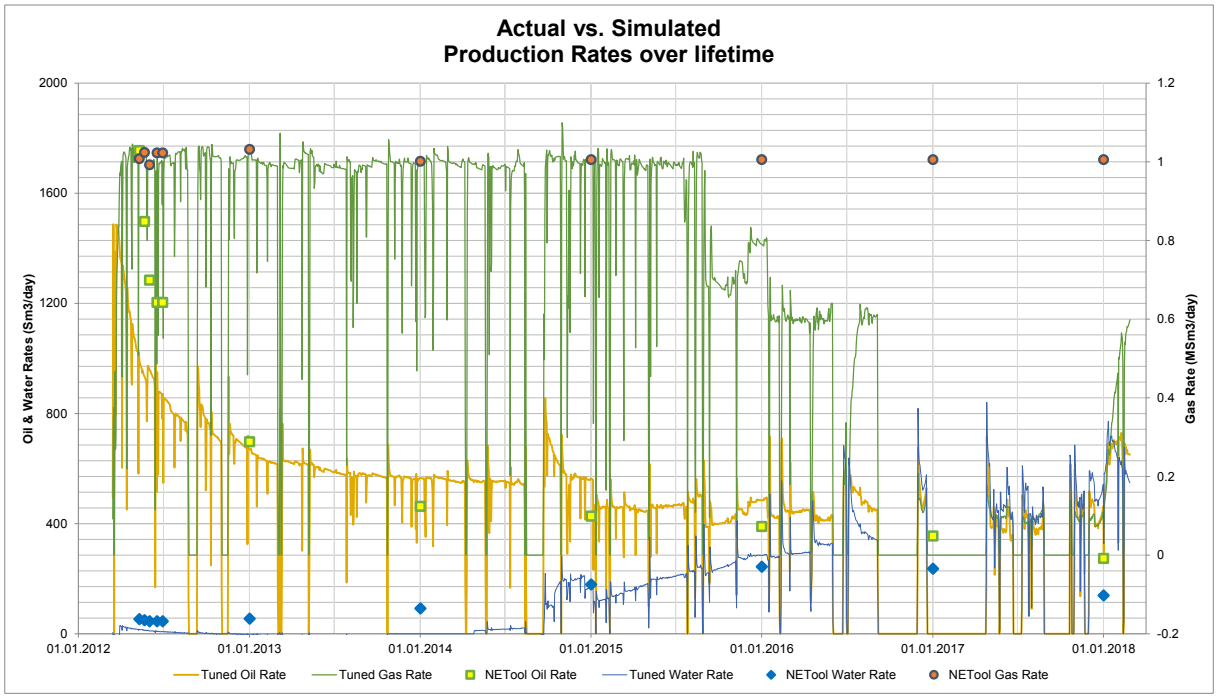

Figure B-18: *B1-AHT3 Case 7: Actual vs. Simulated Production*

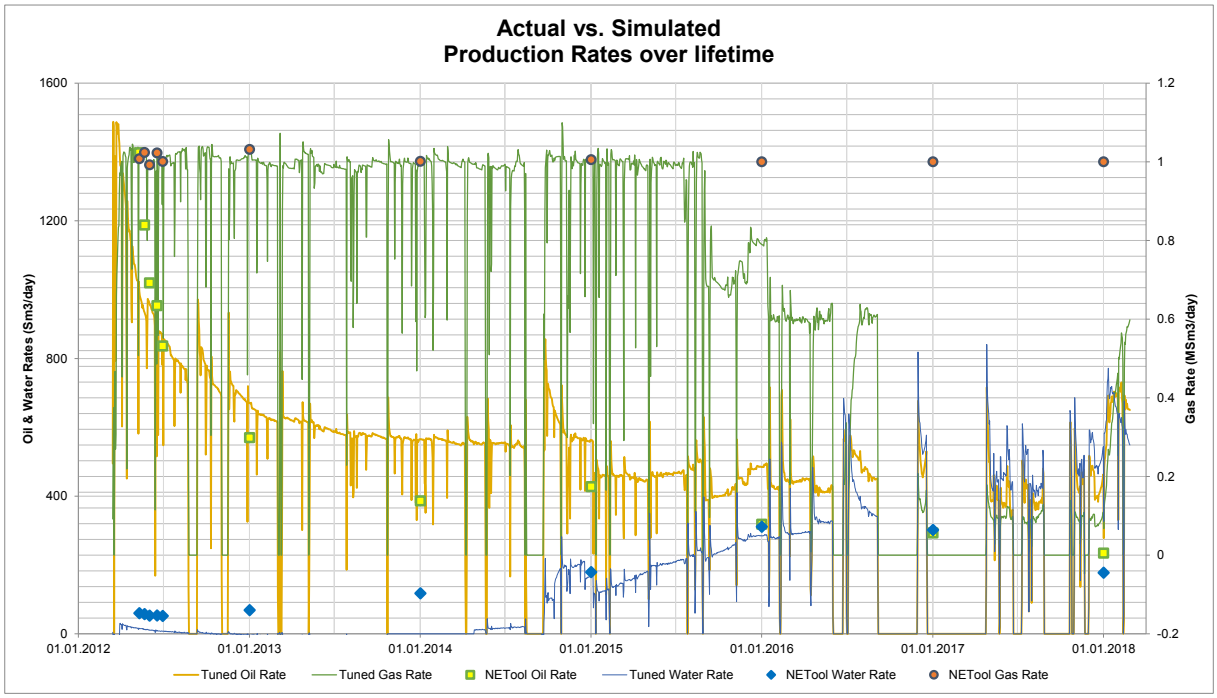

Figure B-19: *B1-AHT3 Case 8: Actual vs. Simulated Production*

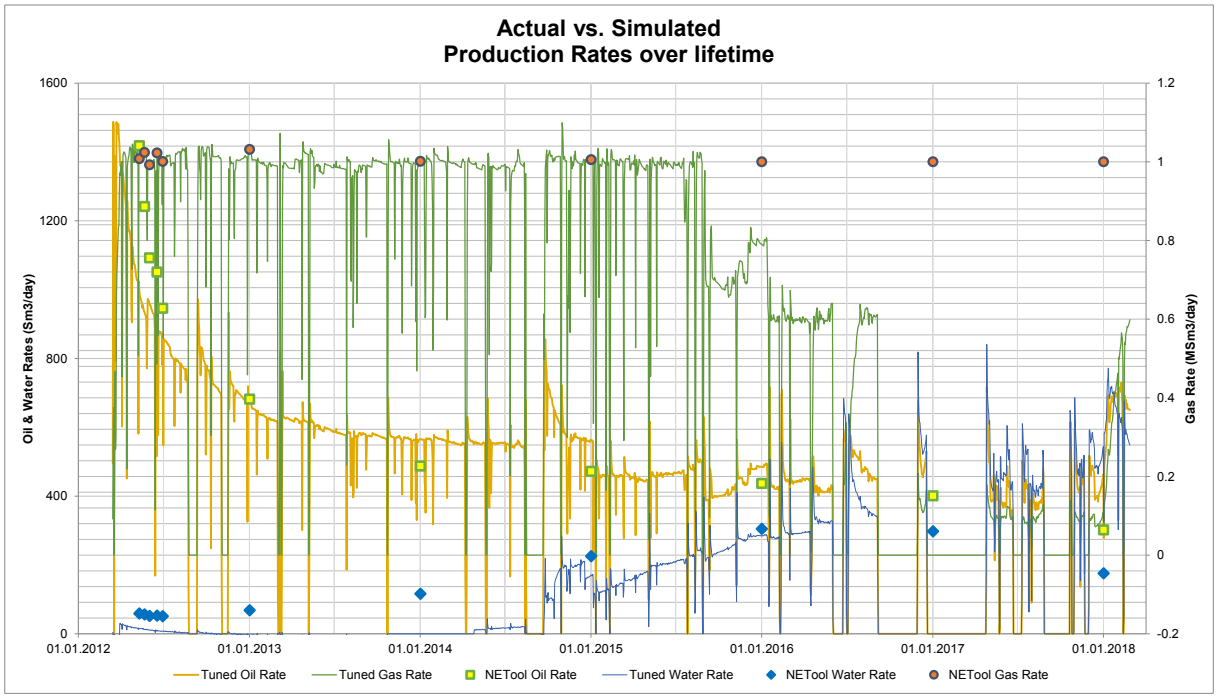

Figure B-20: *B1-AHT3 Case 9: Actual vs. Simulated Production*

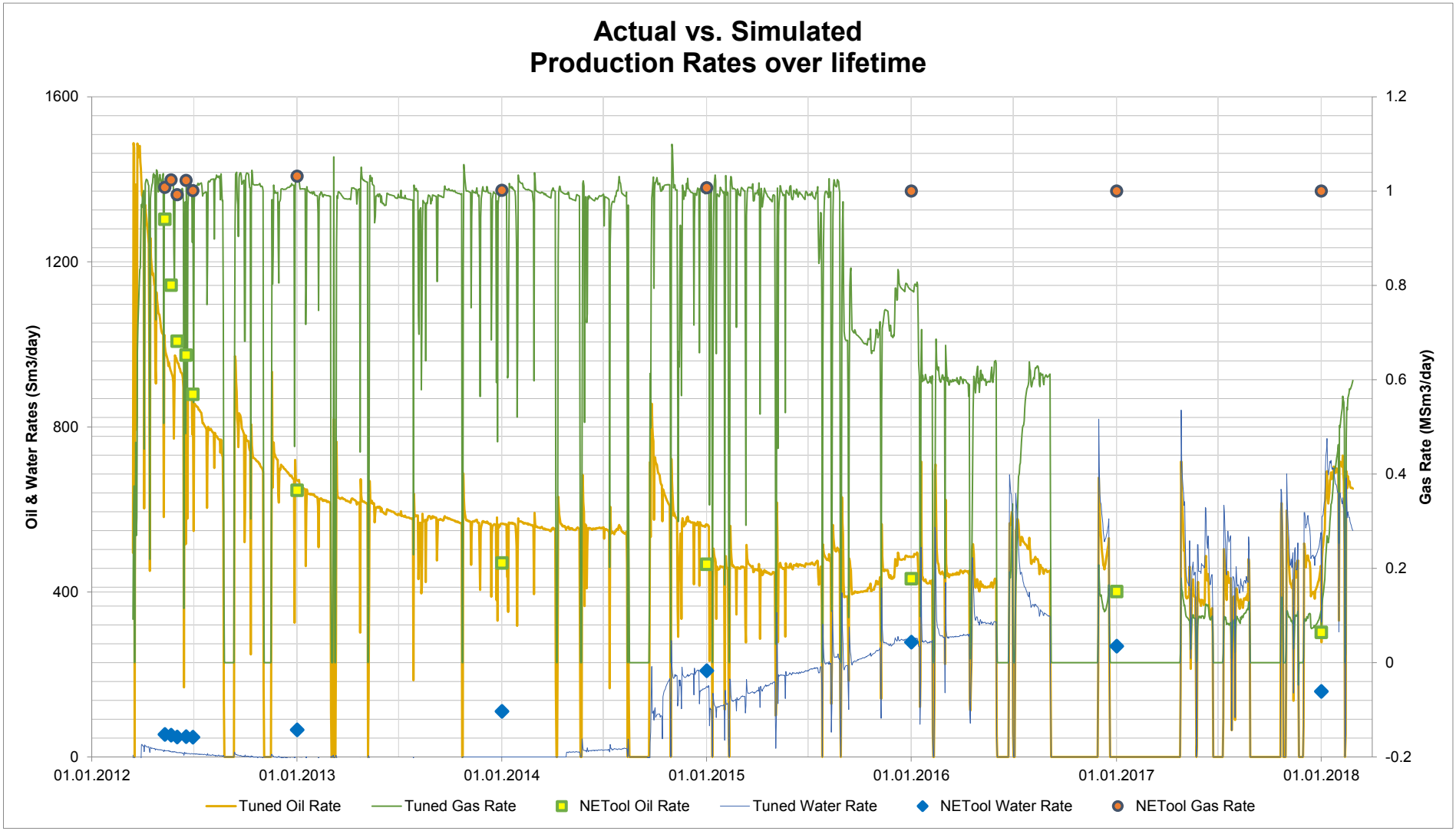

Figure B-21: *B1-AHT3 Case 10: Actual vs. Simulated Production. This will be the reference case (base case) for further simulations*

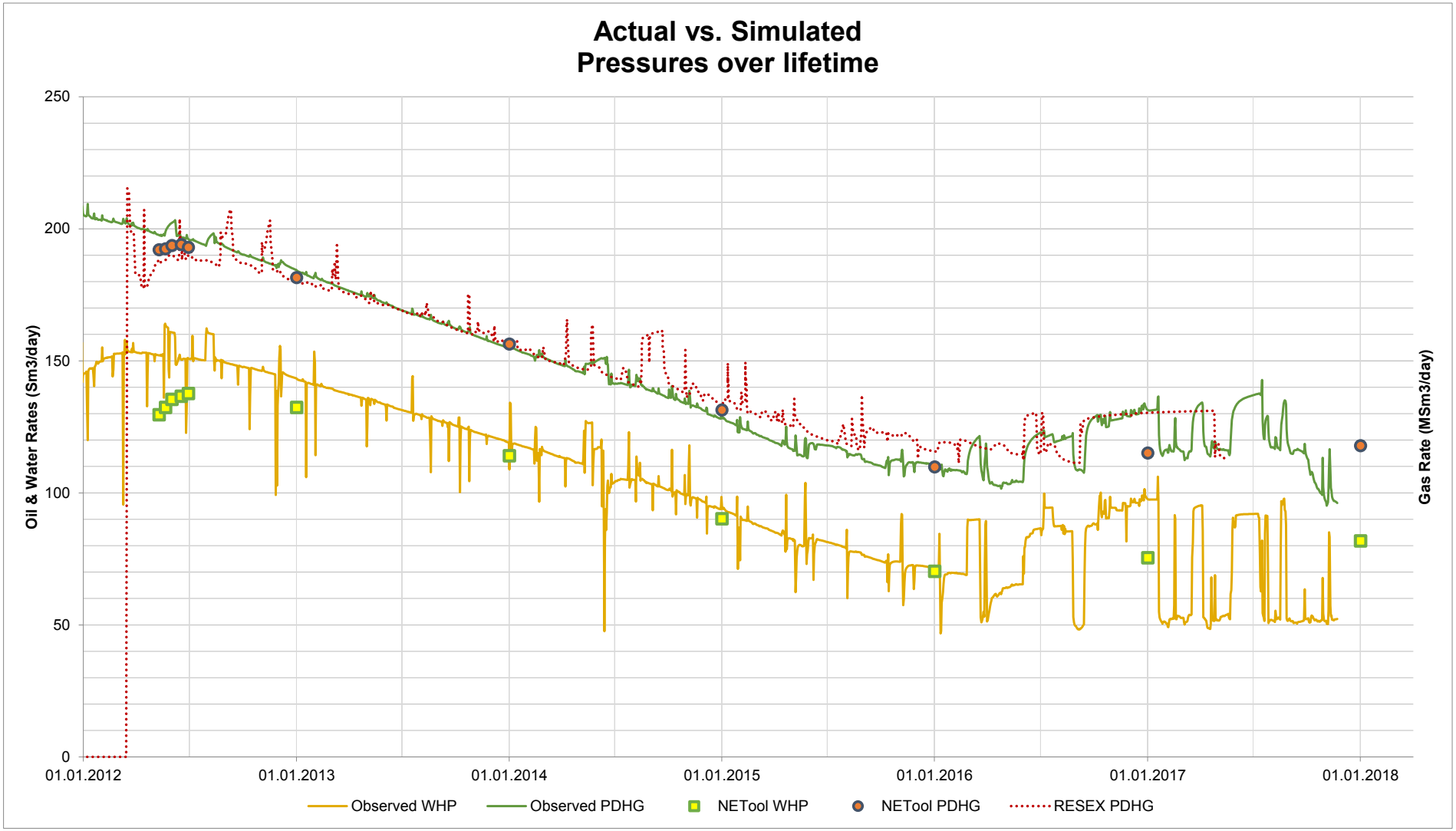

Figure B-22: *B1-AHT3 Case 10: Actual vs. Simulated Pressures. This will be the reference case (base case) for further simulations*

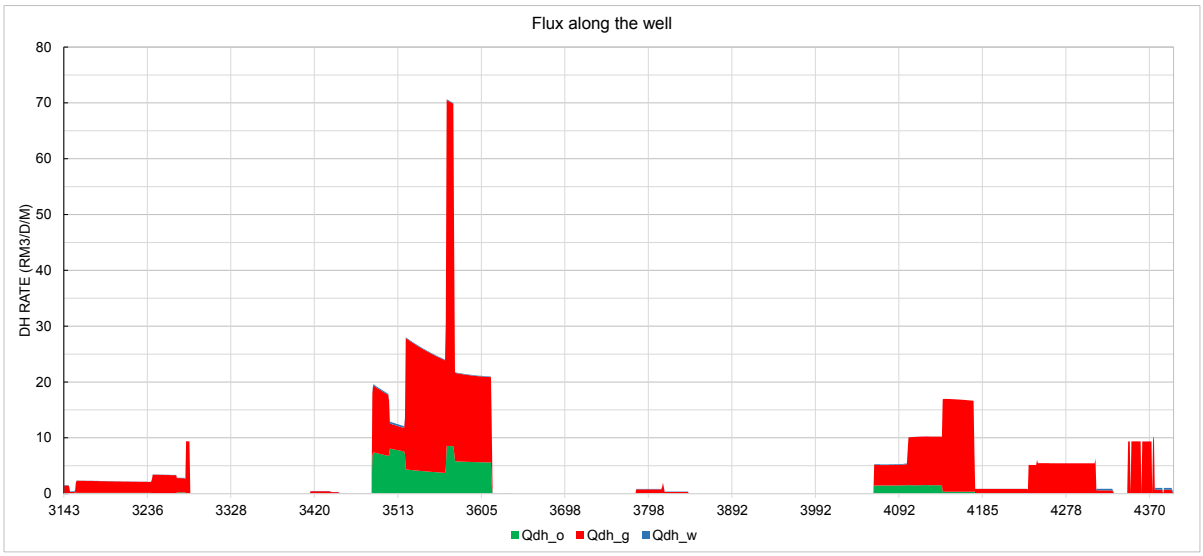

Figure B-23: *B1-AHT3 Case 10: Flux along the well at early-life*

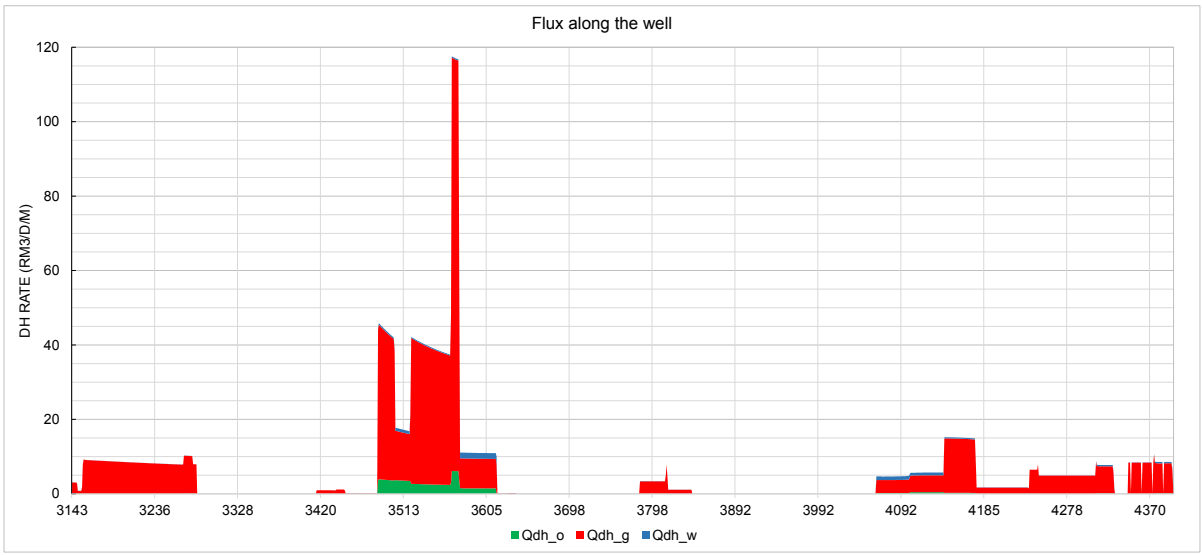

Figure B-24: *B1-AHT3 Case 10: Flux along the well at mid-life*

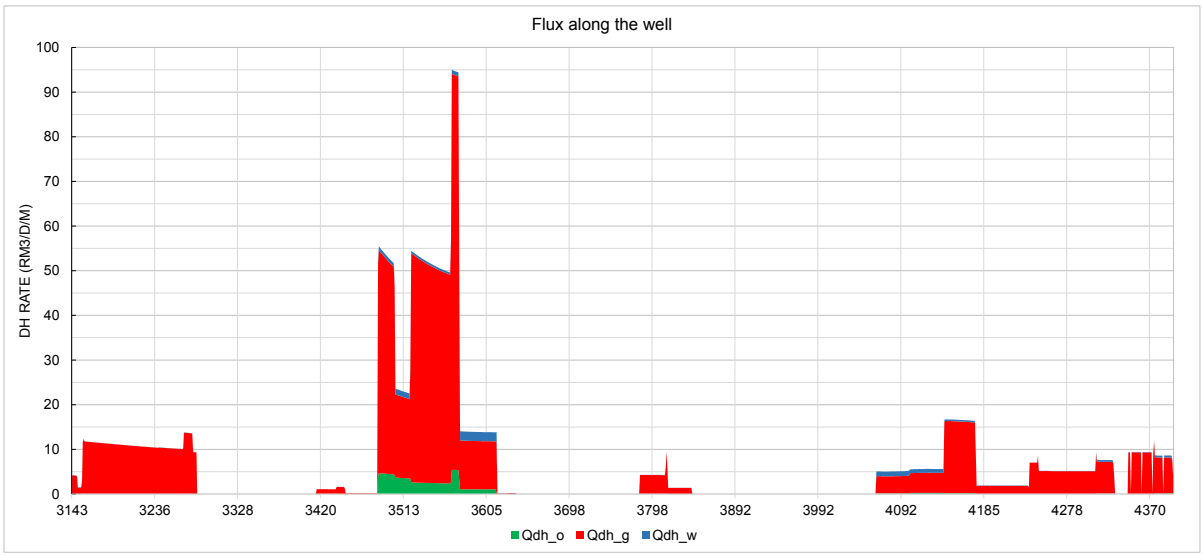

Figure B-25: *B1-AHT3 Case 10: Flux along the well at late-life*

C Input Data for the ICD Cases

C.1 Well B3 NETool ICD Well Design

Hole & Completion

#	Top MD	Seg. Length	Top TVD(SS)	Casing/Liner	Sand Control	Inflow Control
	[m]	[m]	[m]			
1	2613.00	5.55	2040.07	Cemented Blank Pipe	-	-
2	2618.55	3.36	2043.31	Cemented Blank Pipe	-	-
3	2621.91	0.76	2045.26	Cemented Blank Pipe	-	-
4	2622.67	2.06	2045.71	Cemented Blank Pipe	-	-
5	2624.73	0.74	2046.91	Cemented Blank Pipe	-	-
6	2625.47	2.06	2047.34	Cemented Blank Pipe	-	-
7	2627.53	23.95	2048.54	Cemented Blank Pipe	-	-
8	2651.48	3.05	2062.24	Cemented Blank Pipe	-	-
9	2654.53	0.76	2063.97	Cemented Blank Pipe	-	-
10	2655.29	1.97	2064.40	Cemented Blank Pipe	-	-
11	2657.26	22.40	2065.51	Cemented Blank Pipe	-	-
12	2679.66	4.08	2077.97	Cemented Blank Pipe	-	-
13	2683.74	1.28	2080.16	Cemented Blank Pipe	-	-
14	2685.02	3.59	2080.85	Cemented Blank Pipe	-	-
15	2688.61	1.94	2082.75	Cemented Blank Pipe	-	-
16	2690.55	696.44	2083.77	Cemented Blank Pipe	-	-
17	3386.99	2.55	2309.48	Cemented Blank Pipe	-	-
18	3389.54	2.20	2309.73	Cemented Blank Pipe	-	-
19	3391.74	8.01	2309.94	Cemented Blank Pipe	-	-
20	3399.75	0.75	2310.68	Cemented Blank Pipe	Packer	Packer
21	3400.50	1.56	2310.75	Cemented Blank Pipe	Packer	Packer
22	3402.06	38.44	2310.88	Cemented Blank Pipe	Packer	Packer
23	3440.50	335.10	2313.48	-	Packer	Packer
24	3775.60	11.70	2313.67	-	Screen	Inflow Control Device
25	3787.30	0.30	2313.67	-	Packer	Packer
26	3787.60	11.70	2313.67	-	Screen	Inflow Control Device
27	3799.30	0.30	2313.70	-	Packer	Packer
28	3799.60	11.70	2313.70	-	Screen	Inflow Control Device
29	3811.30	0.30	2313.75	-	Packer	Packer
30	3811.60	11.70	2313.75	-	Screen	Inflow Control Device
31	3823.30	0.30	2313.80	-	Packer	Packer
32	3823.60	11.70	2313.80	-	Screen	Inflow Control Device
33	3835.30	0.30	2313.85	-	Packer	Packer
34	3835.60	11.70	2313.85	-	Screen	Inflow Control Device
35	3847.30	0.30	2313.89	-	Packer	Packer
36	3847.60	11.70	2313.89	-	Screen	Inflow Control Device
37	3859.30	0.30	2313.90	-	Packer	Packer
38	3859.60	11.70	2313.90	-	Screen	Inflow Control Device
39	3871.30	0.30	2313.90	-	Packer	Packer
40	3871.60	11.70	2313.90	-	Screen	Inflow Control Device
41	3883.30	0.30	2313.90	-	Packer	Packer
42	3883.60	11.70	2313.90	-	Screen	Inflow Control Device
43	3895.30	0.30	2313.91	-	Packer	Packer
44	3895.60	11.70	2313.91	-	Screen	Inflow Control Device
45	3907.30	0.30	2313.92	-	Packer	Packer
46	3907.60	11.70	2313.92	-	Screen	Inflow Control Device
47	3919.30	0.30	2313.95	-	Packer	Packer
48	3919.60	11.70	2313.95	-	Screen	Inflow Control Device
49	3931.30	0.30	2313.97	-	Packer	Packer
50	3931.60	11.70	2313.97	-	Screen	Inflow Control Device
51	3943.30	0.30	2313.96	-	Packer	Packer
52	3943.60	11.70	2313.96	-	Screen	Inflow Control Device
53	3955.30	0.30	2313.93	-	Packer	Packer
54	3955.60	11.70	2313.93	-	Screen	Inflow Control Device
55	3967.30	0.30	2313.89	-	Packer	Packer
56	3967.60	11.70	2313.89	-	Screen	Inflow Control Device

Figure C-1: *B3-HT2 ICD Completion setup Part 1. Every screen joint is equipped with a 0.3m swellable packer for annular compartmentalization. The screen layer is equipped with inflow control technology. Every joint is set as 12m unless a pup joint is needed for spacing out the original completion length. Blank pipe sections are, as previously, set as packers. Applies to B3 Simulation cases 8-17.*

Hole & Completion

#	Top MD	Seg. Length	Top TVD(SS)	Casing/Liner	Sand Control	Inflow Control
	[m]	[m]	[m]			
57	3979.30	0.30	2313.86	-	Packer	Packer
58	3979.60	11.70	2313.86	-	Screen	Inflow Control Device
59	3991.30	0.30	2313.84	-	Packer	Packer
60	3991.60	11.70	2313.84	-	Screen	Inflow Control Device
61	4003.30	0.30	2313.82	-	Packer	Packer
62	4003.60	11.70	2313.82	-	Screen	Inflow Control Device
63	4015.30	0.30	2313.81	-	Packer	Packer
64	4015.60	11.70	2313.81	-	Screen	Inflow Control Device
65	4027.30	0.30	2313.81	-	Packer	Packer
66	4027.60	11.70	2313.80	-	Screen	Inflow Control Device
67	4039.30	0.30	2313.79	-	Packer	Packer
68	4039.60	11.70	2313.79	-	Screen	Inflow Control Device
69	4051.30	0.30	2313.79	-	Packer	Packer
70	4051.60	11.70	2313.79	-	Screen	Inflow Control Device
71	4063.30	0.30	2313.81	-	Packer	Packer
72	4063.60	11.70	2313.81	-	Screen	Inflow Control Device
73	4075.30	2.71	2313.84	-	Packer	Packer
74	4078.01	397.69	2313.84	-	Packer	Packer
75	4475.70	11.70	2313.87	-	Screen	Inflow Control Device
76	4487.40	0.30	2313.83	-	Packer	Packer
77	4487.70	11.70	2313.83	-	Screen	Inflow Control Device
78	4499.40	0.30	2313.79	-	Packer	Packer
79	4499.70	11.70	2313.79	-	Screen	Inflow Control Device
80	4511.40	0.30	2313.76	-	Packer	Packer
81	4511.70	11.70	2313.76	-	Screen	Inflow Control Device
82	4523.40	0.30	2313.74	-	Packer	Packer
83	4523.70	11.70	2313.74	-	Screen	Inflow Control Device
84	4535.40	0.30	2313.72	-	Packer	Packer
85	4535.70	11.70	2313.72	-	Screen	Inflow Control Device
86	4547.40	0.30	2313.71	-	Packer	Packer
87	4547.70	11.70	2313.71	-	Screen	Inflow Control Device
88	4559.40	0.30	2313.71	-	Packer	Packer
89	4559.70	11.70	2313.71	-	Screen	Inflow Control Device
90	4571.40	0.30	2313.71	-	Packer	Packer
91	4571.70	11.70	2313.71	-	Screen	Inflow Control Device
92	4583.40	0.30	2313.72	-	Packer	Packer
93	4583.70	11.70	2313.72	-	Screen	Inflow Control Device
94	4595.40	0.30	2313.72	-	Packer	Packer
95	4595.70	11.70	2313.72	-	Screen	Inflow Control Device
96	4607.40	0.30	2313.69	-	Packer	Packer
97	4607.70	11.70	2313.69	-	Screen	Inflow Control Device
98	4619.40	0.30	2313.64	-	Packer	Packer
99	4619.70	11.70	2313.63	-	Screen	Inflow Control Device
100	4631.40	0.30	2313.57	-	Packer	Packer
101	4631.70	11.70	2313.57	-	Screen	Inflow Control Device
102	4643.40	0.30	2313.52	-	Packer	Packer
103	4643.70	11.70	2313.52	-	Screen	Inflow Control Device
104	4655.40	0.30	2313.49	-	Packer	Packer
105	4655.70	11.70	2313.49	-	Screen	Inflow Control Device
106	4667.40	0.30	2313.47	-	Packer	Packer
107	4667.70	11.70	2313.47	-	Screen	Inflow Control Device
108	4679.40	0.30	2313.48	-	Packer	Packer
109	4679.70	11.70	2313.48	-	Screen	Inflow Control Device
110	4691.40	0.30	2313.51	-	Packer	Packer
111	4691.70	11.70	2313.51	-	Screen	Inflow Control Device
112	4703.40	0.30	2313.56	-	Packer	Packer

Figure C-2: *B3-HT2 ICD Completion setup Part 2*

Hole & Completion

#	Top MD	Seg. Length	Top TVD(SS)	Casing/Liner	Sand Control	Inflow Control
	[m]	[m]	[m]			
113	4703.70	11.70	2313.56	-	Screen	Inflow Control Device
114	4715.40	0.30	2313.61	-	Packer	Packer
115	4715.70	11.70	2313.62	-	Screen	Inflow Control Device
116	4727.40	0.30	2313.64	-	Packer	Packer
117	4727.70	11.70	2313.64	-	Screen	Inflow Control Device
118	4739.40	0.30	2313.63	-	Packer	Packer
119	4739.70	11.70	2313.63	-	Screen	Inflow Control Device
120	4751.40	0.30	2313.58	-	Packer	Packer
121	4751.70	11.70	2313.58	-	Screen	Inflow Control Device
122	4763.40	0.30	2313.49	-	Packer	Packer
123	4763.70	11.70	2313.48	-	Screen	Inflow Control Device
124	4775.40	0.30	2313.38	-	Packer	Packer
125	4775.70	11.70	2313.38	-	Screen	Inflow Control Device
126	4787.40	0.30	2313.31	-	Packer	Packer
127	4787.70	11.70	2313.31	-	Screen	Inflow Control Device
128	4799.40	0.30	2313.27	-	Packer	Packer
129	4799.70	11.70	2313.27	-	Screen	Inflow Control Device
130	4811.40	0.30	2313.26	-	Packer	Packer
131	4811.70	11.70	2313.26	-	Screen	Inflow Control Device
132	4823.40	0.30	2313.29	-	Packer	Packer
133	4823.70	11.70	2313.29	-	Screen	Inflow Control Device
134	4835.40	0.30	2313.32	-	Packer	Packer
135	4835.70	11.70	2313.32	-	Screen	Inflow Control Device
136	4847.40	0.30	2313.33	-	Packer	Packer
137	4847.70	11.70	2313.33	-	Screen	Inflow Control Device
138	4859.40	0.30	2313.33	-	Packer	Packer
139	4859.70	11.70	2313.33	-	Screen	Inflow Control Device
140	4871.40	0.30	2313.32	-	Packer	Packer
141	4871.70	11.70	2313.32	-	Screen	Inflow Control Device
142	4883.40	0.30	2313.30	-	Packer	Packer
143	4883.70	11.70	2313.30	-	Screen	Inflow Control Device
144	4895.40	0.30	2313.28	-	Packer	Packer
145	4895.70	11.70	2313.28	-	Screen	Inflow Control Device
146	4907.40	0.30	2313.31	-	Packer	Packer
147	4907.70	11.70	2313.31	-	Screen	Inflow Control Device
148	4919.40	0.30	2313.35	-	Packer	Packer
149	4919.70	11.70	2313.35	-	Screen	Inflow Control Device
150	4931.40	0.30	2313.40	-	Packer	Packer
151	4931.70	11.70	2313.40	-	Screen	Inflow Control Device
152	4943.40	0.30	2313.45	-	Packer	Packer
153	4943.70	11.70	2313.45	-	Screen	Inflow Control Device
154	4955.40	0.30	2313.48	-	Packer	Packer
155	4955.70	11.70	2313.48	-	Screen	Inflow Control Device
156	4967.40	0.30	2313.48	-	Packer	Packer
157	4967.70	11.70	2313.48	-	Screen	Inflow Control Device
158	4979.40	0.30	2313.47	-	Packer	Packer
159	4979.70	11.70	2313.47	-	Screen	Inflow Control Device
160	4991.40	0.30	2313.45	-	Packer	Packer
161	4991.70	11.70	2313.45	-	Screen	Inflow Control Device
162	5003.40	0.30	2313.44	-	Packer	Packer
163	5003.70	11.70	2313.44	-	Screen	Inflow Control Device
164	5015.40	0.30	2313.44	-	Packer	Packer
165	5015.70	11.70	2313.44	-	Screen	Inflow Control Device
166	5027.40	0.30	2313.45	-	Packer	Packer
167	5027.70	11.70	2313.45	-	Screen	Inflow Control Device
168	5039.40	0.30	2313.46	-	Packer	Packer

Figure C-3: *B3-HT2 ICD Completion setup Part 3*

Hole & Completion

#	Top MD [m]	Seg. Length [m]	Top TVD(SS) [m]	Casing/Liner	Sand Control	Inflow Control
155	4955.70	11.70	2313.48	-	Screen	Inflow Control Device
156	4967.40	0.30	2313.48	-	Packer	Packer
157	4967.70	11.70	2313.48	-	Screen	Inflow Control Device
158	4979.40	0.30	2313.47	-	Packer	Packer
159	4979.70	11.70	2313.47	-	Screen	Inflow Control Device
160	4991.40	0.30	2313.45	-	Packer	Packer
161	4991.70	11.70	2313.45	-	Screen	Inflow Control Device
162	5003.40	0.30	2313.44	-	Packer	Packer
163	5003.70	11.70	2313.44	-	Screen	Inflow Control Device
164	5015.40	0.30	2313.44	-	Packer	Packer
165	5015.70	11.70	2313.44	-	Screen	Inflow Control Device
166	5027.40	0.30	2313.45	-	Packer	Packer
167	5027.70	11.70	2313.45	-	Screen	Inflow Control Device
168	5039.40	0.30	2313.46	-	Packer	Packer
169	5039.70	11.70	2313.46	-	Screen	Inflow Control Device
170	5051.40	0.30	2313.46	-	Packer	Packer
171	5051.70	11.70	2313.46	-	Screen	Inflow Control Device
172	5063.40	0.30	2313.47	-	Packer	Packer
173	5063.70	11.70	2313.47	-	Screen	Inflow Control Device
174	5075.40	0.30	2313.47	-	Packer	Packer
175	5075.70	11.70	2313.47	-	Screen	Inflow Control Device
176	5087.40	0.30	2313.48	-	Packer	Packer
177	5087.70	11.70	2313.48	-	Screen	Inflow Control Device
178	5099.40	0.30	2313.48	-	Packer	Packer
179	5099.70	11.70	2313.48	-	Screen	Inflow Control Device
180	5111.40	0.30	2313.46	-	Packer	Packer
181	5111.70	11.70	2313.46	-	Screen	Inflow Control Device
182	5123.40	0.30	2313.45	-	Packer	Packer
183	5123.70	11.70	2313.45	-	Screen	Inflow Control Device
184	5135.40	0.30	2313.44	-	Packer	Packer
185	5135.70	11.70	2313.44	-	Screen	Inflow Control Device
186	5147.40	0.30	2313.43	-	Packer	Packer
187	5147.70	11.70	2313.43	-	Screen	Inflow Control Device
188	5159.40	0.30	2313.44	-	Packer	Packer
189	5159.70	11.70	2313.44	-	Screen	Inflow Control Device
190	5171.40	0.30	2313.46	-	Packer	Packer
191	5171.70	11.70	2313.46	-	Screen	Inflow Control Device
192	5183.40	0.30	2313.48	-	Packer	Packer
193	5183.70	11.70	2313.49	-	Screen	Inflow Control Device
194	5195.40	0.30	2313.51	-	Packer	Packer
195	5195.70	11.70	2313.52	-	Screen	Inflow Control Device
196	5207.40	0.30	2313.55	-	Packer	Packer
197	5207.70	11.70	2313.55	-	Screen	Inflow Control Device
198	5219.40	0.30	2313.57	-	Packer	Packer
199	5219.70	11.70	2313.58	-	Screen	Inflow Control Device
200	5231.40	0.30	2313.60	-	Packer	Packer
201	5231.70	11.70	2313.60	-	Screen	Inflow Control Device
202	5243.40	0.30	2313.61	-	Packer	Packer
203	5243.70	11.70	2313.61	-	Screen	Inflow Control Device
204	5255.40	0.30	2313.61	-	Packer	Packer
205	5255.70	11.70	2313.61	-	Screen	Inflow Control Device
206	5267.40	0.30	2313.61	-	Packer	Packer
207	5267.70	11.70	2313.61	-	Screen	Inflow Control Device
208	5279.40	0.30	2313.59	-	Packer	Packer
209	5279.70	9.20	2313.59	-	Screen	Inflow Control Device
210	5288.90	71.20	2313.58	-	Packer	Packer

Figure C-4: *B3-HT2 ICD Completion setup Part 4*

Diameters

#	Top MD	Seg. Length	Top TVD(SS)	Wellbore Diameter	Casing/Liner ID	Sand Control OD	Sand Control ID	Inflow Control OD	Inflow Control ID
	[m]	[m]	[m]	[in]	[in]	[in]	[in]	[in]	[in]
1	2613.00	5.55	2040.07	10.5	6.184	-	-	-	-
2	2618.55	3.36	2043.31	10.5	5.8	-	-	-	-
3	2621.91	0.76	2045.26	10.5	4.78	-	-	-	-
4	2622.67	2.06	2045.71	10.5	4.67	-	-	-	-
5	2624.73	0.74	2046.91	10.5	4.696	-	-	-	-
6	2625.47	2.06	2047.34	10.5	4.67	-	-	-	-
7	2627.53	23.95	2048.54	10.5	4.67	-	-	-	-
8	2651.48	3.05	2062.24	10.5	4.67	-	-	-	-
9	2654.53	0.76	2063.97	10.5	4.67	-	-	-	-
10	2655.29	1.97	2064.40	10.5	6.184	-	-	-	-
11	2657.26	22.40	2065.51	10.5	6.184	-	-	-	-
12	2679.66	4.08	2077.97	10.5	6.184	-	-	-	-
13	2683.74	1.28	2080.16	10.5	5.75	-	-	-	-
14	2685.02	3.59	2080.85	10.5	5.75	-	-	-	-
15	2688.61	1.94	2082.75	10.5	6.184	-	-	-	-
16	2690.55	696.44	2083.77	10.5	6.184	-	-	-	-
17	3386.99	2.55	2309.48	10.5	5.891	-	-	-	-
18	3389.54	2.20	2309.73	10.5	5.75	-	-	-	-
19	3391.74	8.01	2309.94	10.5	8.553	-	-	-	-
20	3399.75	0.75	2310.68	10.5	8.553	-	7.0	-	5.92
21	3400.50	1.56	2310.75	10.5	8.553	-	7.0	-	5.92
22	3402.06	38.44	2310.88	10.5	8.553	-	7.0	-	5.92
23	3440.50	335.10	2313.48	8.5	-	-	7.0	-	5.92
24	3775.60	11.70	2313.67	8.5	-	7.299	7.0	6.625	5.92
25	3787.30	0.30	2313.67	8.5	-	-	7.0	-	5.92
26	3787.60	11.70	2313.67	8.5	-	7.299	7.0	6.625	5.92
27	3799.30	0.30	2313.70	8.5	-	-	7.0	-	5.92
28	3799.60	11.70	2313.70	8.5	-	7.299	7.0	6.625	5.92
29	3811.30	0.30	2313.75	8.5	-	-	7.0	-	5.92
30	3811.60	11.70	2313.75	8.5	-	7.299	7.0	6.625	5.92
31	3823.30	0.30	2313.80	8.5	-	-	7.0	-	5.92
32	3823.60	11.70	2313.80	8.5	-	7.299	7.0	6.625	5.92
33	3835.30	0.30	2313.85	8.5	-	-	7.0	-	5.92
34	3835.60	11.70	2313.85	8.5	-	7.299	7.0	6.625	5.92
35	3847.30	0.30	2313.89	8.5	-	-	7.0	-	5.92
36	3847.60	11.70	2313.89	8.5	-	7.299	7.0	6.625	5.92
37	3859.30	0.30	2313.90	8.5	-	-	7.0	-	5.92
38	3859.60	11.70	2313.90	8.5	-	7.299	7.0	6.625	5.92
39	3871.30	0.30	2313.90	8.5	-	-	7.0	-	5.92
40	3871.60	11.70	2313.90	8.5	-	7.299	7.0	6.625	5.92
41	3883.30	0.30	2313.90	8.5	-	-	7.0	-	5.92
42	3883.60	11.70	2313.90	8.5	-	7.299	7.0	6.625	5.92
43	3895.30	0.30	2313.91	8.5	-	-	7.0	-	5.92
44	3895.60	11.70	2313.91	8.5	-	7.299	7.0	6.625	5.92

Figure C-5: *B3-HT2 ICD Completion diameters. Sand Control ID represents the inner diameter of the sandscreen, while the Inflow Control OD represents the base pipe OD, where the inflow control device is mounted. Lastly, the inflow control ID corresponds to the base pipe ID, which also corresponds to the base case model. The diameters from 3775mMD to 3967mMD is representative for the remaining completion, to ∼5350mMD. Applies to B3 Simulation cases 8-17.*

Inflow Control Device

#	Top MD [m]	Seg. Length [m]	Top TVD(SS) [m]	ICD Design	Joint Length [m]
1	2613.00	5.55	2040.07	-	-
2	2618.55	3.36	2043.31	-	-
3	2621.91	0.76	2045.26	-	-
4	2622.67	2.06	2045.71	-	-
5	2624.73	0.74	2046.91	-	-
6	2625.47	2.06	2047.34	-	-
7	2627.53	23.95	2048.54	-	-
8	2651.48	3.05	2062.24	-	-
9	2654.53	0.76	2063.97	-	-
10	2655.29	1.97	2064.40	-	-
11	2657.26	22.40	2065.51	-	-
12	2679.66	4.08	2077.97	-	-
13	2683.74	1.28	2080.16	-	-
14	2685.02	3.59	2080.85	-	-
15	2688.61	1.94	2082.75	-	-
16	2690.55	696.44	2083.77	-	-
17	3386.99	2.55	2309.48	-	-
18	3389.54	2.20	2309.73	-	-
19	3391.74	8.01	2309.94	-	-
20	3399.75	0.75	2310.68	-	-
21	3400.50	1.56	2310.75	-	-
22	3402.06	38.44	2310.88	-	-
23	3440.50	335.10	2313.48	-	-
24	3775.60	11.70	2313.67	Generic Nozzle ICD	11.7
25	3787.30	0.30	2313.67	-	-
26	3787.60	11.70	2313.67	Generic Nozzle ICD	11.7
27	3799.30	0.30	2313.70	-	-
28	3799.60	11.70	2313.70	Generic Nozzle ICD	11.7
29	3811.30	0.30	2313.75	-	-
30	3811.60	11.70	2313.75	Generic Nozzle ICD	11.7
31	3823.30	0.30	2313.80	-	-
32	3823.60	11.70	2313.80	Generic Nozzle ICD	11.7
33	3835.30	0.30	2313.85	-	-
34	3835.60	11.70	2313.85	Generic Nozzle ICD	11.7
35	3847.30	0.30	2313.89	-	-
36	3847.60	11.70	2313.89	Generic Nozzle ICD	11.7
37	3859.30	0.30	2313.90	-	-
38	3859.60	11.70	2313.90	Generic Nozzle ICD	11.7
39	3871.30	0.30	2313.90	-	-
40	3871.60	11.70	2313.90	Generic Nozzle ICD	11.7
41	3883.30	0.30	2313.90	-	-
42	3883.60	11.70	2313.90	Generic Nozzle ICD	11.7
43	3895.30	0.30	2313.91	-	-
44	3895.60	11.70	2313.91	Generic Nozzle ICD	11.7
45	3907.30	0.30	2313.92	-	-
46	3907.60	11.70	2313.92	Generic Nozzle ICD	11.7
47	3919.30	0.30	2313.95	-	-
48	3919.60	11.70	2313.95	Generic Nozzle ICD	11.7
49	3931.30	0.30	2313.97	-	-
50	3931.60	11.70	2313.97	Generic Nozzle ICD	11.7
51	3943.30	0.30	2313.96	-	-
52	3943.60	11.70	2313.96	Generic Nozzle ICD	11.7
53	3955.30	0.30	2313.93	-	-
54	3955.60	11.70	2313.93	Generic Nozzle ICD	11.7
55	3967.30	0.30	2313.89	-	-
56	3967.60	11.70	2313.89	Generic Nozzle ICD	11.7

Figure C-6: *B3-HT2 ICD Completion Input. The input from 3775mMD to 3967mMD is representative for the remaining completion, to ~5350mMD.Applies to B3 Simulation cases 8-10, 15 and 16.*

Generic Nozzle ICD

#	Top MD	Seg. Length	Top TVD(SS)	Nozzle Diameter	N Parallel Nozzles	Use Discharge or L...	Discharge Depends...	Discharge Coefficient
	[m]	[m]	[m]	[mm]				
1	2613.00	5.55	2040.07	-	-	-	-	-
2	2618.55	3.36	2043.31	-	-	-	-	-
3	2621.91	0.76	2045.26	-	-	-	-	-
4	2622.67	2.06	2045.71	-	-	-	-	-
5	2624.73	0.74	2046.91	-	-	-	-	-
6	2625.47	2.06	2047.34	-	-	-	-	-
7	2627.53	23.95	2048.54	-	-	-	-	-
8	2651.48	3.05	2062.24	-	-	-	-	-
9	2654.53	0.76	2063.97	-	-	-	-	-
10	2655.29	1.97	2064.40	-	-	-	-	-
11	2657.26	22.40	2065.51	-	-	-	-	-
12	2679.66	4.08	2077.97	-	-	-	-	-
13	2683.74	1.28	2080.16	-	-	-	-	-
14	2685.02	3.59	2080.85	-	-	-	-	-
15	2688.61	1.94	2082.75	-	-	-	-	-
16	2690.55	696.44	2083.77	-	-	-	-	-
17	3386.99	2.55	2309.48	-	-	-	-	-
18	3389.54	2.20	2309.73	-	-	-	-	-
19	3391.74	8.01	2309.94	-	-	-	-	-
20	3399.75	0.75	2310.68	-	-	-	-	-
21	3400.50	1.56	2310.75	-	-	-	-	-
22	3402.06	38.44	2310.88	-	-	-	-	-
23	3440.50	335.10	2313.48	-	-	-	-	-
24	3775.60	11.70	2313.67	2.65	3	Use discharge coeff.	☐	0.93
25	3787.30	0.30	2313.67	-	-	-	-	-
26	3787.60	11.70	2313.67	2.65	3	Use discharge coeff.	☐	0.93
27	3799.30	0.30	2313.70	-	-	-	-	-
28	3799.60	11.70	2313.70	2.65	3	Use discharge coeff.	☐	0.93
29	3811.30	0.30	2313.75	-	-	-	-	-
30	3811.60	11.70	2313.75	2.65	3	Use discharge coeff.	☐	0.93
31	3823.30	0.30	2313.80	-	-	-	-	-
32	3823.60	11.70	2313.80	2.65	3	Use discharge coeff.	☐	0.93
33	3835.30	0.30	2313.85	-	-	-	-	-
34	3835.60	11.70	2313.85	2.65	3	Use discharge coeff.	☐	0.93
35	3847.30	0.30	2313.89	-	-	-	-	-
36	3847.60	11.70	2313.89	2.65	3	Use discharge coeff.	☐	0.93
37	3859.30	0.30	2313.90	-	-	-	-	-
38	3859.60	11.70	2313.90	2.65	3	Use discharge coeff.	☐	0.93
39	3871.30	0.30	2313.90	-	-	-	-	-
40	3871.60	11.70	2313.90	2.65	3	Use discharge coeff.	☐	0.93
41	3883.30	0.30	2313.90	-	-	-	-	-
42	3883.60	11.70	2313.90	2.65	3	Use discharge coeff.	☐	0.93
43	3895.30	0.30	2313.91	-	-	-	-	-
44	3895.60	11.70	2313.91	2.65	3	Use discharge coeff.	☐	0.93

Figure C-7: *B3-HT2: An example of the ICD Settings in NETool showing the input for case 15. For cases 8-10, the only thing that is changed is the Nozzle Diameter, in accordance with Table 7. The input from 3775mMD to 3967mMD is representative for the remaining completion, to ∼5350mMD.*

C.2 Well B1 NETool ICD Well Design

Hole & Completion

#	Top MD	Seg. Length	Top TVD(SS)	Casing/Liner	Sand Control	Inflow Control
	[m]	[m]	[m]			
1	2607.00	1.83	2061.70	Cemented Blank Pipe	-	-
2	2608.83	3.05	2062.94	Cemented Blank Pipe	-	-
3	2611.88	1.45	2064.99	Cemented Blank Pipe	-	-
4	2613.33	2.06	2065.97	Cemented Blank Pipe	-	-
5	2615.39	22.00	2067.36	Cemented Blank Pipe	-	-
6	2637.39	3.05	2082.21	Cemented Blank Pipe	-	-
7	2640.44	3.66	2084.27	Cemented Blank Pipe	-	-
8	2644.10	0.58	2086.73	Cemented Blank Pipe	-	-
9	2644.68	2.00	2087.13	Cemented Blank Pipe	-	-
10	2646.68	0.70	2088.47	Cemented Blank Pipe	-	-
11	2647.38	2.00	2088.95	Cemented Blank Pipe	-	-
12	2649.38	25.00	2090.29	Cemented Blank Pipe	-	-
13	2674.38	3.00	2107.15	Cemented Blank Pipe	-	-
14	2677.38	0.60	2109.18	Cemented Blank Pipe	-	-
15	2677.98	2.00	2109.58	Cemented Blank Pipe	-	-
16	2679.98	2.05	2110.94	Cemented Blank Pipe	-	-
17	2682.03	1.15	2112.32	Cemented Blank Pipe	-	-
18	2683.18	3.74	2113.10	Cemented Blank Pipe	-	-
19	2686.92	2.09	2115.62	Cemented Blank Pipe	-	-
20	2689.01	3.00	2117.03	Cemented Blank Pipe	-	-
21	2692.01	4.75	2119.05	Cemented Blank Pipe	-	-
22	2696.76	49.22	2122.24	Cemented Blank Pipe	-	-
23	2745.98	294.02	2154.25	Cemented Blank Pipe	-	-
24	3040.00	6.00	2306.10	Cemented Blank Pipe	-	-
25	3046.00	1.90	2307.21	Cemented Blank Pipe	-	-
26	3047.90	3.00	2307.54	Cemented Blank Pipe	-	-
27	3050.90	3.00	2308.03	Cemented Blank Pipe	-	-
28	3053.90	0.57	2308.49	Cemented Blank Pipe	-	-
29	3054.47	2.58	2308.58	Cemented Blank Pipe	-	-
30	3057.05	48.93	2308.94	Cemented Blank Pipe	Packer	-
31	3105.98	25.28	2312.47	Cemented Blank Pipe	Packer	-
32	3131.26	12.05	2312.97	Cemented Blank Pipe	Packer	-
33	3143.31	11.70	2313.04	-	Screen	Inflow Control Device
34	3155.01	0.30	2313.10	-	Packer	Packer
35	3155.31	11.70	2313.11	-	Screen	Inflow Control Device
36	3167.01	0.30	2313.13	-	Packer	Packer
37	3167.31	11.70	2313.13	-	Screen	Inflow Control Device
38	3179.01	0.30	2313.13	-	Packer	Packer
39	3179.31	11.70	2313.13	-	Screen	Inflow Control Device
40	3191.01	0.30	2313.12	-	Packer	Packer
41	3191.31	11.70	2313.12	-	Screen	Inflow Control Device
42	3203.01	0.30	2313.11	-	Packer	Packer
43	3203.31	11.70	2313.11	-	Screen	Inflow Control Device
44	3215.01	0.30	2313.09	-	Packer	Packer
45	3215.31	11.70	2313.09	-	Screen	Inflow Control Device
46	3227.01	0.30	2313.06	-	Packer	Packer
47	3227.31	11.70	2313.06	-	Screen	Inflow Control Device
48	3239.01	0.30	2313.03	-	Packer	Packer
49	3239.31	11.70	2313.03	-	Screen	Inflow Control Device
50	3251.01	0.30	2313.00	-	Packer	Packer
51	3251.31	11.70	2313.00	-	Screen	Inflow Control Device
52	3263.01	0.30	2312.97	-	Packer	Packer
53	3263.31	11.70	2312.97	-	Screen	Inflow Control Device
54	3275.01	0.30	2312.94	-	Packer	Packer
55	3275.31	11.70	2312.94	-	Screen	Inflow Control Device

Figure C-8: *B1-AHT3 ICD Completion setup Part 1. Every screen joint is equipped with a 0.3m swellable packer for annular compartmentalization. The screen layer is equipped with inflow control technology. Every joint is set as 12m unless a pup joint is needed for spacing out the original completion length. Blank pipe sections are, as previously, set as packers. Applies to B1 Simulation cases 8-17.*

Hole & Completion

#	Top MD	Seg. Length	Top TVD(SS)	Casing/Liner	Sand Control	Inflow Control
	[m]	[m]	[m]			
55	3275.31	11.70	2312.94	-	Screen	Inflow Control Device
56	3287.01	0.30	2312.92	-	Packer	Packer
57	3287.31	11.70	2312.92	-	Screen	Inflow Control Device
58	3299.01	0.30	2312.89	-	Packer	Packer
59	3299.31	11.70	2312.89	-	Screen	Inflow Control Device
60	3311.01	0.30	2312.87	-	Packer	Packer
61	3311.31	11.70	2312.87	-	Screen	Inflow Control Device
62	3323.01	0.30	2312.85	-	Packer	Packer
63	3323.31	11.70	2312.85	-	Screen	Inflow Control Device
64	3335.01	0.30	2312.83	-	Packer	Packer
65	3335.31	11.70	2312.83	-	Screen	Inflow Control Device
66	3347.01	0.30	2312.80	-	Packer	Packer
67	3347.31	11.70	2312.80	-	Screen	Inflow Control Device
68	3359.01	0.30	2312.77	-	Packer	Packer
69	3359.31	11.70	2312.77	-	Screen	Inflow Control Device
70	3371.01	0.30	2312.74	-	Packer	Packer
71	3371.31	11.70	2312.74	-	Screen	Inflow Control Device
72	3383.01	0.30	2312.69	-	Packer	Packer
73	3383.31	11.70	2312.69	-	Screen	Inflow Control Device
74	3395.01	0.30	2312.63	-	Packer	Packer
75	3395.31	11.70	2312.63	-	Screen	Inflow Control Device
76	3407.01	0.30	2312.59	-	Packer	Packer
77	3407.31	11.70	2312.59	-	Screen	Inflow Control Device
78	3419.01	0.30	2312.60	-	Packer	Packer
79	3419.31	11.70	2312.60	-	Screen	Inflow Control Device
80	3431.01	0.30	2312.65	-	Packer	Packer
81	3431.31	11.70	2312.66	-	Screen	Inflow Control Device
82	3443.01	0.30	2312.74	-	Packer	Packer
83	3443.31	11.70	2312.74	-	Screen	Inflow Control Device
84	3455.01	0.30	2312.86	-	Packer	Packer
85	3455.31	11.70	2312.87	-	Screen	Inflow Control Device
86	3467.01	0.30	2313.00	-	Packer	Packer
87	3467.31	11.70	2313.00	-	Screen	Inflow Control Device
88	3479.01	0.30	2313.15	-	Packer	Packer
89	3479.31	11.70	2313.15	-	Screen	Inflow Control Device
90	3491.01	0.30	2313.29	-	Packer	Packer
91	3491.31	11.70	2313.30	-	Screen	Inflow Control Device
92	3503.01	0.30	2313.41	-	Packer	Packer
93	3503.31	11.70	2313.42	-	Screen	Inflow Control Device
94	3515.01	0.30	2313.52	-	Packer	Packer
95	3515.31	11.70	2313.53	-	Screen	Inflow Control Device
96	3527.01	0.30	2313.63	-	Packer	Packer
97	3527.31	11.70	2313.63	-	Screen	Inflow Control Device
98	3539.01	0.30	2313.73	-	Packer	Packer
99	3539.31	11.70	2313.73	-	Screen	Inflow Control Device
100	3551.01	0.30	2313.84	-	Packer	Packer
101	3551.31	11.70	2313.84	-	Screen	Inflow Control Device
102	3563.01	0.30	2313.97	-	Packer	Packer
103	3563.31	11.70	2313.97	-	Screen	Inflow Control Device
104	3575.01	0.30	2314.09	-	Packer	Packer
105	3575.31	11.70	2314.10	-	Screen	Inflow Control Device
106	3587.01	0.30	2314.20	-	Packer	Packer
107	3587.31	11.70	2314.20	-	Screen	Inflow Control Device
108	3599.01	0.30	2314.26	-	Packer	Packer
109	3599.31	11.70	2314.26	-	Screen	Inflow Control Device

Figure C-9: *B1-AHT3 ICD Completion setup Part 2*

Hole & Completion

#	Top MD	Seg. Length	Top TVD(SS)	Casing/Liner	Sand Control	Inflow Control
	[m]	[m]	[m]			
108	3599.01	0.30	2314.26	-	Packer	Packer
109	3599.31	11.70	2314.26	-	Screen	Inflow Control Device
110	3611.01	0.30	2314.30	-	Packer	Packer
111	3611.31	11.70	2314.30	-	Screen	Inflow Control Device
112	3623.01	0.30	2314.29	-	Packer	Packer
113	3623.31	11.70	2314.29	-	Screen	Inflow Control Device
114	3635.01	0.30	2314.27	-	Packer	Packer
115	3635.31	11.70	2314.27	-	Screen	Inflow Control Device
116	3647.01	0.30	2314.25	-	Packer	Packer
117	3647.31	11.70	2314.25	-	Screen	Inflow Control Device
118	3659.01	0.30	2314.25	-	Packer	Packer
119	3659.31	11.70	2314.25	-	Screen	Inflow Control Device
120	3671.01	0.30	2314.25	-	Packer	Packer
121	3671.31	6.17	2314.25	-	Screen	Inflow Control Device
122	3677.48	148.44	2314.25	-	Packer	Packer
123	3825.92	11.70	2314.04	-	Screen	Inflow Control Device
124	3837.62	0.30	2314.03	-	Packer	Packer
125	3837.92	11.70	2314.03	-	Screen	Inflow Control Device
126	3849.62	0.30	2314.02	-	Packer	Packer
127	3849.92	11.70	2314.02	-	Screen	Inflow Control Device
128	3861.62	0.30	2314.01	-	Packer	Packer
129	3861.92	11.70	2314.01	-	Screen	Inflow Control Device
130	3873.62	0.30	2314.00	-	Packer	Packer
131	3873.92	11.70	2314.00	-	Screen	Inflow Control Device
132	3885.62	0.30	2313.99	-	Packer	Packer
133	3885.92	2.59	2313.99	-	Screen	Inflow Control Device
134	3888.51	221.05	2313.98	-	Packer	Packer
135	4109.56	11.70	2313.46	-	Screen	Inflow Control Device
136	4121.26	0.30	2313.42	-	Packer	Packer
137	4121.56	11.70	2313.41	-	Screen	Inflow Control Device
138	4133.26	0.30	2313.38	-	Packer	Packer
139	4133.56	11.70	2313.38	-	Screen	Inflow Control Device
140	4145.26	0.30	2313.37	-	Packer	Packer
141	4145.56	11.70	2313.37	-	Screen	Inflow Control Device
142	4157.26	0.30	2313.42	-	Packer	Packer
143	4157.56	11.70	2313.42	-	Screen	Inflow Control Device
144	4169.26	0.30	2313.49	-	Packer	Packer
145	4169.56	11.70	2313.50	-	Screen	Inflow Control Device
146	4181.26	0.30	2313.59	-	Packer	Packer
147	4181.56	11.70	2313.59	-	Screen	Inflow Control Device
148	4193.26	0.30	2313.68	-	Packer	Packer
149	4193.56	11.70	2313.69	-	Screen	Inflow Control Device
150	4205.26	0.30	2313.77	-	Packer	Packer
151	4205.56	11.70	2313.78	-	Screen	Inflow Control Device
152	4217.26	0.30	2313.85	-	Packer	Packer
153	4217.56	11.70	2313.85	-	Screen	Inflow Control Device
154	4229.26	0.30	2313.91	-	Packer	Packer
155	4229.56	11.70	2313.91	-	Screen	Inflow Control Device
156	4241.26	0.30	2313.92	-	Packer	Packer
157	4241.56	11.70	2313.92	-	Screen	Inflow Control Device
158	4253.26	0.30	2313.91	-	Packer	Packer
159	4253.56	11.70	2313.91	-	Screen	Inflow Control Device
160	4265.26	0.30	2313.89	-	Packer	Packer
161	4265.56	11.70	2313.89	-	Screen	Inflow Control Device
162	4277.26	0.30	2313.88	-	Packer	Packer

Figure C-10: *B1-AHT3 ICD Completion setup Part 3*

Hole & Completion

#	Top MD [m]	Seg. Length [m]	Top TVD(SS) [m]	Casing/Liner	Sand Control	Inflow Control
129	3861.92	11.70	2314.01	-	Screen	Inflow Control Device
130	3873.62	0.30	2314.00	-	Packer	Packer
131	3873.92	11.70	2314.00	-	Screen	Inflow Control Device
132	3885.62	0.30	2313.99	-	Packer	Packer
133	3885.92	2.59	2313.99	-	Screen	Inflow Control Device
134	3888.51	221.05	2313.98	-	Packer	Packer
135	4109.56	11.70	2313.46	-	Screen	Inflow Control Device
136	4121.26	0.30	2313.42	-	Packer	Packer
137	4121.56	11.70	2313.41	-	Screen	Inflow Control Device
138	4133.26	0.30	2313.38	-	Packer	Packer
139	4133.56	11.70	2313.38	-	Screen	Inflow Control Device
140	4145.26	0.30	2313.37	-	Packer	Packer
141	4145.56	11.70	2313.37	-	Screen	Inflow Control Device
142	4157.26	0.30	2313.42	-	Packer	Packer
143	4157.56	11.70	2313.42	-	Screen	Inflow Control Device
144	4169.26	0.30	2313.49	-	Packer	Packer
145	4169.56	11.70	2313.50	-	Screen	Inflow Control Device
146	4181.26	0.30	2313.59	-	Packer	Packer
147	4181.56	11.70	2313.59	-	Screen	Inflow Control Device
148	4193.26	0.30	2313.68	-	Packer	Packer
149	4193.56	11.70	2313.69	-	Screen	Inflow Control Device
150	4205.26	0.30	2313.77	-	Packer	Packer
151	4205.56	11.70	2313.78	-	Screen	Inflow Control Device
152	4217.26	0.30	2313.85	-	Packer	Packer
153	4217.56	11.70	2313.85	-	Screen	Inflow Control Device
154	4229.26	0.30	2313.91	-	Packer	Packer
155	4229.56	11.70	2313.91	-	Screen	Inflow Control Device
156	4241.26	0.30	2313.92	-	Packer	Packer
157	4241.56	11.70	2313.92	-	Screen	Inflow Control Device
158	4253.26	0.30	2313.91	-	Packer	Packer
159	4253.56	11.70	2313.91	-	Screen	Inflow Control Device
160	4265.26	0.30	2313.89	-	Packer	Packer
161	4265.56	11.70	2313.89	-	Screen	Inflow Control Device
162	4277.26	0.30	2313.88	-	Packer	Packer
163	4277.56	11.70	2313.88	-	Screen	Inflow Control Device
164	4289.26	0.30	2313.87	-	Packer	Packer
165	4289.56	11.70	2313.87	-	Screen	Inflow Control Device
166	4301.26	0.30	2313.85	-	Packer	Packer
167	4301.56	11.70	2313.85	-	Screen	Inflow Control Device
168	4313.26	0.30	2313.82	-	Packer	Packer
169	4313.56	11.70	2313.82	-	Screen	Inflow Control Device
170	4325.26	0.30	2313.78	-	Packer	Packer
171	4325.56	11.70	2313.78	-	Screen	Inflow Control Device
172	4337.26	0.30	2313.72	-	Packer	Packer
173	4337.56	11.70	2313.72	-	Screen	Inflow Control Device
174	4349.26	0.30	2313.67	-	Packer	Packer
175	4349.56	11.70	2313.67	-	Screen	Inflow Control Device
176	4361.26	0.30	2313.63	-	Packer	Packer
177	4361.56	11.70	2313.63	-	Screen	Inflow Control Device
178	4373.26	0.30	2313.59	-	Packer	Packer
179	4373.56	11.70	2313.59	-	Screen	Inflow Control Device
180	4385.26	0.30	2313.54	-	Packer	Packer
181	4385.56	11.97	2313.54	-	Screen	Inflow Control Device
182	4397.53	12.37	2313.49	-	Packer	Packer
183	4409.90	0.24	2313.44	-	Packer	Packer

Figure C-11: *B1-AHT3 ICD Completion setup Part 4*

Diameters

#	Top MD	Seg. Length	Top TVD(SS)	Wellbore Diameter	Casing/Liner ID	Sand Control OD	Sand Control ID	Inflow Control OD	Inflow Control ID
	[m]	[m]	[m]	[in]	[in]	[in]	[in]	[in]	[in]
1	2607.00	1.83	2061.70	8.5	6.18	-	-	-	-
2	2608.83	3.05	2062.94	8.5	6.184	-	-	-	-
3	2611.88	1.45	2064.99	8.5	6.072	-	-	-	-
4	2613.33	2.06	2065.97	8.5	6.184	-	-	-	-
5	2615.39	22.00	2067.36	8.5	6.184	-	-	-	-
6	2637.39	3.05	2082.21	8.5	6.184	-	-	-	-
7	2640.44	3.66	2084.27	8.5	5.8	-	-	-	-
8	2644.10	0.58	2086.73	8.5	4.758	-	-	-	-
9	2644.68	2.00	2087.13	8.5	4.67	-	-	-	-
10	2646.68	0.70	2088.47	8.5	4.588	-	-	-	-
11	2647.38	2.00	2088.95	8.5	4.67	-	-	-	-
12	2649.38	25.00	2090.29	8.5	4.67	-	-	-	-
13	2674.38	3.00	2107.15	8.5	4.67	-	-	-	-
14	2677.38	0.60	2109.18	8.5	4.778	-	-	-	-
15	2677.98	2.00	2109.58	8.5	6.184	-	-	-	-
16	2679.98	2.05	2110.94	8.5	6.184	-	-	-	-
17	2682.03	1.15	2112.32	8.5	5.75	-	-	-	-
18	2683.18	3.74	2113.10	8.5	5.75	-	-	-	-
19	2686.92	2.09	2115.62	8.5	6.184	-	-	-	-
20	2689.01	3.00	2117.03	8.5	6.184	-	-	-	-
21	2692.01	4.75	2119.05	8.5	6.094	-	-	-	-
22	2696.76	49.22	2122.24	8.5	5.75	-	-	-	-
23	2745.98	294.02	2154.25	8.5	6.184	-	-	-	-
24	3040.00	6.00	2306.10	8.5	6.184	-	-	-	-
25	3046.00	1.90	2307.21	8.5	6.184	-	-	-	-
26	3047.90	3.00	2307.54	8.5	6.184	-	-	-	-
27	3050.90	3.00	2308.03	8.5	6.184	-	-	-	-
28	3053.90	0.57	2308.49	8.5	6.184	-	-	-	-
29	3054.47	2.58	2308.58	8.5	6.184	-	-	-	-
30	3057.05	48.93	2308.94	8.5	6.184	-	3.96	-	-
31	3105.98	25.28	2312.47	8.5	6.184	-	3.96	-	-
32	3131.26	12.05	2312.97	8.5	6.184	-	3.96	-	-
33	3143.31	11.70	2313.04	6.0	-	5.31	5.0	4.5	3.913
34	3155.01	0.30	2313.10	6.0	-	-	5.0	-	3.96
35	3155.31	11.70	2313.11	6.0	-	5.31	5.0	4.5	3.913
36	3167.01	0.30	2313.13	6.0	-	-	5.0	-	3.96
37	3167.31	11.70	2313.13	6.0	-	5.31	5.0	4.5	3.913
38	3179.01	0.30	2313.13	6.0	-	-	5.0	-	3.96
39	3179.31	11.70	2313.13	6.0	-	5.31	5.0	4.5	3.913
40	3191.01	0.30	2313.12	6.0	-	-	5.0	-	3.96
41	3191.31	11.70	2313.12	6.0	-	5.31	5.0	4.5	3.913
42	3203.01	0.30	2313.11	6.0	-	-	5.0	-	3.96
43	3203.31	11.70	2313.11	6.0	-	5.31	5.0	4.5	3.913
44	3215.01	0.30	2313.09	6.0	-	-	5.0	-	3.96
45	3215.31	11.70	2313.09	6.0	-	5.31	5.0	4.5	3.913
46	3227.01	0.30	2313.06	6.0	-	-	5.0	-	3.96
47	3227.31	11.70	2313.06	6.0	-	5.31	5.0	4.5	3.913
48	3239.01	0.30	2313.03	6.0	-	-	5.0	-	3.96
49	3239.31	11.70	2313.03	6.0	-	5.31	5.0	4.5	3.913
50	3251.01	0.30	2313.00	6.0	-	-	5.0	-	3.96
51	3251.31	11.70	2313.00	6.0	-	5.31	5.0	4.5	3.913
52	3263.01	0.30	2312.97	6.0	-	-	5.0	-	3.96
53	3263.31	11.70	2312.97	6.0	-	5.31	5.0	4.5	3.913
54	3275.01	0.30	2312.94	6.0	-	-	5.0	-	3.96
55	3275.31	11.70	2312.94	6.0	-	5.31	5.0	4.5	3.913

Figure C-12: *B1-AHT3 ICD Completion diameters. Sand Control ID represents the inner diameter of the sandscreen, while the Inflow Control OD represents the base pipe OD, where the inflow control device is mounted. Lastly, the inflow control ID corresponds to the base pipe ID, which also corresponds to the base case model. The diameters from 3143mMD to 3275mMD is representative for the remaining completion, to ~4410mMD. Applies to B1 Simulation cases 11-14.*

Inflow Control Device

#	Top MD	Seg. Length	Top TVD(SS)	ICD Design	Joint Length
	[m]	[m]	[m]		[m]
28	3053.90	0.57	2308.49	-	-
29	3054.47	2.58	2308.58	-	-
30	3057.05	48.93	2308.94	-	-
31	3105.98	25.28	2312.47	-	-
32	3131.26	12.05	2312.97	-	-
33	3143.31	11.70	2313.04	Generic Nozzle ICD	11.7
34	3155.01	0.30	2313.10	-	-
35	3155.31	11.70	2313.11	Generic Nozzle ICD	11.7
36	3167.01	0.30	2313.13	-	-
37	3167.31	11.70	2313.13	Generic Nozzle ICD	11.7
38	3179.01	0.30	2313.13	-	-
39	3179.31	11.70	2313.13	Generic Nozzle ICD	11.7
40	3191.01	0.30	2313.12	-	-
41	3191.31	11.70	2313.12	Generic Nozzle ICD	11.7
42	3203.01	0.30	2313.11	-	-
43	3203.31	11.70	2313.11	Generic Nozzle ICD	11.7
44	3215.01	0.30	2313.09	-	-
45	3215.31	11.70	2313.09	Generic Nozzle ICD	11.7
46	3227.01	0.30	2313.06	-	-
47	3227.31	11.70	2313.06	Generic Nozzle ICD	11.7
48	3239.01	0.30	2313.03	-	-
49	3239.31	11.70	2313.03	Generic Nozzle ICD	11.7
50	3251.01	0.30	2313.00	-	-
51	3251.31	11.70	2313.00	Generic Nozzle ICD	11.7
52	3263.01	0.30	2312.97	-	-
53	3263.31	11.70	2312.97	Generic Nozzle ICD	11.7
54	3275.01	0.30	2312.94	-	-
55	3275.31	11.70	2312.94	Generic Nozzle ICD	11.7
56	3287.01	0.30	2312.92	-	-
57	3287.31	11.70	2312.92	Generic Nozzle ICD	11.7
58	3299.01	0.30	2312.89	-	-
59	3299.31	11.70	2312.89	Generic Nozzle ICD	11.7
60	3311.01	0.30	2312.87	-	-
61	3311.31	11.70	2312.87	Generic Nozzle ICD	11.7
62	3323.01	0.30	2312.85	-	-
63	3323.31	11.70	2312.85	Generic Nozzle ICD	11.7
64	3335.01	0.30	2312.83	-	-
65	3335.31	11.70	2312.83	Generic Nozzle ICD	11.7
66	3347.01	0.30	2312.80	-	-
67	3347.31	11.70	2312.80	Generic Nozzle ICD	11.7
68	3359.01	0.30	2312.77	-	-
69	3359.31	11.70	2312.77	Generic Nozzle ICD	11.7
70	3371.01	0.30	2312.74	-	-
71	3371.31	11.70	2312.74	Generic Nozzle ICD	11.7
72	3383.01	0.30	2312.69	-	-
73	3383.31	11.70	2312.69	Generic Nozzle ICD	11.7
74	3395.01	0.30	2312.63	-	-
75	3395.31	11.70	2312.63	Generic Nozzle ICD	11.7
76	3407.01	0.30	2312.59	-	-
77	3407.31	11.70	2312.59	Generic Nozzle ICD	11.7
78	3419.01	0.30	2312.60	-	-
79	3419.31	11.70	2312.60	Generic Nozzle ICD	11.7
80	3431.01	0.30	2312.65	-	-
81	3431.31	11.70	2312.66	Generic Nozzle ICD	11.7
82	3443.01	0.30	2312.74	-	-

Figure C-13: *B1-AHT3 ICD Completion Input. The input from 3143mMD to 3275mMD is representative for the remaining completion, to ~4410mMD.Applies to B1 Simulation cases 11-13.*

Generic Nozzle ICD

#	Top MD	Seg. Length	Top TVD(SS)	Nozzle Diameter	N Parallel Nozzles	Use Discharge or L...	Discharge Depends...	Discharge Coefficient
	[m]	[m]	[m]	[mm]				
31	3105.98	25.28	2312.47	-	-	-	-	-
32	3131.26	12.05	2312.97	-	-	-	-	-
33	3143.31	11.70	2313.04	3.0	3	Use discharge coeff.	☐	0.93
34	3155.01	0.30	2313.10	-	-	-	-	-
35	3155.31	11.70	2313.11	3.0	3	Use discharge coeff.	☐	0.93
36	3167.01	0.30	2313.13	-	-	-	-	-
37	3167.31	11.70	2313.13	3.0	3	Use discharge coeff.	☐	0.93
38	3179.01	0.30	2313.13	-	-	-	-	-
39	3179.31	11.70	2313.13	3.0	3	Use discharge coeff.	☐	0.93
40	3191.01	0.30	2313.12	-	-	-	-	-
41	3191.31	11.70	2313.12	3.0	3	Use discharge coeff.	☐	0.93
42	3203.01	0.30	2313.11	-	-	-	-	-
43	3203.31	11.70	2313.11	3.0	3	Use discharge coeff.	☐	0.93
44	3215.01	0.30	2313.09	-	-	-	-	-
45	3215.31	11.70	2313.09	3.0	3	Use discharge coeff.	☐	0.93
46	3227.01	0.30	2313.06	-	-	-	-	-
47	3227.31	11.70	2313.06	3.0	3	Use discharge coeff.	☐	0.93
48	3239.01	0.30	2313.03	-	-	-	-	-
49	3239.31	11.70	2313.03	3.0	3	Use discharge coeff.	☐	0.93
50	3251.01	0.30	2313.00	-	-	-	-	-
51	3251.31	11.70	2313.00	3.0	3	Use discharge coeff.	☐	0.93
52	3263.01	0.30	2312.97	-	-	-	-	-
53	3263.31	11.70	2312.97	3.0	3	Use discharge coeff.	☐	0.93
54	3275.01	0.30	2312.94	-	-	-	-	-
55	3275.31	11.70	2312.94	3.0	3	Use discharge coeff.	☐	0.93
56	3287.01	0.30	2312.92	-	-	-	-	-
57	3287.31	11.70	2312.92	3.0	3	Use discharge coeff.	☐	0.93
58	3299.01	0.30	2312.89	-	-	-	-	-
59	3299.31	11.70	2312.89	3.0	3	Use discharge coeff.	☐	0.93
60	3311.01	0.30	2312.87	-	-	-	-	-
61	3311.31	11.70	2312.87	3.0	3	Use discharge coeff.	☐	0.93
62	3323.01	0.30	2312.85	-	-	-	-	-
63	3323.31	11.70	2312.85	3.0	3	Use discharge coeff.	☐	0.93
64	3335.01	0.30	2312.83	-	-	-	-	-
65	3335.31	11.70	2312.83	3.0	3	Use discharge coeff.	☐	0.93
66	3347.01	0.30	2312.80	-	-	-	-	-
67	3347.31	11.70	2312.80	3.0	3	Use discharge coeff.	☐	0.93
68	3359.01	0.30	2312.77	-	-	-	-	-
69	3359.31	11.70	2312.77	3.0	3	Use discharge coeff.	☐	0.93
70	3371.01	0.30	2312.74	-	-	-	-	-
71	3371.31	11.70	2312.74	3.0	3	Use discharge coeff.	☐	0.93
72	3383.01	0.30	2312.69	-	-	-	-	-
73	3383.31	11.70	2312.69	3.0	3	Use discharge coeff.	☐	0.93
74	3395.01	0.30	2312.63	-	-	-	-	-
75	3395.31	11.70	2312.63	3.0	3	Use discharge coeff.	☐	0.93
76	3407.01	0.30	2312.59	-	-	-	-	-
77	3407.31	11.70	2312.59	3.0	3	Use discharge coeff.	☐	0.93
78	3419.01	0.30	2312.60	-	-	-	-	-
79	3419.31	11.70	2312.60	3.0	3	Use discharge coeff.	☐	0.93
80	3431.01	0.30	2312.65	-	-	-	-	-
81	3431.31	11.70	2312.66	3.0	3	Use discharge coeff.	☐	0.93
82	3443.01	0.30	2312.74	-	-	-	-	-
83	3443.31	11.70	2312.74	3.0	3	Use discharge coeff.	☐	0.93
84	3455.01	0.30	2312.86	-	-	-	-	-
85	3455.31	11.70	2312.87	3.0	3	Use discharge coeff.	☐	0.93

Figure C-14: *B1-AHT3 Simulation Case 11 ICD Settings. For cases 12 and 13, the only thing that is changed is the Nozzle Diameter, in accordance with Table 9 The input from 3143mMD to 3275mMD is representative for the remaining completion, to ~4410mMD.*

D Results from ICD Case Simulations

D.1 Well B3 ICD Case Results

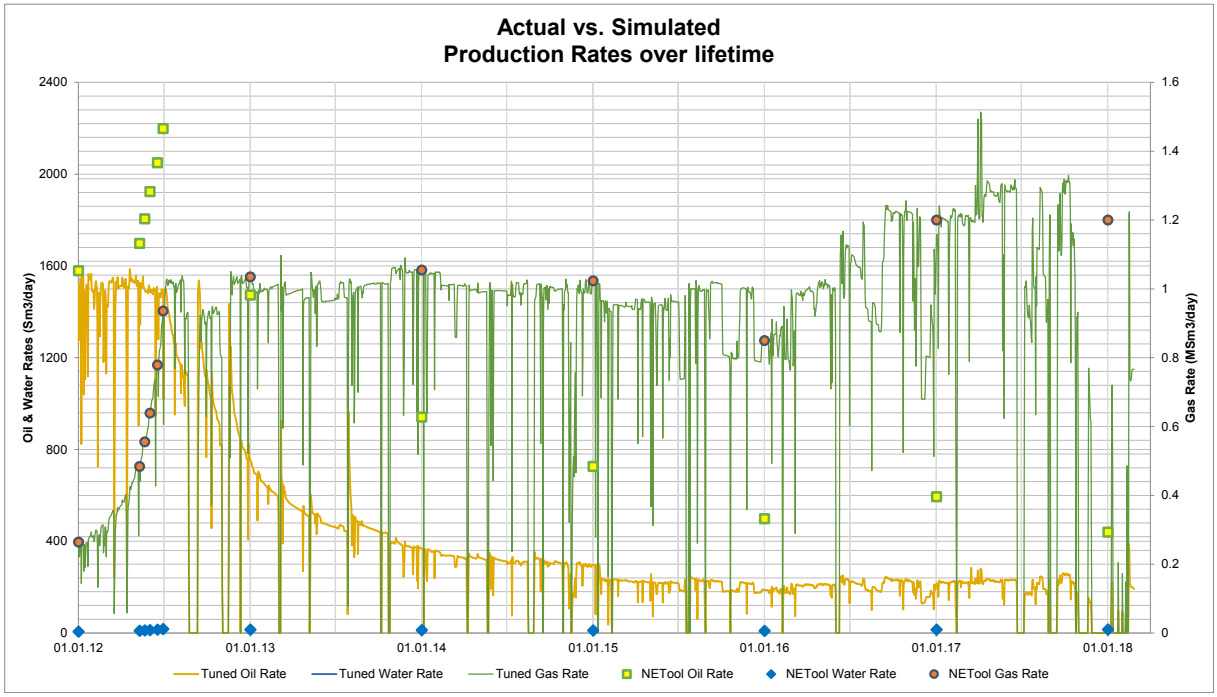

Figure D-1: *B3-HT2 Case 8: Actual vs. Simulated Production*

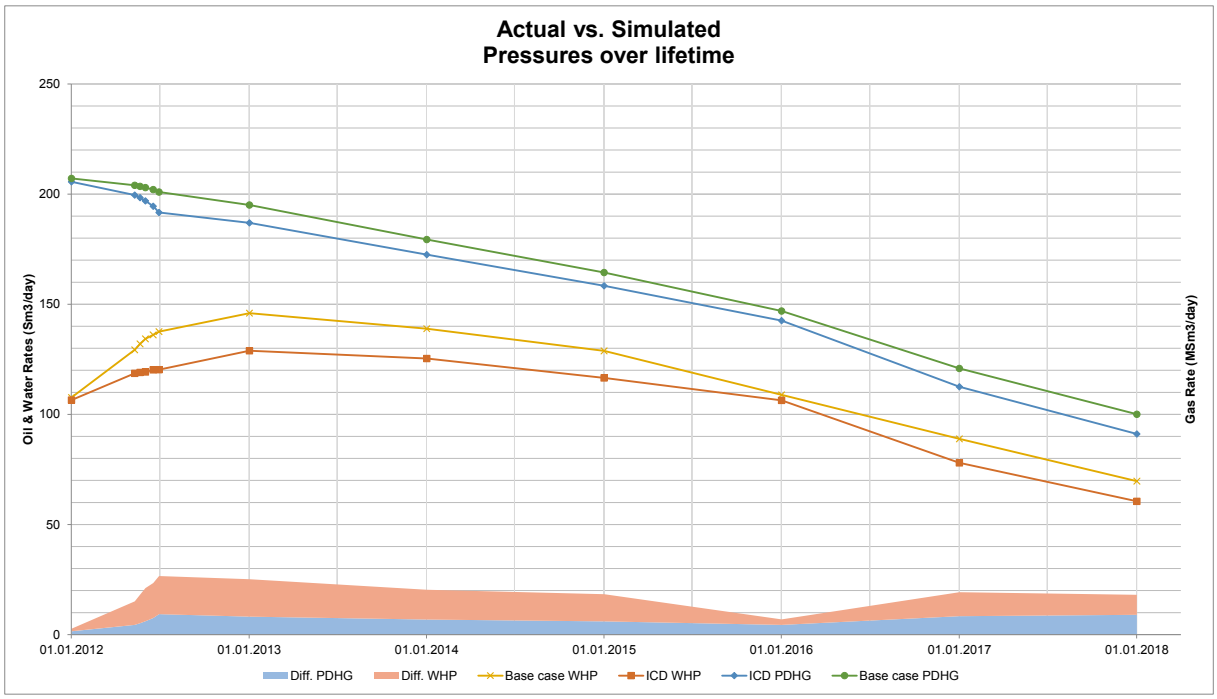

Figure D-2: *B3-HT2 Case 8: Simulated vs. Reference case pressures*

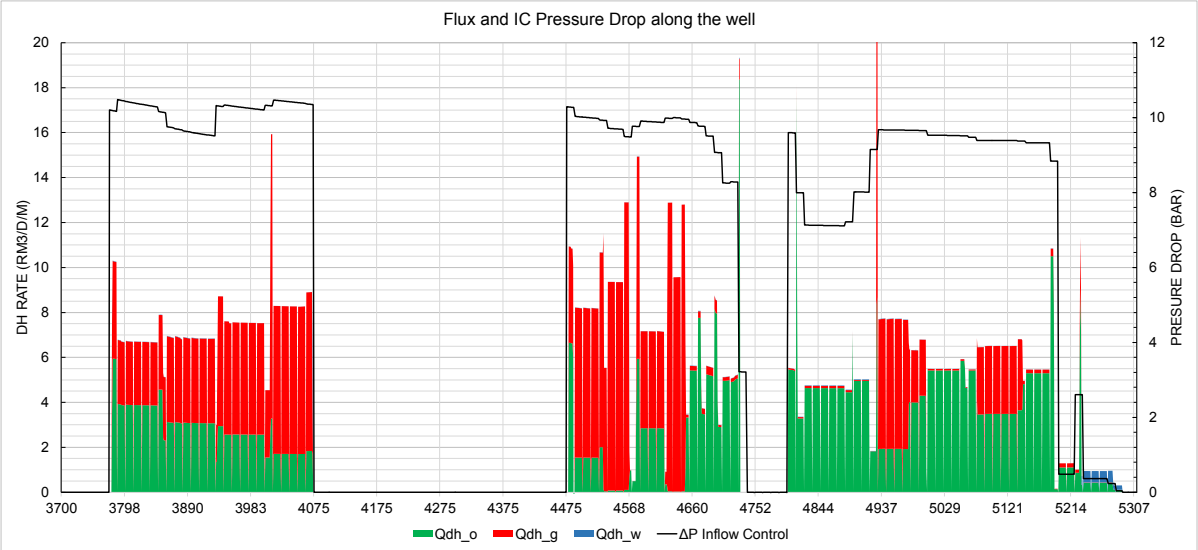

Figure D-3: *B3-HT2 Case 8: Flux and IC pressure drop along the well at early-life*

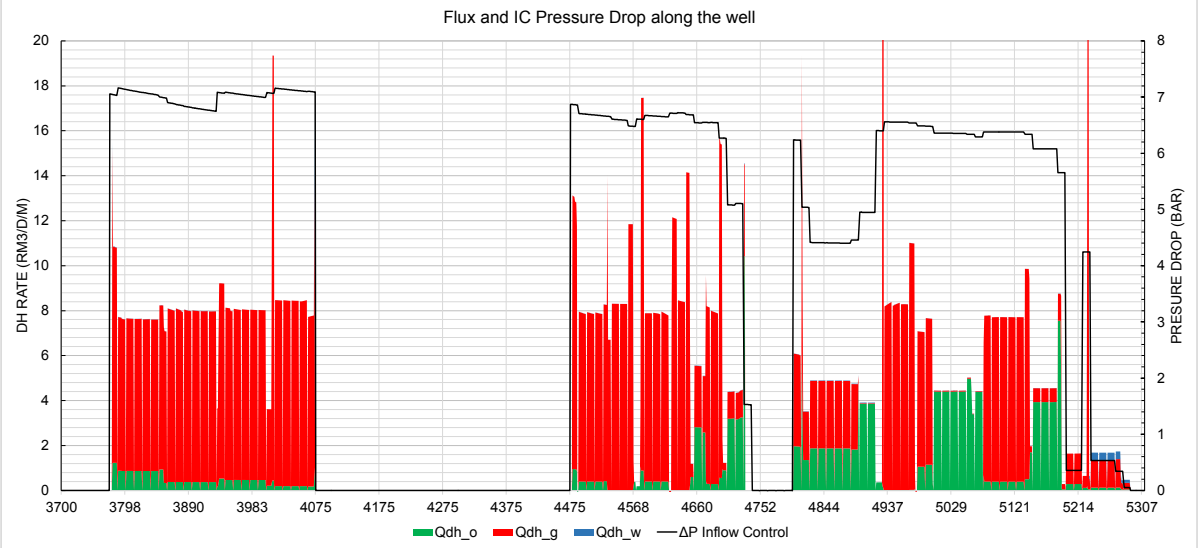

Figure D-4: *B3-HT2 Case 8: Flux and IC pressure drop along the well at mid-life*

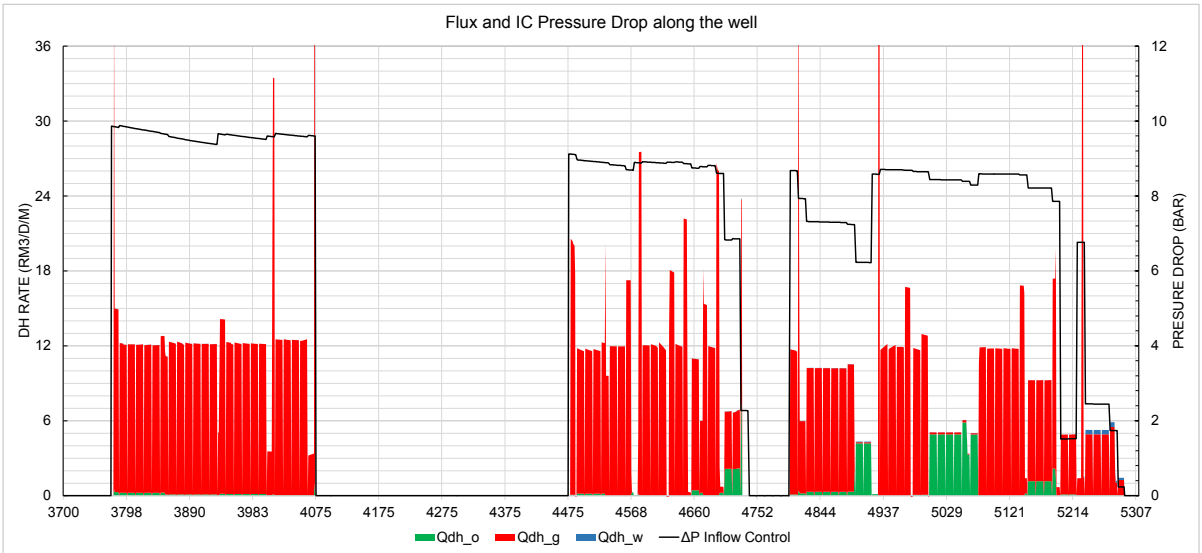

Figure D-5: *B3-HT2 Case 8: Flux and IC pressure drop along the well at late-life*

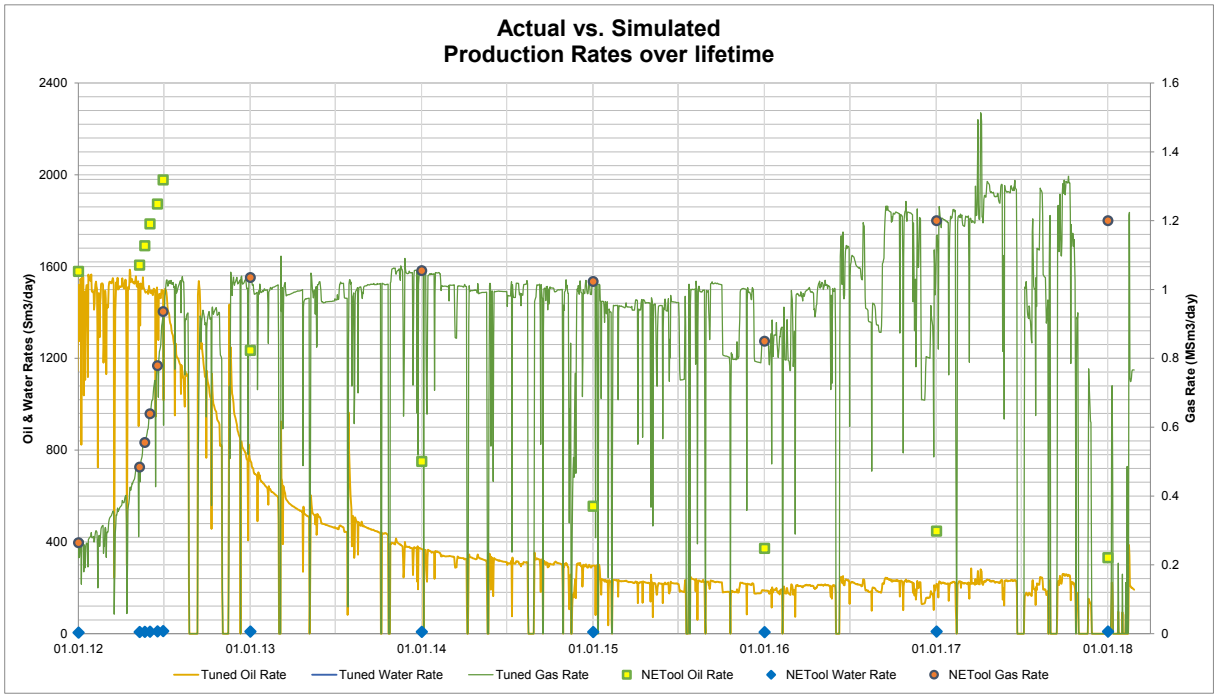

Figure D-6: *B3-HT2 Case 9: Actual vs. Simulated Production*

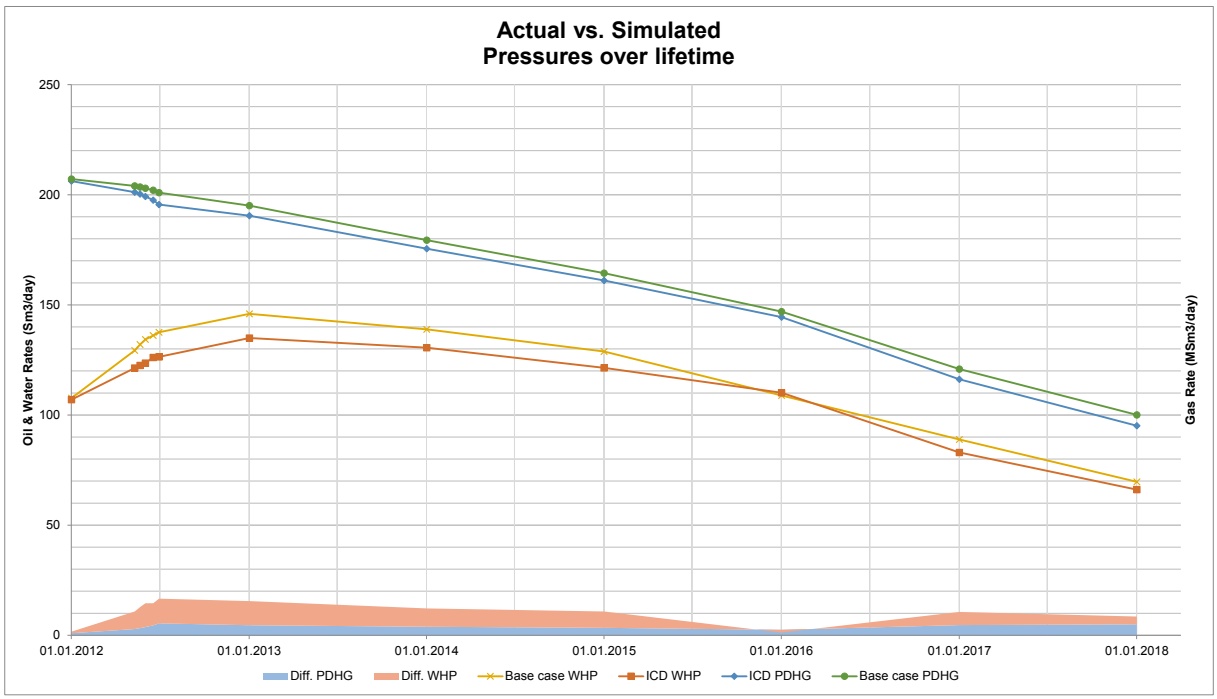

Figure D-7: *B3-HT2 Case 9: Simulated vs. Reference case pressures*

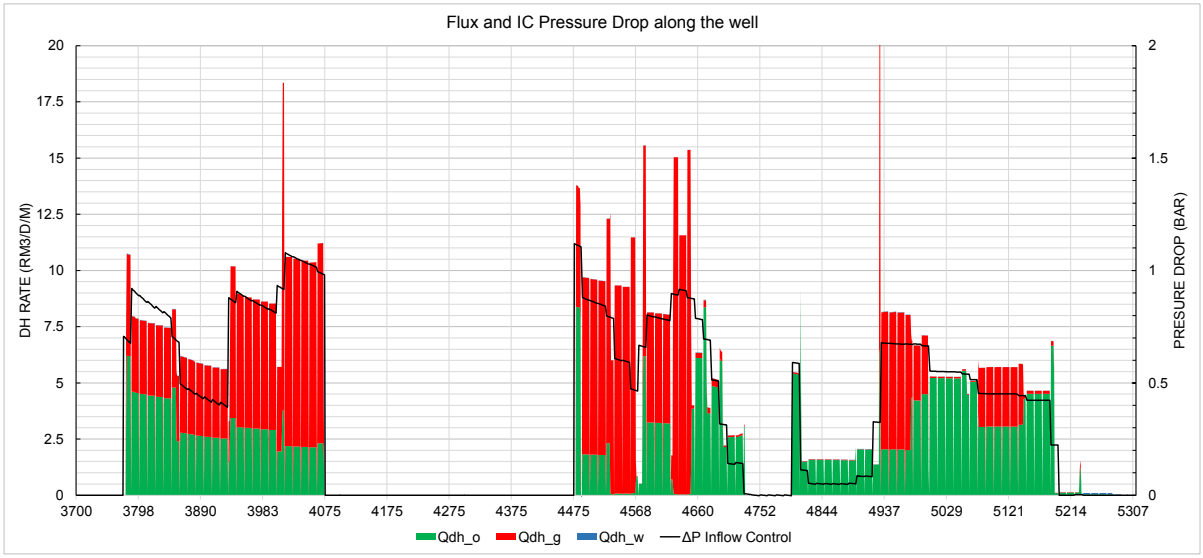

Figure D-8: *B3-HT2 Case 9: Flux and IC pressure drop along the well at early-life*

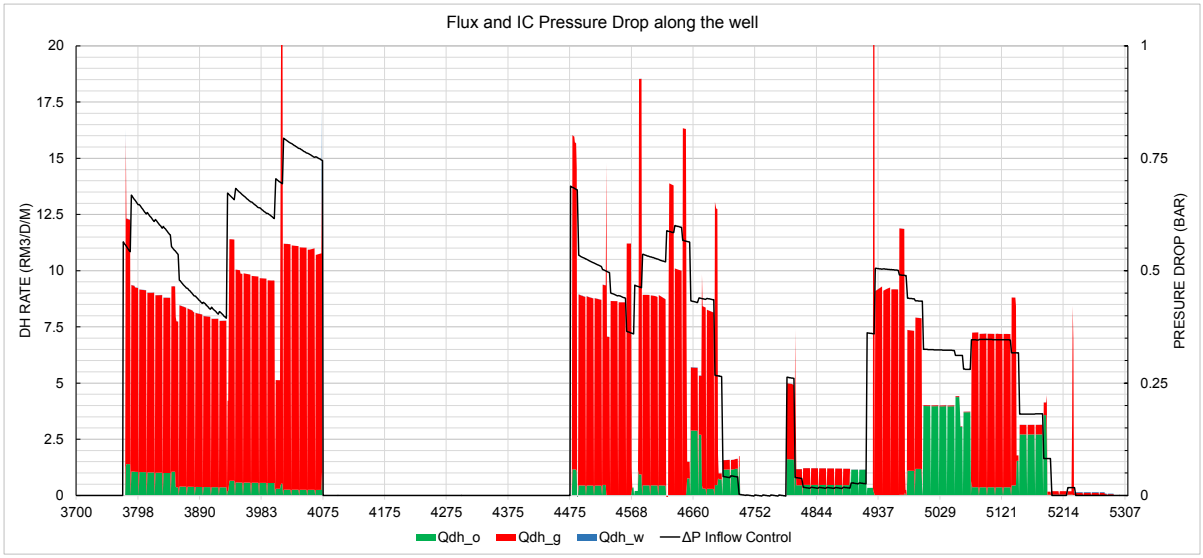

Figure D-9: *B3-HT2 Case 9: Flux and IC pressure drop along the well at mid-life*

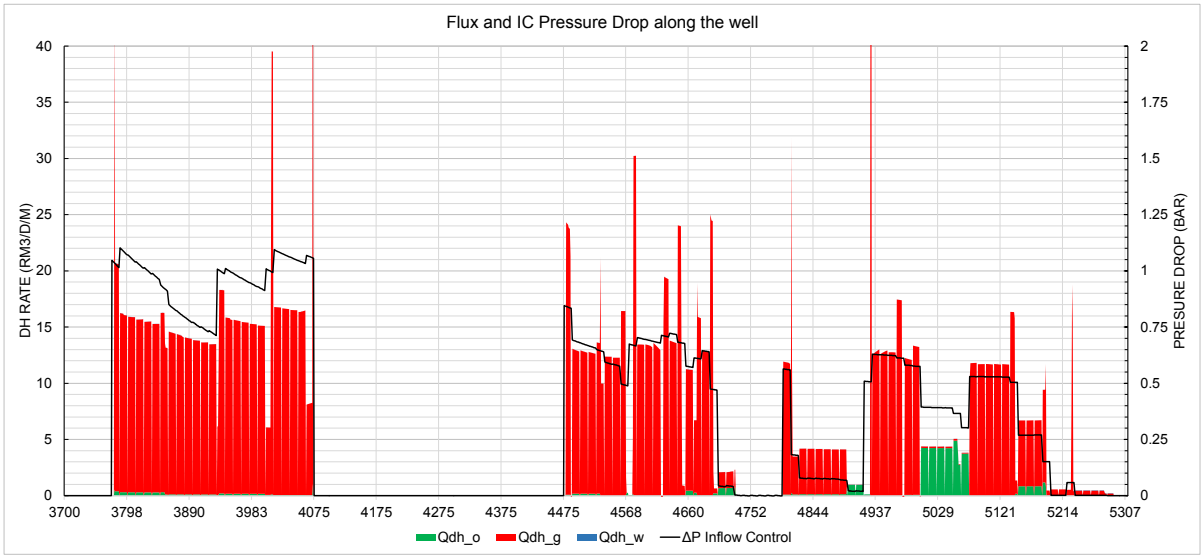

Figure D-10: *B3-HT2 Case 9: Flux and IC pressure drop along the well at late-life*

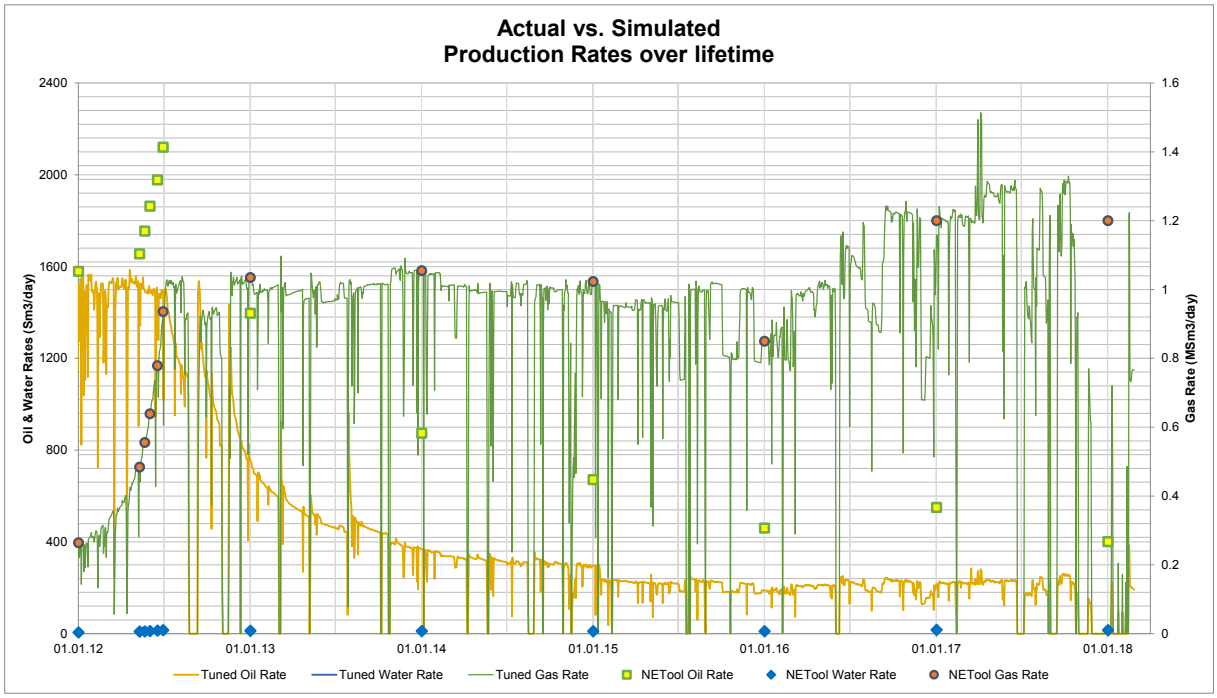

Figure D-11: *B3-HT2 Case 10: Actual vs. Simulated Production*

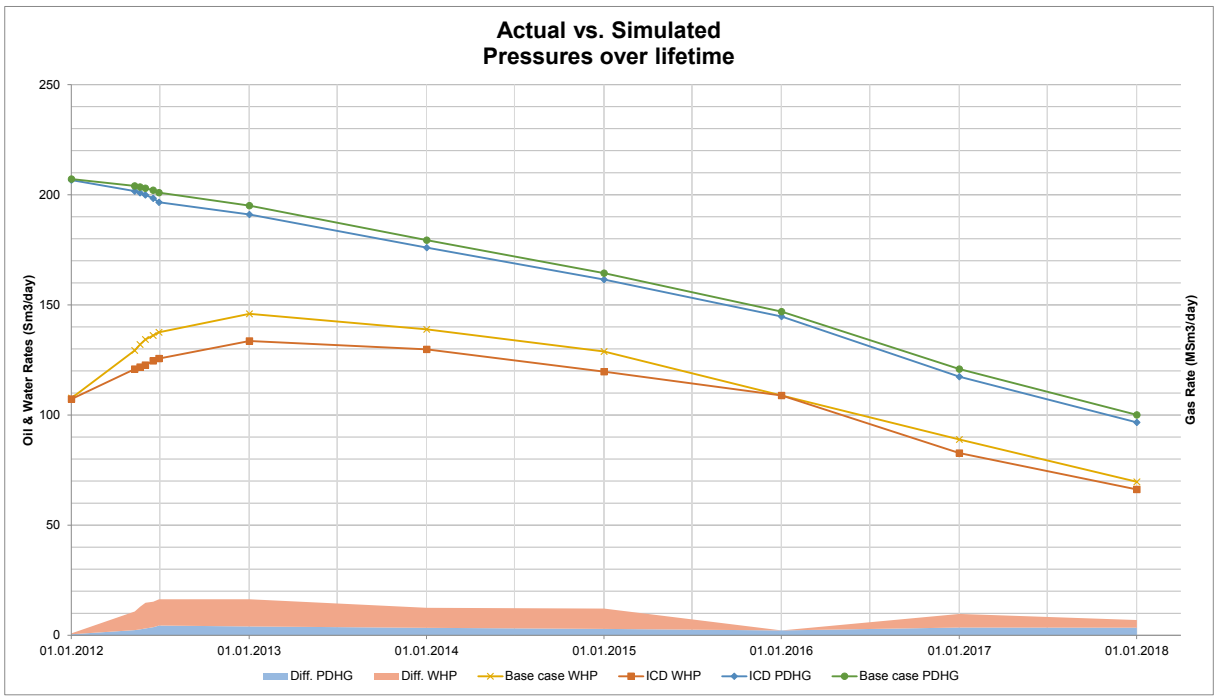

Figure D-12: *B3-HT2 Case 10: Simulated vs. Reference case pressures*

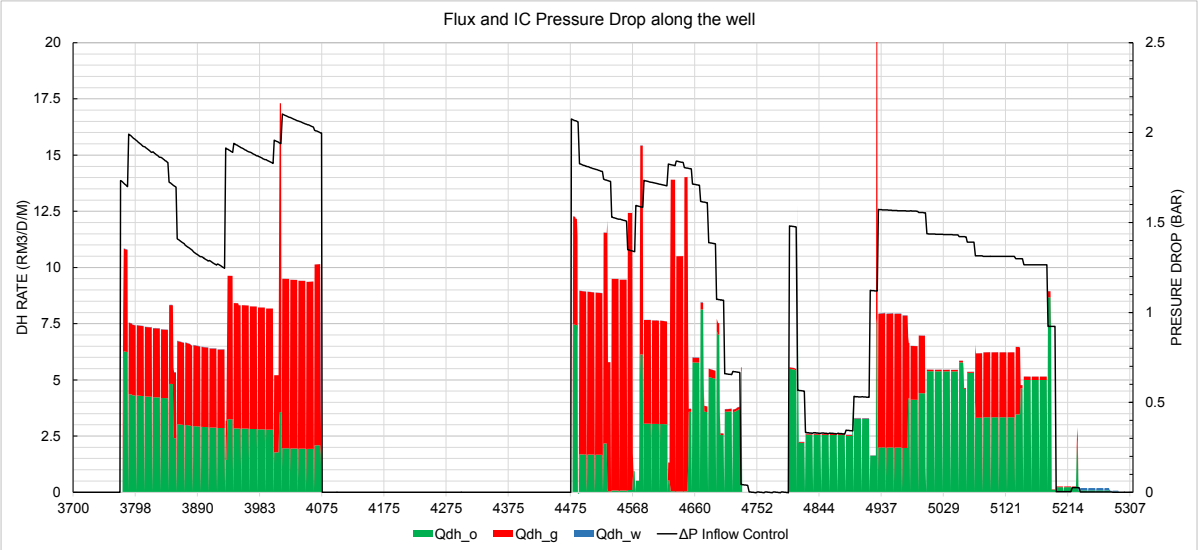

Figure D-13: *B3-HT2 Case 10: Flux and IC pressure drop along the well at early-life*

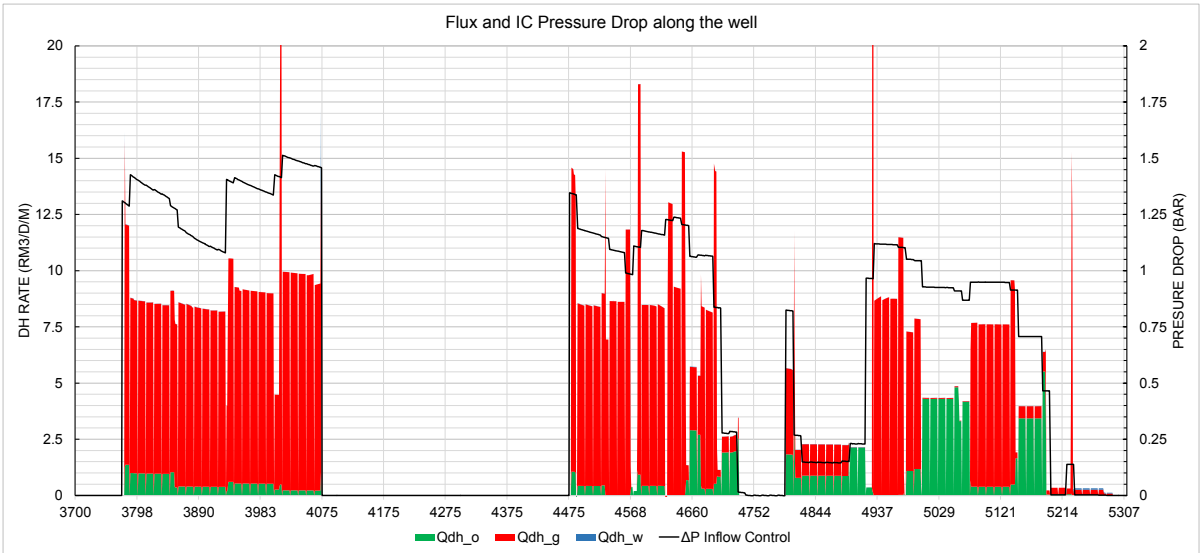

Figure D-14: *B3-HT2 Case 10: Flux and IC pressure drop along the well at mid-life*

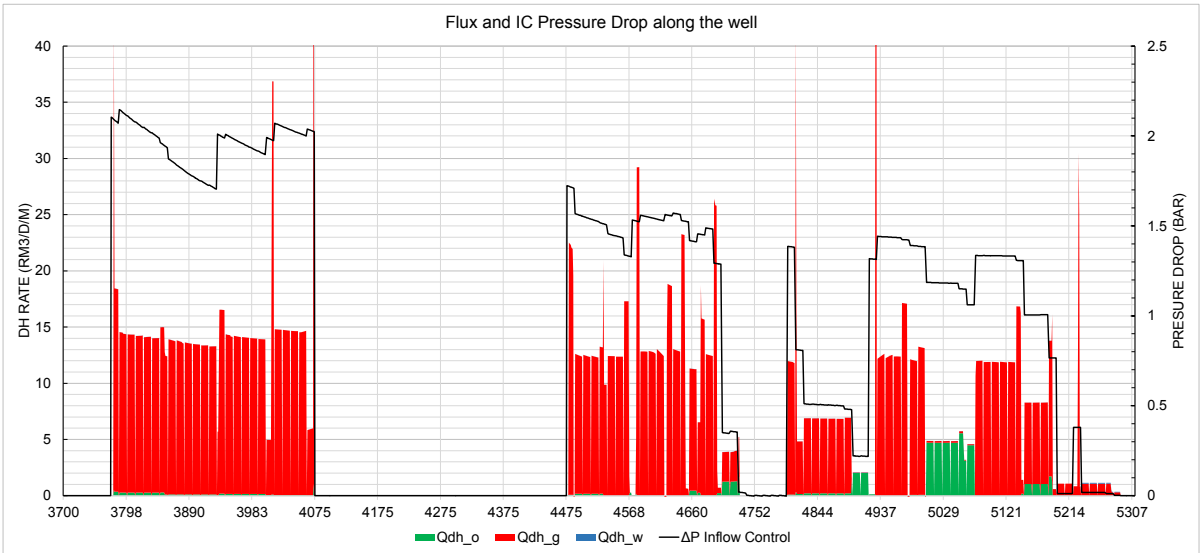

Figure D-15: *B3-HT2 Case 10: Flux and IC pressure drop along the well at late-life*

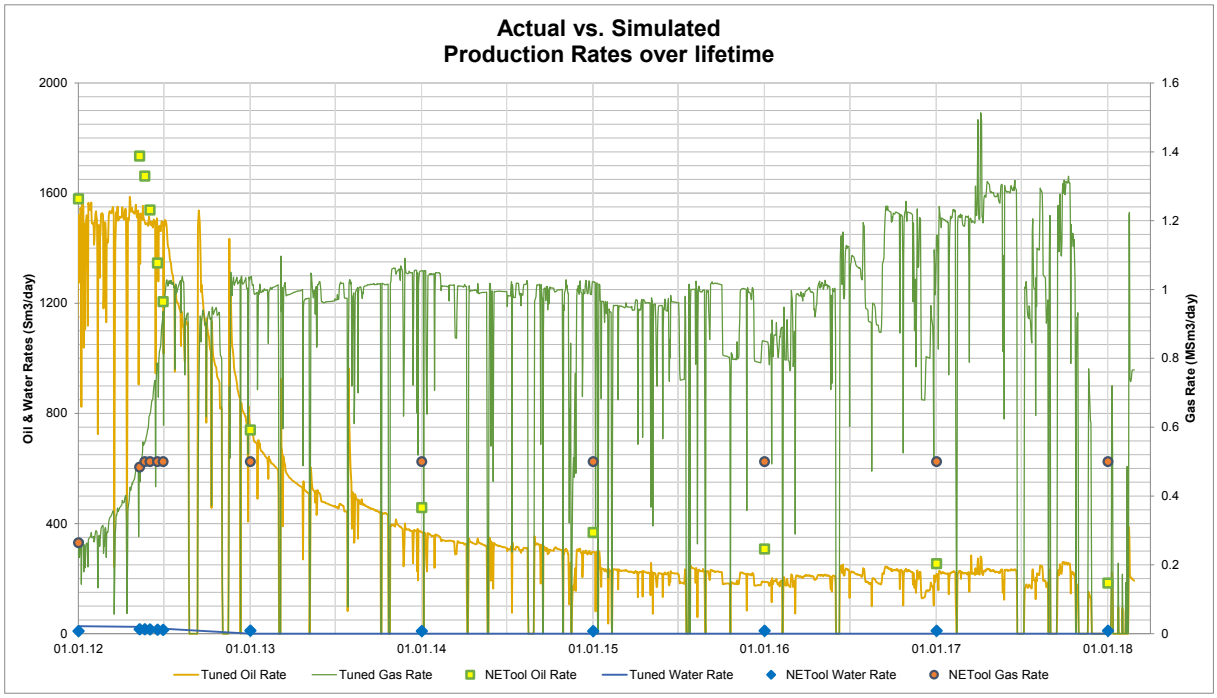

Figure D-16: *B3-HT2 Case 15: Actual vs. Simulated Production*

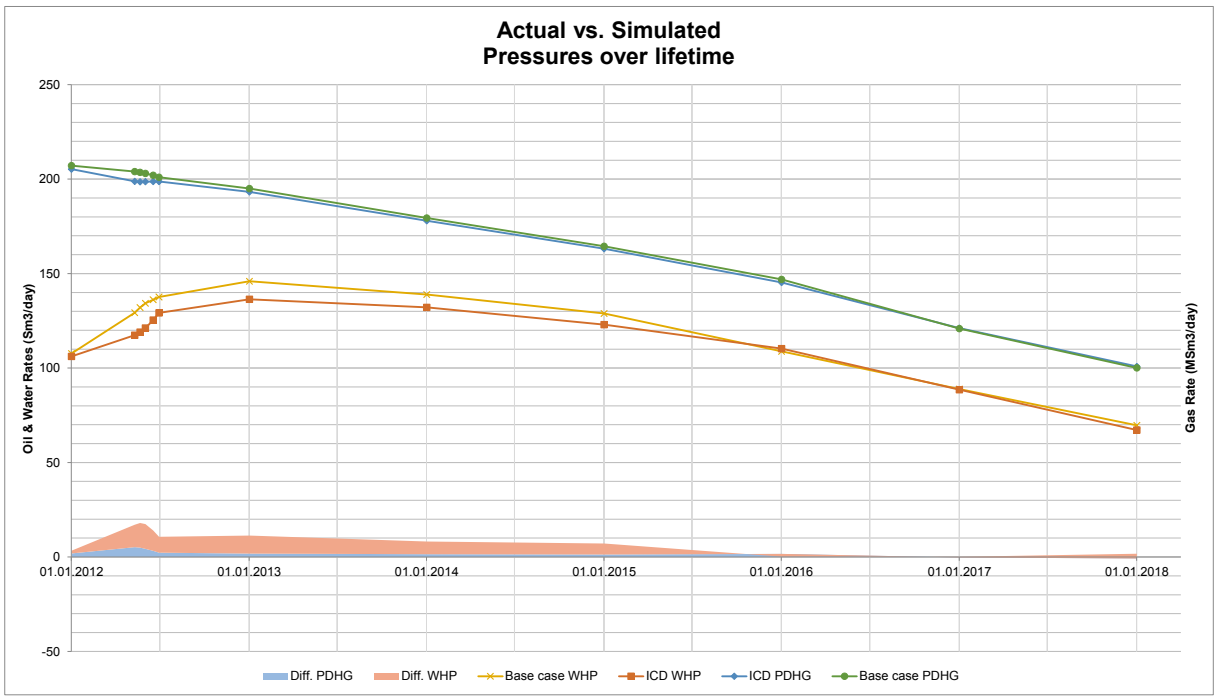

Figure D-17: *B3-HT2 Case 15: Simulated vs. Reference case pressures*

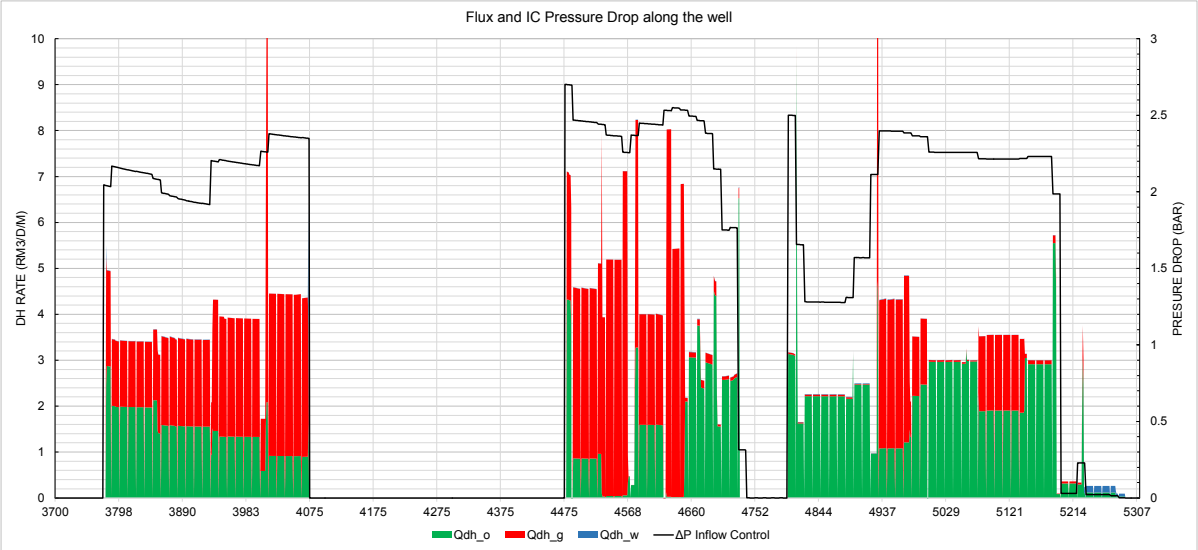

Figure D-18: *B3-HT2 Case 15: Flux and IC pressure drop along the well at early-life*

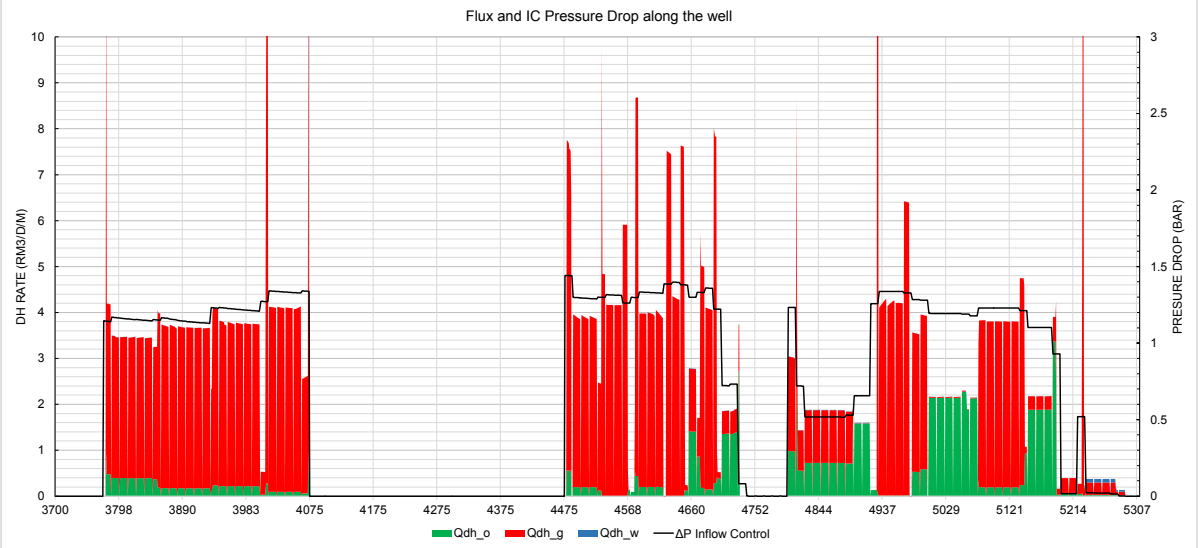

Figure D-19: *B3-HT2 Case 15: Flux and IC pressure drop along the well at mid-life*

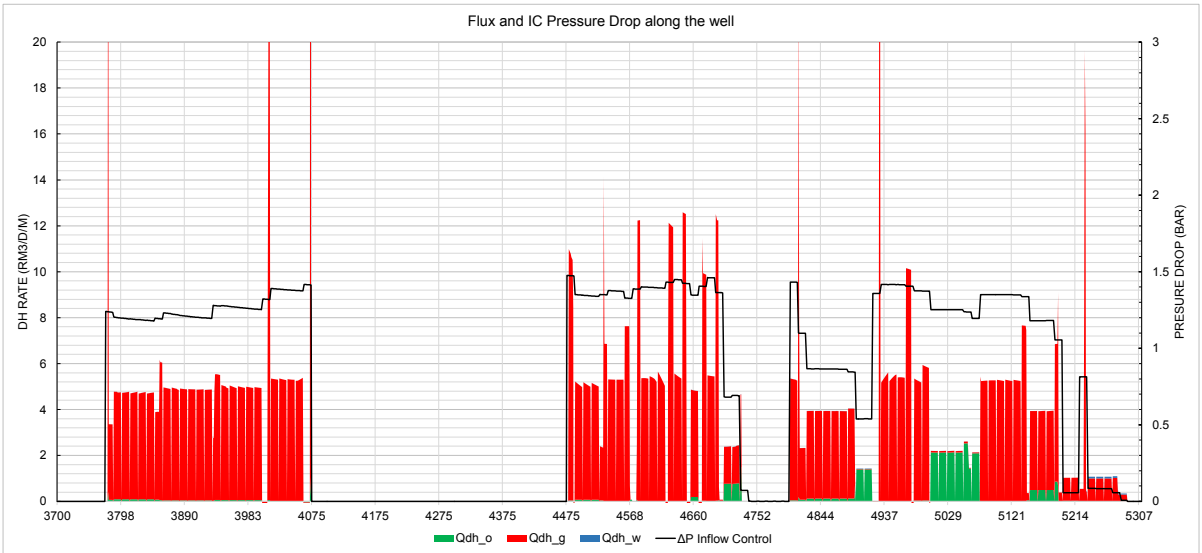

Figure D-20: *B3-HT2 Case 15: Flux and IC pressure drop along the well at late-life*

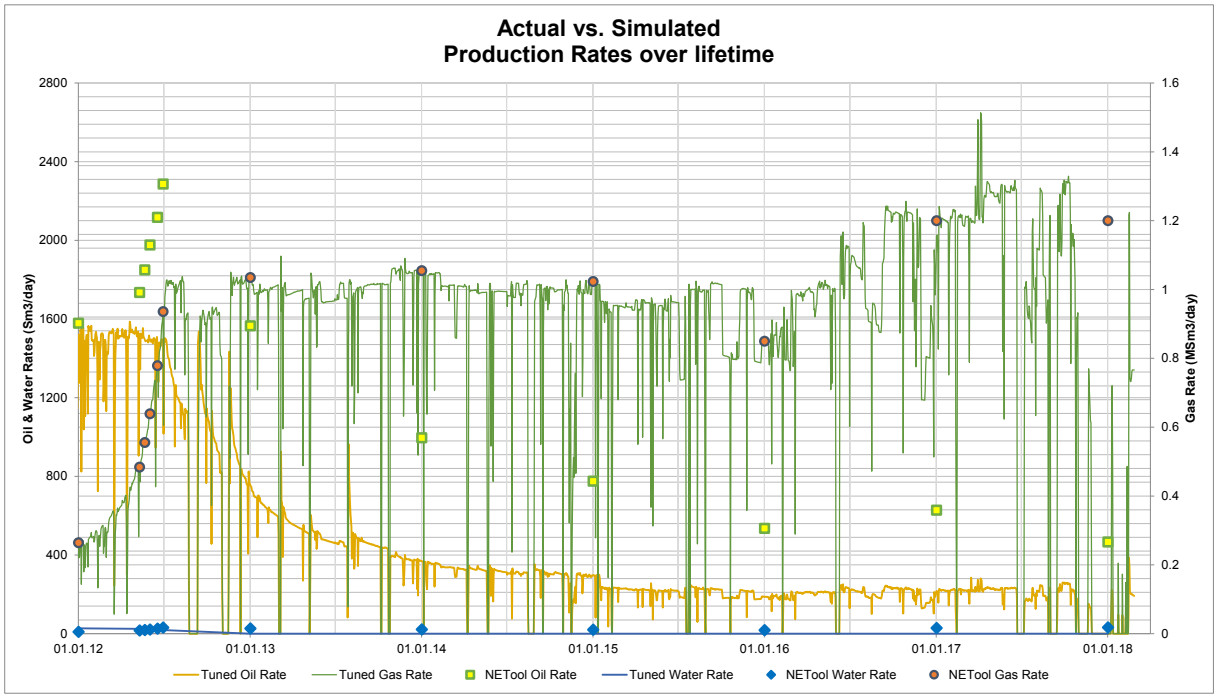

Figure D-21: *B3-HT2 Case 16: Actual vs. Simulated Production*

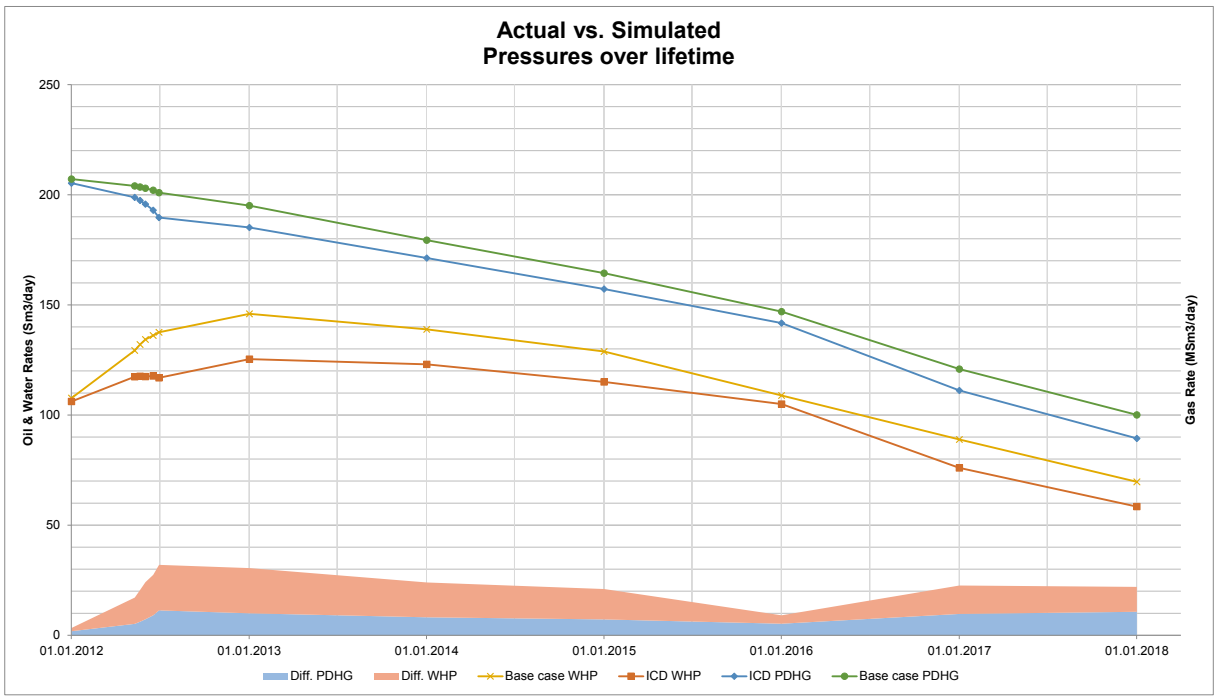

Figure D-22: *B3-HT2 Case 16: Actual vs. Simulated Pressures.*

D.2 Well B1 ICD Case Results

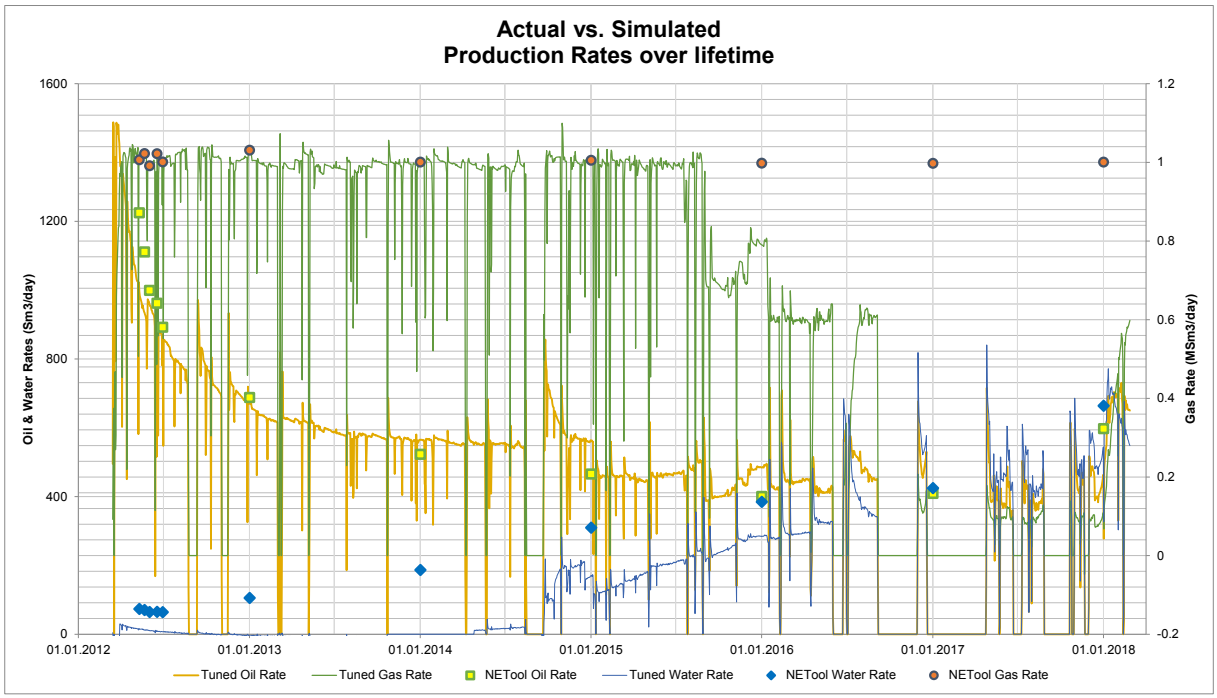

Figure D-23: *B1-AHT3 Case 11: Actual vs. Simulated Production*

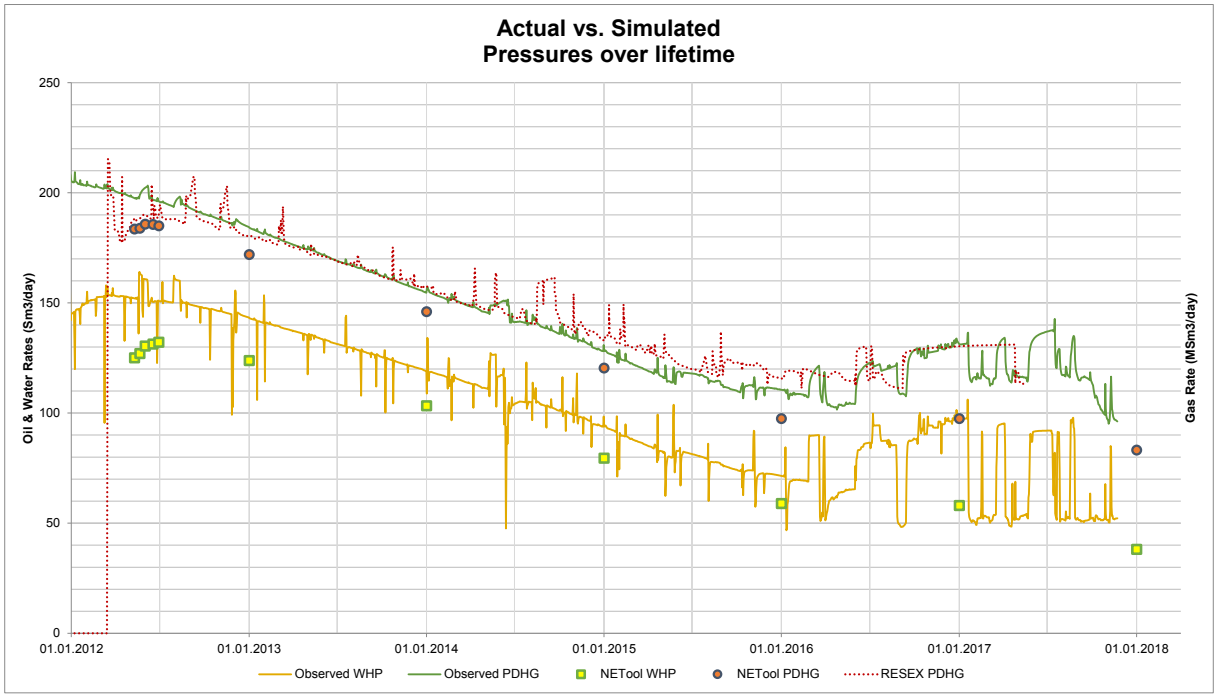

Figure D-24: *B1-AHT3 Case 11: Actual vs. Simulated Pressures*

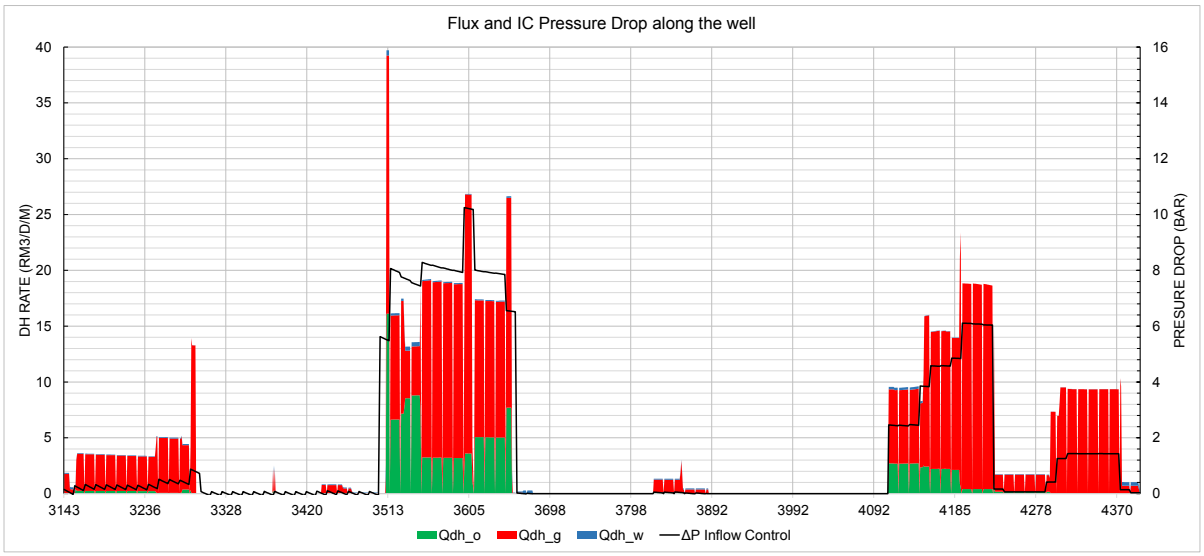

Figure D-25: *B1-AHT3 Case 11: Flux and IC pressure drop along the well at early-life*

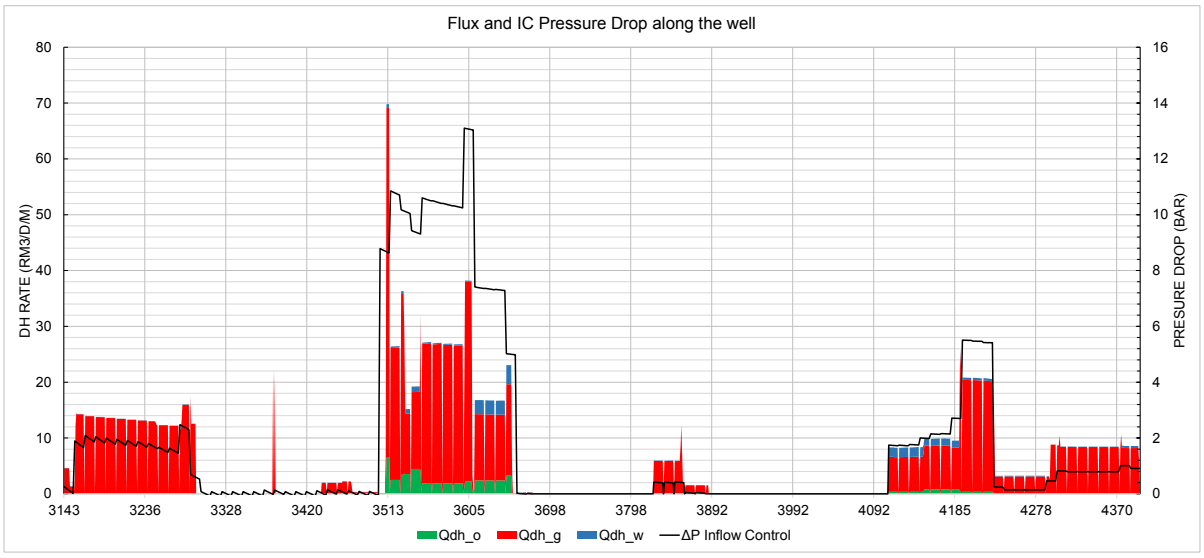

Figure D-26: *B1-AHT3 Case 11: Flux and IC pressure drop along the well at mid-life*

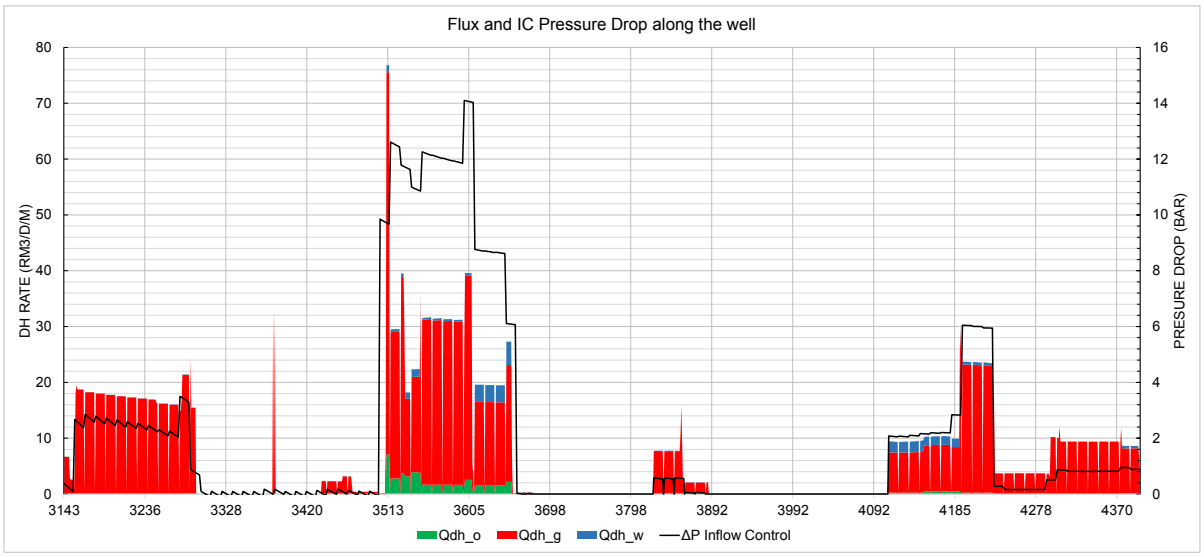

Figure D-27: *B1-AHT3 Case 11: Flux and IC pressure drop along the well at late-life*

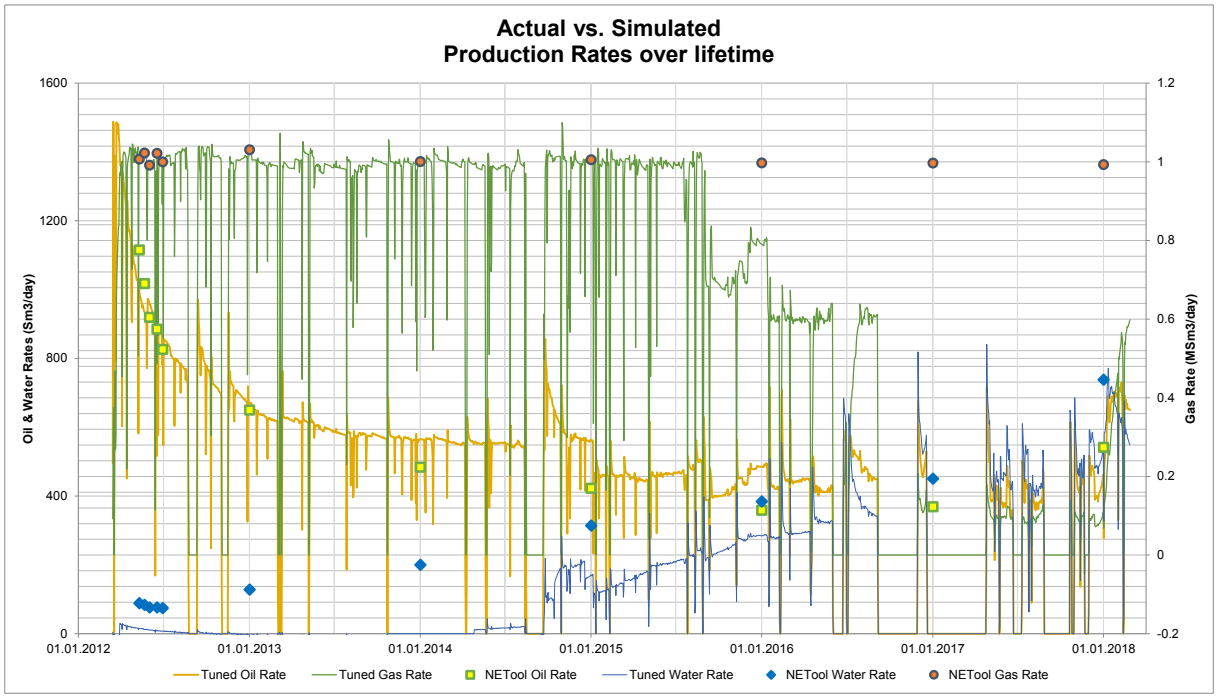

Figure D-28: *B1-AHT3 Case 12: Actual vs. Simulated Production*

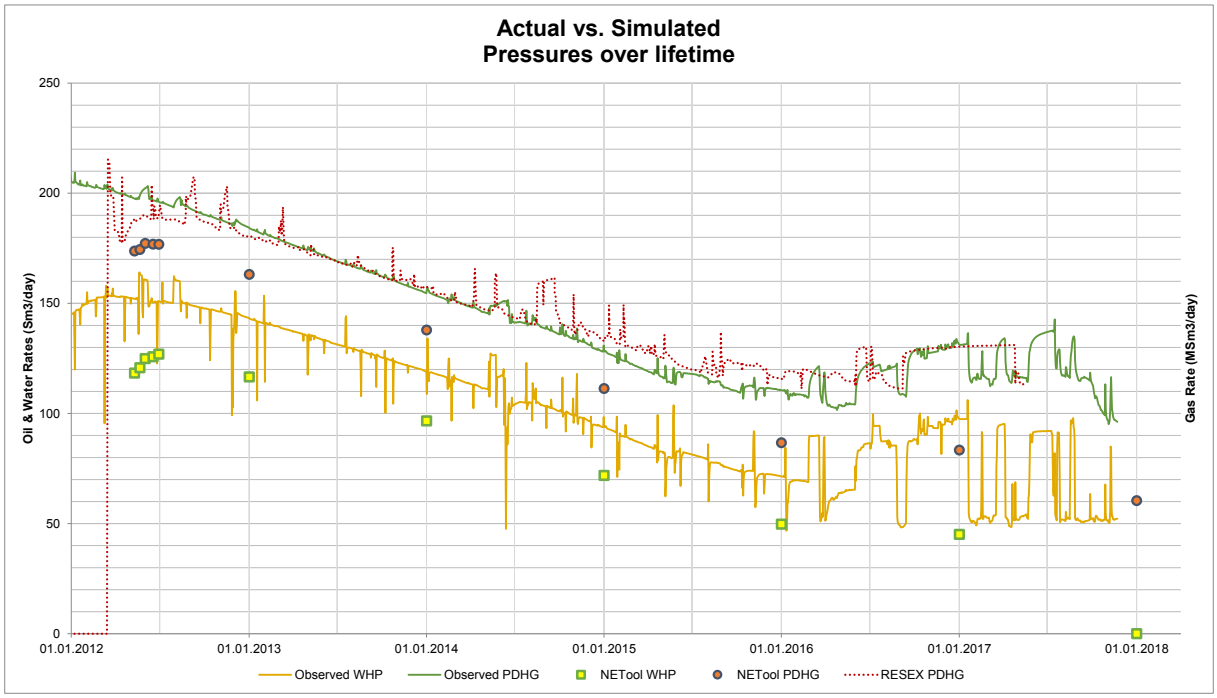

Figure D-29: *B1-AHT3 Case 12: Actual vs. Simulated Pressures*

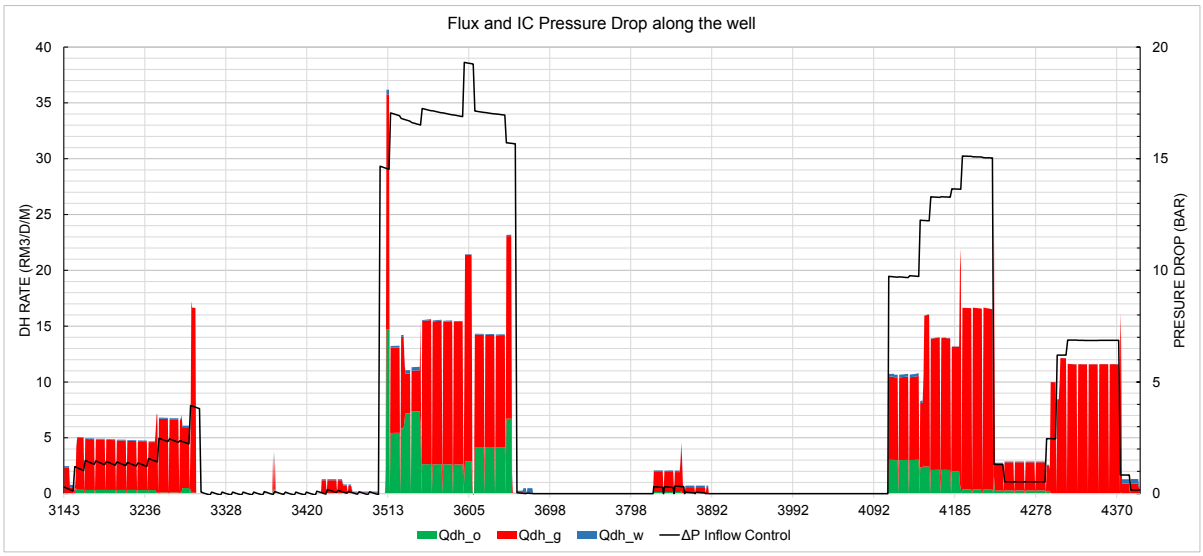

Figure D-30: *B1-AHT3 Case 12: Flux and IC pressure drop along the well at early-life*

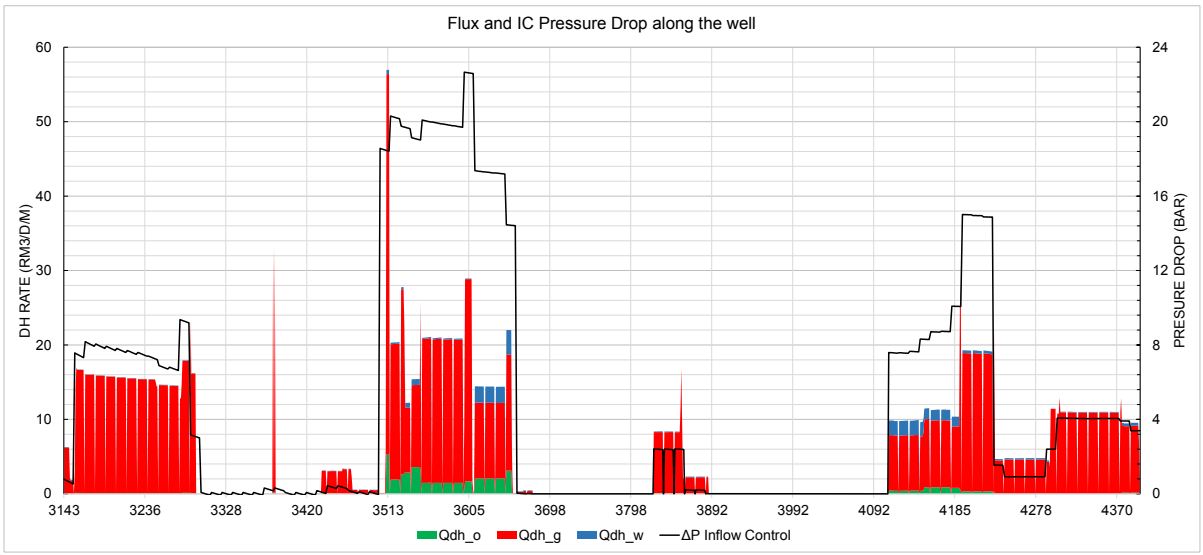

Figure D-31: *B1-AHT3 Case 12: Flux and IC pressure drop along the well at mid-life*

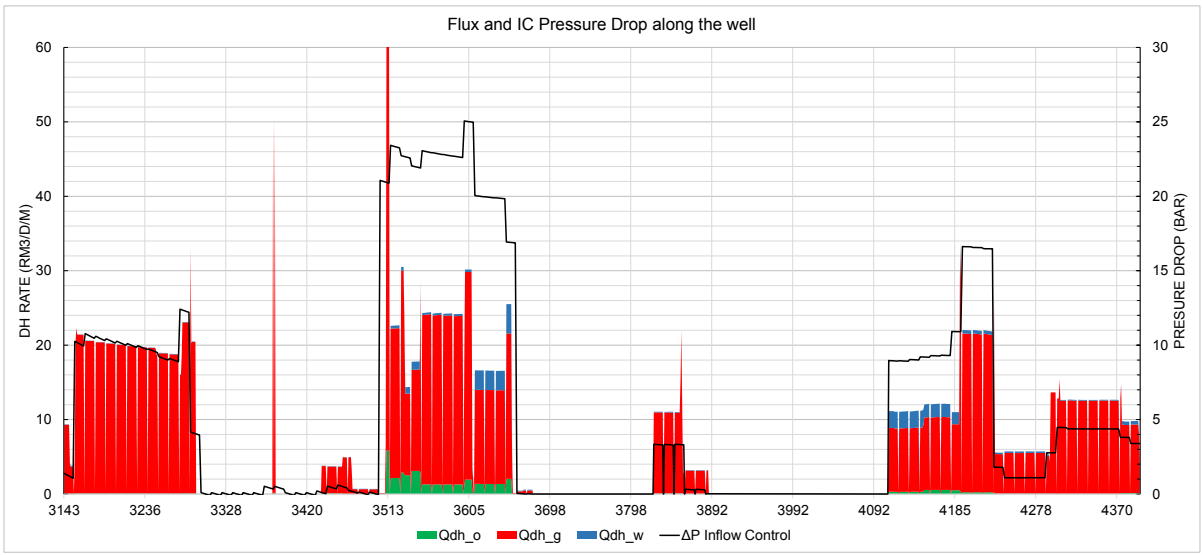

Figure D-32: *B1-AHT3 Case 12: Flux and IC pressure drop along the well at late-life*

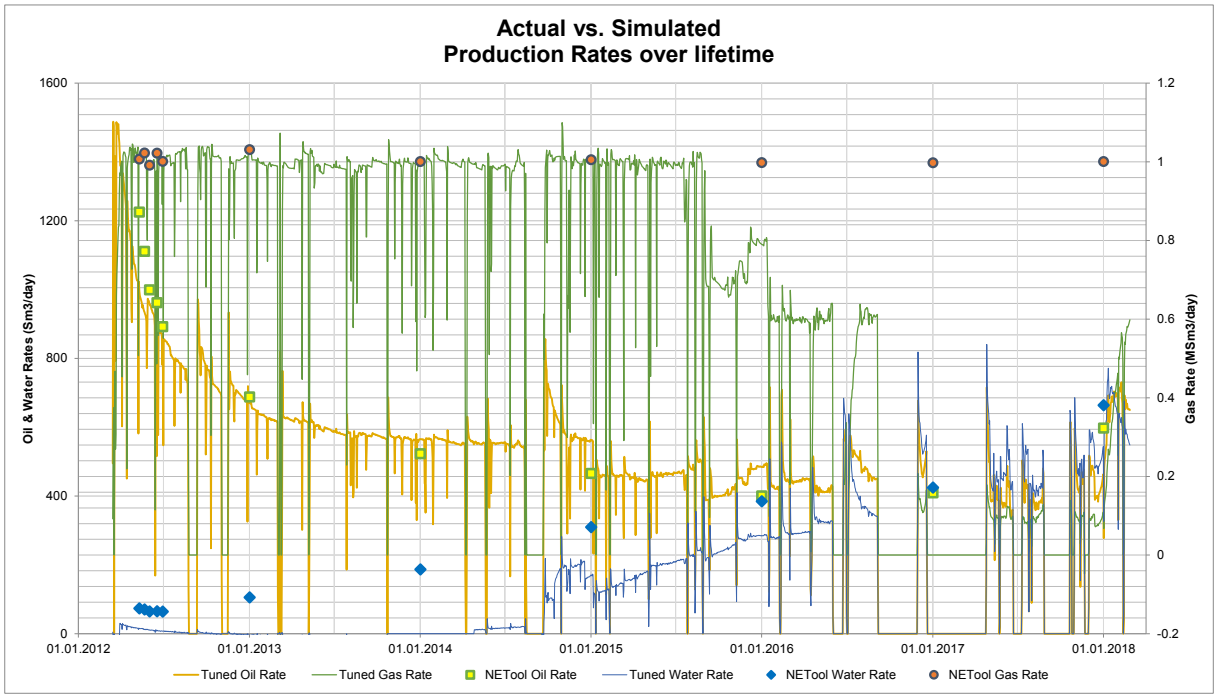

Figure D-33: *B1-AHT3 Case 13: Actual vs. Simulated Production*

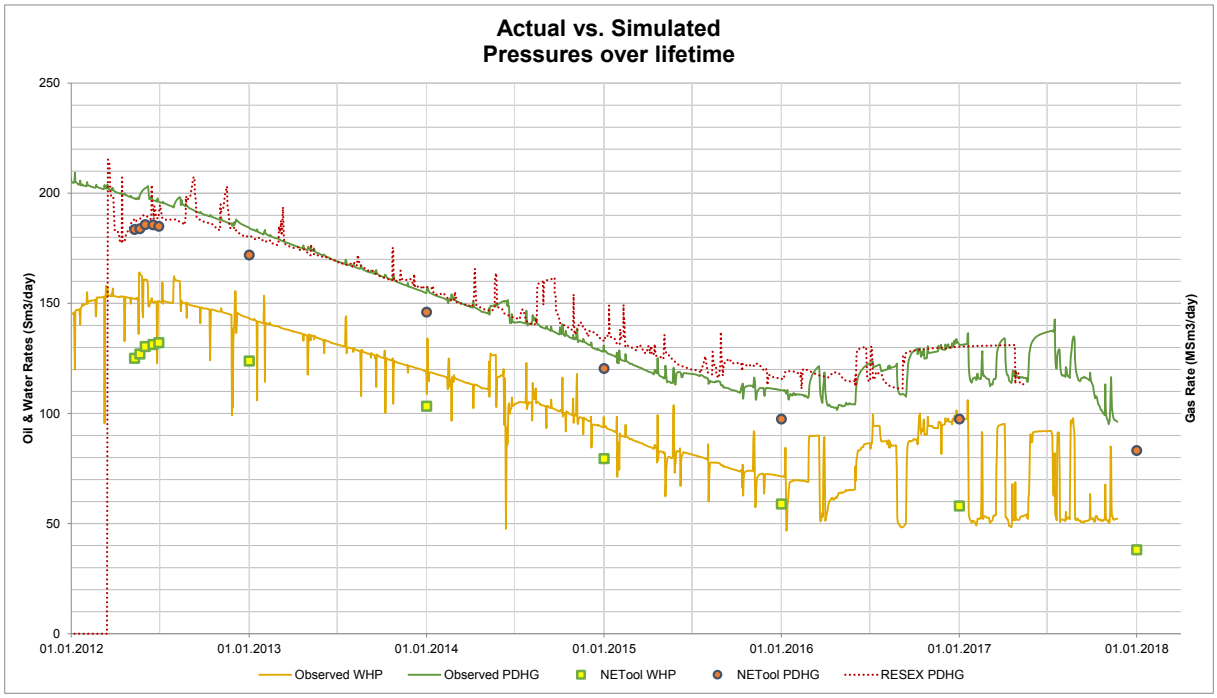

Figure D-34: *B1-AHT3 Case 13: Actual vs. Simulated Pressures*

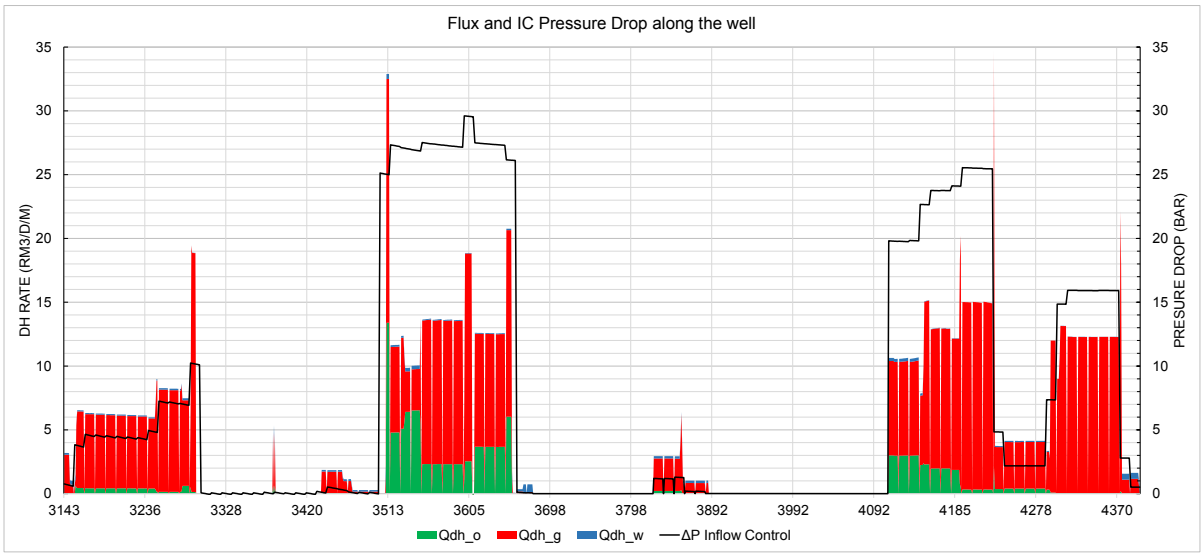

Figure D-35: *B1-AHT3 Case 13: Flux and IC pressure drop along the well at early-life*

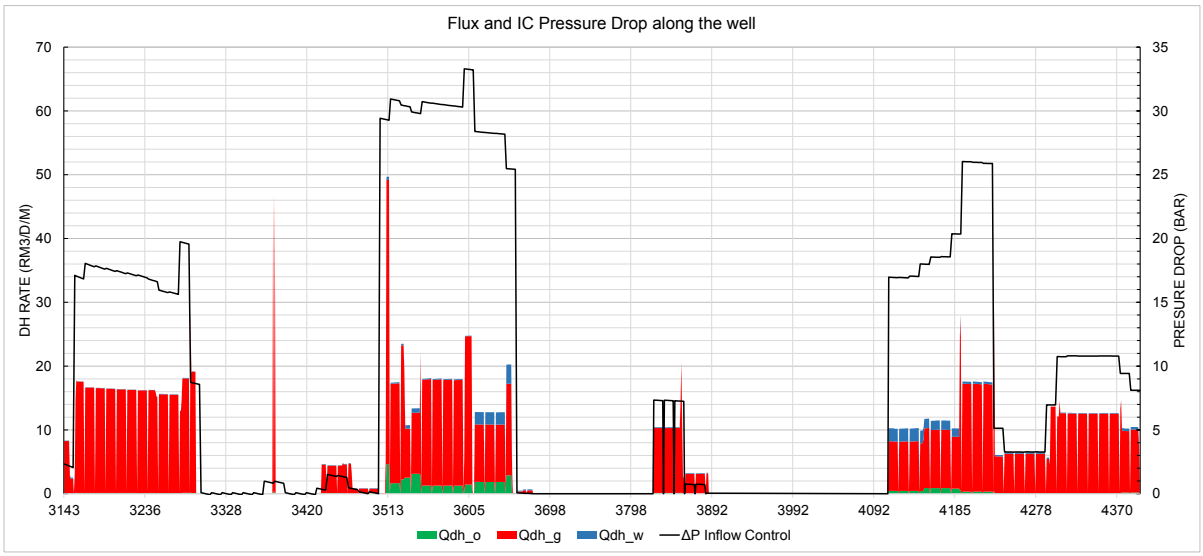

Figure D-36: *B1-AHT3 Case 13: Flux and IC pressure drop along the well at mid-life*

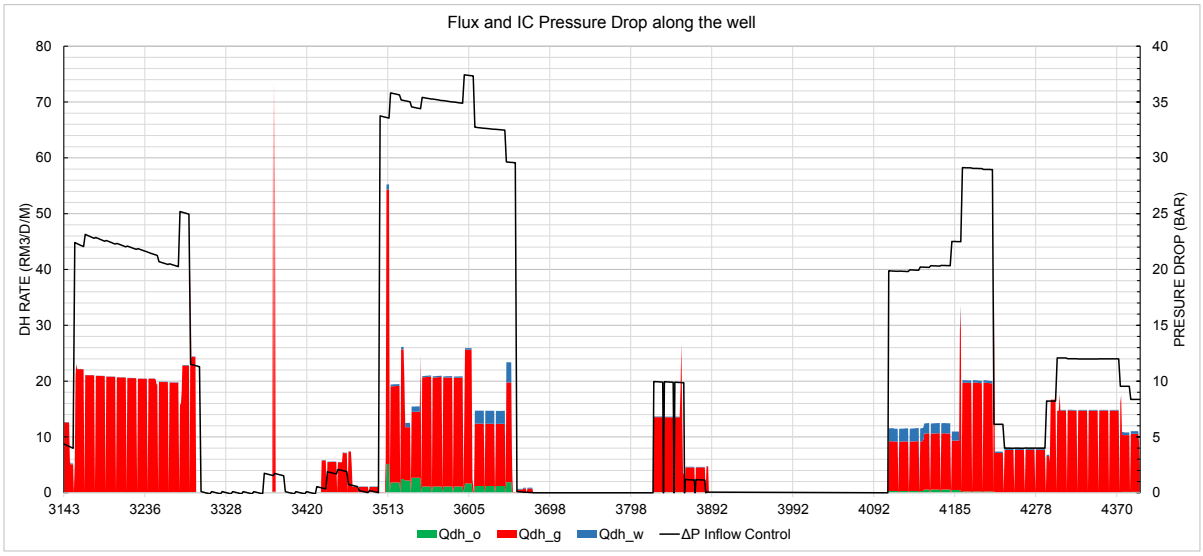

Figure D-37: *B1-AHT3 Case 13: Flux and IC pressure drop along the well at late-life*

E Input Data for the AICV Cases

When modeling AICVs within NETool, the input is quite similar to that of the ICD cases. For well B3, this includes the input data presented in Figure C-1 to C-4, as well as Figure C-5. Similarly, for well B1 the input data presented in Figure C-8 to C-11, as well as Figure C-12 will be the same for the AICV cases. The input that differs for the AICV cases will be presented in the following appendix.

E.1 Well B3 NETool AICV Well Design

Inflow Control Device

#	Top MD [m]	Seg. Length [m]	Top TVD(SS) [m]	ICD Design	Joint Length [m]
1	2613.00	5.55	2040.07	-	-
2	2618.55	3.36	2043.31	-	-
3	2621.91	0.76	2045.26	-	-
4	2622.67	2.06	2045.71	-	-
5	2624.73	0.74	2046.91	-	-
6	2625.47	2.06	2047.34	-	-
7	2627.53	23.95	2048.54	-	-
8	2651.48	3.05	2062.24	-	-
9	2654.53	0.76	2063.97	-	-
10	2655.29	1.97	2064.40	-	-
11	2657.26	22.40	2065.51	-	-
12	2679.66	4.08	2077.97	-	-
13	2683.74	1.28	2080.16	-	-
14	2685.02	3.59	2080.85	-	-
15	2688.61	1.94	2082.75	-	-
16	2690.55	696.44	2083.77	-	-
17	3386.99	2.55	2309.48	-	-
18	3389.54	2.20	2309.73	-	-
19	3391.74	8.01	2309.94	-	-
20	3399.75	0.75	2310.68	-	-
21	3400.50	1.56	2310.75	-	-
22	3402.06	38.44	2310.88	-	-
23	3440.50	335.10	2313.48	-	-
24	3775.60	11.70	2313.67	Autonomous ICD (RCP Valve)	11.7
25	3787.30	0.30	2313.67	-	-
26	3787.60	11.70	2313.67	Autonomous ICD (RCP Valve)	11.7
27	3799.30	0.30	2313.70	-	-
28	3799.60	11.70	2313.70	Autonomous ICD (RCP Valve)	11.7
29	3811.30	0.30	2313.75	-	-
30	3811.60	11.70	2313.75	Autonomous ICD (RCP Valve)	11.7
31	3823.30	0.30	2313.80	-	-
32	3823.60	11.70	2313.80	Autonomous ICD (RCP Valve)	11.7
33	3835.30	0.30	2313.85	-	-
34	3835.60	11.70	2313.85	Autonomous ICD (RCP Valve)	11.7
35	3847.30	0.30	2313.89	-	-
36	3847.60	11.70	2313.89	Autonomous ICD (RCP Valve)	11.7
37	3859.30	0.30	2313.90	-	-
38	3859.60	11.70	2313.90	Autonomous ICD (RCP Valve)	11.7
39	3871.30	0.30	2313.90	-	-
40	3871.60	11.70	2313.90	Autonomous ICD (RCP Valve)	11.7
41	3883.30	0.30	2313.90	-	-
42	3883.60	11.70	2313.90	Autonomous ICD (RCP Valve)	11.7
43	3895.30	0.30	2313.91	-	-
44	3895.60	11.70	2313.91	Autonomous ICD (RCP Valve)	11.7
45	3907.30	0.30	2313.92	-	-
46	3907.60	11.70	2313.92	Autonomous ICD (RCP Valve)	11.7
47	3919.30	0.30	2313.95	-	-
48	3919.60	11.70	2313.95	Autonomous ICD (RCP Valve)	11.7
49	3931.30	0.30	2313.97	-	-
50	3931.60	11.70	2313.97	Autonomous ICD (RCP Valve)	11.7
51	3943.30	0.30	2313.96	-	-
52	3943.60	11.70	2313.96	Autonomous ICD (RCP Valve)	11.7
53	3955.30	0.30	2313.93	-	-
54	3955.60	11.70	2313.93	Autonomous ICD (RCP Valve)	11.7
55	3967.30	0.30	2313.89	-	-
56	3967.60	11.70	2313.89	Autonomous ICD (RCP Valve)	11.7

Figure E-1: *B3-HT2 AICV Completion Input. The input from 3775mMD to 3967mMD is representative for the remaining completion, to ~5350mMD. Applies to B3 Simulation cases 11-14 and 17.*

Autonomous ICD (RCP Valve)

#	Top MD	Seg. Length	Top TVD(SS)	N Parallel Valves	a	x	y	d	e	f	ρ_cal	μ_cal
	[m]	[m]	[m]								[kg/Rm³]	[cP]
1	2613.00	5.55	2040.07	-	-	-	-	-	-	-	-	-
2	2618.55	3.36	2043.31	-	-	-	-	-	-	-	-	-
3	2621.91	0.76	2045.26	-	-	-	-	-	-	-	-	-
4	2622.67	2.06	2045.71	-	-	-	-	-	-	-	-	-
5	2624.73	0.74	2046.91	-	-	-	-	-	-	-	-	-
6	2625.47	2.06	2047.34	-	-	-	-	-	-	-	-	-
7	2627.53	23.95	2048.54	-	-	-	-	-	-	-	-	-
8	2651.48	3.05	2062.24	-	-	-	-	-	-	-	-	-
9	2654.53	0.76	2063.97	-	-	-	-	-	-	-	-	-
10	2655.29	1.97	2064.40	-	-	-	-	-	-	-	-	-
11	2657.26	22.40	2065.51	-	-	-	-	-	-	-	-	-
12	2679.66	4.08	2077.97	-	-	-	-	-	-	-	-	-
13	2683.74	1.28	2080.16	-	-	-	-	-	-	-	-	-
14	2685.02	3.59	2080.85	-	-	-	-	-	-	-	-	-
15	2688.61	1.94	2082.75	-	-	-	-	-	-	-	-	-
16	2690.55	696.44	2083.77	-	-	-	-	-	-	-	-	-
17	3386.99	2.55	2309.48	-	-	-	-	-	-	-	-	-
18	3389.54	2.20	2309.73	-	-	-	-	-	-	-	-	-
19	3391.74	8.01	2309.94	-	-	-	-	-	-	-	-	-
20	3399.75	0.75	2310.68	-	-	-	-	-	-	-	-	-
21	3400.50	1.56	2310.75	-	-	-	-	-	-	-	-	-
22	3402.06	38.44	2310.88	-	-	-	-	-	-	-	-	-
23	3440.50	335.10	2313.48	-	-	-	-	-	-	-	-	-
24	3775.60	11.70	2313.67	4	1.215e-5	2.38	0.763	1.0	1.0	1.0	1000.0	1.0
25	3787.30	0.30	2313.67	-	-	-	-	-	-	-	-	-
26	3787.60	11.70	2313.67	4	1.215e-5	2.38	0.763	1.0	1.0	1.0	1000.0	1.0
27	3799.30	0.30	2313.70	-	-	-	-	-	-	-	-	-
28	3799.60	11.70	2313.70	4	1.215e-5	2.38	0.763	1.0	1.0	1.0	1000.0	1.0
29	3811.30	0.30	2313.75	-	-	-	-	-	-	-	-	-
30	3811.60	11.70	2313.75	4	1.215e-5	2.38	0.763	1.0	1.0	1.0	1000.0	1.0
31	3823.30	0.30	2313.80	-	-	-	-	-	-	-	-	-
32	3823.60	11.70	2313.80	4	1.215e-5	2.38	0.763	1.0	1.0	1.0	1000.0	1.0
33	3835.30	0.30	2313.85	-	-	-	-	-	-	-	-	-
34	3835.60	11.70	2313.85	4	1.215e-5	2.38	0.763	1.0	1.0	1.0	1000.0	1.0
35	3847.30	0.30	2313.89	-	-	-	-	-	-	-	-	-
36	3847.60	11.70	2313.89	4	1.215e-5	2.38	0.763	1.0	1.0	1.0	1000.0	1.0
37	3859.30	0.30	2313.90	-	-	-	-	-	-	-	-	-
38	3859.60	11.70	2313.90	4	1.215e-5	2.38	0.763	1.0	1.0	1.0	1000.0	1.0
39	3871.30	0.30	2313.90	-	-	-	-	-	-	-	-	-
40	3871.60	11.70	2313.90	4	1.215e-5	2.38	0.763	1.0	1.0	1.0	1000.0	1.0
41	3883.30	0.30	2313.90	-	-	-	-	-	-	-	-	-
42	3883.60	11.70	2313.90	4	1.215e-5	2.38	0.763	1.0	1.0	1.0	1000.0	1.0
43	3895.30	0.30	2313.91	-	-	-	-	-	-	-	-	-

Figure E-2: *B3-HT2 AICV Settings for Simulation Cases 11-13. For case 14, N Parallel Valves are set to 2 instead of 4. The input from 3775mMD to 3967mMD is representative for the remaining completion, to ∼5350mMD.*

Autonomous ICD (RCP Valve)

#	Top MD	Seg. Length	Top TVD(SS)	N Parallel Valves	a	x	y	d	e	f	ρ_cal	μ_cal
	[m]	[m]	[m]								[kg/Rm³]	[cP]
1	2613.00	5.55	2040.07	-	-	-	-	-	-	-	-	-
2	2618.55	3.36	2043.31	-	-	-	-	-	-	-	-	-
3	2621.91	0.76	2045.26	-	-	-	-	-	-	-	-	-
4	2622.67	2.06	2045.71	-	-	-	-	-	-	-	-	-
5	2624.73	0.74	2046.91	-	-	-	-	-	-	-	-	-
6	2625.47	2.06	2047.34	-	-	-	-	-	-	-	-	-
7	2627.53	23.95	2048.54	-	-	-	-	-	-	-	-	-
8	2651.48	3.05	2062.24	-	-	-	-	-	-	-	-	-
9	2654.53	0.76	2063.97	-	-	-	-	-	-	-	-	-
10	2655.29	1.97	2064.40	-	-	-	-	-	-	-	-	-
11	2657.26	22.40	2065.51	-	-	-	-	-	-	-	-	-
12	2679.66	4.08	2077.97	-	-	-	-	-	-	-	-	-
13	2683.74	1.28	2080.16	-	-	-	-	-	-	-	-	-
14	2685.02	3.59	2080.85	-	-	-	-	-	-	-	-	-
15	2688.61	1.94	2082.75	-	-	-	-	-	-	-	-	-
16	2690.55	696.44	2083.77	-	-	-	-	-	-	-	-	-
17	3386.99	2.55	2309.48	-	-	-	-	-	-	-	-	-
18	3389.54	2.20	2309.73	-	-	-	-	-	-	-	-	-
19	3391.74	8.01	2309.94	-	-	-	-	-	-	-	-	-
20	3399.75	0.75	2310.68	-	-	-	-	-	-	-	-	-
21	3400.50	1.56	2310.75	-	-	-	-	-	-	-	-	-
22	3402.06	38.44	2310.88	-	-	-	-	-	-	-	-	-
23	3440.50	335.10	2313.48	-	-	-	-	-	-	-	-	-
24	3775.60	11.70	2313.67	2	6.0e-5	2.5	2.0	1.0	1.0	1.0	1009.0	0.4
25	3787.30	0.30	2313.67	-	-	-	-	-	-	-	-	-
26	3787.60	11.70	2313.67	2	6.0e-5	2.5	2.0	1.0	1.0	1.0	1009.0	0.4
27	3799.30	0.30	2313.70	-	-	-	-	-	-	-	-	-
28	3799.60	11.70	2313.70	2	6.0e-5	2.5	2.0	1.0	1.0	1.0	1009.0	0.4
29	3811.30	0.30	2313.75	-	-	-	-	-	-	-	-	-
30	3811.60	11.70	2313.75	2	6.0e-5	2.5	2.0	1.0	1.0	1.0	1009.0	0.4
31	3823.30	0.30	2313.80	-	-	-	-	-	-	-	-	-
32	3823.60	11.70	2313.80	2	6.0e-5	2.5	2.0	1.0	1.0	1.0	1009.0	0.4
33	3835.30	0.30	2313.85	-	-	-	-	-	-	-	-	-
34	3835.60	11.70	2313.85	2	6.0e-5	2.5	2.0	1.0	1.0	1.0	1009.0	0.4
35	3847.30	0.30	2313.89	-	-	-	-	-	-	-	-	-
36	3847.60	11.70	2313.89	2	6.0e-5	2.5	2.0	1.0	1.0	1.0	1009.0	0.4
37	3859.30	0.30	2313.90	-	-	-	-	-	-	-	-	-
38	3859.60	11.70	2313.90	2	6.0e-5	2.5	2.0	1.0	1.0	1.0	1009.0	0.4
39	3871.30	0.30	2313.90	-	-	-	-	-	-	-	-	-
40	3871.60	11.70	2313.90	2	6.0e-5	2.5	2.0	1.0	1.0	1.0	1009.0	0.4
41	3883.30	0.30	2313.90	-	-	-	-	-	-	-	-	-
42	3883.60	11.70	2313.90	2	6.0e-5	2.5	2.0	1.0	1.0	1.0	1009.0	0.4
43	3895.30	0.30	2313.91	-	-	-	-	-	-	-	-	-

Figure E-3: *B3-HT2 AICV Settings for Simulation Case 17. The input from 3775mMD to 3967mMD is representative for the remaining completion, to ~5350mMD.*

E.2 Well B1 NETool AICV Well Design

Inflow Control Device

#	Top MD [m]	Seg. Length [m]	Top TVD(SS) [m]	ICD Design	Joint Length [m]
1	2607.00	1.83	2061.70	-	-
2	2608.83	3.05	2062.94	-	-
3	2611.88	1.45	2064.99	-	-
4	2613.33	2.06	2065.97	-	-
5	2615.39	22.00	2067.36	-	-
6	2637.39	3.05	2082.21	-	-
7	2640.44	3.66	2084.27	-	-
8	2644.10	0.58	2086.73	-	-
9	2644.68	2.00	2087.13	-	-
10	2646.68	0.70	2088.47	-	-
11	2647.38	2.00	2088.95	-	-
12	2649.38	25.00	2090.29	-	-
13	2674.38	3.00	2107.15	-	-
14	2677.38	0.60	2109.18	-	-
15	2677.98	2.00	2109.58	-	-
16	2679.98	2.05	2110.94	-	-
17	2682.03	1.15	2112.32	-	-
18	2683.18	3.74	2113.10	-	-
19	2686.92	2.09	2115.62	-	-
20	2689.01	3.00	2117.03	-	-
21	2692.01	4.75	2119.05	-	-
22	2696.76	49.22	2122.24	-	-
23	2745.98	294.02	2154.25	-	-
24	3040.00	6.00	2306.10	-	-
25	3046.00	1.90	2307.21	-	-
26	3047.90	3.00	2307.54	-	-
27	3050.90	3.00	2308.03	-	-
28	3053.90	0.57	2308.49	-	-
29	3054.47	2.58	2308.58	-	-
30	3057.05	48.93	2308.94	-	-
31	3105.98	25.28	2312.47	-	-
32	3131.26	12.05	2312.97	-	-
33	3143.31	11.70	2313.04	Autonomous ICD (RCP Valve)	11.7
34	3155.01	0.30	2313.10	-	-
35	3155.31	11.70	2313.11	Autonomous ICD (RCP Valve)	11.7
36	3167.01	0.30	2313.13	-	-
37	3167.31	11.70	2313.13	Autonomous ICD (RCP Valve)	11.7
38	3179.01	0.30	2313.13	-	-
39	3179.31	11.70	2313.13	Autonomous ICD (RCP Valve)	11.7
40	3191.01	0.30	2313.12	-	-
41	3191.31	11.70	2313.12	Autonomous ICD (RCP Valve)	11.7
42	3203.01	0.30	2313.11	-	-
43	3203.31	11.70	2313.11	Autonomous ICD (RCP Valve)	11.7
44	3215.01	0.30	2313.09	-	-
45	3215.31	11.70	2313.09	Autonomous ICD (RCP Valve)	11.7
46	3227.01	0.30	2313.06	-	-
47	3227.31	11.70	2313.06	Autonomous ICD (RCP Valve)	11.7
48	3239.01	0.30	2313.03	-	-
49	3239.31	11.70	2313.03	Autonomous ICD (RCP Valve)	11.7
50	3251.01	0.30	2313.00	-	-
51	3251.31	11.70	2313.00	Autonomous ICD (RCP Valve)	11.7
52	3263.01	0.30	2312.97	-	-
53	3263.31	11.70	2312.97	Autonomous ICD (RCP Valve)	11.7
54	3275.01	0.30	2312.94	-	-
55	3275.31	11.70	2312.94	Autonomous ICD (RCP Valve)	11.7

Figure E-4: *B1-AHT3 AICV Completion Input. The input from 3143mMD to 3275mMD is representative for the remaining completion, to ~4410mMD. Applies to B1 Simulation cases 14.*

Autonomous ICD (RCP Valve)

#	Top MD	Seg. Length	Top TVD(SS)	N Parallel Valves	a	x	y	d	e	f	ρ_cal	μ_cal
	[m]	[m]	[m]								[kg/Rm³]	[cP]
1	2607.00	1.83	2061.70	-	-	-	-	-	-	-	-	-
2	2608.83	3.05	2062.94	-	-	-	-	-	-	-	-	-
3	2611.88	1.45	2064.99	-	-	-	-	-	-	-	-	-
4	2613.33	2.06	2065.97	-	-	-	-	-	-	-	-	-
5	2615.39	22.00	2067.36	-	-	-	-	-	-	-	-	-
6	2637.39	3.05	2082.21	-	-	-	-	-	-	-	-	-
7	2640.44	3.66	2084.27	-	-	-	-	-	-	-	-	-
8	2644.10	0.58	2086.73	-	-	-	-	-	-	-	-	-
9	2644.68	2.00	2087.13	-	-	-	-	-	-	-	-	-
10	2646.68	0.70	2088.47	-	-	-	-	-	-	-	-	-
11	2647.38	2.00	2088.95	-	-	-	-	-	-	-	-	-
12	2649.38	25.00	2090.29	-	-	-	-	-	-	-	-	-
13	2674.38	3.00	2107.15	-	-	-	-	-	-	-	-	-
14	2677.38	0.60	2109.18	-	-	-	-	-	-	-	-	-
15	2677.98	2.00	2109.58	-	-	-	-	-	-	-	-	-
16	2679.98	2.05	2110.94	-	-	-	-	-	-	-	-	-
17	2682.03	1.15	2112.32	-	-	-	-	-	-	-	-	-
18	2683.18	3.74	2113.10	-	-	-	-	-	-	-	-	-
19	2686.92	2.09	2115.62	-	-	-	-	-	-	-	-	-
20	2689.01	3.00	2117.03	-	-	-	-	-	-	-	-	-
21	2692.01	4.75	2119.05	-	-	-	-	-	-	-	-	-
22	2696.76	49.22	2122.24	-	-	-	-	-	-	-	-	-
23	2745.98	294.02	2154.25	-	-	-	-	-	-	-	-	-
24	3040.00	6.00	2306.10	-	-	-	-	-	-	-	-	-
25	3046.00	1.90	2307.21	-	-	-	-	-	-	-	-	-
26	3047.90	3.00	2307.54	-	-	-	-	-	-	-	-	-
27	3050.90	3.00	2308.03	-	-	-	-	-	-	-	-	-
28	3053.90	0.57	2308.49	-	-	-	-	-	-	-	-	-
29	3054.47	2.58	2308.58	-	-	-	-	-	-	-	-	-
30	3057.05	48.93	2308.94	-	-	-	-	-	-	-	-	-
31	3105.98	25.28	2312.47	-	-	-	-	-	-	-	-	-
32	3131.26	12.05	2312.97	-	-	-	-	-	-	-	-	-
33	3143.31	11.70	2313.04	4	1.23e-5	2.386	0.757	1.0	1.0	1.0	1000.0	1.0
34	3155.01	0.30	2313.10	-	-	-	-	-	-	-	-	-
35	3155.31	11.70	2313.11	4	1.23e-5	2.386	0.757	1.0	1.0	1.0	1000.0	1.0
36	3167.01	0.30	2313.13	-	-	-	-	-	-	-	-	-
37	3167.31	11.70	2313.13	4	1.23e-5	2.386	0.757	1.0	1.0	1.0	1000.0	1.0
38	3179.01	0.30	2313.13	-	-	-	-	-	-	-	-	-
39	3179.31	11.70	2313.13	4	1.23e-5	2.386	0.757	1.0	1.0	1.0	1000.0	1.0
40	3191.01	0.30	2313.12	-	-	-	-	-	-	-	-	-
41	3191.31	11.70	2313.12	4	1.23e-5	2.386	0.757	1.0	1.0	1.0	1000.0	1.0
42	3203.01	0.30	2313.11	-	-	-	-	-	-	-	-	-
43	3203.31	11.70	2313.11	4	1.23e-5	2.386	0.757	1.0	1.0	1.0	1000.0	1.0
44	3215.01	0.30	2313.09	-	-	-	-	-	-	-	-	-
45	3215.31	11.70	2313.09	4	1.23e-5	2.386	0.757	1.0	1.0	1.0	1000.0	1.0
46	3227.01	0.30	2313.06	-	-	-	-	-	-	-	-	-
47	3227.31	11.70	2313.06	4	1.23e-5	2.386	0.757	1.0	1.0	1.0	1000.0	1.0
48	3239.01	0.30	2313.03	-	-	-	-	-	-	-	-	-
49	3239.31	11.70	2313.03	4	1.23e-5	2.386	0.757	1.0	1.0	1.0	1000.0	1.0
50	3251.01	0.30	2313.00	-	-	-	-	-	-	-	-	-
51	3251.31	11.70	2313.00	4	1.23e-5	2.386	0.757	1.0	1.0	1.0	1000.0	1.0
52	3263.01	0.30	2312.97	-	-	-	-	-	-	-	-	-
53	3263.31	11.70	2312.97	4	1.23e-5	2.386	0.757	1.0	1.0	1.0	1000.0	1.0
54	3275.01	0.30	2312.94	-	-	-	-	-	-	-	-	-
55	3275.31	11.70	2312.94	4	1.23e-5	2.386	0.757	1.0	1.0	1.0	1000.0	1.0

Figure E-5: *B1-AHT3 Simulation Case 14 AICV Settings. The input from 3143mMD to 3275mMD is representative for the remaining completion, to ~4410mMD.*

F Results from AICV Case Simulations

F.1 Well B3 AICV Case Results

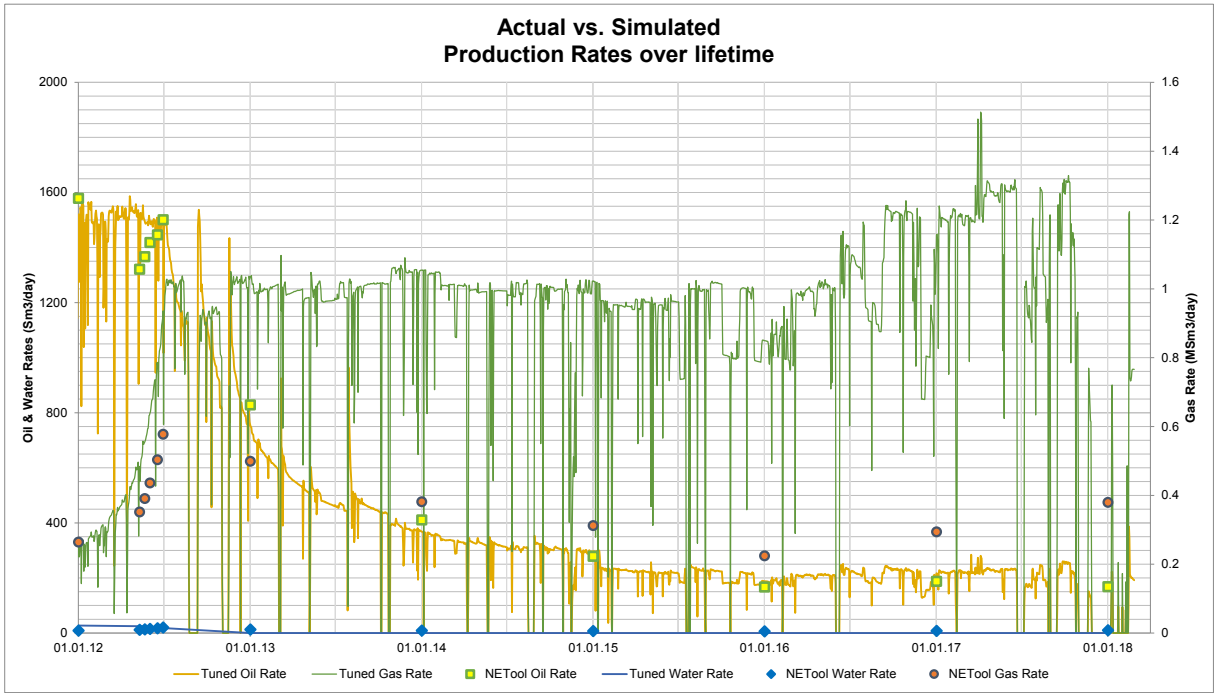

Figure F-1: *B3-HT2 Case 11: Actual vs. Simulated Production.*

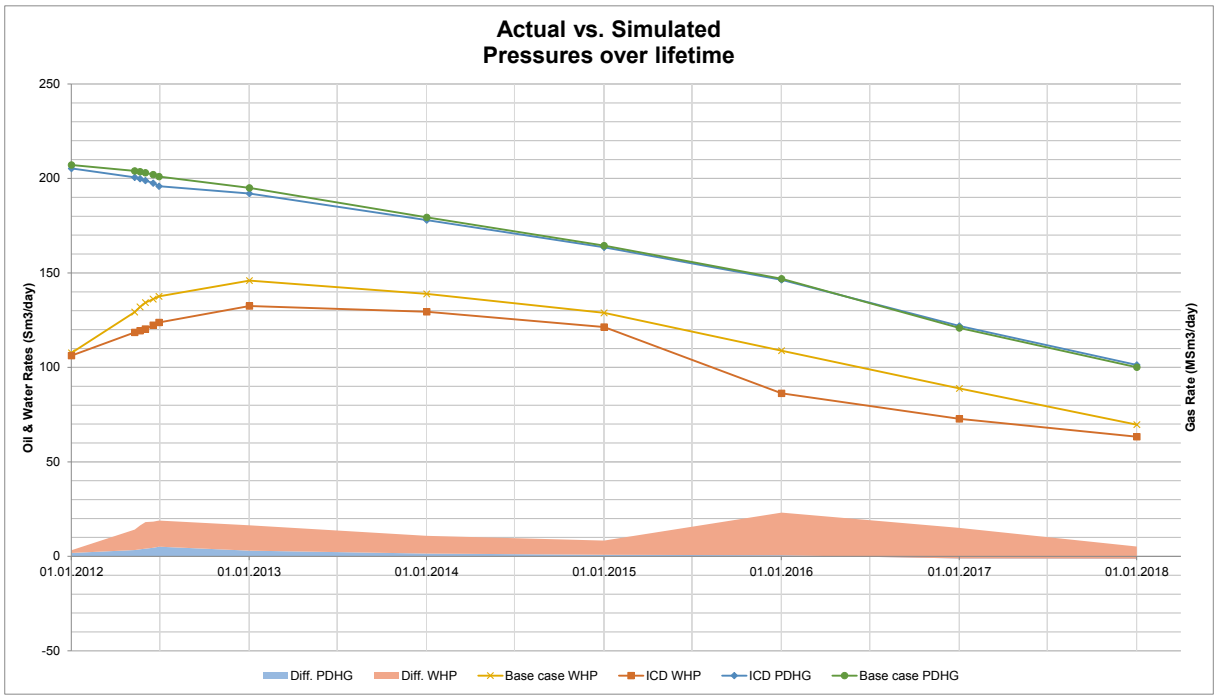

Figure F-2: *B3-HT2 Case 11: Actual vs. Simulated Pressures.*

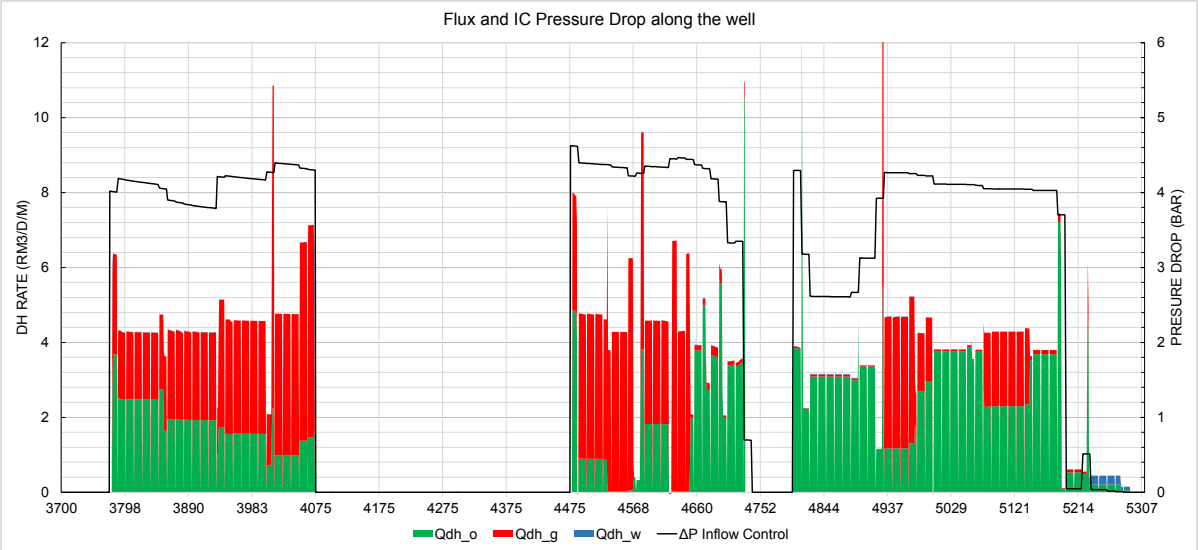

Figure F-3: *B3-HT2 Case 11: Flux and IC pressure drop along the well at early-life*

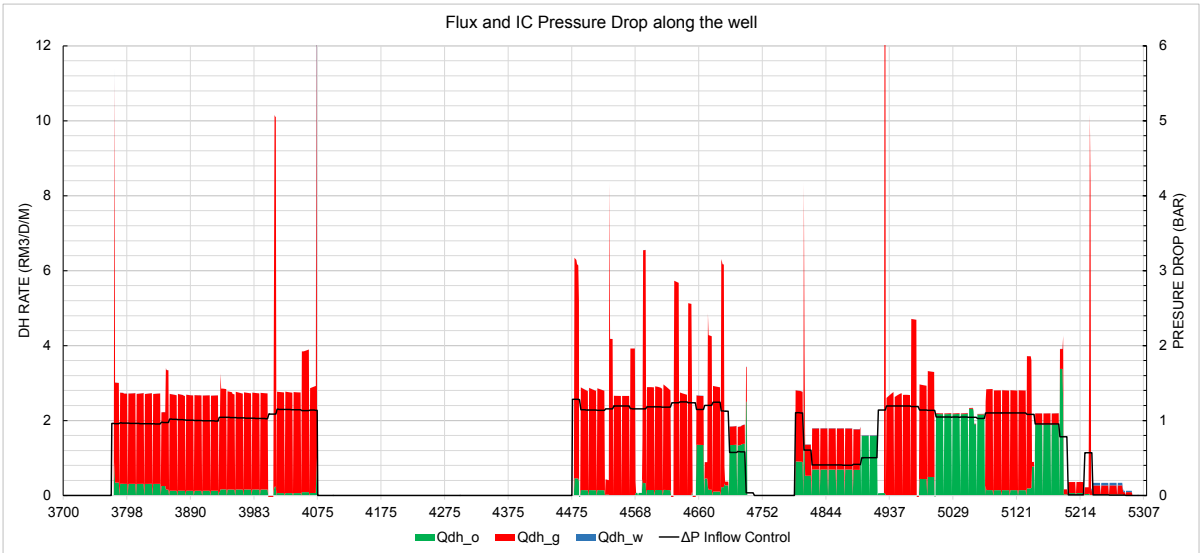

Figure F-4: *B3-HT2 Case 11: Flux and IC pressure drop along the well at mid-life*

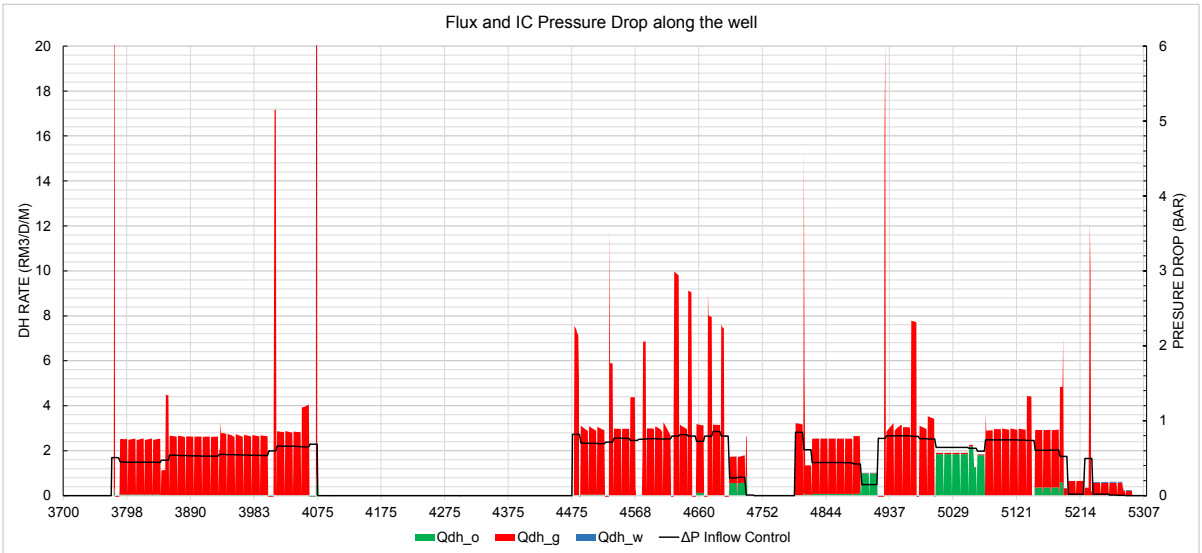

Figure F-5: *B3-HT2 Case 11: Flux and IC pressure drop along the well at late-life*

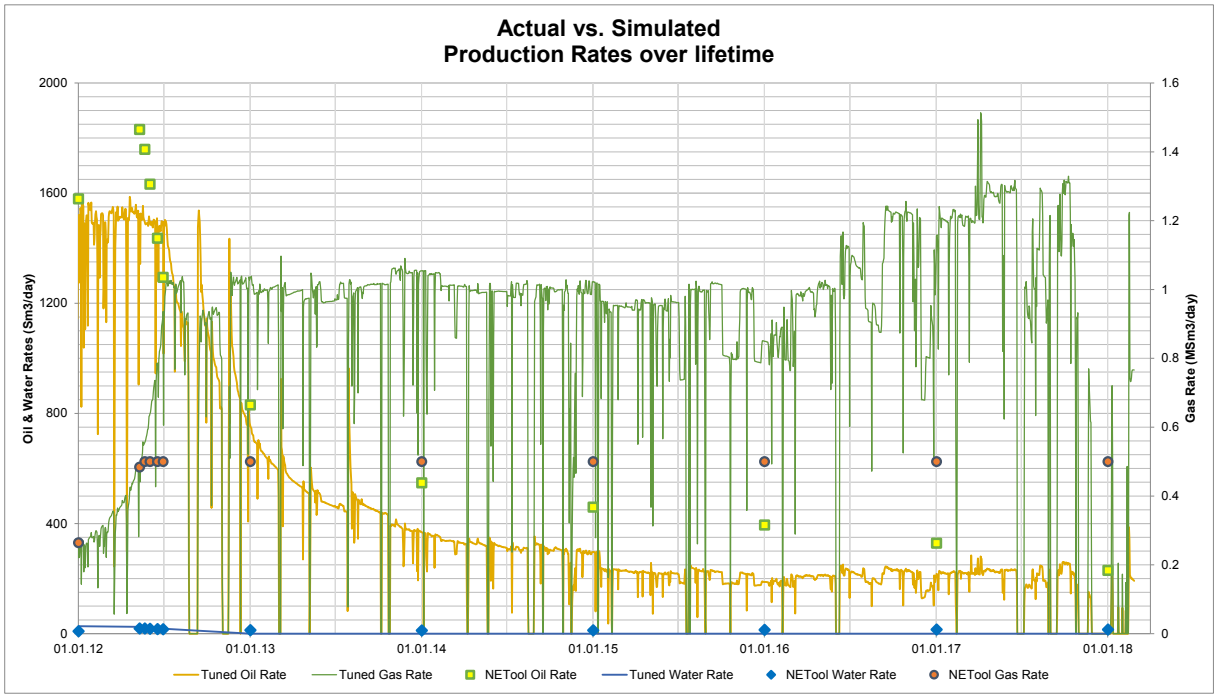

Figure F-6: *B3-HT2 Case 12: Actual vs. Simulated Production*

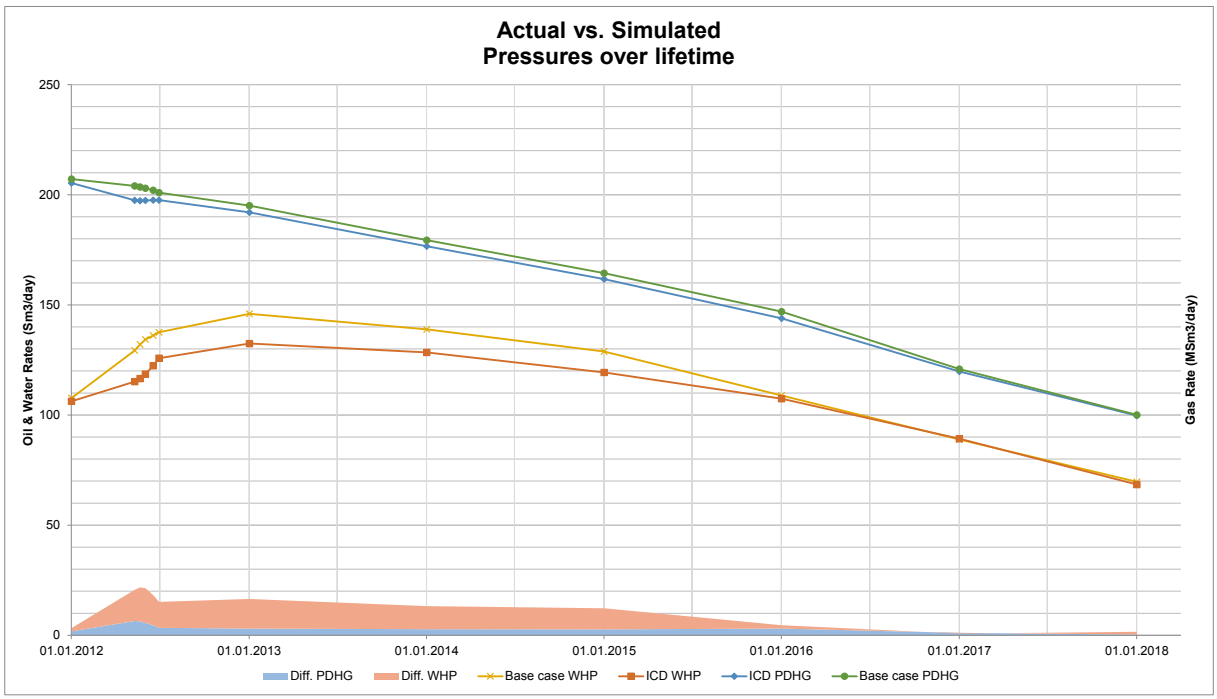

Figure F-7: *B3-HT2 Case 12: Actual vs. Simulated Pressures.*

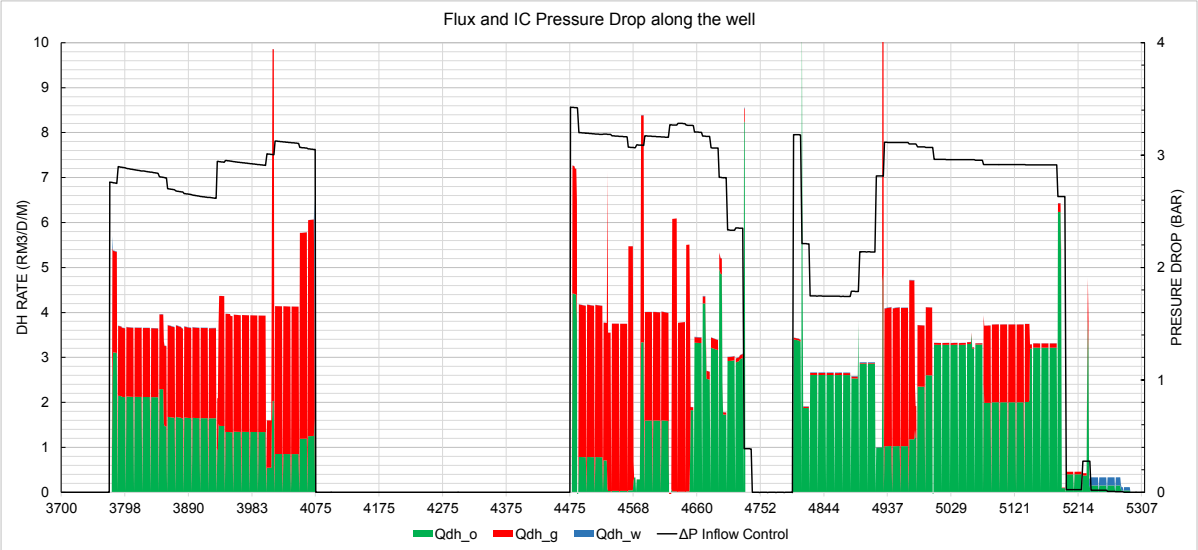

Figure F-8: *B3-HT2 Case 12: Flux and IC pressure drop along the well at early-life*

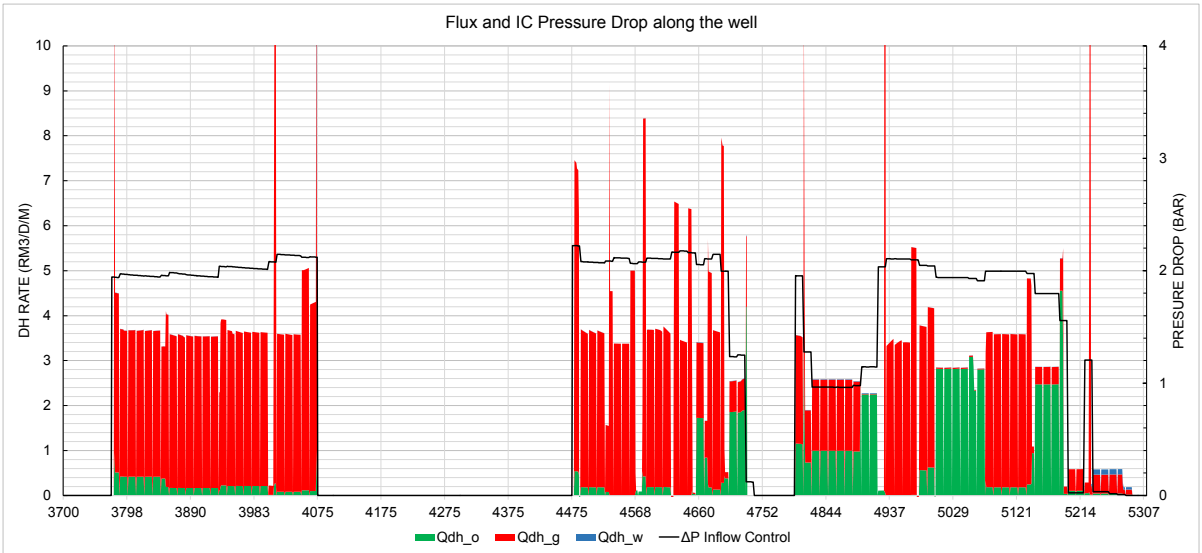

Figure F-9: *B3-HT2 Case 12: Flux and IC pressure drop along the well at mid-life*

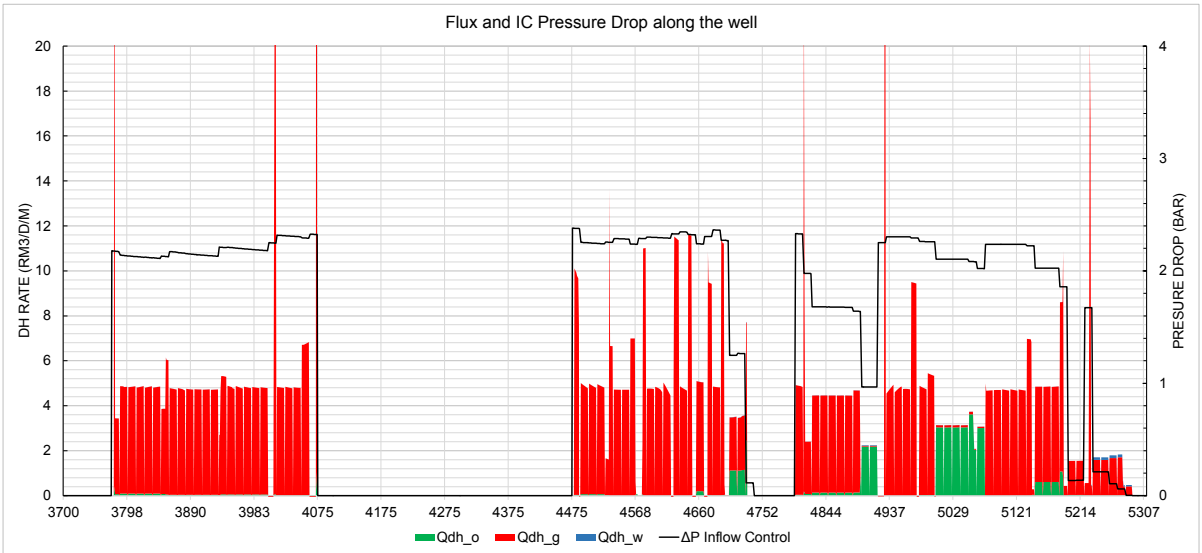

Figure F-10: *B3-HT2 Case 12: Flux and IC pressure drop along the well at late-life*

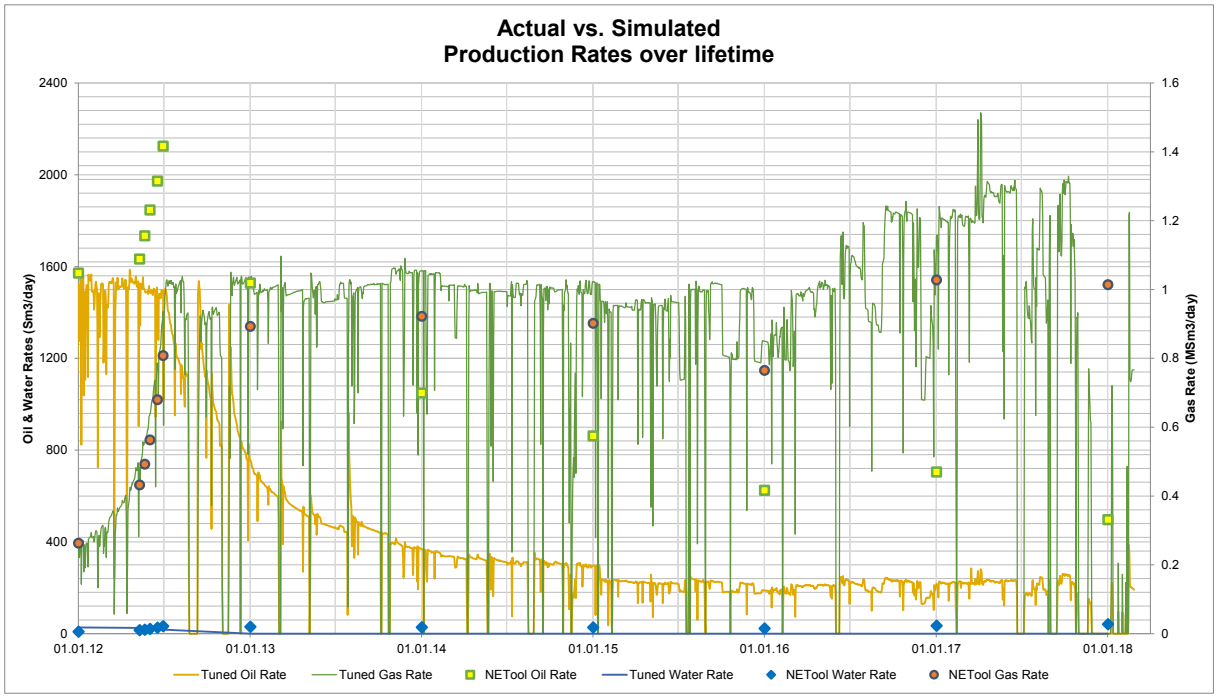

Figure F-11: *B3-HT2 Case 13: Actual vs. Simulated Production*

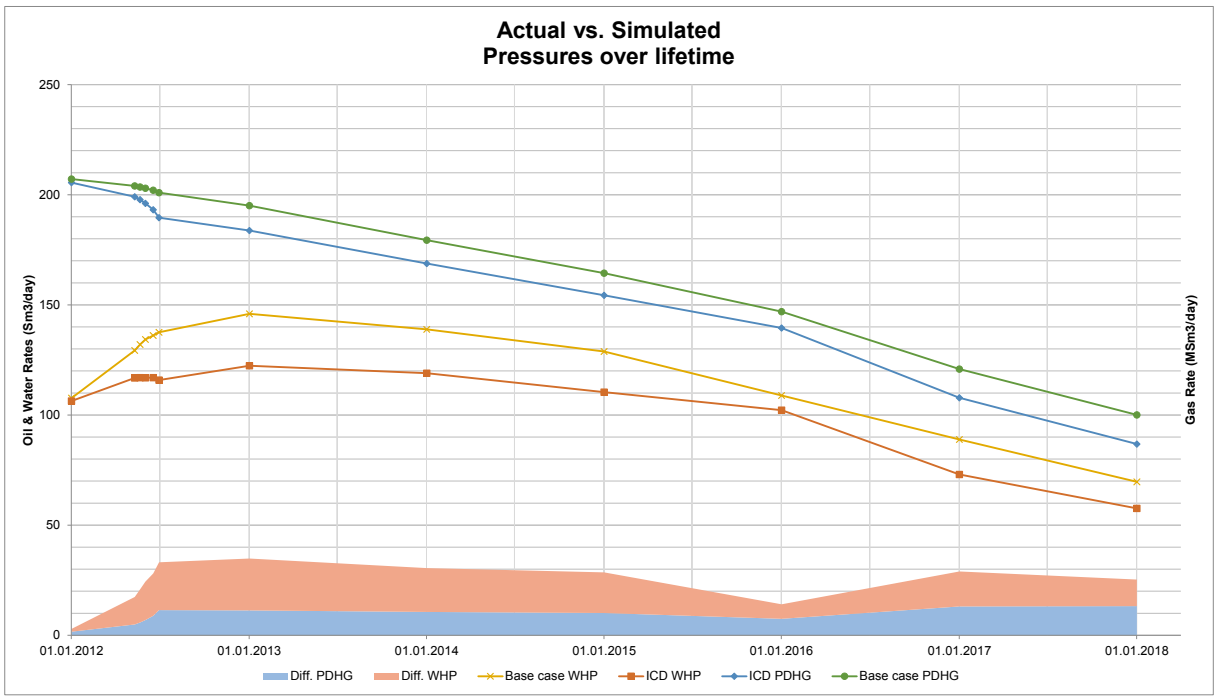

Figure F-12: *B3-HT2 Case 13: Actual vs. Simulated Pressures.*

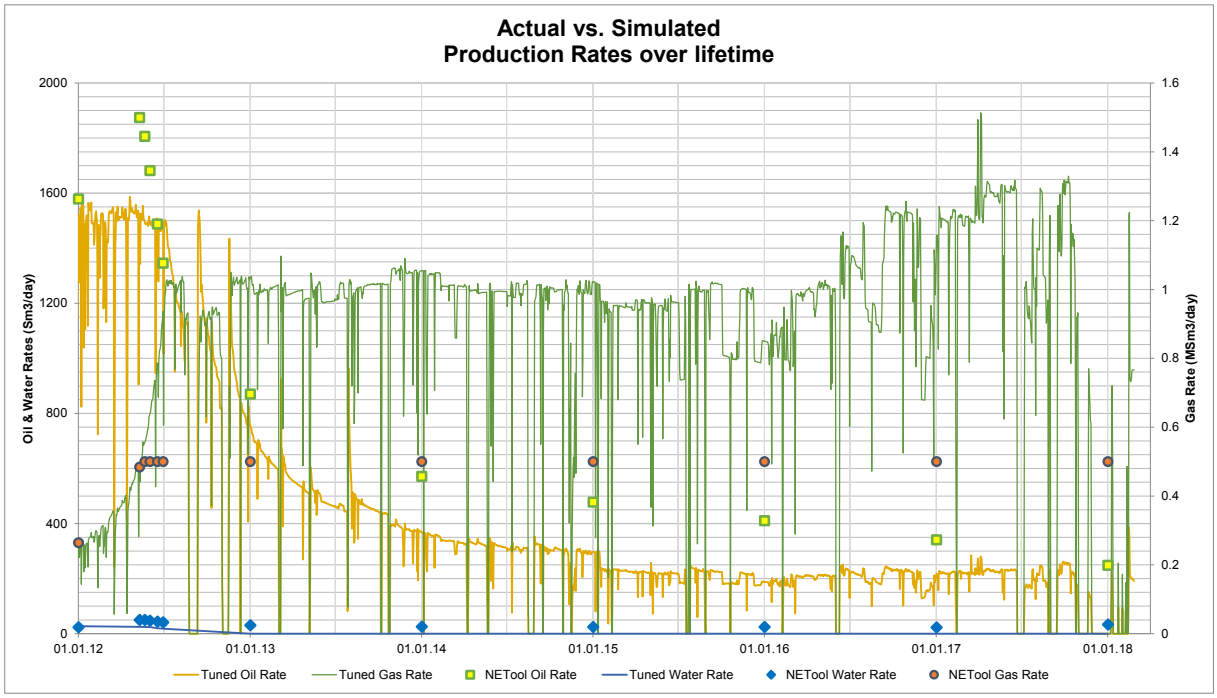

Figure F-13: *B3-HT2 Case 14: Actual vs. Simulated Production*

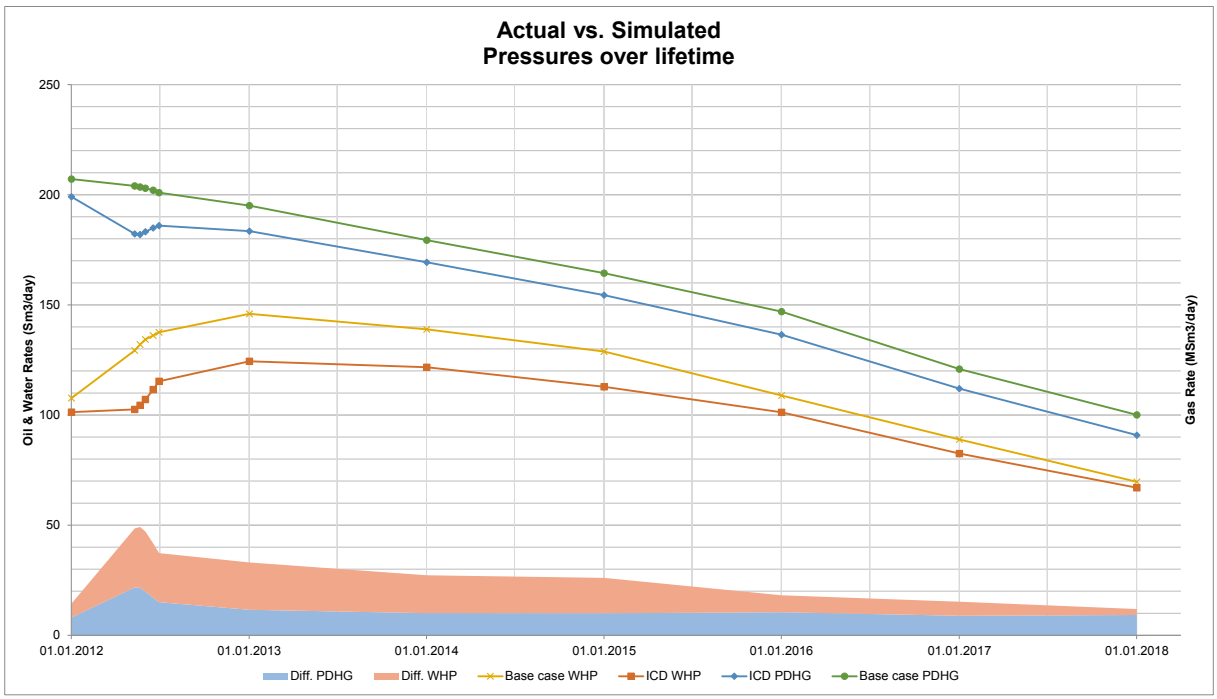

Figure F-14: *B3-HT2 Case 14: Actual vs. Simulated Pressures.*

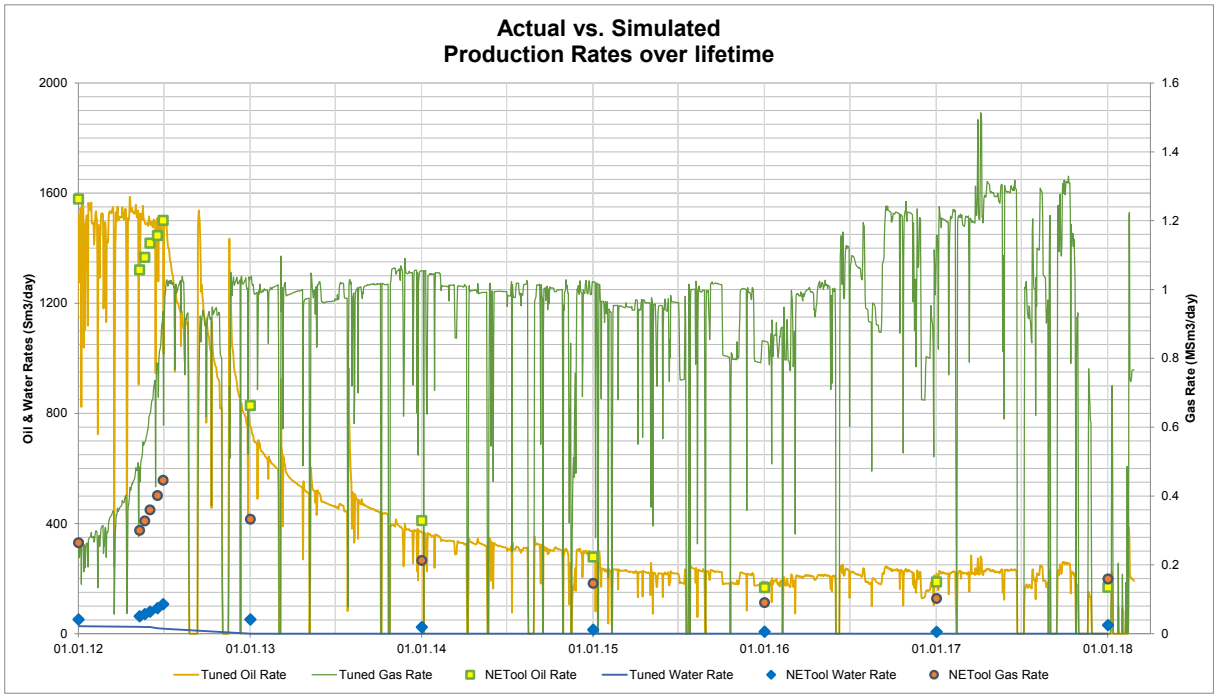

Figure F-15: *B3-HT2 Case 17: Actual vs. Simulated Production*

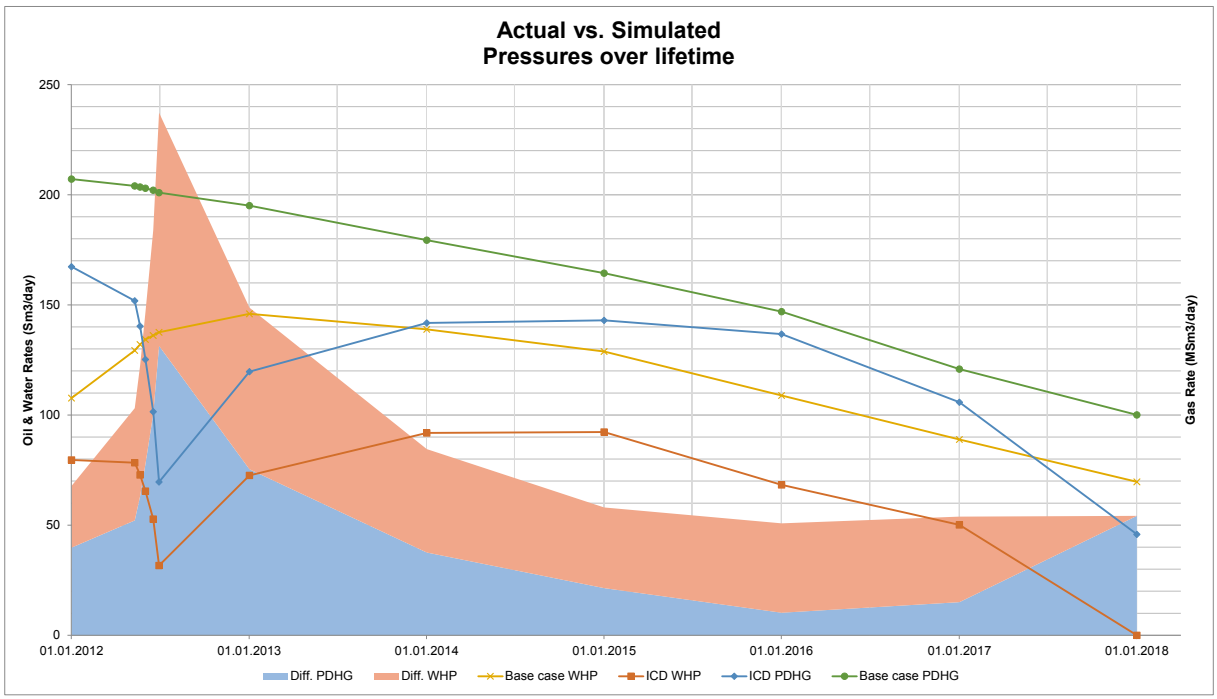

Figure F-16: *B3-HT2 Case 17: Actual vs. Simulated Pressures.*

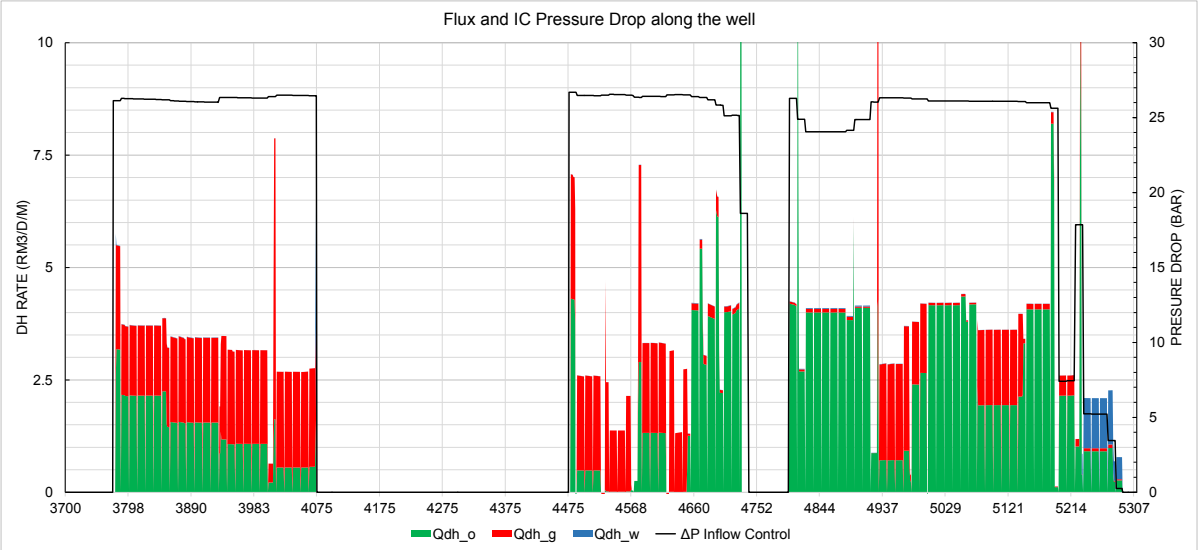

Figure F-17: *B3-HT2 Case 17: Flux and IC pressure drop along the well at early-life*

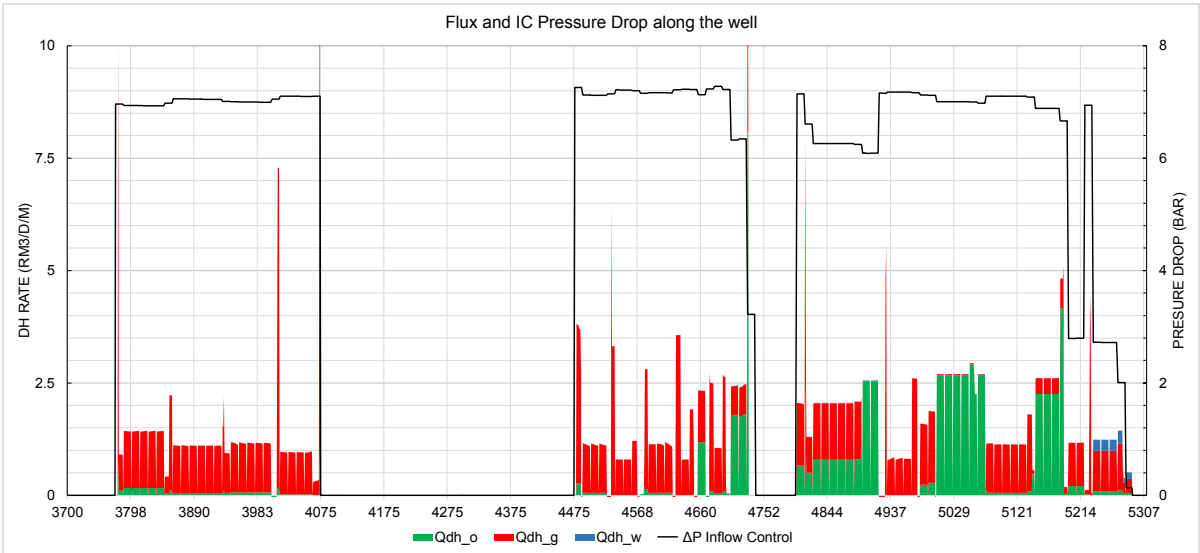

Figure F-18: *B3-HT2 Case 17: Flux and IC pressure drop along the well at mid-life*

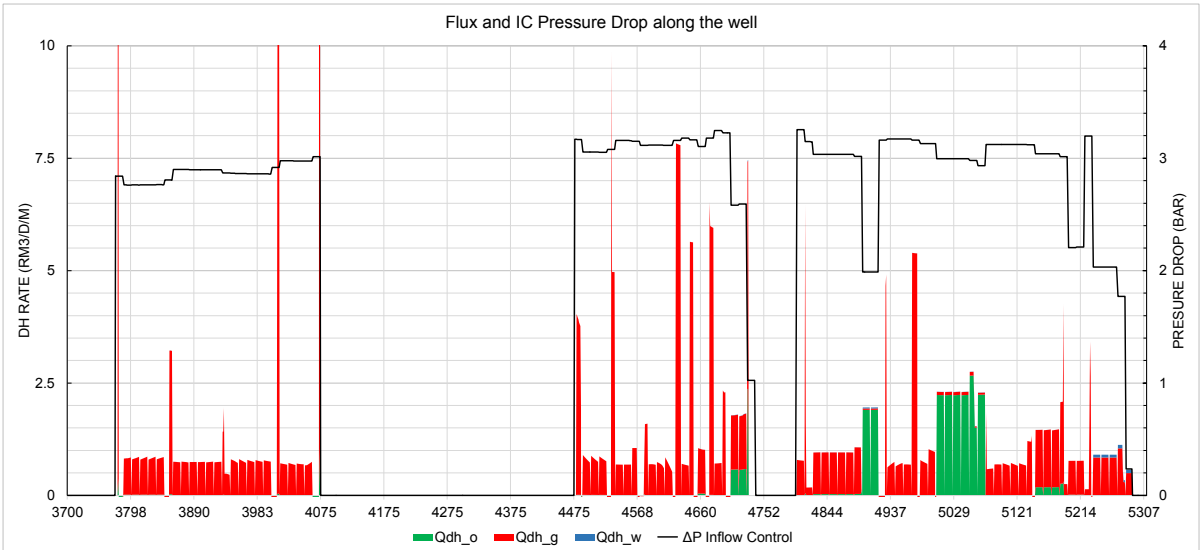

Figure F-19: *B3-HT2 Case 17: Flux and IC pressure drop along the well at late-life*

F.2 Well B1 AICV Case Results

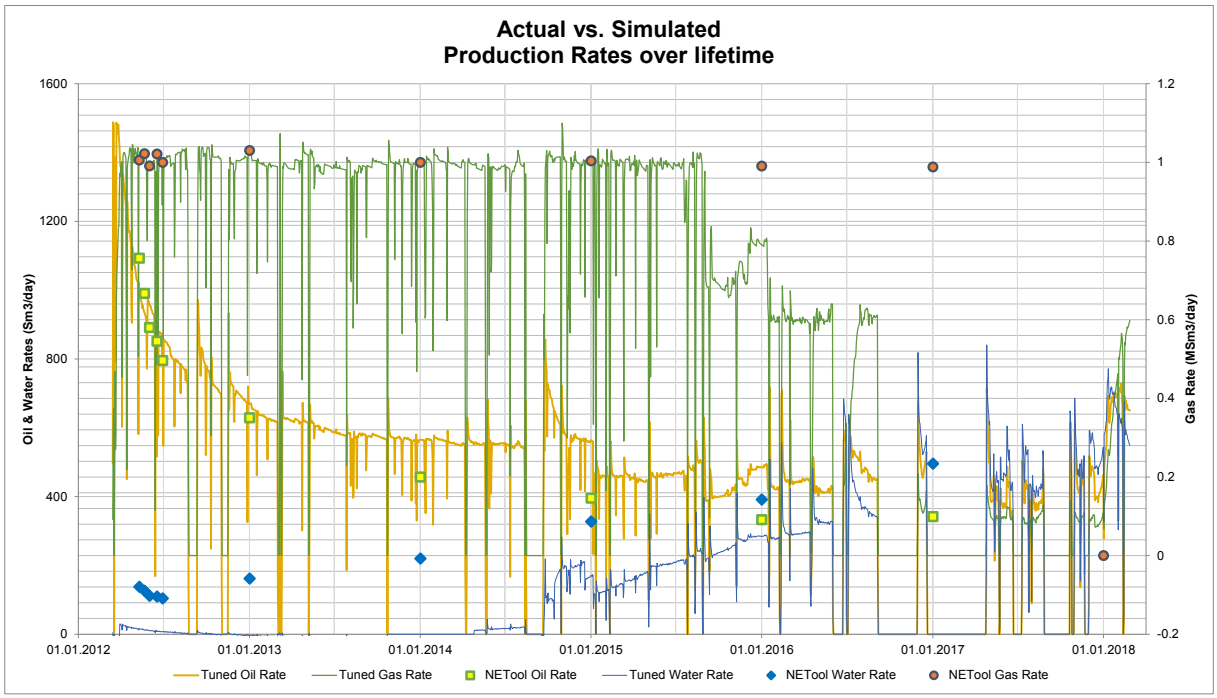

Figure F-20: *B1-AHT3 Case 14: Actual vs. Simulated Production*

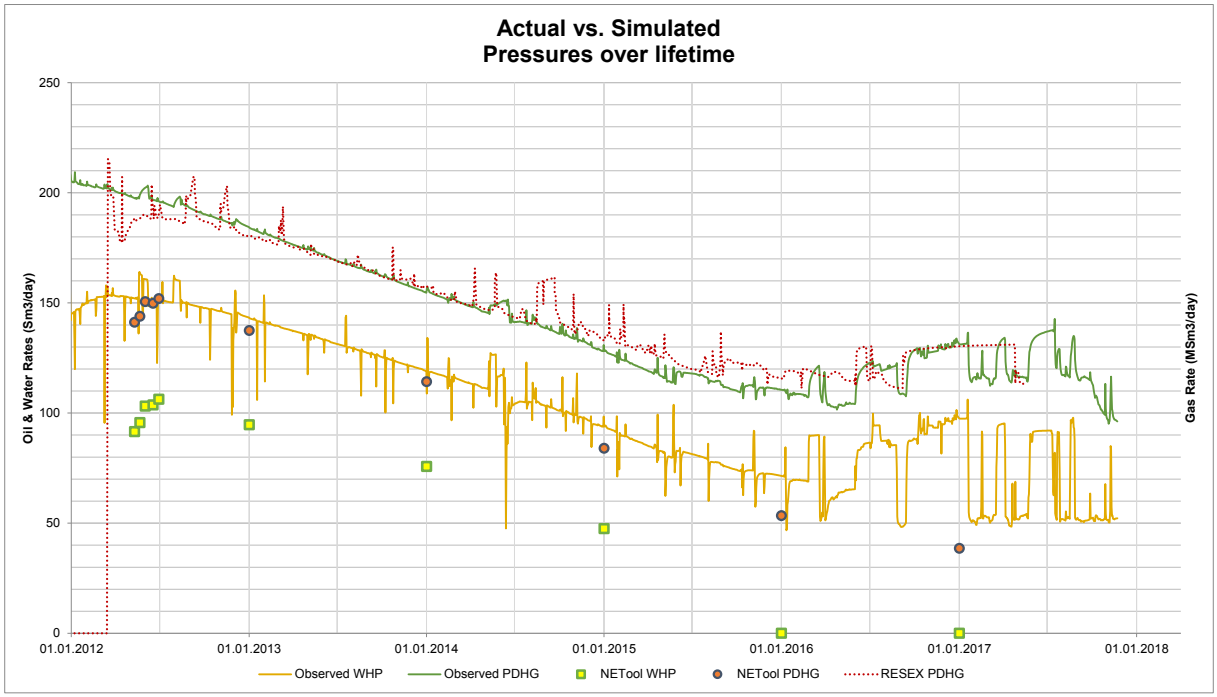

Figure F-21: *B1-AHT3 Case 14: Actual vs. Simulated Pressures*

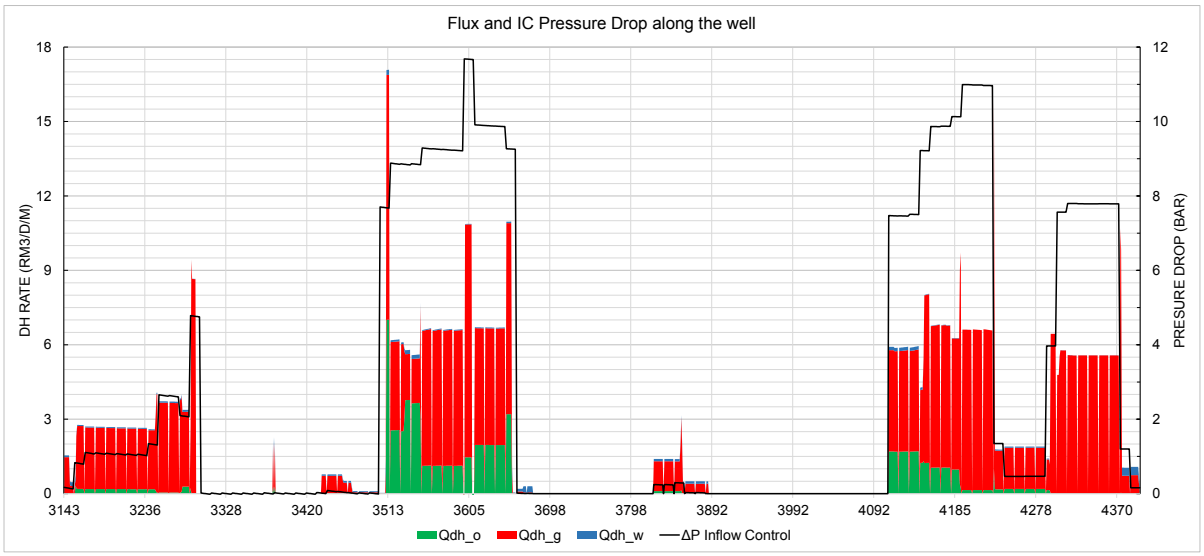

Figure F-22: *B1-AHT3 Case 14: Flux and IC pressure drop along the well at early-life*

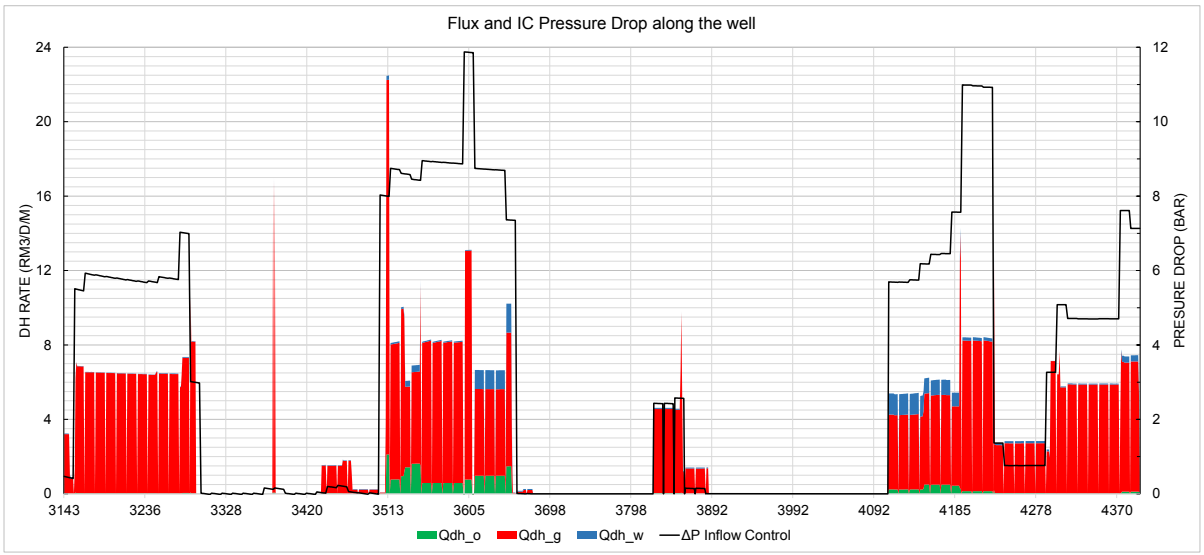

Figure F-23: *B1-AHT3 Case 14: Flux and IC pressure drop along the well at mid-life*

G Miscellaneous

G.1 Well Schematics

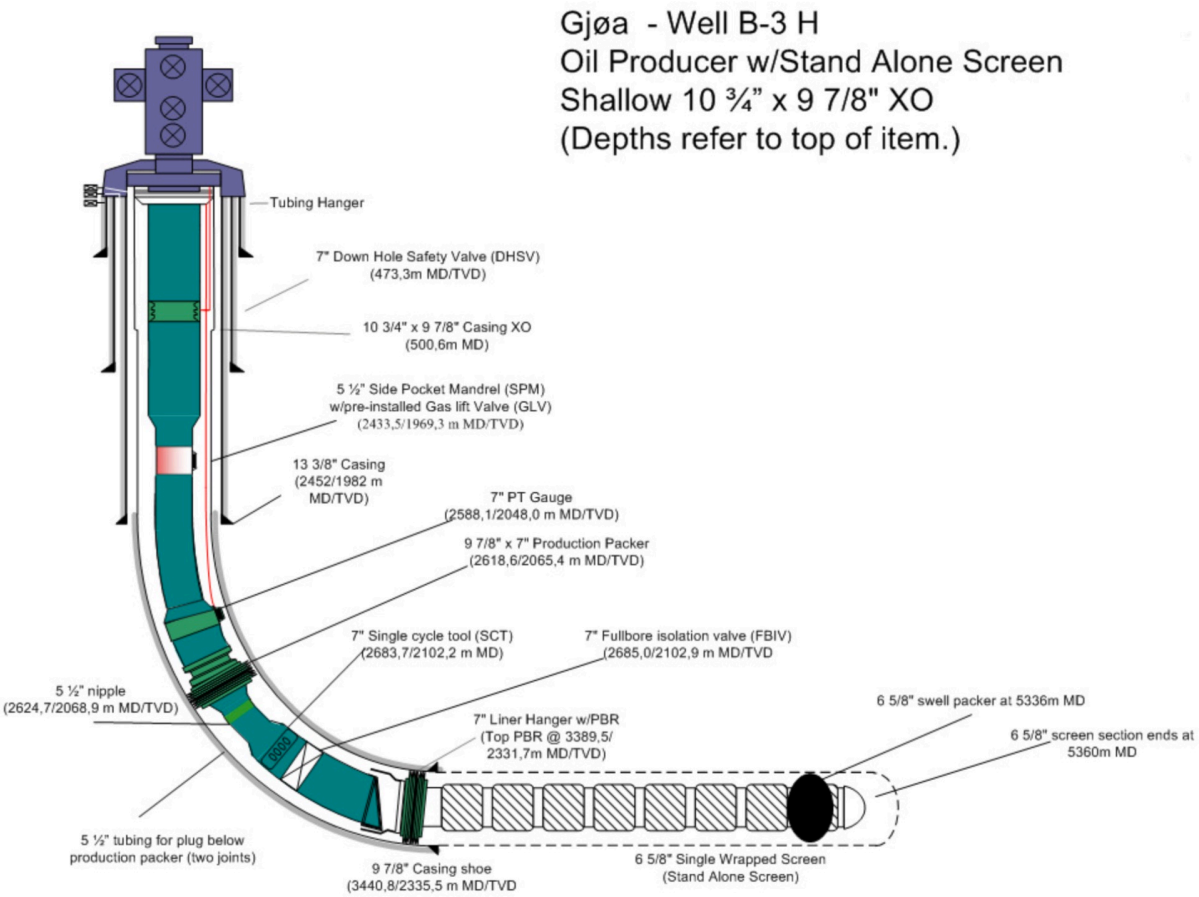

Figure G-24: *Well Schematic for well B3, [6]*

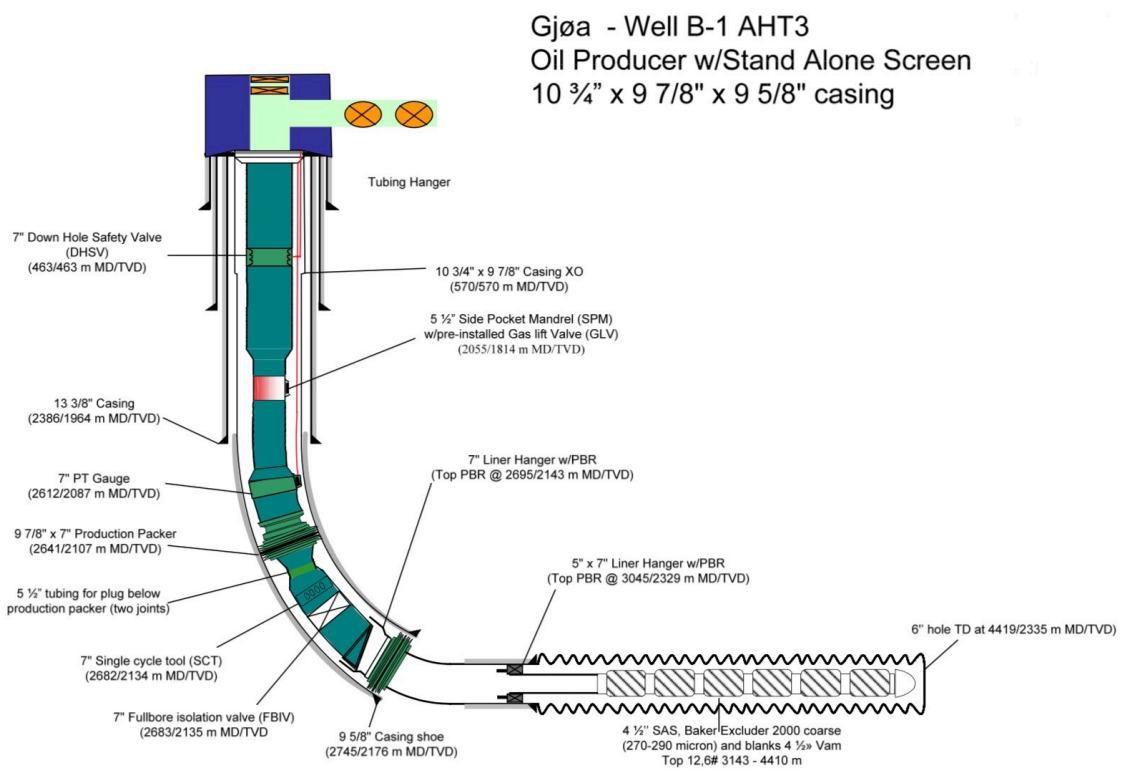

Figure G-25: *Well Schematic for well B1, [9]*

G.2 Well logs

The following pictures show the well logs for the producing sections of the two wells. *PHIE* designates the porosity log, while the *KLOGH* column shows the horizontal permeability. Furthermore, *SW* shows the water saturation. The rightmost column shows the sections of the well completed with blank pipes (*closed*), and sandscreens (*open*).

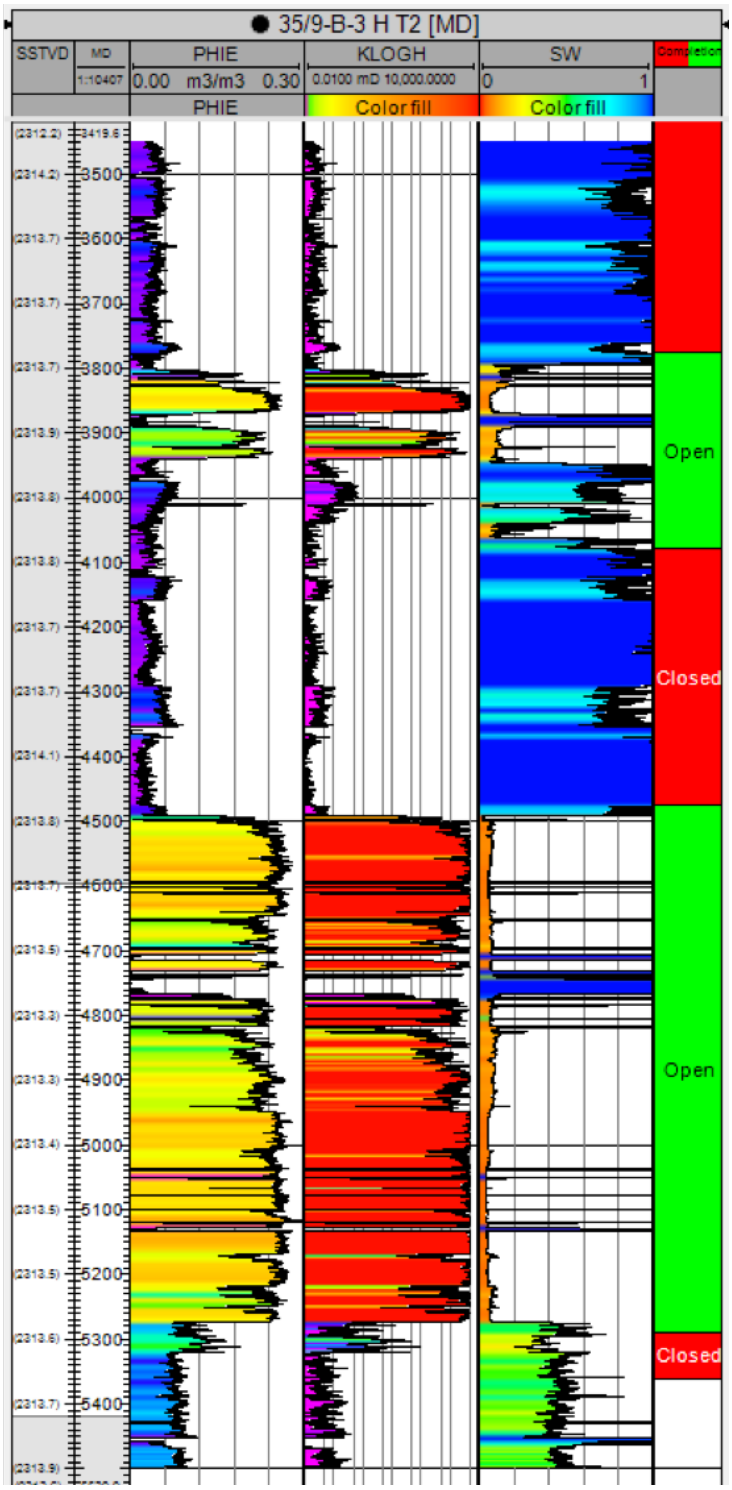

Figure G-26: *Well log for well B3, [10]*

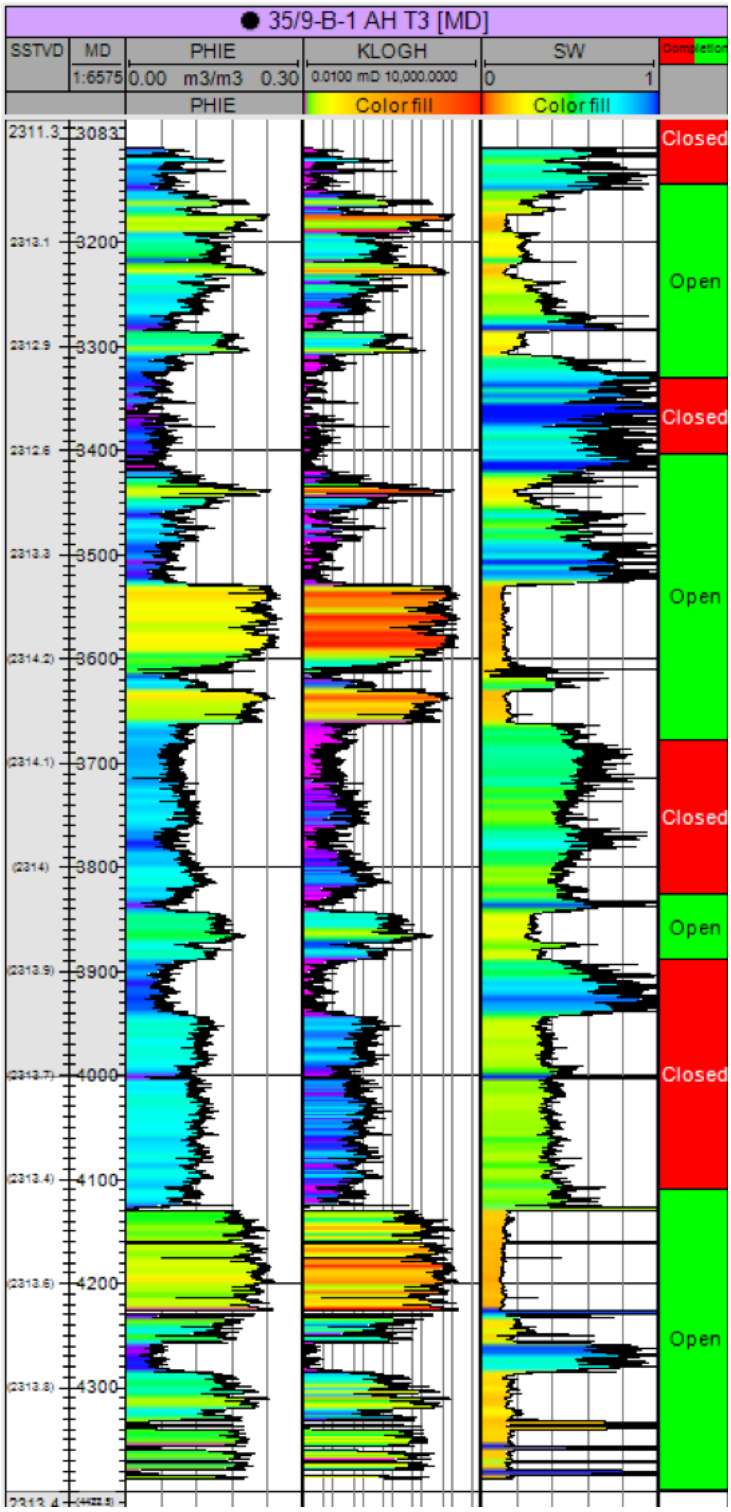

Figure G-27: *Well log for well B1, [10]*

G.3 Relative Permeability curves for well B1

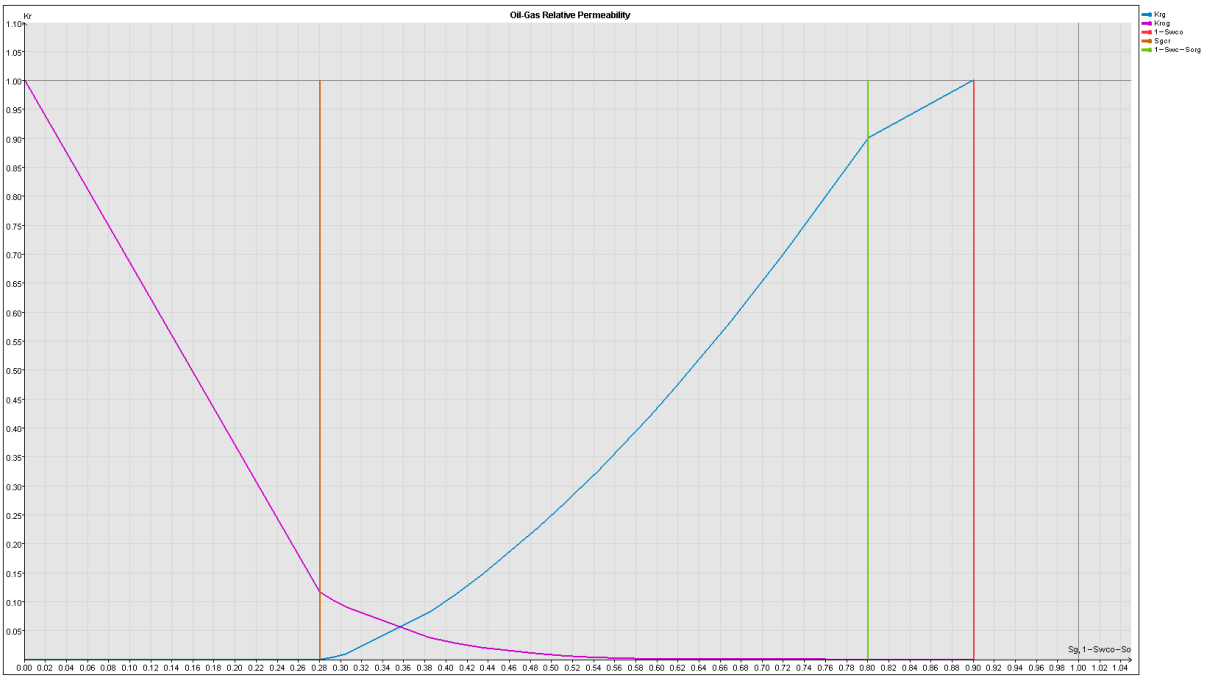

Figure G-28: *B1-AHT3: Oil-Gas relative permeability*

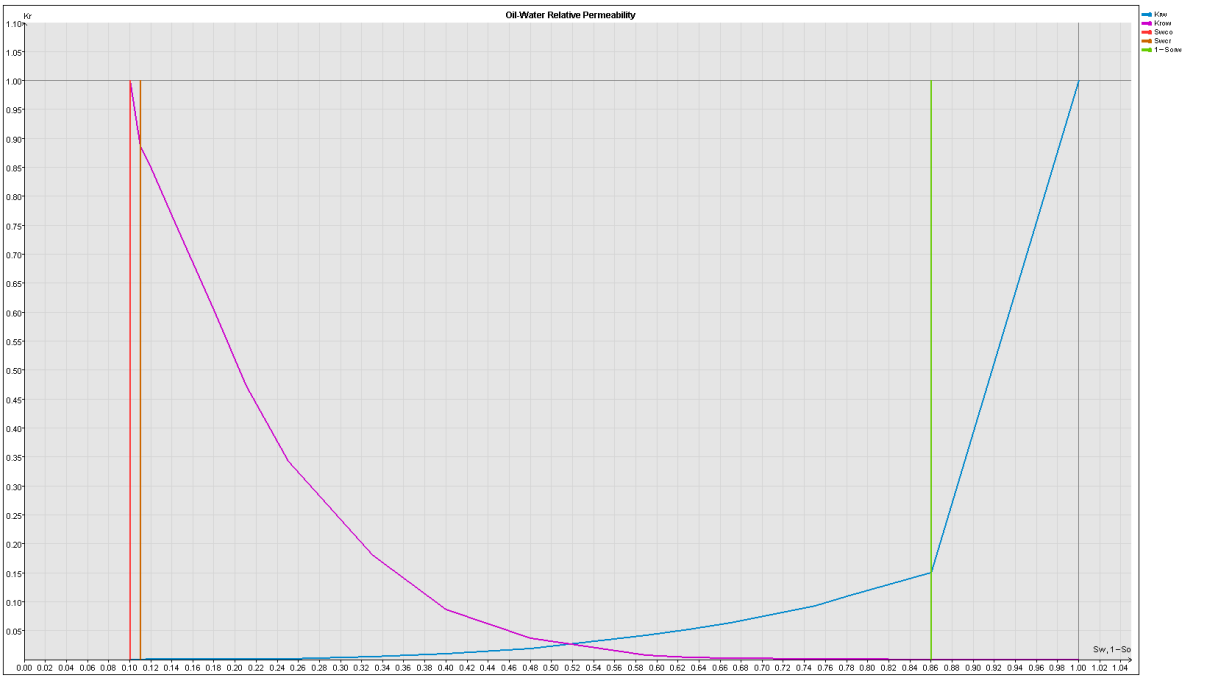

Figure G-29: *B1-AHT3: Oil-Water relative permeability*